ProQuest LLC.
789 East Eisenhower Parkway
P.O. Box 1346
Ann Arbor, MI 48106 – 1346

Development and Applications of Electrically-Driven Separation Methods.

David R Ellis

A thesis submitted in partial fulfilment of the requirements of
Sheffield Hallam University
for the degree of Doctor of Philosophy.

December 2002

ABSTRACT.

The use of non-aqueous media in CE was investigated primarily in an attempt to identify alternative mobile phases for application in CEC. Several solvents were found to support a rapid EOF even without the presence of a supporting electrolyte. These initial experiments led to the development of a separation involving an active pharmaceutical ingredient (Cimetidine) and a series of related materials. The latter displayed alternative selectivity relative to a comparable aqueous-based separation and offered a number of advantages. However, the underlying fundamental principles that govern separations in non-aqueous media were not well understood and method development was somewhat of a "black art". Further studies were therefore undertaken in order to gain an understanding of the mechanisms that influence separations in non-aqueous media. Under certain conditions the mode of separation appeared to be based on some form of interaction with the background electrolyte and the choice of a suitable EOF marker was not straightforward.

HPLC separations of EPA priority pollutant phthalate esters were developed to assess the ease by which they could be transferred to CEC and determine any advantages offered by the electrically-driven technique. The practicalities of fabricating columns for CEC separations are critically discussed along with the unsuitability of some of the stationary phases employed. Attempts to utilise non-aqueous media in CEC separations are also described.

A series of "real" applications were undertaken to assess the practicality of various electrically-driven separation techniques. The latter comprised a series of alkyltin compounds, the pesticide pirimicarb and its related metabolites and the determination of ethylenediammine (EDA). No meaningful separations were achieved with alkyltin compounds. However, the use of NMF as a non-aqueous mobile phase for CEC was demonstrated. Investigations involving EDA also did not lead to a successful separation. However, issues with the proposed derivatisation schemes were uncovered. The separations involving pirimicarb clearly demonstrated the enhanced scope available for method development offered by the various modes of CE that are available. Only partial separations were possible using CE in both aqueous and non-aqueous media. However, complete resolution of the 4 structurally similar materials was achieved using MEKC.

ACKNOWLEDGEMENTS.

To reminisce, digress or inform? To reveal, portray or exonorate? For whom and for why?
Ian Dury

The work presented in this thesis was performed between March 1996 and March 1998. This thesis took considerably longer to write and reach you in its final form due to me being jumped on and bludgeoned by the 'black dog' of depression.

Although the work presented within this thesis is my own I am extremely keen and proud to acknowledge the contributions of the various individuals without whom.....

Words cannot express my gratitude for the support (both emotional and financial) given to me by my mother over the years.

I wish I had the words to describe my feelings for Suzanne who walked into my life and changed it immeasurably for the better. The birth of our first child (Lennon Samuel 1 Sept 2001, 15:47) has made me the happiest and proudest man alive.

It was once stated that 1000 monkeys each with their own typewriter would eventually produce the complete works of William Shakespeare. I'm sure that my supervisors Dr Lee Tetler and Dr Malcolm Clench would state that this would have been a faster strategy for getting this thesis completed! I cannot thank them enough for their patience and support and understanding during the production of this thesis. I thank Lee for giving me the opportunity of undertaking this work and all of his advice over the years.

Thanks to all of my fantastic friends and colleagues at Hallam University over the years. Extra special mentions to Dave Douce, Jackie Mawhinney (now Dr Morton) and Ben Zeitlin for consistently being friends above and beyond the call of duty.

The help and support of the wonderful technical staff at the University is gratefully acknowledged. Hopefully after all this time they will have forgiven me for breaking that UV cell! The help and support of the Research Office and library staff is also gratefully acknowledged.

Many sincere thanks to Duncan and all the staff at the Health and Safety laboratory for their helpful discussions and use of their CE.

Undertaking a PhD is a tough life. It was made so much easier by the wonderful Brown family with whom I lodged.

Must go, my tea's ready.
Dave Ellis 16:51 3/11/02

Dr Lee Tetler

Lee was tragically killed in a motoring accident on 13 Dec 2000 whilst returning to his home in Broadbottom. I am deeply saddened by the fact that he never saw the completed version of this thesis.

Try as I might I cannot find words to describe Lee that can top those used by a speaker at his memorial service so I shall repeat them here:

Lee Tetler: "A great bloke".

This thesis is dedicated to Lee.

AIMS OF THIS WORK.

At the time of undertaking this research electrically-driven separations based on CE were subject to a significant wave of interest fuelled mainly by the "rediscovery" of capillary electrochromatography (CEC).

Several groups had begun to publish impressive CEC separations but these typically involved model test compounds such as mixtures of PAHs using only a few simple mobile phases. Furthermore, workers in this field were obliged to fabricate their own columns "in-house" since they were not readily commercially available. Development of the technique in the research community therefore required fabrication techniques that could ideally be applied within any laboratory. Additionally, clear demonstrations were necessary that the technique could meet pharmaceutical industry and other regulatory criteria, be successfully applied to complex and/or "real" samples and that conversion of established HPLC methods was straightforward.

The addition of organic solvents to CE separation media is a well-established method of manipulating selectivity. The literature contained several intriguing reports of CE and CEC separations effected in totally non-aqueous media. Unfortunately, none of the authors involved appeared to fully understand the fundamental processes involved in this conceptually difficult area and many reports did not discuss important separation parameters such as repeatability.

This research initially aimed to verify reported observations of a rapid EOF in non-aqueous solvents. It was then intended to identify and understand the fundamental processes involved and determine their effect(s) on the resulting separation. This would allow a generic method development procedure to be proposed and ultimately applied to "real" samples comprising complex matrices. The latter would be used as a challenging test to evaluate whether the technique was capable of achieving typical performance criteria found in industry. Applications were to be carefully chosen to demonstrate the perceived advantages offered by non-aqueous media such as the analysis of hydrophobic materials.

The application of non-aqueous media to CEC was also envisaged. It was anticipated that this would significantly enhance the scope available during method development and hence the potential application range of the technique. However, it was first necessary to evaluate the advantages offered by the technique compared to HPLC. This was to be assessed by transferring a method developed for HPLC to CEC.

Published procedures for the fabrication of CEC columns had generally been developed by well-established groups. Financial constraints necessitated that columns were fabricated "in-house". This allowed the feasibility and limitations of manufacturing columns in a small laboratory without the aid of specialised equipment or access to speciality stationary phases to be evaluated.

CONTENTS.

CHAPTER 1.

INTRODUCTION.

1.1. BACKGROUND.

This introductory chapter reviews the fundamental principles of high performance capillary zone electrophoresis (CE, CZE or HPCE). Alternative modes of separation that allow CE instrumentation to be employed for the separation of a wide range of analytes are also introduced and discussed. Finally, the work of various researchers in this field is reviewed. The latter focuses on major developments in the field of electrically-driven separations as well as considering representative applications.

1.2. OVERVIEW.

CE is a versatile technique that has emerged over the past 15-20 years into the forefront of separation science. It is capable of effecting rapid separations exhibiting unprecedented efficiencies. Additionally, sample sizes and solvent requirements are far lower when compared to HPLC. Originally considered primarily for the separation of biological macromolecules, the development of new separation modes[1] has considerably broadened the potential application range of electrically-driven techniques to cover a broad spectrum of analytes including uncharged materials.

An additional attractive feature of CE is the relatively simple instrumentation involved. Briefly, the ends of a narrow bore separation capillary are placed into two vials containing a background electrolyte (or buffer) and electrodes that provide electrical contact between the capillary and a high voltage supply. Instruments are typically configured such that the inlet vial contains the positive electrode (anode) as shown in figure 1.1.

Figure 1.1 Schematic representation of a typical CE instrument.

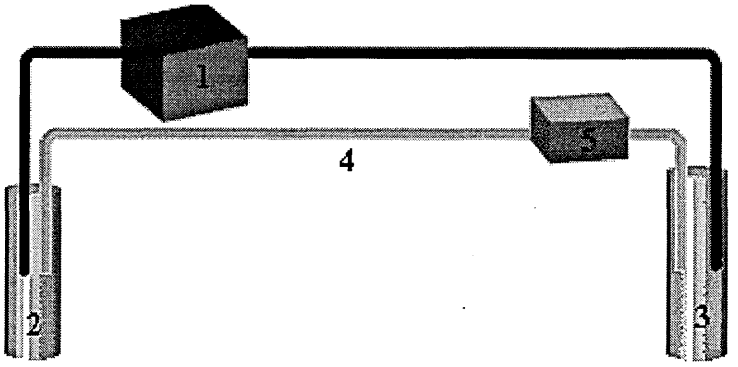

1 High voltage power source.
2 Inlet vial and positive electrode
3 Outlet vial and negative electrode
4 Separation capillary
5 On-capillary absorbance detection.

Samples are loaded onto the capillary at the inlet side. The sample vial is then replaced with one containing a background electrolyte (also referred to as buffer or separation media). Separations are accomplished via the application of a high voltage (typically in the order of 10-30 kV) across the capillary. Optical detection is usually performed through the capillary near to the outlet (or receiver vial). Most commercially available instruments include a high degree of safety features and an autosampler as standard. The latter allows high sample throughput and unsupervised operation. Important dimensions and parameters that will be discussed in subsequent sections can differ significantly between instrument brands.

1.2.1. Separation capillaries.

Fused silica capillaries (FSCs) are most commonly employed to effect CE separations[2]. They are typically coated with a thin layer of polyimide to impart mechanical strength. However, this coating strongly absorbs in the UV region and a small section must be removed to provide a window for optical detection. Polyimide removal may be effected by carefully heating in a small flame, scraping with a sharp blade or via chemical attack with hot concentrated sulphuric acid. A far more convenient and reproducible method is to use a commercially available device involving a resistively heated wire coil [3].

1.3. HISTORICAL DEVELOPMENT OF CE.

Electrophoresis involves the migration of charged entities in solution under the influence of an external electrical field. It is beyond the scope of this thesis to provide a comprehensive historical account of the development of electrophoretic techniques. However, an excellent summary has been provided by Vesterberg[4].

The origins of modern electrophoretic separations may be traced back to the pioneering work of Tiselius who was awarded a Nobel Prize in 1948. He is commonly credited with introducing electrophoresis as an analytical technique initially through his postgraduate research and subsequently through improved experiments[5]. He observed that the rate and direction in which components of a protein test mixture migrated in a simple electrophoresis experiment were based upon their charge and mobility. These free solution experiments were limited by both the instability of apparatus and more significantly by the convection processes caused by thermal heating induced by the applied electrical field.

The next major development of the technique was the introduction of support media such as gels, paper and cellulose acetate. The purpose of such support media was to contain the separation buffer and impede free movement of the analyte and thus limit the random influence of diffusion. However, separations that employed such anti-convective stabilisers required long analysis times and the resulting efficiencies were generally low. Efficiency was limited by zone broadening mechanisms such as interactions between the analyte and the anti-convective medium and/or eddy migration along the channels formed by the stabiliser. In addition to these difficulties, detection could be problematic and automation of the techniques for high sample throughput was not straightforward.

An alternative to the slab gel format involved performing the electrophoretic separation in a narrow bore tube or capillary. Such capillaries were found to exert an anti-convective "wall effect" [6] due to the viscosity of the electrophoretic medium and hence stabilising media were not required. Furthermore, the anti-convective and heat transfer properties were found to increase as the internal diameter of the capillary was reduced.

Hjerten[7] performed zone electrophoresis in a 3 mm quartz glass capillary coated with methylcellulose. The detrimental effects caused by the relatively large internal diameter were reduced via rotation of the capillary along its longitudinal axis. Although the feasibility of zone electrophoresis in capillaries was clearly demonstrated by this work, subsequent development was severely limited by the complexity of the instrumentation involved. Other workers subsequently performed electrophoresis in narrow bore (<200μm i.d) tubes but the predicted high efficiencies were not achieved[6, 8].

The true potential of free solution electrophoresis was finally demonstrated by the work of Jorgenson and Lukacs[9-11] in the early 1980s. These workers achieved highly efficient separations in 75 μm i.d untreated glass capillaries of 80-100 cm total length and employed sensitive on-column fluorescence detection.

1.4. THEORETICAL ASPECTS.

In a vacuum, an ion in an electrical field will continue to accelerate until it leaves the field The accelerating force, F, is given by equation 1.1.

$$F_e = qE \qquad \textit{Equation 1.1}$$

Where:

q is the charge of the ion.

E is the applied electrical field strength (applied voltage/capillary length).

However, in a fluid medium it will experience an opposing viscous resistance, ρ, that increases with increasing velocity. The frictional force experienced by a spherical ion is given by equation 1.2 which is termed the Stokes equation.

$$\rho = 6\,\pi\eta r v \qquad \textit{Equation 1.2}$$

Where:

η is the viscosity of the electrophoretic medium.

r is the radius of the charged ion.

v is the velocity of ion.

The rate of electrophoretic motion rapidly reaches a steady state and the ion moves at a constant velocity that is proportional to the applied electrical field as shown in equation 1.3.

$$v = \mu_e E = \mu_e V/L \qquad \textit{Equation 1.3}$$

The proportionality constant, μ_e, termed the electrophoretic mobility, is characteristic for a given ion in a given medium at a given temperature. The electrical and frictional effects become equal and opposite in magnitude during the steady state as shown in equation 1.4.

$$qE = 6\,\pi\eta r v \qquad \textit{Equation 1.4}$$

Solving equation 1.4 in terms of ion velocity and then substituting into equation 1.3 yields equation 1.5 that describes μ_e in terms of various parameters.

$$\mu_e = q/6\,\pi\eta r \qquad \textit{Equation 1.5}$$

Although this is a fairly crude model it does allow a useful insight into the electrophoretic process. Equation 1.5 clearly accounts for the influence of the viscosity of the background electrolyte. The relationship between temperature and ion mobility is also suggested since viscosity is temperature dependent. The presence of the charge and radius terms indicate that small, highly charged ions will have higher electrophoretic mobilities than larger, lesser charged species.

1.4.1. The electrical double layer.

The electrical double layer is a feature of any surface that is immersed in a solution. Consider a negatively charged surface such as silica in contact with an electrolyte solution. A thin area of excess opposite charge will exist in solution at the surface boundary to balance the fixed negative charges. Excess charge at the solid surface/liquid boundary involves a fairly immobile layer of ions that adhere tightly. The remainder of the excess charge is distributed amongst a mobile layer of ions that freely exchange with those in the bulk solution. The excess charge density and associated electrical potential decreases rapidly as the distance from the surface increases. The potential at the boundary between the fixed and mobile layers is termed the zeta potential, denoted by ζ. This will be discussed in greater in section 1.4.2.

The fall-off of electrical potential with distance from the surface is roughly exponential. The distance at over which ζ falls by a factor of *e* is termed the double layer thickness denoted by δ. The latter is often denoted by $1/\kappa$ (κ is the Debye length) which may be determined using equation 1.6.

$$\delta = \sqrt{(\varepsilon_r \varepsilon_o RT)/(4 \pi F^2 \Sigma_i C_i Z_i^2)} \qquad \textit{Equation 1.6}$$

Where:

ε_r is the dielectric constant of the electrolyte solution.

ε_o is the permittivity of a vacuum.

R is the gas constant.

T is the absolute temperature.

F is the Faraday constant.

C_i is the molar concentration of any ion in the solution phase.

Z_i is the ion valency of any ion in the solution phase.

1.4.2. Electroosmotic flow.

Electroosmotic flow (EOF) is an electrophoretic phenomenon that results in bulk flow of solution through the separation capillary. It results from effect of the applied high voltage on the electrical double layer and is key to all capillary-electroseparation methods.

The following discussion is restricted to untreated fused silica capillaries as they are most commonly employed in electrophoretic separations. The inner walls of such capillaries may become charged either via ionisation (acid-base equilibria) or adsorption processes. The inner surface of a fused silica capillary consists of silanol groups, (Si-OH). These groups become ionised above approximately pH 3 to yield negatively charged silanoate, ($Si\text{-}O^-$) groups. It is common practise to enhance this ionisation process by pre-treating a separation capillary with a base such as sodium hydroxide.

This ionisation process results in a layer of negative charge at the capillary wall. Cations from the background electrolyte solution are attracted to form a tightly held immobile layer at the capillary wall/solution interface (the Stern layer). This process cannot sufficiently neutralise the negative charges exhibited by the silanoate groups resulting in the formation of a second layer of cations. The second layer is not as tightly bound as the Stern layer and is referred to as the mobile (or diffuse) layer.

An electrical imbalance termed the zeta potential or electrokinetic potential, ζ, is created at a plane of shear which exists between the Stern and diffuse layers as shown in figure 1.2.

Figure 1.2 The electrical double layer

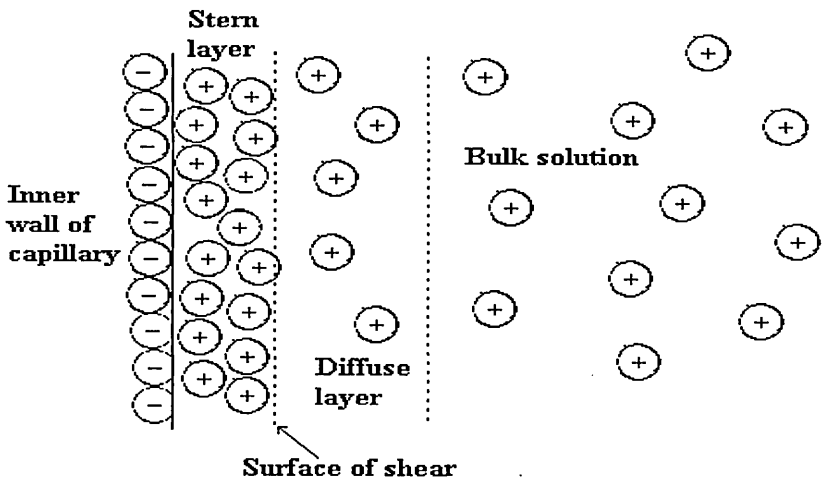

Application of a high voltage across the length of the capillary causes the mobile layer of cations to be attracted towards the cathode. The cations are solvated and hence their movement causes the bulk solution in the capillary to be dragged with them yielding a net flow from anode to cathode. The flow velocity is generated uniformly along the capillary and is independent of its internal diameter.

The magnitude of the EOF is proportional to the zeta potential that is in turn proportional to the thickness of the diffuse double layer. The magnitude of the zeta potential is given by equation 1.7.

$$\zeta = \frac{4\pi\delta e}{\varepsilon} \qquad \textit{Equation 1.7}$$

Where:

ε is the dielectric constant of the electrolyte medium.

δ is the thickness of the electrical double layer.

e is the charge per unit surface area.

The magnitude of the EOF is dependent on the internal diameter of the capillary, d, and the thickness of the electrical double layer, δ. Rice and Whitehead[12] stated that the EOF velocity would be independent of d only when d is significantly greater than δ. They concluded that as the internal diameter of the capillary was reduced and the value of d approached that of δ, double layer overlap would result in parabolic flow profile that would limit efficiency. Double layer overlap is therefore unlikely to pose a problem under typical CE operating conditions. A consideration of double layer overlap in terms of capillary electrochromatography (CEC) is given in section 1.8.5.2.

1.4.2.1. Important characteristics of EOF.

EOF has a plug-like flow profile that is totally in contrast to the typical pumped (or laminar) flow associated with HPLC as indicated in figure 1.3. Parabolic flow is caused by the difference in flow velocity between the centre and the walls of the separation column. The velocity at the centre of the tube is twice the average velocity whilst at the walls it is virtually zero.

Figure 1.3 Comparison of EOF and pressure-driven flow profiles.

The EOF profile is essentially plug-like apart from an insignificantly small area adjacent to the capillary wall that moves at a slower rate than the bulk solution due to friction. All solute molecules experience the same velocity component from the EOF regardless of their cross sectional position within the capillary and hence elute as narrow bands. In contrast, laminar flow leads to relatively broad peaks since solutes in the centre of the capillary move faster than those nearer the wall. It is this property that is responsible for yielding the sharp peaks and high efficiencies associated with CE.

1.4.2.2. EOF velocity and mobilities.

The electroosmotic velocity, ν_{EOF}, is given by equation 1.8.

$$\nu_{EOF} = \frac{\varepsilon \xi}{4\pi\eta} \cdot E \qquad \textit{Equation 1.8}$$

The electroosmotic mobility, μ_{EOF}, is given by equation 1.9.

$$\mu_{EOF} = \frac{\varepsilon \zeta}{4\pi\eta} \qquad \textit{Equation 1.9}$$

It is clear from equation 1.9 that the EOF mobility is independent of the applied voltage and is solely based upon dielectric constant and viscosity which are characteristic of the separation medium that is employed.

The cumulative effects of electrophoretic mobility and EOF result in all species being carried through the capillary from the inlet vial to the detector. Cationic species migrate fastest and hence elute first since their electrophoretic attraction towards the cathode and the EOF are in the same direction. The electrophoretic mobility of an electrically neutral (uncharged) species is zero. Hence all neutral species move through the capillary together at the same rate as the EOF and are not separated. Anions are carried towards the cathode since the EOF is generally greater than their electrophoretic attraction towards the anode. They therefore migrate slowest and hence elute last as demonstrated in figure 1.4. However, under certain conditions the electrophoretic mobility of an anion can be greater than the EOF resulting in migration towards the anode and the material not being detected.

Figure 1.4 Migration order in CE (flow from + to -).

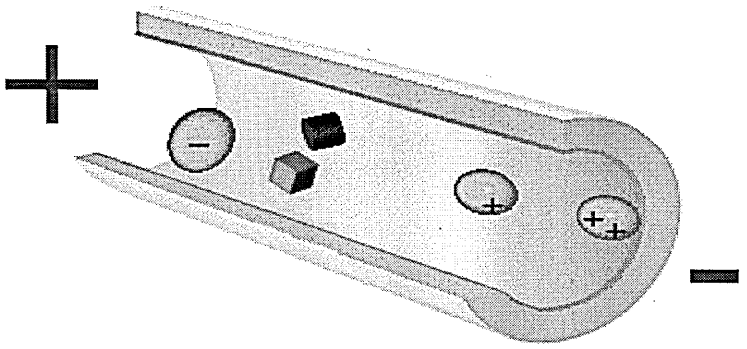

Charged species may therefore be separated from each other on the basis of differences in their electrophoretic mobilities. Neutral compounds may be separated from charged species but not from each other. Without EOF some very large and/or weakly charged ions would require a extremely long time to migrate to the point of detection and it would be impossible to separate anions and cations in a single analysis.

1.5. DEVELOPMENT OF SEPARATIONS.

1.5.1. Control of EOF.

Reproducible separations are dependent on efficient control of the EOF. The EOF may be manipulated via alteration of the surface charge on the capillary inner wall or the properties of the buffer. Conditions that alter the surface charge of the wall such as buffer pH often also affect analytes. Successful separations are the result of optimising both the EOF and analyte mobilities.

Alternative modes of electrophoretic separation such as isoelectric focussing and isotachophoresis (both covered in section 1.8) often require suppression of the EOF. There are several means of manipulating EOF that are briefly discussed in the following sections. These parameters are further discussed in section 1.5 in terms of their influence when developing separations.

1.5.1.1. Applied electrical field.

Lowering the applied electrical voltage will decrease the EOF (equation 1.8.5.1). However, this strategy typically results in detrimental effects to resolution, efficiency and separation time. Conversely, raising the applied voltage will yield a faster EOF but the increased current may result in Joule heating (section 1.5.3.1).

1.5.1.2. Buffer.

The EOF may also be manipulated by simply altering the pH of the buffer. However, this may also affect the charge and mobility of analytes. The EOF varies with pH because of alteration in the charge density at the capillary wall.

The concentration and ionic strength of the buffer also influence the magnitude of the EOF [13]. Typical buffer concentrations range from 10-100mM. High buffer concentrations can be useful for limiting coulombic interactions between analytes and the capillary by lowering the effective charge at the capillary wall.

1.5.1.3. Modification of the capillary wall.

The EOF may be increased, decreased or even reversed via modification of the capillary wall. Modification may be accomplished using either dynamic coatings involving buffer additives or by employing capillaries whereby the inner wall has been permanently chemically modified.

1.5.2. Solute mobilities and migration times.

Measured separations occur in the section of the capillary defined by L_d whereas the electrical field strength is measured across the total capillary length, L_t as shown in figure 1.5.

Figure 1.5 Definition of the two capillary dimensions employed in CE.

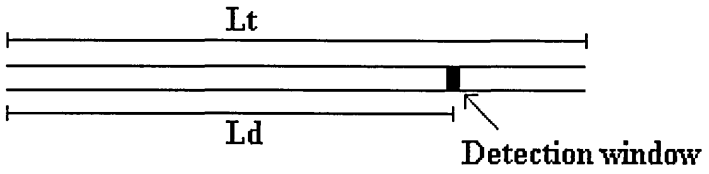

The magnitude of the two length terms is instrument specific and minimum capillary dimensions are often fixed. The latter restraint has been overcome using the so-called "short end injection" technique[14, 15] whereby the sample is introduced at the end of the capillary that is closest to the detector.

The migration time of a solute is simply the time taken for it to migrate to the point of detection. The observed electrophoretic velocity ν_{OBS} may be determined using equation 1.10.

$$\nu_{OBS} = L_d/t_m \qquad \textit{Equation 1.10}$$

Analyte mobilities may be calculated using equation 1.11.

$$\mu_{app} = \frac{L_d.L_t}{t_m.V} \qquad \textit{Equation 1.11}$$

Where:

μ_{app} is the apparent (observed) mobility ($cm^2\ V^{-1}\ s^{-1}$).

V is the applied voltage (V).

t_m is the migration time (s).

L_d is the effective capillary length i.e. length from inlet to detection window (cm).

L_t is the total capillary length (cm).

In some instrumental configurations the difference between these two length terms is negligible and $L_d L_t$ in equation 1.11 has been reduced to L^2. Analyte mobilities calculated in this manner are termed apparent mobilities since they include the contribution from the EOF. The effective (or true) mobility of an analyte, $\mu_{eff,}$ may be determined by subtracting μ_{EOF} from μ_{app} as demonstrated in equation 1.12

$$\mu_{eff} = \mu_{app} - \mu_{EOF} \qquad \textit{Equation 1.12}$$

The magnitude of μ_{EOF} may be determined experimentally via the injection of a neutral marker compound such as acetone, thiourea or mesityl oxide that travels through the capillary at an identical rate to that of the EOF. Such compounds are typically included within sample solutions during their preparation.

1.5.3. EFFICIENCY AND ZONE BROADENING.

The time taken for an analyte to migrate the entire length of the capillary is given by equation 1.13.

$$t = \frac{L}{v} \qquad \textit{Equation 1.13}$$

Substituting the expression for velocity in equation 1.3 yields equation 1.14.

$$t = \frac{L^2}{\mu_e V} \qquad \textit{Equation 1.14}$$

It is evident from equation 1.14 that the analysis time is proportional to the square of the capillary length and inversely proportional to the applied voltage. Assuming that molecular diffusion is the sole contributor to sample zone broadening, the spatial variance, σ^2, of a sample zone after time, t, is given by equation 1.15 that is termed the Einstein equation.

$$\sigma^2 = 2Dt \qquad \textit{Equation 1.15}$$

Where D is the diffusion coefficient of the analyte.

Substituting the expression for time in equation 1.14 into equation 1.15 yields equation 1.16.

$$\sigma^2 = 2DL^2/\mu_e V \qquad \textit{Equation 1.16}$$

The expression for the number of theoretical plates, N, in electrophoretic separations derived by Giddings[16] is given in equation 1.17

$$N = L^2/\sigma^2 \qquad \textit{Equation 1.17}$$

Substitution of equation 1.16 into equation 1.17 yields an important expression in electrophoretic separations that is given in equation 1.18[11].

$$N = \frac{\mu_e V}{2D} \qquad \textit{Equation 1.18.}$$

These equations must be modified in the presence of EOF. Efficiency in terms of number of theoretical plates in the presence of EOF is given by equation 1.19.

$$N = \frac{(\mu_{EOF} + \mu_e)V}{2D} \qquad \textit{Equation 1.19.}$$

It is clear from equation 1.19 that efficiency is independent of the capillary length. Although the efficiency is proportional to the diffusion coefficient and mobility of the analyte, these are intrinsic properties of the compound(s) in question and hence their manipulation to increase N is not straightforward.

Van Deemter and co-workers[17] determined that there was an optimum mobile phase velocity in chromatography at which band broadening is a minimum and column efficiency is greatest. They also defined three processes (A, B and C) that contribute towards band broadening. Under ideal conditions the sole contribution to analyte zone broadening in CE is the van Deemter B term, longitudinal diffusion (i.e. along the length of the capillary). However, other dispersive effects are often present as described in the following sections[18]. Note, the van Deemter equation is discussed in greater detail in section 1.8.5.1 as an introduction to capillary electrochromatography.

1.5.3.1. Temperature effects: Joule heating.

Efficiency is directly proportional to the applied voltage (equation 1.19) whereas separation time is proportional to the square of the capillary length (equation 1.14). It would therefore be reasonable to assume optimum separation in terms of speed and efficiency would be achieved using a very high voltage and a short capillary. Jorgenson and Lukacs[19] reported that a plot of efficiency versus applied voltage was a straight line except for a negative deviation from linearity at high voltages. They predicted that the inability to dissipate generated heat was a limiting factor to the use of high separation voltages.

Joule heat is generated by the passage of current through a background electrolyte within a capillary. Heat is generated uniformly throughout the capillary but is only dissipated at the inner walls and ends. This results in a parabolic temperature gradient across the capillary such that the centre becomes warmer than at the inner walls[20]. Under extreme circumstances the temperature difference between the walls and centre is so great that the electrophoretic process can breakdown completely. However, the effects of Joule heat are more commonly observed as reduced efficiency.

Reduced efficiency is a consequence of increased analyte mobility caused by a change in the viscosity of the aqueous buffer. The latter increases by approximately 2-3% for every 1°C rise in temperature. Under these conditions analyte molecules at the warmer centre of the capillary migrate faster than those at the walls resulting in broadening of the sample zone.

The radial position of analyte molecules is constantly changing due to diffusion across the capillary. Reducing the internal diameter of the capillary effectively enhances this radial diffusion of analyte molecules back and forth across the temperature gradient thus averaging their velocities and minimising the effects of Joule heat. The magnitude of the radial temperature gradient is proportional to the square of the capillary radius and hence reduction of the internal diameter significantly reduces any temperature differences across the capillary.

The majority of commercially available instruments incorporate some form of cooling system to maintain a constant separation temperature[21]. Zare *et al.*[22] patented a design for a capillary with a rectangular cross-section that was claimed to efficiently dissipate heat.

1.5.3.2. Interaction between analytes and the capillary wall.

Adsorption of solutes to the capillary wall can lead to a variety of problems such as alteration of the EOF, irreproducible migration times, degradation of efficiency, capillary fouling and loss of sample.

The large surface area to volume ratio of the separation capillary enhances the likelihood of such effects occurring. The main causes of adsorption are ionic interactions between the negatively charged capillary wall and cationic analytes and hydrophobic interactions. It is perhaps not surprising that peptides are the most commonly cited examples of these adsorptive effects since they possess numerous charges and hydrophobic groups. A number of strategies may be employed to reduce analyte-wall interactions such as increased buffer concentrations, operation at extremes of pH and use of coated capillaries.

1.5.3.3. Electromigration dispersion.

Peak shape distortion occurs when the conductivity of the sample zone is appreciably different from that of the separation medium. The field strength becomes non-uniform along the capillary resulting in asymmetric zones. Dispersion of this kind is particularly evident with samples comprising analytes with a wide range of mobilities[23].

The leading edge of the sample zone will be diffuse and the trailing edge sharp (termed tailing) when the sample zone has a higher mobility than the separation medium. Conversely, the leading edge will be sharp and the trailing edge diffuse (termed fronting) when the sample conductivity is lower than the separation media. No distortion is observed when the sample and media conductivities are equal. Each situation is illustrated in figure 1.6.

Figure 1.6 Electrodispersion resulting from mismatched sample and buffer conductivities.

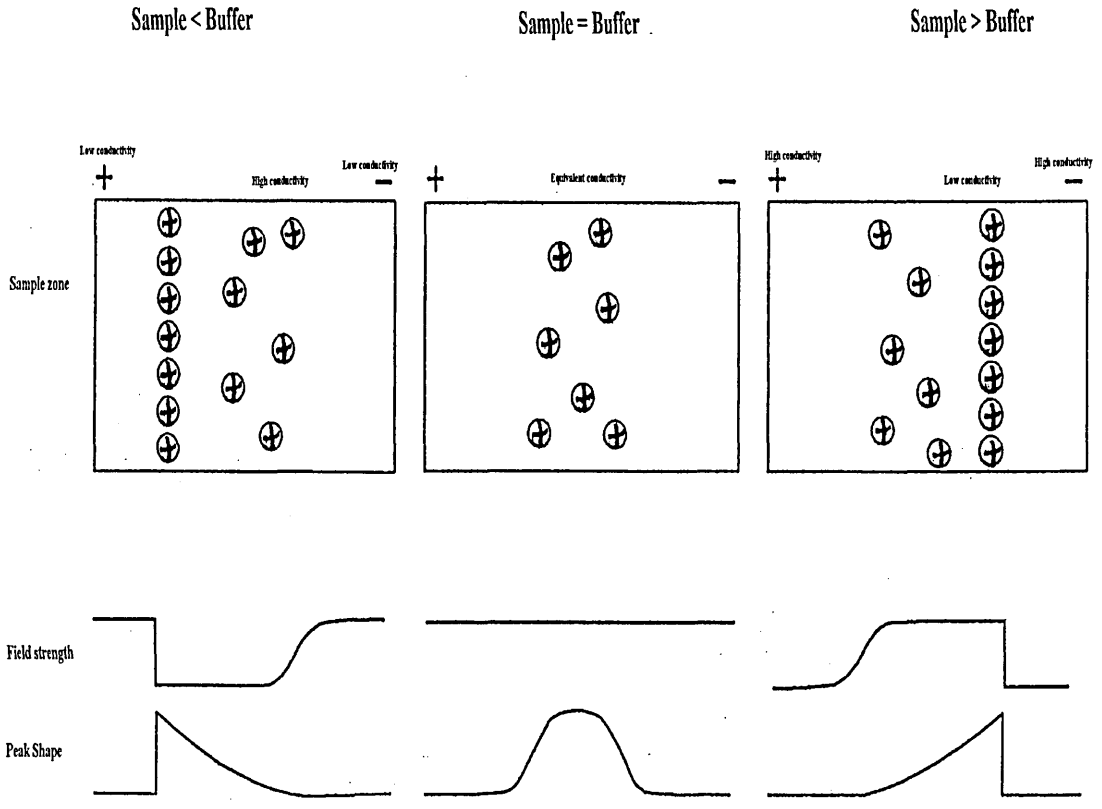

1.5.3.4. Length of sample injection plug.

An excessively long sample plug will have a detrimental effect on resolution and efficiency. Injection zone lengths typically do not exceed 1-2% of the total capillary length. However, even a 1% plug length may be excessive in many instances[24].

Issues with detection limits (section 1.6.3) under typical conditions often necessitate longer plug lengths. Methods of improving detection limits without compromising efficiency are discussed in section 1.6.3.2.

1.5.4. RESOLUTION.

Resolution in electrophoresis is given in equation 1.20[18].

$$R_s = \frac{\sqrt{N}}{4} \cdot \frac{\Delta v}{v_{avg}} \qquad \textit{Equation 1.20}$$

The relative velocity difference between the two analyte zones ($\Delta v/v_{avg}$) is defined in equations 1.21 and 1.22 (with and without the presence of EOF respectively).

$$\frac{\Delta v}{v_{avg}} = \frac{\mu_1 - \mu_2}{\mu_{avg} + \mu_{EOF}} \qquad \textit{Equation 1.21}$$

$$\frac{\Delta v}{v_{avg}} = \frac{\mu_1 - \mu_2}{\mu_{avg}} \qquad \textit{Equation 1.22}$$

Where:

μ_1 and μ_2 are the mobilities of the two analytes.

μ_{avg} is the average mobility of the pair.

It is evident from equation 1.21 that a large μ_{EOF} will reduce the relative velocity difference between the two analyte zones.

Substitution of equations 1.19 and 1.21 into equation 1.20 followed by rearrangement yields equation 1.23 which is an important expression for resolution in electrophoretic separations[11].

$$R_s = 0.177\,(\mu_1-\mu_2)\sqrt{V/[D(\mu_{avg}+\mu_{EOF})]} \qquad \textit{Equation 1.23}$$

A linear gain in resolution with increased applied voltage is not observed due to the square root term. The separation voltage must therefore be quadrupled to effect a two-fold increase in resolution. However, this strategy is ultimately restricted by the generation of Joule heat.

It is evident from equation 1.23 that a large EOF in the same direction as the analytes will reduce the resolution between the pair. Jorgenson and Lukacs[11] compared the separation of a series of derivatised amino acids in both a normal glass capillary and a glass capillary in which the inner surface was modified to suppress EOF. Enhanced resolution was achieved in the coated capillary but this was at the expense of increased separation time.

Optimum resolution will be achieved when the when the magnitude of the EOF is equal but opposite to the migration of the analytes (i.e. $\mu_{EOF} = -\mu_{avg}$). Under such conditions it should be possible to resolve analytes with extremely similar mobilities.

1.5.5. SEPARATION SELECTIVITY.

Resolution in CE is improved via the alteration of important separation parameters[25]. The most common strategies involve variation of buffer pH and/or the use of additives such as surfactants, chiral selectors and organic solvents.

1.5.5.1 Buffer.

Variations in buffer preparation have less pronounced effects in HPLC than in CE. Some workers have proposed standardising the documentation of CE buffer preparation procedures and other important operating parameters[26]. Altria[27] has recently detailed several generic buffers that are applicable for a variety of applications.

Crucial separation parameters such as migration velocity and efficiency are sensitive to changes in buffer characteristics. In particular, pH is of crucial importance. Buffering capacity (a quantitative measure of buffering efficiency/ability) must be sufficient to ensure that local pH and conductivity do not change significantly as a result of sample injection. Valko and co-workers[28] demonstrated that adequate buffering is crucial to obtaining reproducible migration times.

An effective buffer exhibits a range of approximately 2 pH units centred on its pKa value. A number of commonly used buffers and their useful pH ranges are listed in table 1.1. Polybasic buffers such as phosphate and citrate have more than one pKa value and hence can be employed in more than one pH range. Additionally, the buffer should exhibit a low absorbance at the relevant detection wavelength and possess a low mobility to minimise current generation. The commonly termed biological buffers such as TRIS are especially useful in terms of the latter property. Hjerten and Liao[29] investigated and subsequently patented a series of low conductivity buffers.

Table 1.1. Commonly employed materials for the preparation of CE separation media.

Name	**pKa**[30]
Phosphate	2.12 (pKa1), 7.21 (pKa2), 12.32 (pKa3).
Citrate	3.06 (pKa1), 4.74 (pKa2), 5.40 (pKa3).
Formate	3.75
Borate	9.24
Acetate	4.71
TRIS	8.30

Alteration of buffer pH is a powerful means of manipulating selectivity since it affects both the EOF and analyte mobilities. Small changes in pH can result in the separation of closely migrating analytes. Altria and Simpson[31] observed that mobility was inversely proportional to buffer concentration and that a logarithmic plot of concentration Vs mobility was linear.

1.5.5.2 Surfactants.

The following discussion is limited to surfactants that are added to the buffer at a concentration below the relevant critical micelle concentration (CMC). Surfactant concentrations above the CMC result in an alternative mode of separation termed micellar electrokinetic chromatography that is discussed in section 1.8.4.

Ionic surfactant molecules may act as solubilising agents for hydrophobic solutes, ion-pairing reagents or as capillary-wall modifiers. The latter may be used to modify the EOF and/or limit adsorption of analytes onto the capillary wall. Cationic surfactants such as CTAB adhere to the wall via ionic interactions. Hydrophobic interactions of free CTAB molecules with those adhered results in the generation of a positive charge in the vicinity of the wall and a reversal of the EOF flow.

1.5.5.3 Chiral selectors.

Selectivity may be manipulated by adjusting the identity and concentration of a chiral selector. Cyclodextrins (CDs) are the most widely employed chiral additives in CE. They are natural cyclic oligimers of glycopyranose units produced by enzymatic reactions with starch. The most commonly encountered CDs in analytical chemistry are those comprising 6, 7 and 8 units termed α, β and γ respectively. Their structure is best described as a truncated cone containing a relatively hydrophobic cavity and two openings of different sizes that are relatively hydrophilic due to the presence of hydroxyl groups.

It is possible to introduce a variety of compounds into the hydrophobic cavity via a mechanism termed guest-host (or inclusion) complexation. After dissolution the cavity of a cyclodextrin will "host" a water molecule. The latter is in an energetically unfavourable situation since the cavity is hydrophobic. Hence, molecules such as aromatics that can form non polar-non polar interactions with the cavity readily replace it. Further stabilisation is possible if the "guest" molecule also possesses a hydrophilic region that can interact with the opening of the CD cavity. CDs are dextrorotatory as a result of the chiral D-(+)-glycopyranose units present in their structure. Hence they can be employed as a chiral environment for the resolution of enantiomers[32-34].

Another popular means of effecting enantiomeric separations in CE is via the use of crown ethers. Crown ethers are macrocyclic polyethers that form stable inclusion complexes with alkali, alkaline earth and primary ammonium cations. Khun[35] gave an extensive review of the practical applications of crown ethers.

1.5.5.4. Temperature.

Most CE systems are thermostatically controlled to maintain capillary temperature and to dissipate Joule heat[21]. However, temperature may be employed to manipulate separations. An elevated or reduced temperature will alter buffer viscosity, EOF and analysis time. It may also be used to alter reaction kinetics and chemical equilibria.

1.5.5.5. Modification of the capillary wall.

It has already been stated that interactions between analytes and the capillary wall can have a detrimental effect on efficiency. Working at pH extremes is an effective means of reducing such issues. However, this strategy is unsuitable for some applications such as proteins whereby sample structure can be adversely affected. An alternative approach is to employ high ionic strength buffers but Joule heating resulting from the high currents generated ultimately restricts this strategy.

The most common form of permanent modification involves silylation followed by deactivation with a functional group. However, the siloxane (Si-O-Si) bond is stable only between pH 4-7 and hydrolysis may limit long term stability of some capillaries. Neutral deactivation with polyacrylamide, polyethylene glycol or similar eliminates EOF whereas deactivation with a cationic material reverses the EOF. Deactivation with amphoteric materials such as an amino acid yields a reversible EOF that is dependent on the buffer pH and the pI of the coating.

1.5.6. The Role of Organic solvents in CE.

Solvents such as acetonitrile and methanol have been employed in CE as either pure materials or constituents of an aqueous-organic mixture. The use of pure solvents is referred to as non-aqueous capillary electrophoresis (NACE)[36, 37]. Separation selectivity may be radically altered since the acid-base properties of analytes are different in organic solvents. Additionally, migration is dependent upon the physiochemical properties of the of the separation media (ζ, η) and the radius of the solvated ion which will be different in a non-aqueous environment.

Separation selectivity may be manipulated via the addition of organic solvents to CE buffers due to their effects on the physiochemical parameters that are decisive for separation (ζ, EOF, $\mu_{analyte}$)[38, 39].

1.5.6.1. Classification of solvents.

A variety of solvent classification schemes have been proposed. Many involve initially distinguishing two broad classes based on dielectric constant with a dividing value of 30 typically chosen. Each broad class is then further sub-divided into hydrogen-bonded (protic) solvents and non-hydrogen-bonded (aprotic) solvents. This classification is illustrated with examples in table 1.2. An excellent overview of the properties and chemistry of non-aqueous solvents is available[40]

Table 1.2 Classification of solvents.

High dielectric constant		Low dielectric constant	
H-Bonded	Non H-bonded	H-Bonded	Non H-bonded
Water	Acetonitrile	Ethanol	Acetone
Methanol	Dimethylsulphoxide	iso-propanol	Benzene
Formic acid	Nitrobenzene	Acetic acid	Chloroform
N-methylformamide			

Further division of each subclass may be made according to acidic or basic properties. For example formic acid is an acidic (or protogenic) solvent whereas dimethylsulphoxide is a basic (or protophilic) solvent. A third category may be assigned involving *amphiprotic* solvents that display both acidic and basic properties. These solvents are characterised by appreciable self-ionisation (or autoprotolysis) as illustrated in equation 1.24.

$$SH + SH \rightleftharpoons SH_2^+ + S^- \qquad \textit{Equation 1.24}$$

1.5.6.2. Levelling and differentiation.

In solvents undergoing autoprotolysis the strongest acid is the solvent cation SH_2^+ and the strongest base is the solvent anion S^-. Water completely converts strong acids to their conjugate anions and H_3O^+ (the solvent cation). Hence, strong acids such as HNO_3, HCl and $HClO_4$ appear to be of identical strength. Likewise, bases such as NH_2^- and CH_3O^- are completely converted to their conjugate acids and OH^- (the solvent anion). Strongly acidic and basic species are said to be levelled by water.

The intrinsic differences in the strength of acids and bases are not levelled in solvents such as acetonitrile and are said to be differentiated. The differentiation limits of a solvent are defined by the autoprotolysis constant. In water studies are restricted to acids with pKa values between 0 and 14 units whereas in acetonitrile it is possible to study acids with pKa values between 0 and 32.

1.5.6.3. Non-Aqueous Capillary Electrophoresis (NACE).

This area has received considerable interest during the past 5 years. Although impressive separations have been reported the technique is still not well understood. NACE was recently reviewed by Riekkola *et al.*[37].

1.5.6.4. EOF in pure solvents.

EOF has been observed in a number of solvents even without the addition of electrolyte. Whitaker and Sepaniak[41] observed cathodic flow rates in pure acetonitrile that were around three times faster than in typical aqueous media. Meanwhile, Wright and co-workers[42] reported rapid EOF in various organic solvents (acetonitrile, methanol, N,N-dimethylformamide and DMF).

Many organic solvents have lower dielectric constants than water resulting in less free ions to facilitate charge transfer. Hence lower currents are generated and higher electrical field strengths may be employed to effect separations. Reduced Joule heat effects can result in enhanced efficiencies compared to aqueous systems under optimised conditions[24]. Jansson and Roeraade[43] exploited the high field strengths possible with NACE and separated propranolol from felodipine in less than 35 seconds.

EOF in plain acetonitrile typically results in currents of less than 0.1μA[41, 42, 44]. Lister and co-workers[44] determined the current generated in a range of pure solvents. No relationship was apparent between the measured current and the EOF generated in each solvent.

The ratio of dielectric constant to viscosity (ε/η) has been shown[41, 42] to be a convenient means of predicting the magnitude of the EOF generated in a given solvent. Solvents with an ε/η similar to that of water should therefore provide rapid flow as long as a significant ζ exists.

N-methyl formamide (NMF) has both a high dielectric constant and an autoprotolysis constant that is comparable to water. It is understood that all species are solvated, principally by hydrogen bonding with the solvent. Jansson and Roeraade[43] demonstrated a reproducible EOF was possible without the presence of background electrolyte. However, NMF contains impurities such as hydrolysis products that are likely to influence the EOF and ζ.

1.5.6.5. NACE separations involving background electrolytes.

The term pH* has been adopted as a means of describing acidity and basicity in NACE since the concept of pH is arguably only valid in dilute aqueous solutions. Many workers have chosen to determine such values using commercially available pH probes. A recent paper by Espinosa and co-workers[45] provides an excellent insight into the complexity of pH measurements in non-aqueous media.

A number of studies have employed non-aqueous media of relatively low pH* comprising methanol and/or acetonitrile containing an electrolyte such as ammonium or sodium acetate with acetic acid present to aid dissolution[46-53]. The selectivity of basic analytes in non-aqueous media of this type is markedly different from equivalent aqueous-based separations[47, 48, 51-53] and may be manipulated via alteration of the relative compositions of the organic solvents[46-48, 53]. Additionally, separations involving highly hydrophobic analytes may be undertaken [48].

Altria and co-workers[54] used high pH* non-aqueous media for the separation of acidic species. Sodium acetate and sodium hydroxide were used to increase pH*. Fillet and co-workers[55] effected the separation of non-steroidal anti-inflammatory drugs using a methanolic buffer comprising 50mM ammonium acetate/13.75mM ammonium acetate (pH* 8.5).

Conversely, Senior *et al.*[49] employed low pH* (<7) NACE buffers to effect the separation of acidic compounds. Samples were injected at the outlet side of the capillary and the resulting negatively charged species migrated against the EOF.

Water in concentrations of up to 0.5% v/v has been shown to have only a minor effect on the separation selectivity, efficiency and EOF achieved in NACE[56]. In a separate study Hansen and co-workers[53] reported that the addition of up to 1% v/v water did not have any significant effect on the selectivity obtained for a series of test compounds.

Temperature control is crucial for obtaining reproducible separations in NACE. Leung and co-workers[46] obtained a significant improvement in the repeatability of migration times when they transferred their NACE separation to an instrument with superior thermostatic control.

1.5.6.6. Separation of neutral analytes using NACE.

Non-aqueous solvents have also been employed in the electrophoretic separation of electrically neutral compounds. Separation is based upon the interaction between neutral analyes and ionic buffer additives such as tetraalkylammonium ions that are well solvated in dipolar aprotic solvents such as acetonitrile. The resulting positively charged species are capable of migration in the electrical field. This technique has been used to separate PAHs[57]. Tjørnlund and Hansen[58] studied the effect of alkyl chain length on the separation of uncharged analytes in propylene carbonate and acetonitrile. The fastest mobilities in each solvent were achieved using tetrabutylammonium chloride.

Miller *et al.*[59] exploited the principle of heteroconjugation between Brønsted acids and small inorganic anions in acetonitrile to effect the separation of phenols, carboxylic acids and alcohols. The resulting heteroconjugated anions migrated towards the anode. Meanwhile, Wright and Dorsey[60] applied the principles of argentation chromatography to NACE. Silver (I) complexation was demonstrated to be an effective means of manipulating selectivity for heterocyclic containing materials.

1.5.6.7. Enantiomeric separations.

Many organic solvents have dielectric constants lower than water which facilitate ion-pair formation or ion-dipole interactions between analytes and chiral selectors that may not be possible in aqueous buffers. Quinine has been used to resolve dinitrobenzoyl amino acids in methanol[61] whilst pharmaceutical enantiomers have been separated using camphorsulphonate in acetonitrile[62].

Some cyclodextrins (CDs) exhibit limited solubility in water making NACE an attractive alternative to aqueous-based separations. Formamide and NMF are particularly good solvents for CDs but association constants have been shown to be lower than in water. However, successful separations have been reported[63]. Enantiomeric NACE separations employing a crown ether as the chiral selector have also been reported[64].

1.5.6.8. Quantitative analysis.

Concerns have been expressed regarding whether NACE methods employing volatile separation media are sufficiently stable and repeatable to be employed in quantitative assays.

Bjørnsdottir and Hansen[52] exploited the different selectivities possible with NACE to the separation of morphine from related opium alkaloids. The levels of morphine determined in three drug formulations using a validated NACE assay were found to be comparable with results from an aqueous CE and HPLC methods.

Cherkaoui and co-workers[50] developed a NACE assay for several atropine and scopolamine related compounds. Method robustness was demonstrated using a full factoral design at two levels. The method was successfully validated and applied to the determination of N-butylscopolamine in pharmaceutical formulations.

1.5.6.9. Preparative applications employing wide-bore capillaries.

The low currents associated with NACE have led to the development of separations on a preparative scale[65]. Relatively large solvent volumes are transported from the inlet to outlet vials when wide-bore capillaries are employed in NACE. This is a consequence of reduced viscosity compared to aqueous systems. The resulting difference in liquid levels can lead to a siphoning effect that induces a deviation from the plug-like flow profile. Palonen and co-workers[66] compensated for this effect by lifting the inlet vial. A separation of bumetadine and ethacrynic acid was presented using a 530 μm id capillary.

1.6. INSTRUMENTAL AND OPERATIONAL ASPECTS.

1.6.1. Sample injection techniques.

The high efficiency separations associated with CE may only be realised when the sample injection system does not significantly contribute towards band broadening. Separations typically involve on-capillary loadings of only a few nanolitres. Quantitative and reproducible loading of such small volumes of sample may be achieved using a number of injection techniques.

The two most widely employed procedures are hydodynamic (pressure) and electrokinetic (applied voltage) loading. Sample introduction by siphoning has been used by workers employing home-built CE systems. The 3 techniques are shown in figure 1.7 and discussed in the following sections.

Figure 1.7 Comparison of hydrodynamic (A), Siphoning (B) and Electrokinetic (C) sample introdution.

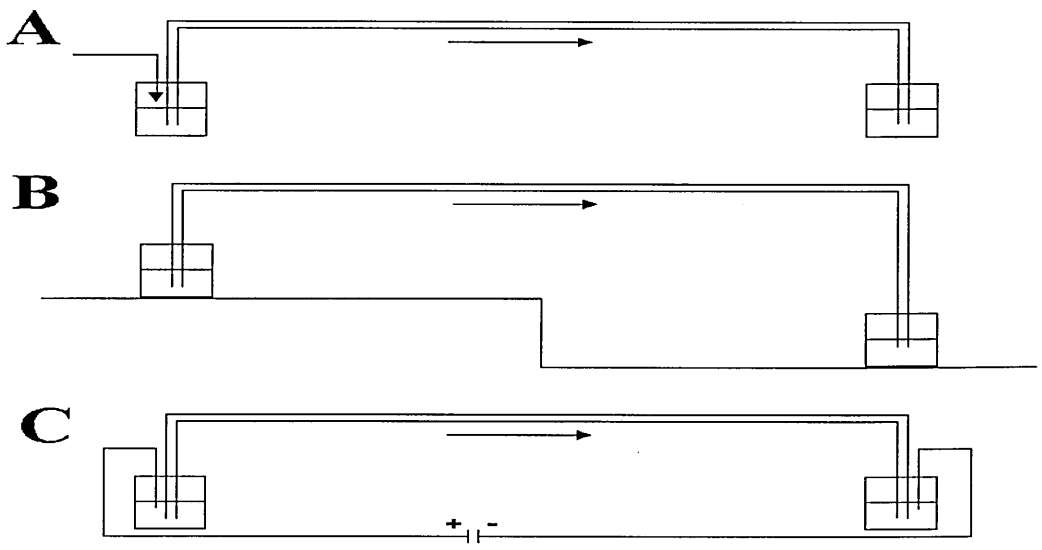

1.6.1.1. Hydrodynamic injection.

Hydrodynamic or hydrostatic injection sample injection is the most widely used injection procedure since it does not suffer from the sample composition-based discrimination inherent with electrokinetic injection. It has been shown to have very little effect on separation efficiency and to have an RSD of 2.9% when automated [67].

Sample introduction is accomplished by the application of pressure (25-100 mbar) at the inlet end of the capillary. The volume of sample, V_s, loaded may be determined using equation 1.25 that is termed the Hagen-Poiseuille equation.

$$V_s = \frac{\Delta P\, d^4 \pi\, t}{128\, \eta\, L_t} \qquad \textit{Equation 1.25}$$

Where:

ΔP is the pressure differential across the capillary.

d is the internal diameter of the capillary.

t is the duration of the injection.

η is the viscosity of the background electrolyte.

1.6.1.2. Siphoning.

Hydrodynamic-like injection may be effected in systems that do not have the capability to perform pressure injection via a siphoning process. This is typically performed by elevating the inlet vial such that it is 5-10 cm above the outlet vial for a period of time. The pressure differential in siphoning injection is given by equation 1.26. This value is then employed in equation 1.25 to determine the sample loading.

$$\Delta P = \rho g \Delta h \qquad \textit{Equation 1.26}$$

Where:

ρ is the density of the background electrolyte.

g is a gravitational constant.

Δh is the difference in height between the two buffer vials.

1.6.1.3. Electrokinetic injection.

Electrokinetic injection essentially involves utilising the combination of electrophoresis and EOF to load sample into the capillary. Injections are accomplished by replacing the inlet buffer vial with the relevant sample vial and applying a high voltage across the capillary. This is typically lower than the voltage that is employed to effect the separation.

The amount of sample, A_s, loaded may be determined using equation 1.27

$$A_s = \frac{(\mu_{analyte} + \mu_{EOF})\, V\, \pi\, r^2\, C_{analyte}\, t}{L_t} \qquad \textit{Equation 1.27}$$

Where:

$\mu_{analyte}$ is the electrophoretic mobility of the analyte.

μ_{EOF} is the EOF mobility.

V is the applied voltage (kV)

r is the radius of the capillary.

$C_{analyte}$ is concentration of the sample.

t is the injection time (s).

L_t is the total length of the capillary (cm).

It is clear from equation 1.27 that sample loading is dependant on analyte mobility and that biased loading will occur in samples containing species with widely differing mobilities[68]. In this situation, sample constituents with high mobilities will be injected onto the capillary in larger quantities than less mobile components.

The resistance of the injected sample solution also influences electrokinetic loading. This is inversely proportional to the conductivity of the background electrolyte. Huang and co-workers[68] demonstrated that more sample is injected in solutions with a high resistance. The authors suggested that this was due to ν_{EOF} and $\nu_{analyte}$ increasing with decreasing electrolyte concentration and hence ν_{total} (where $\nu_{total} = \nu_{EOF} + \nu_{analyte}$) varies almost linearly with the resistance of the sample solution.

1.6.1.4. Other injection modes.

Specialised alternative methods of sample introduction have been also been reported. Commercially available HPLC rotary injectors are unsuitable for CE due to generation of bubbles via electrochemical reactions at the surface of metal components. Tsuda *et al.*[69] designed a rotary-type injector for CE constructed from ceramics and tetrafluoroethylene resins. Meanwhile, Deml and co-workers[70] developed an electric sample splitter.

1.6.2. Repeatability of CE methods.

CE methods have a reputation for poor repeatability. Understanding and control of various key factors are crucial to establishing good routine methods[71]. For example, the buffer solution employed in a CE separation is subject to alteration via a number of processes that are discussed in the following sections[72].

1.6.2.1. Unequal buffer reservoirs.

A siphoning effect termed levelling is induced when the levels of background electrolyte in the two reservoirs are unequal[72]. This results in a laminar flow being superimposed onto the EOF leading to loss of efficiency and poor migration time repeatability[73].

1.6.2.2. Contamination.

Sample carryover during injection and/or the separation can lead to contamination of the buffer reservoirs. Additionally, impurities on vial caps may cause the applied voltage to skim away from the capillary and be grounded.

1.6.2.3. Electrolysis effects.

Extensive application of a voltage across an electrolyte during a series of replicate assays results in an effect termed buffer depletion [74, 75]. Essentially, a pH gradient is formed along the length of the capillary that can effect migration time repeatability and peak efficiency. Approaches to address this issue were discussed by Kelly *et al.*[76]. The extent of such effects is application dependent but it is generally considered good practice to renew the buffer after a number of replicate separations especially if analytes have pKa values close to the pH of the buffer[77]. Improved reproducibility has been reported using an automated buffer replenishment system[78]

Note that a decrease (or increase) in migration time results in a decrease (or increase) in peak area since bandwidth is proportional to the time taken for a solute to pass the detector. One strategy to eliminate this irreproducibility is to normalise peak areas by dividing by the migration time[79, 80].

Comparison of separations effected via application of constant voltage and constant current found that the latter resulted in better migration time repeatability in both successive injections and day to day analysis[81]. Wätzig and Dette[82] proposed that separation voltages and associated currents should be recorded when performing routine analyses for the purposes of traceability and good GLP.

1.6.2.4. Evaporation.

Vial caps cannot be fully sealed in CE since there is a requirement to insert the capillary and electrode into the buffer. Loss of analytes and/or solvents is therefore possible via evaporation especially during long run sequences such as overnight separation. The use of so-called star caps with cross-slotted openings has been shown to reduce losses via evaporation[83].

1.6.2.5. Alteration of the capillary wall.

Rinsing with some form of wash solvent followed by the relevant buffer is commonly performed between replicate separations to remove adsorbed materials, avoid sample carryover and re-equilibrate the capillary. Considerable time may be necessary to re-equilibrate the capillary in some applications[84]. It has been stated[85] that a reproducible EOF is not achieved until a capillary has been regularly used for a period of one to four months. When a capillary has been used for an extended period the inner wall may become altered. Additionally, EOF tends to gradually reduce as the capillary ages[77].

1.6.3. Detection.

1.6.3.1 On-capillary absorbance detection.

The most widely employed mode of detection is on-column UV/vis absorbance which is standard on most commercially available CE instrumentation. Many instruments also have diode array options that can be interfaced with data acquisition software[86].

The first wave of commercially available CE detectors were closely based upon established HPLC instrumentation. Conversion for CE detection required only the additional sphere (or ball) optics to collimate light across the diameter of the capillary. On-capillary UV absorbance detection rapidly became almost universal for all CE application involving organic compounds containing a chromophore. However, concentration detection limits are poor compared to HPLC due to the combination of the narrow detection light path and nl quantities of materials involved.

Increasing the capillary diameter increases both the amount of sample injected onto the capillary and the length of the UV detection light path. However, wide bore capillaries generate higher currents that cannot be efficiently dissipated leading to the detrimental effects of Joule heating. Hence the use of wide-bore capillaries to improve sensitivity may not be suitable for all applications.

Separation capillaries with modified detection windows are now commercially available. The most common and least expensive example is the so-called "bubble cell" in which the internal diameter of the detection window is significantly larger than the remainder of the capillary. Typical sensitivity enhancements are in the order of 3-5 fold. Djordjevic and co-workers[87] compared the performance of a sleeve cell extended light path design with a commercially available bubble cell capillary and on-column detection in a 75 μm id capillary. An abrupt change in capillary diameter in the sleeve cell (50 to 220 μm) did not result in excessive band broadening and was found to improve peak symmetry.

The "Z cell" capillary[88] offers a higher sensitivity gain than the bubble cell but is significantly more expensive. Essentially, the capillary is bent into a Z shape to yield a detection window. Detection is then performed along the length of this window (typically 1-3 mm long) i.e. at right angles to the remainder of the capillary. Typical sensitivity enhancements of 20-40 fold increases have been quoted. Improved sensitivity via an increased path length is also possible with rectangular capillaries[22].

1.6.3.2. Preconcentration.

Several methods utilising properties of the electrophoretic process may be employed to concentrate (or stack) a sample on the capillary prior to separation. These methods employ different kinds of discontinuous buffers to invoke different velocities to the same analyte molecules resulting in sharpening of the sample band. An excellent review of this area was recently provided by Shihabi[89].

Sharpening may be accomplished by simply dissolving the sample in an injection solvent with a lower ionic strength than the separation buffer. A similar effect may be achieved by dissolving the analyte in a solvent with a lower viscosity than water such as acetonitrile. Stacking in this manner typically yields a 5 to 30-fold increase in concentration factor bringing limits closer to HPLC. The isotachophoresis process (section 1.8.2) has also been utilised as a means of sample pre-concentration.

1.6.3.3. Alternative detection strategies.

Fluorescence [90] and laser-induced fluorescence detection (LIFD) [91] have been utilised due to their improved sensitivity compared to UV/Vis. Detection limits in fluorescence are usually in the range of femtomoles. Compounds without native fluorescence may be detected via pre-, on- or post-capillary derivatisation with a "tag" such as quinine sulphate, dansyl chloride or fluorescein isothiocyanate (FITC).

H^1 NMR[92] CE-MS[93, 94] and have been employed for structure elucidation. Chemiluminescence detection has shown great promise for CE applications but is still at an early stage of development[95, 96].

Commercially available radiation detection technology offers high sensitivity and unrivalled selectivity since only radiolabelled compounds are detected. Interfacing such devices with CE offers exciting possibilities in applications such as tracer studies. Zare and co-workers [97, 98] have described three on-line radioisotope detectors for CE designed to respond to γ and high-energy β emissions.

Other reported detection methods include electrochemical [99], X-ray fluorescence [100], flame photometric[101], conductivity[102] and ICP-MS[103, 104]. Swinney and Bornhop[105] have recently reviewed detection in CE

1.7. SELECTED APPLICATIONS.

CE is commonly associated with applications such as the separation of peptides[106], biopolymers[107] and simple ionic species[108]. The ease of method development and alteration of selectivity associated with CE has led workers to undertake a variety of challenging new applications. An excellent summary of recent significant developments in CE may be found in the latest of a series of biannual reviews[109].

The following sections briefly focus on two expanding areas of interest that are pertinent to this thesis namely the pharmaceutical industry and environmental applications.

1.7.1. Pharmaceuticals.

CE is beginning to gain popularity within the pharmaceutical industry[110-113]. Some companies working within this highly regulated environment were initially frustrated when attempting to convert established validated HPLC and GC methods into CE assays. Gains in speed and efficiency were often lost in precision and accuracy making it difficult to validate methods using accepted criteria for submission to regulatory authorities. However, developments in instrumentation and a better understanding of method development have improved performance and CE has become regarded as a viable alternative to HPLC in some applications. For example in a CE assay for diclofenac sodium using end-column amperometric detection the limit of detection was 5.2fmol and repeatability of migration times was 0.8%[114].

Various authors[115-118] have discussed approaches for the validation of CE methods within regulated environments. The performance of chromatographic instrumentation must be assessed prior to the commencement of an assay via a system suitability test[119]. The use of such tests for CE assays has been proposed[117]. Additionally, key regulatory aspects such as instrumental qualification have been discussed[120].

Altria and co-workers[121] validated a CE assay suitable for a range of basic drugs. Acceptable precision was achieved by employing an internal standard whilst optimal sensitivity was obtained using low (200nm) UV wavelengths. Wynia and co-workers[122] validated an assay for the quantitative determination of mirtazipine and related substances. Batch analysis results were reported to be similar to those obtained via the HPLC release test for mirtazipine. Poor injection precision was overcome via the use of an internal standard.

1.7.1.1. Representative applications.

A CE method for use in dissolution release testing of tablets has been reported[15]. It was demonstrated that there was no significant difference between the results of the CE method and the stated Pharmacopoeial ion-pair HPLC test. CE has also been employed in the routine analysis of pharmaceutical raw materials and excipients[123], in drug metabolism studies[124], pharmacokinetics[125] and to validate cleaning procedures in manufacturing areas[126].

1.7.2. Environmental.

Analysis of environmental samples is a challenging application for CE due to the low concentrations typically involved. Representative reported examples include quaternary ammonium herbicides such as Paraquat and Diquat [127-130], Chlorophenols[131] and alkyltin compounds[132]. Nielson[133] discussed trace enrichment strategies for environmental samples.

1.8. OTHER MODES OF SEPARATION.

1.8.1. CAPILLARY ISOELECTRIC FOCUSSING.

Capillary isoelectric focussing (CIEF)[134] is a well-established means of separating species such as proteins and peptides on the basis of their isoelectric (pI) points. The latter is the pH at which the number of positive charges possessed by a molecule exactly equals the number of negative charges.

Separation involves the formation of a pH gradient along the capillary using zwitterionic molecules termed ampholytes. The latter are typically synthetic polyamino, polysulphonic or polycarboxylic acids. The ampholytes become ordered on the basis of their pI values upon the application of an electrical field resulting in a pH gradient. They are kept within the capillary by employing a low pH solution at the anode and a high pH solution at the cathode. Amphoteric analytes such as proteins behave in a similar fashion to the ampholytes and become focussed as they migrate to a point corresponding to their pI.

EOF is problematic in CIEF since it may cause analytes to be swept through the capillary prior to focussing. Additionally, it can introduce some of the low pH anodic solution entering the capillary and disturb the pH gradient. EOF is usually either totally suppressed using coated capillaries or controlled using additives such as methylcellulose. In the latter case the focussed analytes will eventually pass through the detection window under the influence of the reduced EOF. CIEF separations involving zero-EOF environments require the addition of a salt to either the anode or cathode to cause the analytes to gain a charge and migrate towards the opposite electrode past the detector.

1.8.2. CAPILLARY ISOTACHOPHORESIS.

The term isotachophoresis (ITP)[135] is derived from Greek: iso meaning equal; tacho meaning velocity. This mode of CE employs a discontinuous buffer comprising a leading and terminating electrolyte to yield a steady state in which separated zones move at the same velocity. Choice of a suitable buffer system can often be problematic.

A major limitation of ITP is that anions and cations cannot be separated simultaneously and therefore must be separated independently. When separating anions the buffer involves a leading electrolyte containing an anion with an effective mobility that is higher than that of the analytes whilst the terminating electrolyte must exhibit a lower mobility. When an external voltage is applied the individual anions migrate towards the anode in discrete zones but all move at an identical velocity that is defined by the leading anion.

The electrical field in each zone adjusts to maintain constant velocity (velocity = mobility x field strength). Sharp boundaries are maintained between each zone since an ion diffusing into a neighbouring zone will immediately undergo a change in velocity and return to its original zone.

The on-line combination of ITP and CE has been employed as an effective means of increasing sensitivity[136, 137]. Chen and Lee[138] described an automated ITP-CE system where the sample was pre-concentrated in an initial capillary prior to being repeatedly injected into a second smaller diameter capillary for separation by CE. ITP-CE in a single capillary has also been reported[139, 140] in which detection limits were lowered by a factor of 170.

1.8.3. CAPILLARY GEL ELECTROPHORESIS.

Slab gel electrophoresis is a widely employed technique in biological analysis for the separation of proteins on the basis of their size. Separation is effected via electrophoresis of the analytes through a suitable polymer that acts as a molecular sieve. Capillary gel electrophoresis (CGE) employs an identical separation mechanism. The use of a capillary is advantageous since higher electrical fields can be applied without resulting in Joule heating, detection can be performed on-capillary and high-throughput automation is possible. Additionally, the capacity to mimic the preparative separations available with slab electrophoresis is possible to a certain extent via the use of wide-bore capillaries.

Capillaries filled with linear or cross-linked polyacrylamide gels are often used to effect separations. The buffer pH should be selected such that the analytes are ionised. Mixed TRIS/borate and TRIS/phosphate buffers at pH 8.6 are typical examples. Denaturing solubilising additives such as urea may also be added. Sample injection is typically accomplished via electrokinetic loading as the gel exerts too much resistance for hydrodynamic techniques.

1.8.4. MICELLAR ELECTROKINETIC CHROMATOGRAPHY.

Terabe and co-workers[141-143] developed electrophoretic separations of uncharged analytes using a chromatographic-like partitioning process employing charged micelles as a pseudo-stationary phase. This mode of CE developed rapidly and is now universally referred to as *micellar electrokinetic chromatography* (MEKC or MECC)[144, 145]. MEKC has many similarities to HPLC[146] that will become apparent in subsequent sections.

1.8.4.1 Theoretical aspects.

Essentially, a surfactant is added to the separation buffer at a level exceeding the critical micelle concentration (CMC). Aggregation of surfactant molecules results in orientation of the hydrocarbon chains towards the centre of the structure forming a hydrophobic core whilst the hydrophilic groups point out into the aqueous medium. Uncharged analytes form distribution equilibrium between the aqueous and micellar phases and hence may be separated via differences in their partition coefficients. Elution order in MEKC is generally related to hydrophobicity with strongly hydrophobic species being solubilised (i.e. retained) to a greater extent by the micelles than hydrophilic compounds. The latter was confirmed by Yang *et al.*[147] using linear solvation energy relationships (LSER).

Micelles are generally charged and will migrate either with or against the EOF upon the application of a high voltage across the capillary. Anionic micelles such as those formed by sodium dodecyl sulphate (SDS) migrate against the EOF. The magnitude of the EOF velocity, μ_{EOF} is generally greater than the electrophoretic mobility of the anionic micelles, $\mu_{Micelle}$ at neutral and basic pH. Hence, the micellar phase will migrate in the same direction as the EOF but at a lower net velocity (i.e. $\nu_{EOF} > \nu_{Micelle}$). A neutral analyte distributed between the aqueous and micellar phases will therefore migrate at a velocity between ν_{EOF} and $\nu_{Micelle}$ (i.e. $\nu_{EOF} > \nu_{Analyte} > \nu_{Micelle}$). The migration times of uncharged analytes are therefore limited between the migration time of the EOF and the micelles. This finite elution range is termed either the time window or elution range.

The retention or capacity factor, k' is defined as the ratio of analyte molecules incorporated within the micelles to the number of analyte molecules in the aqueous phase. This is analogous to the classical LC equation involving partitioning between a mobile and stationary phase. In MEKC k' may be determined experimentally using equation 1.28[142]

$$k' = \frac{t_r - t_o}{t_o(1-t_r/t_{mc})} \qquad \textit{Equation 1.28}$$

Where:

t_r is the migration time of the analyte

t_o is the migration time of the EOF (capillary dead time).

t_{mc} is the migration time of the micelle.

The EOF is determined via injection of a marker compound. Methanol has been widely employed since it is poorly incorporated into the micellar phase and is easily detected using UV/VIS absorbance as a baseline disturbance caused by a change in refractive index. Other materials such as acetone and formamide have also been used. The migration time of the micellar phase is obtained via injection of a material that is assumed to be totally solubilised. Lipophilic azo dyes such as Sudan III are often employed.

The size of the time window restricts the peak capacity (maximum number of resolved peaks) and hence the separation of complex samples. Any means by which the time window may be enlarged will clearly yield an increase in the number of resolvable peaks. The actual micellar velocity, v_{mc} is the sum of the micelle velocity and the opposing EOF. Hence manipulation of either the electrophoretic velocity of the micelle or the EOF velocity will alter the magnitude of the time window. Small values of t_o/t_{mc} yield wide migration time windows and hence improved resolution. Expansion of the time window via a reduction in the value of t_o/t_{mc} is easily accomplished via decreasing the EOF velocity.

1.8.4.2. Resolution.

Resolution in MEKC is given by equation 1.29[142].

$$R_s = \frac{\sqrt{N}}{4} \frac{\alpha - 1}{\alpha} \frac{k'_2}{1 + k'_2} \frac{1 - (t_o/t_{mc})}{1 + (t_o/t_{mc})\, k'_1} \qquad \textit{Equation 1.29}$$

Where:

N is the column efficiency (number of theoretical plates).

α is the selectivity factor of two adjacent analyte bands.

k' is the capacity factor.

Equation 1.29 is identical to the classical LC equation apart from the t_o/ t_{mc} term. This is a consequence of the previously discussed limited elution range caused by the movement of the micellar phase. Note that when t_{mc} approaches ∞ where the micelles are a true stationary phase equation 1.29 does reduce to the classical LC equation. It should be stressed that equation 1.29 is only valid for neutral (uncharged) analytes. Charged analytes may also interact with the micelles via electrostatic interactions. Equation 1.29 predicts that resolution may be improved via manipulation of n, α, k' or extending the time window.

1.8.4.3. Choice of micelle forming surfactant.

The micelle is analogous to the stationary phase in HPLC and the aqueous buffer to the mobile phase. Therefore, these two parameters may be adjusted to manipulate selectivity. Use of a different surfactant in MEKC is analogous to changing stationary phase in a HPLC separation. Temperature also influences selectivity in MEKC separations.

The micellar phase must be ionic although non-ionic surfactants have been employed in mixed micelle systems (section 1.8.4.3.6). Additionally, the Kraft point of the surfactant must be considered. The Kraft point is the temperature below which the surfactant solubility is lower than the CMC. An extensive review of micelle forming surfactants in MEKC is given in reference[148]

1.8.4.3.1. Anionic surfactants.

Anionic surfactants, particularly sodium dodecyl sulphate (SDS) have been most frequently employed to effect MEKC separations. Hydrophobic chain length has been shown to have little effect on selectivity [142] suggesting that the choice of alkyl group should be relatively unimportant. However, certain limitations exist in practice.

The relatively high CMC values associated with shorter alkyl chain surfactants limits their application in MEKC. The high concentrations required yield excessive currents leading to joule heating effects. However, sodium decyl sulphate (STS) micelles display large electrophoretic mobilities and have been investigated as a potential means of enhancing the elution range in MEKC[149]. Although a significantly improved elution range was achieved compared to SDS migration time reproducibility and peak asymmetry were found to be extremely poor.

Surfactants with a hydrophobic chain greater than C_{14} are seldom employed in MEKC due to their high Kraft points. The dodecyl group is therefore the most widely used surfactant in MEKC. Ahuja and Foley[150] compared lithium, potassium and sodium dodecyl sulphate (LDS, KDS and SDS respectively) to determine the effect of the counter ion on the resulting MEKC separation. The KDS micelles gave the largest elution range followed by SDS and then LDS. However, a minimum of 15% v/v acetonitrile was required to solubilise the KDS monomers due to the high Kraft point of this surfactant.

1.8.4.3.2. Cationic surfactants.

Cationic surfactants are electrostatically adsorbed onto the inner wall of the separation capillary yielding a net positive charge and a reversed EOF[151]. Under these conditions the electrode polarity of the instrument must be reversed in order to detect the analyte. Cetyltrimethylammonium bromide (CTAB) is the most widely employed cationic surfactant in MEKC. Different selectivity was reported for a series of 22 charged and neutral phenylthiohydantoin-amino acids using dodecyltrimethylammonium bromide (DTAB) and SDS [143].

1.8.4.3.3. Macromolecular surfactants.

High molecular mass surfactants often termed micelle polymers have been employed as pseudostationary phases in MEKC. The CMC of such materials is zero and hence the structure and concentration is unaffected by changes in separation conditions. They may also be employed in the presence of relatively high concentrations of organic modifiers.

Poly(sodium 10-undecylenate) was the first micelle polymer to be employed as a pseudostationary phase in MEKC[152]. Separation selectivity was reported to be significantly different to SDS. However, the migration times and retention factors of test compounds were observed to increase during replicate separations.

Butylacrylate/butyl methacrylate/methacrylic acid (BBMA) copolymer showed similar separation selectivity as SDS for benzene derivatives[153]. However, separation selectivity for napthalene derivatives was different for these two surfactants. The molecular weight distribution of BBMA did not cause significant band broadening.

Yang *et al.*[154] employed a poly(methylmethacrylate/ethyl acrylate/methacrylic acid) block copolymer as pseudostationary phase. Structural integrity was maintained even at a methanol concentration of 70% v/v.

1.8.4.3.4. Bile salts.

Bile salts such as sodium cholate (SC) are a group of naturally occurring steroidal anionic surfactants isolated from biological sources. Their structure is based on a hydroxyl-substituted steroidal backbone. It is believed that they form helical aggregates exhibiting a reverse formation where the hydrophobic portions face the aqueous solution whereas the hydrophilic portions face inwards. This unique conformation tolerates high concentrations of organic solvent modifiers without loss of efficiency or significantly increased separation time.

Bile salts are more polar than SDS thus reducing k' [155, 156]. Hence they have found use in the separation of highly hydrophobic analytes that cannot be resolved using SDS[157]. They are also naturally chiral and have been used to effect enantiomeric separations[158, 159].

1.8.4.3.5. Chiral surfactants.

Enantiomeric resolution of derivatised amino acids has been reported using mixed micelles comprising SDS and the non-ionic surfactant digitonin[160] and SDS with sodium N-dodecanoyl-L-valinate, urea and methanol[161]. A novel surfactant with a chiral head group, N-dodecoxycarbonylvaline was employed to effect enantiomeric separations of 20 basic pharmaceutical compounds[162].

1.8.4.3.6. Mixed surfactants.

The two most popular systems are mixtures of bile salts with SDS and the combination of ionic and non-ionic surfactants. As previously stated, bile salts form micelles with a reverse geometry. The use of bile salt surfactants in combination with SDS therefore results in a pseudo-stationary phase involving micelles with both hydrophobic and hydrophilic outer surfaces. It has been demonstrated[163] that SDS/sodium cholate mixed micelles exhibit only one type of complex micelle. Issaq *et al.*[163] reported that the migration time window was 50% larger in 50:50 SDS/SC compared to 100% SC and 15% larger than in 100% SDS.

This mixed micellar phase is particularly effective for the separation of highly hydrophobic analytes such as corticosteroids[164, 165]. It has been shown[164] that sodium cholate competes with corticosteroids for the SDS micelles. This explains the lower solubilising ability of the mixed system compared to SDS.

Clothier and co-workers[159] compared the chiral resolving abilities of four different bile salts alone and in combination with polyoxyethylene-4-dodecyl ether (C_{12} E_4). Addition of C_{12} E_4 with or without methanol to solutions of sodium cholate and sodium deoxcholate enhanced the chiral resolution of analytes where the chiral centre was separated from major functional groups by a longer alkyl chain. The pure bile salt solutions generally provided improved chiral resolution where the major functional groups were closer to the chiral centre.

Addition of Tween 20 to an SDS-based pseudostationary phase has been shown to improve the separation of hydrophobic cations[166]. The Tween 20 was found to weaken the ionic interactions between the analyte cations and SDS. Adrenaline and its six precursors were fully resolved using this mixed micellar system. Ahuja and co-workers[167] demonstrated that the elution range could be significantly expanded using a non-ionic/anionic system comprising Brij 35 and SDS.

1.8.4.3.7. Other pseudo-stationary phases.

Starburst dendrimers (SBDs)[166] are synthetic polymers with well-defined branched structures and highly specific molecular masses. Unlike ionic surfactants they are stable in buffers containing high concentrations of organic modifiers and can be synthesised to impart unique selectivity. A dodecyl-modified SBD provided similar selectivity to SDS and was capable of resolving the 16 EPA priority PAHs[166]. Greve and co-workers[169] employed zwitterionic surfactants in the separation of closely related peptides via hydrophobic selectivity.

1.8.4.4. Efficiency.

The efficiencies that are achievable with MEKC are superior to HPLC. The main contributions to band broadening in MEKC are molecular diffusion of the analyte, the kinetics of the partitioning process and the heterogeneity of the micelle. The latter two effects are only significant for highly hydrophobic analytes with high capacity factors. With the obvious constraint of Joule heating, the higher the applied voltage, the higher the efficiency.

Terabe[142] demonstrated that the capacity factor increases linearly with surfactant concentration. Hence, k' may be manipulated by altering the surfactant concentration. This procedure essentially involves altering the phase ratio, a process that is extremely limited in HPLC. It must be stressed that increased concentrations of charged surfactants yield high currents and possible Joule heating effects. Surfactant concentrations used in MEKC are typically in the order of 20-100 mM.

1.8.4.5 Addition of aqueous phase modifiers.

1.8.4.5.1. Organic modifiers.

Organic modifiers are routinely employed in MEKC to extend the time window and enhance resolution via a reduction in the EOF velocity. Balchunas and Sepaniak[170] reported that significant loss of efficiency was only observed at higher concentrations of propan-2-ol. However, μ_{EOF} and $\mu_{Micelle.}$ were found to decrease with increasing organic modifier concentration leading to excessive analysis times. Aggregation of surfactant molecules to form micelles is restricted or prevented at high concentrations of organic solvents as a consequence of increased CMC values

Dimethylsulphoxide (DMSO) and acetone have been employed as organic modifiers for SDS-based MEKC[171]. Separation of 8 PAHs was achieved at a DMSO concentration of 50% v/v whereas 13 PAHs were resolved using acetone as a modifier. A detection wavelength of 200nm was employed since acetone has a strong UV absorbance over conventional wavelengths such as 254 nm.

Van Hove and co-workers[172] investigated a series of linear chain alcohols (C_1-C_{12}). Highly polar, short alkyl chain alcohols were found to increase migration times and the magnitude of t_{mc}/t_o. The hydrophobic chain length of the alcohol was found to have a pronounced effect on these increases. At a concentration of 1M modifier propanol and methanol produced t_{MC}/t_o increases of 257% and 12% respectively. Intermediate (C_4-C_6) alcohols initially increased migration times and t_{MC}/t_o to a maximum value before causing a decrease at higher concentrations. The authors attributed this effect to incorporation of the modifier into the micelles resulting in a reduction in their electrophoretic mobility and hence t_{mc}. Longer chain alcohols (C_7-C_{12}) were found to have limited scope as modifiers due to their limited solubility.

1,2 Hexanediol has been shown[173] to improve resolution at concentrations as low as 20 mM. Trends in the retention of test analytes were observed in that analytes capable of forming H-bonds and those that could not exhibited reduced and increased k' respectively upon the addition of the modifier.

Many organic modifiers can cause a gradual decrease in migration times over a series of replicate injection. This is a consequence of the modifier slowly absorbing onto the inner capillary wall altering the zeta potential and hence EOF. However, migration time repeatability was not affected in this fashion when 1,2 hexanol was employed in SDS systems.

1.8.4.5.2. Solvent programming.

Balchunas and Sepaniak[170] were the first workers to explore the possibilities of gradient elution in MEKC. Step-wise gradients were effected by pipetting aliquots of a gradient solvent containing propan-2-ol into the inlet vial at regular intervals. The applied voltage was increased during the separation to partially compensate for reductions in the electroosmotic velocity caused by the increased mole fractions of the modifier. Adding Triton-X-100 to the buffer to effect a similar reduction in the electrophoretic velocity of the micelles also offset reductions in EOF. A gradient MEKC separation of derivatised amines using a home-built instrument was shown to be reproducible (t_m RSD < 2% for n = 5) but required a 25 minute re-equilibration with the initial mobile phase between analyses.

Butehorn and Pyell[174] effected gradient MEKC separations on commercially available instrumentation. Stepwise alteration of the buffer composition was achieved by changing the inlet and outlet vials during the separation. Direct transfer of the method of Balchunas and Sepaniak[170] involving addition of aliquots of a 2-propanol-containing solvent to the inlet vial at predetermined times resulted in an extremely poor separation exhibiting excessive band broadening and poor efficiency. Disappointing results were also obtained in a subsequent gradient separation involving several vial changes during the separation. The authors proposed that the loss of efficiency encountered in their experiments was a consequence of a border zone between the two buffers employed that displayed an irregular flow profile.

1.8.4.5.3. Cyclodextrins.

Cyclodextrin-modified micellar electrokinetic chromatography (CD-MEKC) employs unmodified CDs as additives to alter selectivity. CDs hardly associate with the micellar phase and migrate at the same velocity as the EOF. Their central core provides an alternative hydrophobic environment for analytes with high capacity factors that are totally solubilised by the micelles. Differential analyte migration and chiral separation are therefore the result of differential inclusion complex formation between the CD and the individual analytes[175-177].

Incorporation of ionic groups into the structure of CDs allows them to become charged and possess electrophoretic mobilities. CDs modified in this fashion have been employed as pseudostationary phases in place of micelles in a technique termed cyclodextrin electrokinetic chromatography (CD-EKC)[178]. Any analyte that is included within the cavity of a modified CD will have a different overall charge due to the modified ionic group on the CD and also a modified electrophoretic mobility.

1.8.4.5.4. Urea.

The log k' values for aromatic compounds, corticosteroids and alkyl p-hydroxybenzoates have been shown to decrease linearly with increasing urea concentration[179]. The observed current was also found to decrease in a similar fashion. Selectivity was found to be extremely sensitive to urea concentration in the separation of 23 PTH-amino acids.

1.8.4.6. Effect of pH.

The nature and concentration of the buffer solution generally do not influence the selectivity of a MEKC separation. However, the pH of the buffer may be used to alter the selectivity of ionic analytes. Buffer pH also alters the EOF velocity that in turn affects the magnitude of the migration time window[180].

1.8.4.7. Effect of temperature.

Temperature control is a significant factor in MEKC since it affects both the distribution co-efficient and analyte mobilities[181]. An increase in temperature leads to decreased buffer viscosity resulting in an increase in both υ_{EOF} and υ_{MC}. Temperature may also be critical in terms of the Kraft point. Balchunas and Sepaniak[170] observed peak sharpening for some analytes when the separation temperature was raised from 28 to 39°C. Temperature programming analogous to GC has been employed to effect MEKC separations[182].

1.8.4.8. Detection.

Again, UV absorbance is the most widely employed detection method in MEKC separations. The direct coupling of MEKC with MS can be problematic due to detrimental effects caused by the non-volatile surfactants in the buffers employed. Various approaches for coupling of MEKC with MS were reviewed byYang and Lee[183].

1.8.4.9. SELECTED APPLICATIONS

1.8.4.9.1. PHARMACEUTICALS AND DRUG ANALYSIS.

MEKC has found wide application in drug analysis. Nishi and Terabe[184] reviewed applications such as closely related peptides, drugs in biological samples and complex drug mixtures. In a separate paper the same authors also reviewed pharmaceutical applications of MEKC[1185].

MEKC has been demonstrated to be a viable alternative to HPLC for purity determination of drugs. Reliable assays for the quantification of cephalosporin antibiotics, xanthines and benzodiazepines have been reported[186].

Altria and McLean[187] developed a generic MEKC separation applicable to a wide range of active and excipient materials in pharmaceutical manufacturing environments.

1.8.4.9.2. ENVIRONMENTAL.

Representative example separations include PAHs[188], nitrated-PAHs[144], aromatic sulphonates from industrial processes[189], fungicides[190], carbamate pesticides[191] and various herbicides[192].

1.8.5. CAPILLARY ELECTROCHROMATOGRAPHY.

Capillary electrochromatography (CEC) is a hybrid separation technique combining the high separation efficiency of CE with HPLC[193-195]. CEC employs EOF rather than hydraulic pressure to propel the mobile phase. Separation is based on differential interactions of the analytes between the stationary and mobile phase for neutral (uncharged) species as with HPLC. Electrophoretic separation also occurs under conditions where analytes are charged.

Since there is minimal backpressure it is possible to employ small diameter packings and effect extremely high efficiencies. Smith and Carter-Finch[196] have recently reviewed CEC.

1.8.5.1. Chromatographic band broadening.

The van Deemter equation[17] relates plate height to the average linear velocity of the mobile phase and three identified band broadening parameters termed A, B and C as shown in equation 1.30.

$$H = A + \frac{B}{U} + C_S.U + C_m.U \qquad \textit{Equation 1.30}$$

Where:

A, B and C terms are kinetic and thermodynamic processes which are explained in the following sections.

U is the average linear velocity of the mobile phase that is given by equation 1.31.

$$U = \frac{L}{t_o} \qquad \textit{Equation 1.31}$$

Where:

L is the column length.

t_o is the retention time of an unretained marker compound from which the column dead volume may be determined

A Term: Multiple flow paths (eddy diffusion).

Band broadening occurs as result of analyte molecules travelling different distances through a unit length of column. This is a consequence of the multiple flow paths that they may follow through the irregularly packed bed. The particles of packing material which make up the packed bed may also produce turbulence or eddy currents causing dispersion via mixing processes. The A term is a function of the size of the packing particles and the homogeneity of the packed bed as shown in equation 1.32.

$$A = \lambda d_p \qquad \textit{Equation 1.32}$$

Where:

λ is a geometrical packing factor that increases with decreasing particle size.

d_p is the particle size of the packing material.

The quoted particle diameter for any HPLC packing is the mean value of a size distribution. Most HPLC packing materials have a Gaussian type particle size distribution where the position of the maximum corresponds to the mean particle diameter and the standard deviation represents the distribution width. It is clear from equation 1.32 that small particles with a narrow size range that are uniformly packed will yield the most efficient columns. Note that the A term is independent of the mobile phase.

B term: Longitudinal diffusion.

The B term refers to the natural diffusion of analyte molecules from the concentrated band centre to more dilute regions along length of column, that is parallel to the mobile phase flow. Longitudinal diffusion is proportional to the time an analyte spends in the column and hence is inversely proportional to the mobile phase velocity. The B term is also a dependant on the diffusion coefficient of the analyte in the mobile phase as shown in equation 1.33.

$$B = 2\gamma D \qquad \textit{Equation 1.33}$$

Where:

γ is a hindrance factor based on the characteristics of the packed bed.

D is the diffusion coefficient of the analyte in the mobile phase

The B term may be largely ignored in liquid chromatography due to the low rates of diffusion in liquids.

C terms: Resistance to mass transfer.

The two C terms refer to the finite time taken for mass transfer between the mobile and stationary phases. The transport of analyte molecules between the two phases to attain the equilibrium defined by the distribution ratio is a continuous process during elution.

The C_s term refers to diffusion in the stationary phase. These effects can be largely ignored for solid phases since analyte transfer on and off of the surface is rapid. For liquid phases C_s is directly related to the stationary film thickness and the diffusion coefficient of the analyte in the stationary phase as shown in equation 1.34.

$$C_S = \frac{d_f}{D_S} \qquad \textit{Equation 1.34}$$

Where:

d_f is the film thickness of the stationary phase.

D_s is the diffusion coefficient of the analyte in the stationary phase.

The C_m term describes diffusion of analyte molecules through the mobile phase to the stationary phase. This is dependent on both the size of the packing particles and the diffusion coefficient of the analyte in the stationary phase as shown in equation 1.35.

$$C_m = \frac{d_p}{D_m} \qquad \textit{Equation 1.35}$$

Where:

d_p is the size of the packing particles.

D_m is the diffusion coefficient of the analyte in the stationary phase.

Equation 1.35 demonstrates that efficiency increases with decreasing particle size. However, a limiting factor associated with the use of small particles in HPLC is the increased pressure drop across the column.

1.8.5.2. Theoretical aspects of CEC.

Several authors [194, 195, 197, 198] have extensively discussed the theoretical aspects of the technique and hence only a brief overview of the method is presented.

The markedly different flow profile and enhanced efficiencies obtained when solvent was electrically driven through a packed bed was first observed in 1974[199]. The rapid development of CEC during the last decade owes a great deal to a series of papers published by Knox and co-workers[200-204] that laid the foundations of the current technique.

The linear mean EOF velocity in CEC is given by equation 1.36 that is termed the Helmholtz-Smoluchowski equation.

$$\nu_{EOF} = \frac{\varepsilon o\, \varepsilon r\, \zeta\, E}{\eta} \qquad \textit{Equation 1.36}$$

The average linear velocity in pressure-driven flow is given by equation 1.37.

$$U = \frac{d_p^2\, \Delta P}{\phi \eta L} \qquad \textit{Equation 1.37}$$

Comparison of equations 1.36 and 1.37 demonstrates that the mean linear flow using EOF as a driving force differs from pressure-driven systems in that it is independent of the size of the packing material particles. Additionally, Jorgenson and Lukacs[205] suggested that the EOF should not be affected by any irregularities in the packed section.

In CEC both the silica-based packing material and the wall of the fused silica capillary are capable of supporting EOF. Most workers agree that the main contribution to the generated EOF is from the particles since it has a far greater surface area compared to the inner wall of the capillary.

The significance of capillary diameter, d in relation to double layer overlap has already been discussed for CE (section 1.42). The pore size of the support material is typically around 8-10nm. Hence, EOF will only be generated around the particles since overlap would occur within the pores. In CEC the capillary diameter is therefore replaced by the average diameter of the channels between the particles. The average inter-particle distance has been estimated to be around $^1/_4$ -$^1/_5$ of the particle diameter[200].

Knox and Grant[200] determined that particle sizes as small as 0.4 μm could be employed in CEC without adversely affecting the EOF velocity. Efficient packing of such small particles significantly reduces the A term of the van Deemter equation. This discussion does not apply to porous particles which have been shown capable of supporting through-particle (or perfusive) EOF[206].

1.8.5.3. Development of separations.

The thickness of the double layer and hence ζ are affected by the concentration of electrolyte in the mobile phase. EOF therefore increases as the electrolyte concentration is reduced[202, 207].

Various authors [197, 208, 209] have experimentally confirmed the theoretical prediction that EOF increases linearly with applied voltage. However, non-linear plots of EOF Vs applied voltage have also been reported which were attributed to Joule heating effects[210, 211]. Joule heating in CEC columns results in the formation of bubbles (section 1.8.5.6.2) within the packed bed that affects the current and usually results in breakdown of the EOF. Knox[212] discussed heating effects in electrically-driven separations.

It is generally agreed that EOF increases as the level of organic solvent in the mobile phase increases [209, 213-215]. However, evidence to the contrary has also been reported where the EOF was found to decrease as the concentration of acetonitrile was increased[210, 211]. It has been proposed[195] that these discrepancies may be the result of some workers employing thiourea as an EOF marker. The latter has been shown to be retained under high concentrations of acetonitrile[214]. Kitagawa and Tsuda[216] observed that both electrophoretic and electroosmotic flow velocities remained almost constant between 30-90% v/v methanol in the buffer and then increased above 90% v/v.

The pH of the mobile phase directly affects the EOF via the degree to which the surface silanol groups of the packing particles and capillary wall are ionised[209, 216]. Kitagawa and Tsuda[217] developed an equation relating pH to EOF in ODS columns that could be used to estimate the dissociation constant for unreacted silanol groups.

The length of the injection zone has also been shown to have a large effect on efficiency[213, 218]. Van den Bosch and co-workers[213] reported that this effect decreased with increasing k'.

1.8.5.4. Stationary phases employed in CEC.

1.8.5.4.1. ODS.

The majority of reported applications have employed non-end capped ODS phases ranging from 1.5 to 10μm diameter. Cikalo *et al.*[198] demonstrated the inherent differences between commercially available ODS by comparing published data concerning separation of PAHs using different 3 μm phases.

Zimina and co-workers[219] attempted to correlate the electroosmotic mobilities generated by a series of commercial ODS phases to the surface area, carbon load and free silanol activity of each material. No apparent correlation was established between either the free silanol activity or carbon load of packing and the magnitude of the EOF that it generated. Correlation of surface area to generated EOF was found to be problematic due to uncertainty regarding published data. The highest mobilities were generated by Nucleosil 5 C18 and LiChrospher RP-18. However, these phases were unstable under the test conditions used and chromatography degraded after only 2-10 days. The two highly base-deactivated phases (Partisil ODS 3 and Purospher RP-18) were incapable of generating EOF as expected. Low to moderate EOF was generated by Spherisorb S5 ODS2, Zorbax BP-ODS and Hypersil ODS. All mobilities compared favourably with values determined from data published in the literature for identical or similar packing materials.

1.8.5.4.2. Cationic exchange materials.

The first phases specifically manufactured for CEC involved propylsulphonic acid bonded onto new 3μm silica. Separation of basic pharmaceuticals with this cationic exchange phase resulted in unprecedented efficiencies in excess of 40 x 10^6 plates/m[220]. The latter observation was confirmed by Euerby and co-workers[221].

Unusually high efficiencies have also been reported under reversed phase conditions using a standard ODS phase[222, 223]. An explanation was proposed[223] in terms of non-equilibrium conditions due to pulses of weaker or stronger solvent associated with the sample.

1.8.5.4.3. Physical mixtures of phases.

Djordjevic and co-workers[224] demonstrated that blends of bare silica and ODS reduced the retention of neutral compounds resulting in shortened separation time. Meanwhile, Yang and El Rassi[225] prepared capillaries consisting of two segments. The first was packed with ODS and served as the separation segment. The second was packed with bare silica to act as an EOF accelerator.

Impressive separations of highly polar compounds and acidic, neutral and basic species in a single run have been effected using physical mixtures of SCX and ODS phases[226]. The mixed phase was shown to perform reproducibly over wide ranges of pH and organic modifier concentration.

1.8.5.4.4. Other phases.

Other notable materials employed as stationary phases in CEC include cellulose acetate fibres[227], wide pore aminopropyl silica gel coated with helically chiral poly diphenyl-2-pyridylmethyl methacrylate[228] and vancomycin coated silica gel[229]. A polymerically bonded C30 phase has been employed to separate carotenoid isomers[230].

1.8.5.5. Fabrication of columns for CEC.

The columns that have been employed to effect CEC separations can be divided into two distinct categories namely packed and open-tubular.

1.8.5.5.1. Open-tubular columns.

In open-tubular (OT) columns the stationary phase is attached to the inner walls of the capillary[231]. Tsuda *et al.*[232] fabricated OT columns by drawing large bore soda-lime capillaries and attaching an ODS stationary phase to the inner wall using a chemical reaction. Pesek and Matyska[231] used a chemical etching procedure to increase the inner surface area available for coating with 1-octadecane stationary phase. The hydrosilation reaction employed to effect the surface modification was reported to produce extremely stable phases.

1.8.5.5.2. Packed capillaries.

Some important considerations in the fabrication of packed capillaries were summarised by Boughtflower and co-workers[3]. The majority of reported work has involved production of capillaries using a high-pressure pump to pack slurries of stationary phase and a suitable organic solvent. Essentially, a slurry of the stationary phase and a suitable solvent such as acetone is loaded into some form of packing reservoir. An empty HPLC guard column complete with fittings to attach the fused silica capillary is typically employed. Many workers have immersed the packing reservoir into an ultrasonic bath in an attempt to maintain homogenous packing slurry within the reservoir. Boughtflower *et al.*[233] reported a novel pressurised ultrasound device designed for this purpose.

An alternative strategy to avoid clogging of the slurry during packing has been proposed involving a simple gravity-feed procedure[234]. Briefly, a slurry of C18 ODS packing material in acetone was delivered into a 50 μm I.D capillary by sedimentation. Under these conditions a 20-30 cm section could be packed in around 12 hours. Columns were subsequently pressurised to compress the bed prior to electrochromatographic evaluation.

Frame *et al.*[222] described a simple method of column fabrication that could be applied in any laboratory regardless of resources. Meanwhile, Mayer and co-workers[235] reported a fritless design that utilised the electrophoretic attraction of the packing particles towards the anode. Columns packed with 1.5 μm particles resulted in efficiencies in excess of 500000 plates/m. Softening of fused silica capillaries as a result of microcracks caused by the action of stationary phase particles during packing has been reported[236].

An alternative packing technique involves the in-situ formation of a polymeric network or monolithic stationary phase[237]. Schweitz and co-workers[238] prepared monolithic columns with pre-determined selectivity obtained through molecular imprinting. Chiral separations were presented using a stationary phase were prepared via molecular imprinting of propranolol and metoprolol.

The use of drawn capillaries[202] electrokinetic migration[239] and supercritical fluids[240] have also been reported whilst some procedures have been patented[241, 242]. Electrical measurements have been employed to give an indication of the flow permeability of open and packed CEC capillaries[243].

1.8.5.5.3. Manufacture of frits.

The first stage in the fabrication of a CEC column is the manufacture of a restraining frit to pack the stationary phase against. The frit needs to be mechanically strong in order to withstand the pressures employed during the packing process. It also needs to exhibit good porosity to exhibit minimum flow resistance since variations in packing speed can yield loosely packed sections that can result in the formation of voids.

The majority of reported procedures have packed the bed against a frit prepared by sintering either the relevant stationary phase[206] or bare silica and water[234, 244], potassium silicate and formamide[244, 245] or native silica and an aqueous solution of potassium[244] or sodium[3, 202, 210, 218, 246] silicate. Other workers[197, 213, 219, 222] have packed against temporary frits constructed from microbore HPLC components. A permanent frit was subsequently formed using controlled heat when the bed was suitably packed. Fuchs and co-workers[247] melted fusible glass beads together using electrical sparking.

The initial retaining frit is usually replaced after packing along with a second frit at the outlet end of the packed section. A popular approach due to its reproducibility involves fusing small sections of the stationary phase using either a resistively heated element or a micro torch. Use of a Bunsen burner has been reported to result in pyrolysis of the alkyl chains bonded to the silica surface[248]. These sintering techniques rely on the formation of sodium polysilicate and hence are only suited to packing phases with a high sodium content. Sintering destroys small sections of the protective polyimide coating making columns more susceptible to breakage. Procedures have also been reported where replacement frits were prepared via sintering native silica that was packed into the column after the packing process[214].

1.8.5.6. Practical aspects.

1.8.5.6.1. Detection.

Windows for optical detection are fabricated in an identical fashion to CE. The majority of reported separations involved columns with a detection window located after the packed bed. However, detection through the packed section has also been reported but baselines tend to be noisier due to light scattering by the particles of packing material[41]. Additionally the dimensions of the unpacked pre-detection segment and the packed section may be tailored to afford optimum separation speed and selectivity[249].

Fluorescence[248] and laser-induced fluorescence detection (LIFD)[250] have been employed for separations involving PAHs. In the latter case limits of detection were 10^{-9}-10^{-10} M.

The low flow rates (< 1μL/min) associated with CEC are advantageous for hyphenation with MS since an electrospray source typically requires a liquid make-up flow in the order of 0.75-500 μL/min. The development and applications of this powerful analytical combination have recently been reviewed[251].

1.8.5.6.2. Bubble formation.

The main operating problem in CEC is the formation of bubbles within the column that cause breakdown of current and/or drying out of the packed section. Bubble formation was initially attributed to Joule heating effects caused by variations in factors controlling heat dissipation at frit interfaces[202]. However, it has been stated that Joule heating should not be an issue under typical operating conditions[201]. Rebscher and Pyell[252] reported that bubbles invariably formed at the frit interface between packed and unpacked sections of the column. It is now assumed that a change in the EOF that occurs at this interface results in liquid expansion and hence the formation of bubbles. It has been shown that bubble formation is a function of the length and nature of the frit[253].

Rathore and Horváth[254] investigated the discontinuity of electrochromatographic parameters such as flow velocity, conductivity and electrical field strength at the frit interface between open and packed sections of a capillary. The authors concluded that silica frits have zeta potentials that are significantly different to the bulk packing. This discontinuity was proposed to produce a flow equalising inter-segmental pressure resulting in bubble formation.

There have been many debates as to whether pressurisation of the system is necessary to prevent bubble formation. Many workers have recommended pressurisation although separations have been effected at ambient pressure[208, 213]. Not all commercially available CE systems are capable of pressurising both inlet and outlet vials although modification has been reported[196].

Other strategies have been adopted to address the issue of bubble formation. Many workers have moved towards using low conductivity (or biological) buffers such as MES and TRIS that may be employed at higher concentrations without causing such problems. Other reported solutions include use of open-tubular capillaries[231], re-coating of ODS onto the silica frit after formation using a solution of chlorodimethyloctadecylsilane[253], and addition of SDS (below CMC) to the buffer[255]. The latter was claimed to create a more uniform surface charge density and equalise local differences in the EOF.

1.8.5.6.3. Sample injection.

Sample injection in CEC is mainly effected using electrokinetic injection since hydrodynamic loading cannot overcome the backpressure of the packed column. However, hydrodynamic sample loading has been demonstrated to be comparable to electrokinetic injection using the "short end" geometry[256]. This was presumed to be a consequence of the reduced backpressure associated with the shorter packed section.

1.8.5.6.4. Gradient elution.

The first example of gradient elution in CEC involved a high voltage being superimposed onto a pressure-driven separation[257]. Application of a high voltage to an established microbore HPLC separation of eleven oligonucleotides was shown to significantly improve both resolution and column efficiency and to reduce the analysis time.

Huber and co-workers[258] employed two reciprocating pumps to deliver the desired gradient to the inlet of a CEC column in a modified commercially available CE instrument. Gradients formed in this manner were found to be reproducible with migration time reproducibility of less than 3% RSD (n=5). Extremely promising preliminary separations of both PTH-amino acids and steroid hormones were presented.

The first entirely electrically-driven gradient system was developed by Yan and co-workers [259]. Their computerised system automatically generated gradients by merging the electrically-driven flows from two mobile phase reservoirs using two independent high voltage sources. A test mixture of 16 PAHs were fully resolved in less than 90 minutes.

Euerby and co-workers[260] reported automated step-gradient separations performed on an unmodified commercially available instrument. Essentially, the applied voltage was removed at a pre-determined time during the separation whilst the initial buffer vials were replaced with the final mobile phase conditions whose composition comprised a higher organic modifier content. The voltage was then re-applied to complete the separation. The technique was demonstrated using six diuretic compounds displaying a wide range of polarities that could not be satisfactorily separated by isocratic elution.

Que and co-workers[261] have recently described an easily assembled gradient generator for CEC that allows reproducible stepwise or continuous gradients to be effected. Gradient elution has also been hyphenated with NMR[262]

1.8.5.7. Selected Applications.

1.8.5.7.1. Pharmaceuticals.

CEC and CEC-MS[263] have been evaluated in the pharmaceutical industry. Many workers have concentrated on optimising developed separations[221, 260, 264] whereas others have determined whether it can meet criteria specified by regulatory bodies for HPLC. For example in the assay of a neutral drug candidate mean values (n=11) for the active material by CEC and HPLC were 99.65% (2.23%) and 97.95% (1.22%RSD) respectively which were comparable to HPLC results[265].

The silanol groups that are the basis of the EOF in CEC are detrimental to the separation of basic compounds such as pharmaceuticals. Interaction between basic analytes and the surface silanol groups results in severe peak tailing and loss of efficiency. This problem may be overcome by adding a competing base to the mobile phase. Gillott and co-workers[266] effected the separation of strongly basic pharmaceutical compounds using low pH buffers containing triethylamine and triethanolamine. Simultaneous separation of acidic, neutral and basic compounds in a single run have been reported using this strategy[267]

CEC is typically performed at high pH in order to maximise EOF. However, anionic materials may migrate towards the anode under these conditions and will not be detected[221]. This problem may be overcome using the so-called *ion suppression* mode whereby a low pH buffer causes acidic analytes to be present in their protonated (neutral) form. Even at low pH materials such as Spherisorb ODS-1 are capable of generating sufficient EOF to effect rapid separation of acidic drugs[268].

1.8.5.7.2. Environmental

Many workers have employed PAHs as test mixtures for CEC to demonstrate the improvement in separation compared to HPLC and/or μHPLC. Two notable separations employed non-aqueous mobile phases without a background electrolyte[41, 42]. Whitaker and Sepaniak[41] employed plain acetonitrile containing no background electrolyte as a mobile phase for CEC. THF and methylene chloride were employed as mobile phase modifiers to manipulate k' and effect separations of PAHs.

1.8.5.7.3. Chiral separations.

The first chiral separations were effected using an α_1-acid glycoprotein stationary phase[269]. Separations were also reported by Wolf and co-workers[270] using (S)-Naproxin-derived and (3R,4S)-Whelk-O chiral stationary phases. Meanwhile, Lelièvre and co-workers[214] effected chiral separations using ODS with a cyclodextrin in the mobile phase whilst Li and Lloyd[269] employed a β-cyclodextrin stationary phase.

1.9. THE FUTURE OF ELECTROPHORETIC SEPARATIONS.

Electrically-driven separations form a versatile family of techniques covering a diverse area of applications. The numerous options available to manipulate selectivity make them particularly attractive and are a key selling point. However, CE may never become established to the extent of HPLC and GC and may have to settle with being regarded as a "niche" or complementary technique although it has started to be considered as a practical alternative to ion chromatography[271]. Issues involving detection, precision/quantitative analysis, reliability of CEC columns and so forth still need to be addressed. Unfortunately, instrument manufacturers seem reluctant to invest heavily in electrically-driven techniques.

Acceptance and growth within the pharmaceutical industry in particular is only likely to occur if numerous "real" applications can be validated and accepted by regulatory authorities[272]. There is still no Pharmacopeial monograph regarding CE Although elegant separations have been reported the "explosion" of CE within the industry that was predicted in the 1990s has not occurred and the recent rise in popularity of Near Infrared Spectrometry (NIRS) seems to have pushed it into semi-obscurity. However, enantioresolution of therapeutic compounds is likely to continue to be a popular area of interest due to its cost effectiveness relative to HPLC especially in drug discovery[273].

MS will presumably continue to become a routine detection technique. The use of stable isotope internal standards makes MS capable of quantifying analytes independent of CE migration times and may therefore help to improve the sometimes poorly perceived precision of quantitative CE. However, HPLC is still viewed by many as the most practical means of introducing samples to MS.

Fragility of CEC capillaries and particularly the weakness of retaining frits may lead to further research involving monolithic columns. Acceptance within the pharmaceutical industry is unlikely in the immediate future due to concerns regarding column to column repeatability.

Ending on a more positive note, the electrophoretic process is key to the further development of so-called "Lab on a chip" miniaturisation[274, 275] that is currently a popular area of research.

CHAPTER 2

MATERIALS AND METHODS.

2.1. INTRODUCTION.

This chapter details the recurring procedures and methods that were employed during the acquisition of data for this thesis. More detailed information regarding the procedures employed for specific investigations may be found in the relevant experimental chapters.

2.2. INSTRUMENTATION.

Two instruments were employed to acquire data for this thesis which are described in subsequent sections.

2.2.1. Thermo Unicam Crystal model 310.

The Crystal (Thermo-Unicam, Cambridge, UK) CE is a modular instrument that may be configured to suit requirements. The two main components are an automated sample injection system and a high voltage power supply (HPVS) which are shown in figure 2.1. The latter unit can supply up to 30 kV.

Figure 2.1 Thermo Unicam CE system: Automated sample injection system (left) and HPVS (right).

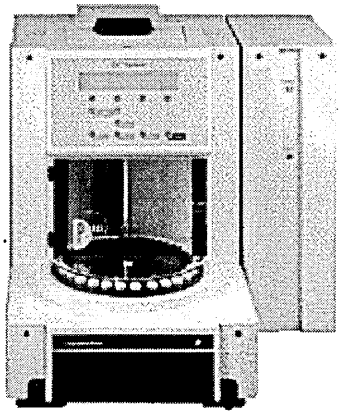

The cathode and associated inlet buffer reservoir (5ml) are incorporated within the sample injection module. The anode and associated outlet buffer vial (50ml) are attached to a remote platform upon which the UV detector is placed (not shown in figure 2.1). Replenishment of buffer could be performed automatically at the inlet side only by loading the sample carousel with several vials and changing the numbered location of the inlet vial several times within the programmed method. The outlet vial was generally removed during pre-injection rinse cycles involving sodium hydroxide and water that were allowed to flow to waste. This strategy ensured that the buffer composition (pH and ionic strength) was identical in both the inlet and outlet vials.

The separation capillary is initially threaded through the top of the autoinjector unit such that the inlet is level with the bottom of the cathode. The outlet half of the capillary is threaded through the cell of detector and into the outlet vial. The latter operation can be troublesome and resulted in a number of capillaries snapping at the detection window.

The instrumental design limited the practical minimum capillary size that could be employed. The minimum dimensions were restricted to L_d = 44 cm and L_t = 60 cm equating to a maximum field strength of 500 V/cm.

Temperature control was achieved via an in-built recycling airflow housed within the autoinjector module. A foam insulation tube was provided with the unit to cover the exposed section of capillary between the autosampler and detector. However, this was found to be inconvenient to use during routine use and hence was rarely employed.

Hydrodynamic and electrokinetic injection were shown to be equivalent in terms of repeatability (0.70% and 0.72%) during a simple study involving 10 replicate injections of a thiourea working standard. Hydrodynamic injection was the mode of choice in the majority of experimental work to avoid the possibility of any sample bias. However, electrokinetic injection was employed for all CEC work since hydrodynamic sample introduction could not overcome the pressure drop of the packed capillaries.

The model employed was a stand-alone unit requiring input from an in-built keypad. The absence of acquisition software necessitated the use of a chart recorder. All electropherograms were therefore plotted using a HP model 3395 integrator. Application of a separation voltage was found to give rise to a significant baseline disturbance. The integrator was therefore programmed to autozero 0.5 minutes into each separation. All electropherograms generated with this instrumentation that are included in this thesis were converted to bitmap images using commercially available scanners.

The system was modified in-house to allow semi-automatic operation. Essentially, the integrator was connected such that it was triggered upon the application of the separation voltage. In addition, an event was programmed into the integrator once the length of time required for a given separation was known. Combination of these two procedures gave rise to a pseudo-automated system that was particularly useful when acquiring analytical data over a series of replicate injections.

2.2.2. Beckman P/ACE 5150.

The Beckman (Fullerton, CA) P/ACE (Preparative/Analytical Capillary Electrophoresis) is a PC-driven instrument incorporating an in-built detector and Windows™ acquisition software as shown in figure 2.2.

Figure 2.2 Beckman P/ACE 5150 CE comprising autosampler and high voltage unit (grey box) and in-built detector (white box on top of autosampler). The former can supply up to 30 kV.

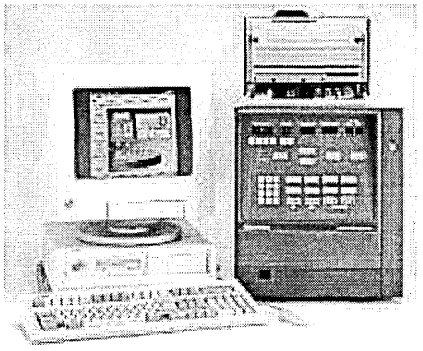

The system is fully automated and parameters (separations, current, diode array spectra) may be monitored in "real time". Electropherograms and associated diode array plots are produced as bitmap files. This allowed images to be conveniently inserted into this thesis. The acquisition software allows the user to design and generate reports involving the electropherogram and a summary of important parameters such as migration times and so forth.

Beckman CE systems employ cartridges to house and align the separation capillary. In addition, the cartridge forms part of the temperature control system. The design incorporates a pre-aligned aperture for optimum on-capillary absorbance detection. Circulation ports permit flow of a heat transfer fluid to ensure efficient temperature control. Care must be taken to ensure an airtight seal is formed when constructing the cartridge otherwise the highly UV absorbing fluid is prone to flooding the detection window. Fitting a capillary into a cartridge was found to be a rather fiddly and time-consuming task. However, once fitted, the capillary was less prone to breakage than the Thermo Unicam system and dedicated capillaries could be rapidly fitted and removed from the instrument. In addition, fewer restrictions exist regarding capillary dimensions, the minimum practical length being approximately 15cm. This permits the use of high field strengths with the obvious limitation of Joule heat effects.

The Beckman P/ACE 5150 autosampler comprises 2 sample carousels, one each for the inlet and outlet vials. Hence, automatic replenishment of the buffer in both the inlet and outlet vials was possible using a strategy similar to that previously discussed for the Thermo Unicam instrument. In addition, the outlet vial could be automatically replaced by a dedicated waste vial during pre-injection rinses thus avoiding the possibility of buffer contamination. The turntables were prone to becoming removed from their drive mechanism during long periods of usage. Rectification of this issue was straightforward but rather time consuming.

The model employed (Health and Safety Laboratory, Sheffield, UK) possessed an in-built diode array detector. This was found to be extremely useful during the development of methods. Briefly, the diode array spectrum of a given analyte peak could be recorded and stored within a library. Migration orders could then be determined during method development via comparison with the library. This strategy was far more convenient than spiking solutions and/or injection of individual compounds.

2.3 MATERIALS AND PROCEDURES.

All fused silica capillary was obtained from Composite Metal Services Ltd (Hallow, UK) and originally sourced from Polymicro Technologies (Phoenix, USA). Separation capillaries were prepared by carefully cutting off the appropriate length with a ceramic tile. Pre-conditioning was effected by flushing with sodium hydroxide (1.0 M, 2000 mbar) for 30 minutes. Residual sodium hydroxide was removed by flushing with water (2000 mbar) for 5 minutes. Detection windows were fabricated using either a disposable lighter or a frit burner obtained from Glaxo (Ware, UK). Subsequent treatment was application-specific and further details may be found in the appropriate experimental chapters.

The majority of reagents employed were obtained from Aldrich (Poole, UK). All materials were reagent grade or better unless otherwise stated. The majority of solvents were obtained from Fisher (Loughborough, UK). All solvents were HPLC grade.

Key practical differences exist between the two CE instruments that required careful consideration when transferring separations between the two units in order to yield equivalent conditions. The Beckman instrument employs flushing and sample loading pressures quoted in PSI whereas the Crystal system uses mbar. The relevant conversion factors are listed below in equation 2.1[276].

$$1\ \text{PSI} \equiv 68.95\ \text{mbar} \equiv 6894.76\ \text{pascal (S.I unit)} \qquad \textit{Equation 2.1}$$

Appropriate scaling of separation voltages was also performed to take into account the different capillary dimensions (L_d, L_t) involved and thus ensure equivalent field strengths.

All pH and pH* (non-aqueous media) measurements were undertaken using commercially available pH meters that were calibrated according to the manufacturers recommendations prior to use. Separation media were always fully prepared prior to the measurement of pH/pH* and performing required pH/pH* adjustments

2.4. DETERMINATION OF KEY SEPARATION PARAMETERS.

2.4.1. Electrophoretic mobilities.

The apparent mobilities of analyte compounds of interest were calculated using equation 1.11. These values were subsequently employed in equation 1.12 to determine associated electrophoretic mobilities.

2.4.2. Resolution between two adjacent bands.

Two strategies were employed which are explained in the following sections.

a) Determination of resolution between 2 discrete bands.

All relevant values were determined using equation 2.2.

$$R_s = \frac{2\,(t_{mb} - t_{ma})}{w_a + w_b} \qquad \textit{Equation 2.2.}$$

Where:

t_{ma} and t_{mb} are the migration times of the two bands (band b migrates behind band a).

W_a and W_b are the base widths of the two peaks.

b) Estimation of resolution using peak and valley measurements.

An alternative means[277] of determining a qualitative estimate resolution was employed in situations where bands overlapped. This strategy is based upon the heights of both bands and the valley between them as shown in figure 2.3.

Figure 2.3 Measurements required for estimation of resolution.

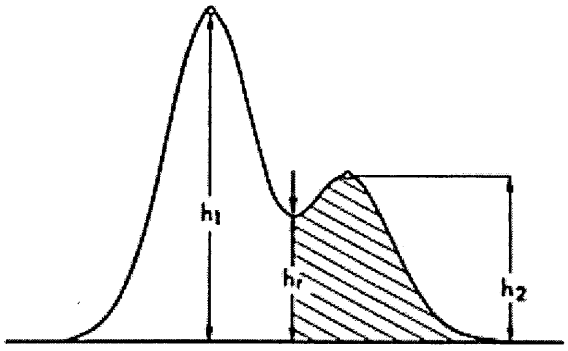

Essentially, the valley height is expressed as a percentage of the height of the smallest band (i.e. h_r/h_2 x 100 in the example shown in figure 2.4) . The ratio of the two band heights (h_1/h_2) is also determined and these values are used to determine an approximate resolution from the standard values in table 2.1[277].

Table 2.1 Estimation of resolution ($R_{estimated}$) from the height of the valley between 2 adjacent bands.

h_r as % of smallest band	1:1	2:1	4:1	8:1
10	1.22	1.26	1.30	-
20	1.07	1.13	1.17	1.31
30	0.97	1.05	1.10	1.22
40	0.89	0.99	1.05	1.13
50	0.83	0.92	1.01	1.07
60	0.78	0.86	0.96	1.01
70	0.74	0.82	0.91	0.96
80	0.70	0.77	0.86	0.92
90	0.66	0.74	0.82	0.89

This is a rather crude method but has been shown to be a useful indication of resolution during method development[278].

2.4.3. Peak efficiencies.

Efficiencies were calculated in terms of number of theoretical plates directly from electropherograms using peak widths and migration times. Peak widths were determined either at the base or at half height as indicated in equations 2.3 and 2.4 respectively.

$$N = 16 (t_m/w_{base})^2 \qquad \textit{Equation 2.3.}$$

$$N = 5.54 (t_m/w_{1/2})^2 \qquad \textit{Equation 2.4.}$$

Where:

t_m is the migration time of the appropriate peak.

w is the width of the appropriate peak (w_{base} signifies width at base, $w_{½}$ signifies width at half peak height).

Chapter 3.

INITIAL EVALUATION OF CE IN NON-AQUEOUS MEDIA.

3.1. INTRODUCTION.

The work discussed in this chapter concerns an evaluation of the practicalities of performing CE in non-aqueous solvents. Several workers[41, 42, 44] have investigated various pure and mixed solvents but did not discuss key parameters such as the repeatability of the generated EOF. It was anticipated that an understanding of the mechanisms involved in non-aqueous media would enhance the applicability of both CE and CEC.

3.2. EXPERIMENTAL PROCEDURES.

All separations were performed using the Crystal CE system. Separation capillaries comprised 60 cm lengths of 50 μm i.d. uncoated fused silica capillary. Unless otherwise stated, all on-capillary absorbance detection was performed at a wavelength of 254 nm at a distance of 44 cm from the inlet (L_d = 44 cm).

The separation capillary was equilibrated at the start of each working day and prior to changing separation media by flushing with sodium hydroxide (0.1 M, 2000 mbar) for 5 minutes. Residual sodium hydroxide was removed by flushing with water (2000 mbar) for 2 minutes. A two-stage equilibration was performed with the appropriate non-aqueous media which was first hydrodynamically pumped (2000 mbar) for 5 minutes and then electrically driven (20 kV) for 5 minutes. The capillary was rinsed using sodium hydroxide (0.1 M, 2000 mbar) for 5 minutes followed by water (2000 mbar) for 2 minutes at the end of each working day prior to careful storage. Unless stated otherwise, all separations were effected at an applied voltage of 20 kV (333 V/cm).

The capillary was rinsed with sodium hydroxide (0.1 M, 2000 mbar) for 0.5 minutes followed by water (2000 mbar) for 1.5 minutes and finally the relevant non-aqueous separation media (2000 mbar) for 2 minutes between replicate injections. Additionally, the first two electropherograms generated using each medium studied were not included in any statistical analysis. Microsoft Excel 97 (Microsoft Corporation, Redmond, USA) was employed to undertake comparisons of data using t-tests.

A thiourea stock standard solution (1mg/ml) was prepared in acetonitrile. Working standards (0.1mg/ml) were prepared as required via appropriate dilution of the stock solution with the media under investigation. The biphenyl working standard that was employed in the silver nitrate studies was prepared in an identical fashion.

All samples were hydrodynamically injected (25 mbar, 0.2 minutes). The magnitude of the EOF generated by each medium was determined via injection of the relevant marker standard. Unless stated otherwise, 10 replicate injections were performed under each set of separation conditions to assess the repeatability of the generated EOF.

The use of the phrase "pure" in relation to the solvents studied implies that the material was used as provided by the supplier without any form of pre-treatment.

3.3. INITIAL EVALUATION OF EOF IN PURE ORGANIC SOLVENTS.

3.3.1. Acetonitrile.

A simple trial investigation was undertaken using pure acetonitrile as the separation medium. Injection of the thiourea working standard gave rise to a sharp peak at a migration time of 1.229 minutes (0.60 cm/s, equating to an EOF of 0.00179 $cm^2 V^{-1} s^{-1}$). A second injection resulted in a peak with a migration time of 1.204 minutes (0.61 cm/s, equating to an EOF of 0.00182 $cm^2 V^{-1} s^{-1}$). Increasing the applied voltage to 30 kV resulted in thiourea eluting after 0.812 minutes (0.90 cm/s, equating to an EOF of 0.00180 $cm^2 V^{-1} s^{-1}$).

The data obtained agreed well with that of Lister and co-workers[42, 44] and Wright and Dorsey[60] who reported EOFs of 0.00199 and 0.000188 $cm^2\ V^{-1}\ s^{-1}$ respectively in plain acetonitrile. In comparison, separations performed within this laboratory using traditional media (10 mM sodium tetraborate, pH 9.2) typically generated an EOF typically in the order of 0.00070 $cm^2\ V^{-1}\ s^{-1}$.

Addition of methylene chloride (10% and 50% v/v) was shown to decrease the EOF (0.00149 $cm^2\ V^{-1}\ s^{-1}$ and 0.00087 $cm^2\ V^{-1}\ s^{-1}$ respectively) further confirming the observations of Whitaker and Sepaniak[41].

Arguably the most interesting observation was that no current was registered on the instrument during any of the investigations. This implied that the generated current was less than 0.1 μA since this is the minimum that the instrument could display. This was consistent with the observations of other workers who reported have currents of <100 nA[41] and 3.4 nA[44] in pure acetonitrile.

3.3.2. Methanol.

Migration times for duplicate injections of thiourea in methanol were 3.511 and 3.440 minutes. The EOF was obviously slower than in acetonitrile (0.00062 and 0.000640 $cm^2\ V^{-1}\ s^{-1}$ respectively) but was again in good agreement with the work of Lister *et al.*[42, 44] who reported an EOF of 0.000582 $cm^2\ V^{-1}\ s^{-1}$.

3.3.3. N-Methyl formamide.

An EOF of 0.000337 $cm^2\ V^{-1}\ s^{-1}$ was observed in N-Methyl formamide (NMF). A relatively high current of 5.4 μA registered on the instrument. This was also observed by Jansson and Roeraade[43] who attributed it to the presence of hydrolysis products and other impurities. Comparison of data with reported values is not straightforward since workers employing NMF in NACE experiments have typically added background electrolytes.

3.4. Assessment of initial findings.

These initial evaluations uncovered some fascinating concepts that initially inspired optimistic speculation regarding the potential applications of NACE. It appeared that a simple medium capable of supporting a fast and reproducible EOF without generating significant Joule heat had been uncovered. Additionally, it was apparently amenable to hydrophobic analytes and CE-MS.

Acetonitrile appeared to be the most promising solvent from these initial experiments. Although NMF exhibited a reasonable EOF, its strong absorbance over the useful analytical detection range was likely to limit subsequent applications. Methanol was also promising but tended to exhibit erratic migration time repeatability and required longer equilibration than acetonitrile.

3.5. Further studies in acetonitrile.

A more thorough study was subsequently undertaken to determine the characteristics of the EOF generated in pure acetonitrile. Replicate injections (n=10) of the thiourea working standard resulted in an average migration time of 2.316 minutes with a repeatability of 0.164 % RSD. The latter was in good agreement with the data of Wright *et al.*[42] who reported an RSD of <2% (n=25). However, the magnitude of the EOF was far lower than had been achieved in the initial experiments. No obvious explanation was immediately apparent. Subsequent experiments therefore focussed on areas that could explain this shift in magnitude.

3.5.1. Influence of water.

The acetonitrile employed to effect the previous separations was used directly from the bottle as supplied and was likely to contain a small percentage of water. It was anticipated that different batches of solvent were likely to exhibit a range of water contents. It was therefore reasonable to assume that a more consistent EOF would be achieved if the acetonitrile were dried prior to use.

Replicate injections (n=10) of the thiourea working standard were undertaken using dried acetonitrile (kindly undertaken by the organic research laboratory at this institution). A control investigation was performed immediately afterwards using acetonitrile taken directly from the same bottle as supplied. A comparison of the resulting data is presented in table 3.1.

Table 3.1. Comparison of EOF generated in dried acetonitrile and that which had not Undergone any form of pre-treatment (n=10).

	Average t_m (min)	Repeatability (% RSD)	EOF ($cm^2 V^{-1} s^{-1}$)
Dried	1.321	0.038	0.001665
Control	1.340	0.022	0.001642

The magnitude of the EOF generated in the dried solvent was more consistent with the initial observations and data reported in the literature[42, 44]. Comparison with the control study implied that no significant benefit would be obtained by drying acetonitrile prior for use in CE separations. This was consistent with reported work involving the effect of water in NACE media involving background electrolytes[53, 56]. However, this hypothesis was rejected at the 0.975 confidence interval (table 3.2).

Table 3.2. Evaluation of experimental data using the student t-test.

	No pre-treatment	*Dried*
Mean	1.3395	1.321
Variance	4.16111×10^{-5}	0.000124444
Observations	10	10
Pooled Variance	8.30278×10^{-5}	
Hypothesized Mean Difference	0	
df	18	
t Stat	4.540	
t Critical one-tail	2.101	

3.5.2. Addition of supporting electrolytes.

It was anticipated that the addition of a background electrolyte might help to stabilise the EOF and address the issues concerning day to day shifts in its magnitude. Unfortunately, the majority of typical CE electrolytes are insoluble in acetonitrile.

3.5.2.1. Ammonium acetate.

Preliminary investigations concerned the addition of ammonium acetate at a concentration of 1 mM. It was discovered that the added electrolyte could not be made to dissolve completely even when ultrasonication was employed. Addition of acetic acid was found to effect total dissolution with 5% v/v typically being required. However, on some occasions total dissolution could be achieved via the addition of less acid (1-2% v/v). The procedure was therefore standardised for all subsequent investigations. The method adopted was addition of 5% v/v acetic acid followed by ultrasonication for a period of 5 minutes.

The magnitude and repeatability of the EOF generated in acetonitrile containing 1 mM ammonium acetate and 5% v/v acetic acid was assessed by performing 10 replicate injections of the thiourea working standard.

As expected, the resulting EOF (0.000330 cm^2 V^{-1} s^{-1}) was slower than in pure acetonitrile. Additionally, migration time repeatability (0.99% RSD) was rather disappointing compared to some of the behaviour that had been observed in pure solvents.

Poor EOF repeatability suggested some issue with the inner capillary surface. It was possible that the capillary surface was not sufficiently equilibrated with non-aqueous media between replicate injections. Hence, the sodium hydroxide and water rinses were removed from pre-injection conditioning program resulting in a modified procedure involving a single flush with the non-aqueous media (2000 mbar, 2 minutes). A further 10 replicate injections of thiourea were performed using the modified rinse procedure. The two sets of data are compared in table 3.3.

Table 3.3. Influence of pre-run conditioning on resulting EOF.

	Average t_m (min)	Repeatability (% RSD)	EOF ($cm^2 V^{-1} s^{-1}$)
Original program	6.669	0.99	0.000330
Modified	5.938	0.32	0.000370

Removal of the aqueous solutions from the rinse cycle appeared to have enhanced the characteristics of the generated EOF. Hence, the modified rinse cycle was employed in all subsequent studies.

Increasing the ammonium acetate concentration firstly to 5 mM and then to 10 mM surprisingly resulted in a faster EOF. The latter conflicts with what would be expected in aqueous media as the background electrolyte is increased. Experimental data are shown in table 3.4.

Table 3.4. Influence of ammonium acetate concentration on EOF.

	5 mM	10 mM
Mean t_m (mins)	4.717	3.382
Repeatability (% RSD)	0.350	4.321
Magnitude of EOF ($cm^2 V^{-1} s^{-1}$)	0.000466	0.000650

3.5.2.2. Silver nitrate.

Silver nitrate was identified as one of the few materials that readily dissolved in acetonitrile without the need for any other materials. However, use of thiourea as an EOF marker in this media was found to be impractical as the resulting peak was extremely ill defined. This was presumed to be a consequence of complexation between thiourea and Ag(I). Anthracene was instead employed as it has been shown not to undergo Ag(I) complexation in argentation liquid chromatography[279].

Replicate injections (n=10) of anthracene were performed at silver nitrate concentrations of 1, 5 and 25 mM. The resulting EOFs were faster than with ammonium acetate and migration time repeatability was better, particularly at an Ag(I) concentration of 25 mM as shown in table 3.5.

Table 3.5. Magnitude and repeatability of the EOF generated at an applied voltage of 20 kV in acetonitrile containing various levels of silver nitrate.

	1 mM	5 mM	25 mM
Mean t_m	2.762	3.252	3.990
Repeatability (% RSD)	0.786	0.341	0.043
EOF ($cm^2 V^{-1} s^{-1}$)	0.000797	0.000677	0.000551

The EOF at 5 mM Ag(I) compared well with data subsequently published by Wright and Dorsey[60] who reported an EOF of 0.000672 $cm^2 V^{-1} s^{-1}$. Agreement at 25 mM was slightly poorer (0.000551 vs 0.000432 $cm^2 V^{-1} s^{-1}$[60]).

3.6. Investigation of temperature gradients.

The Crystal 310 instrument employs an air fan cooling system to maintain a constant separation temperature. However, this strategy appears to be incredibly inefficient since a significant portion of the separation capillary and the outlet buffer vial are exposed to the ambient temperature of the laboratory. It was therefore possible that changes in ambient temperature were leading to poor EOF repeatability. This theory was investigated by artificially inducing a temperature gradient.

A bulk supply of media comprising acetonitrile containing 1 mM ammonium acetate and 5% v/v acetic acid was prepared. The receiver vial was filled and left to chill in a refrigerator prior to use. The inlet vial was filled and loaded into the autosampler as usual. The instrument was programmed to maintain the separation temperature at 20°C. Replicate injections were performed over a period of 2 hours.

It was anticipated that significant variations in the EOF would be apparent over ten injections as the temperature of the thermostated inlet buffer vial increased at a faster rate than the receiver vial. However, this was not the case as shown in table 3.6. The magnitude of the resulting EOF was comparable with previous investigations involving this media (table 3.3).

Table 3.6. Magnitude and repeatability of the EOF generated at an applied voltage of 20 kV in acetonitrile containing 1mM ammonium acetate and 5% v/v acetic acid under an induced temperature gradient.

	Average t_m (min)	Repeatability (% RSD)	EOF ($cm^2 V^{-1} s^{-1}$)
Previous data	5.938	0.32	0.000370
Temp gradient	6.025	0.556	0.000365

Data were again evaluated using the student t-test. The hypothesis that the induced temperature gradient did not significantly influence migration behaviour was rejected at the 0.975 confidence interval (table 3.7)

Table 3.7. Evaluation of experimental data using the student t-test.

	Typical data	*Temp gradient*
Mean	5.938	6.024
Variance	0.0003576	0.001123122
Observations	10	10
Pooled Variance	0.000740361	
Hypothesized Mean Difference	0	
df	18	
t Stat	-7.092	
t Critical one-tail	2.101	

3.7. CONCLUSION.

EOF has been demonstrated in a series of solvents with and without the presence of a supporting electrolyte. Agreement between experimental data and values reported in the literature using different instrumentation was encouraging suggesting robustness of the technique. However, the mechanism by which the EOF was generated was unclear.

A rapid EOF was demonstrated in pure acetonitrile. However, its magnitude was found to vary markedly on a day to day basis. Addition of ammonium acetate initially appeared to stabilise the EOF but repeatability was noticeably poorer at higher electrolyte concentrations. It is presumed that these issues were not a consequence of buffer electrolysis since the magnitude of the receiver vial is designed to dilute such effects. Formation of temperature gradients was also eliminated as a potential cause. Conversely, migration time repeatabilities appeared to improve with increasing levels of silver nitrate.

Addition of relatively high amounts of acid was necessary to effect dissolution of background electrolytes but restricted the magnitude of EOF. Additionally, standardisation of conditions was necessary due to inconsistencies in the amount of acid required to effect full dissolution of ammonium acetate. This area warrants further investigation.

CHAPTER 4.

APPLICATION OF NACE TO THE SEPARATION OF AN ACTIVE PHARMACEUTICAL COMPOUND FROM A SERIES OF RELATED IMPURITY AND DEGRADATION MATERIALS.

4.1. INTRODUCTION.

The benefits of CE in non-aqueous media were evaluated by comparing a method developed for pharmaceutical materials with a separation achieved in a typical aqueous buffer. NACE method development was undertaken in a step-wise fashion in an attempt to gain further understanding of CE in non-aqueous media. An "entrance exam" mini validation was undertaken to critically assess whether the developed NACE separation was capable of meeting the strict criteria required within the highly regulated pharmaceutical industry.

4.2. BACKGROUND.

The regulations governing the manufacture and analysis of medicinal products are rightly extremely stringent[280]. Many of the assays routinely employed for product release testing in pharmaceutical QA laboratories employ isocratic reversed phase HPLC separations using UV absorbance detection. Such separations offer excellent resolution but tend to involve long analysis times of typically 10-30 minutes that are not particularly amenable to high throughput analysis.

Cimetidine (or Tagamet) is a histamine H_2-receptor antagonist that is used to reduce acid secretion in treatment of gastrointestinal ulcers[281, 282]. It is employed in the treatment of gastric ulcers and other complaints that are associated with the production of excess stomach acid. Chemically it is N-cyano-N-methyl-N-[2(5-methyl-1-H-imidazoyl-4-yl)methylthio-ethyl]guanidine. Its pharmacology has been extensively reviewed[283].

4.3. REGULATORY ASPECTS .

The United States Pharmacopoeia (USP) assay for cimetidine in tablet formulations[284] involves an isocratic reverse phase HPLC separation employing UV absorbance detection at 220 nm. The mobile phase comprises 200 ml methanol and 0.3 ml phosphoric acid diluted to 1000 ml with water.

Sample solutions are prepared by adding approximately 100 mg of powdered tablets to a 250 ml flask containing 50 ml methanol. The resulting solution is shaken prior to the addition of 40 ml water. The flask is then ultrasonicated for a period of 15 minutes prior to being diluted to the mark with water. A 5 ml aliquot of this stock solution is then transferred to a 200 ml volumetric flask and diluted to the mark with mobile phase. The assay essentially involves replicate 50 μL injections of this solution under the previously described conditions.

The USP monograph clearly states that the efficiency of the analyte peak should not be less than n=1000 theoretical plates and that the relative standard deviation of the response of 5 replicate injections must be less than 2.0%. These figures would serve as a useful reference against which the performance of developed separations could be critically compared.

4.4. MATERIALS AND METHODS.

The cimetidine and related impurity and degradation compounds were a kind gift supplied by Smithkline Beecham (Harlow, UK). Each compound was nominally assigned an identification letter (A-H) to avoid the use of complex chemical names or proprietary reference codes. The structures of the materials studied are presented in table 4.1.

Table 4.1 Structures of the Pharmaceutical Compounds Employed.

Structure	Identification
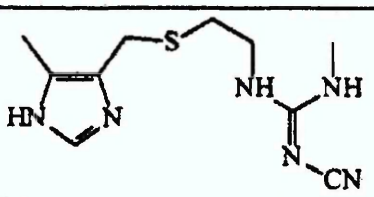	A (Cimetidine)
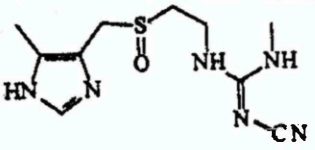	B (Cimetidine Sulphoxide)
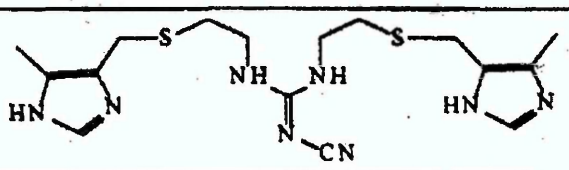	C
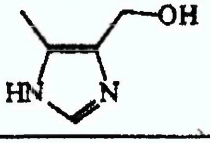	D (Cet-Alcohol)
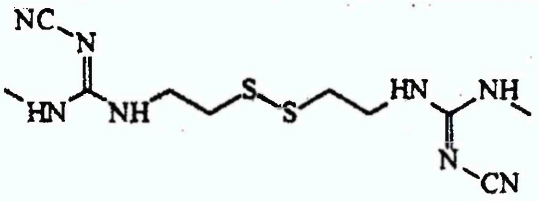	E
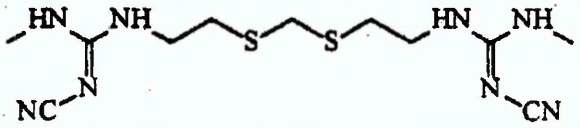	F
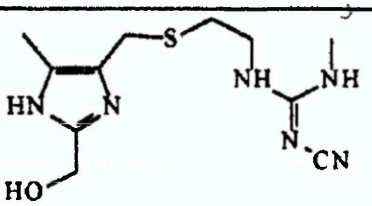	G
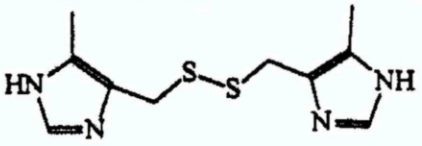	H

4.5. EXPERIMENTAL PROCEDURES.

All separations were performed using the Crystal 310 C.E system using 60 cm lengths of 50 μm i.d. uncoated fused silica capillary. On-capillary UV absorbance detection was performed at 230 nm at a distance of 44 cm from the inlet end (Ld = 44 cm).

Stock solutions (1000 mg/l) of all analyte compounds were prepared by dissolving the appropriate amount of each material in 50/50 % v/v acetonitrile/methanol containing 1 % v/v acetic acid. These were subsequently diluted to a working concentration of 100mg/l when required using the relevant non-aqueous media. All solutions were stored in a refrigerator when not required. However, sample solutions containing compound A (cimetidine) were found to have a limited usable life of only a few weeks even when refrigerated. After this time, a broad peak eluting soon after cimetidine was evident. This extra peak caused significant errors during peak integration and hence parameters such as efficiency could not be calculated with any degree of confidence.

The separation capillary was equilibrated at the start of each working day and prior to changing separation media by flushing with sodium hydroxide (0.1 M, 2000 mbar) for 5 minutes. Residual sodium hydroxide was removed by flushing with acetonitrile (2000 mbar) for 5 minutes. A two-stage equilibration was performed with the appropriate non-aqueous medium which was first hydrodynamically pumped (2000 mbar) for 5 minutes and then electrically driven (20 kV) for 5 minutes. The capillary was rinsed using acetonitrile (2000 mbar) for 5 minutes at the end of each working day prior to careful storage.

The detrimental effects of performing a sodium hydroxide rinse between separations were discussed in the previous chapter. The capillary was therefore only rinsed with the relevant non-aqueous media (2000 mbar, 2 minutes) between replicate injections. Additionally, the first two separations achieved using each medium studied were not included in any statistical analysis.

All samples were hydrodynamically injected (25 mbar, 0.2 minutes). Electroosmotic mobilities were determined by incorporating thiourea as a neutral marker compound within the test samples. Replicate injections were performed at each set of separation conditions to access migration time repeatability. Migration orders were determined by injection of individual compounds and/or spiked standard solutions.

4.6. EXPERIMENTAL.

4.6.1. Initial method development.

Leung and co-workers[46] reported the separation of basic drugs using non-aqueous media comprising a mixture of acetonitrile and methanol containing 1% v/v acetic acid and 20 mM ammonium acetate. The initial investigations with non-aqueous media described in the previous chapter had demonstrated that a fast and reproducible EOF was possible using an ammonium acetate concentration of only 1 mM. Hence, preliminary investigations were performed at this electrolyte concentration. All initial method development was performed using a three component test mix comprising compounds A, B and C (all 1 mg/ml).

4.6.2. Optimum solvent composition of the non-aqueous separation medium.

The dependence of the apparent electrophoretic mobilities of the test compounds on the solvent composition of the non-aqueous media which included ammonium acetate and acetic acid at constant concentrations of 1 mM and 1 % v/v respectively is presented in figure 4.1.

The migration order was B, C, A regardless of solvent composition. The fact that all three compounds eluted ahead of thiourea implied that they carried some form of positive charge.

Figure 4.1 Dependence of the electrophoretic and electroosmotic mobilities of a simple 4 component test mixture on the composition of the non-aqueous medium.

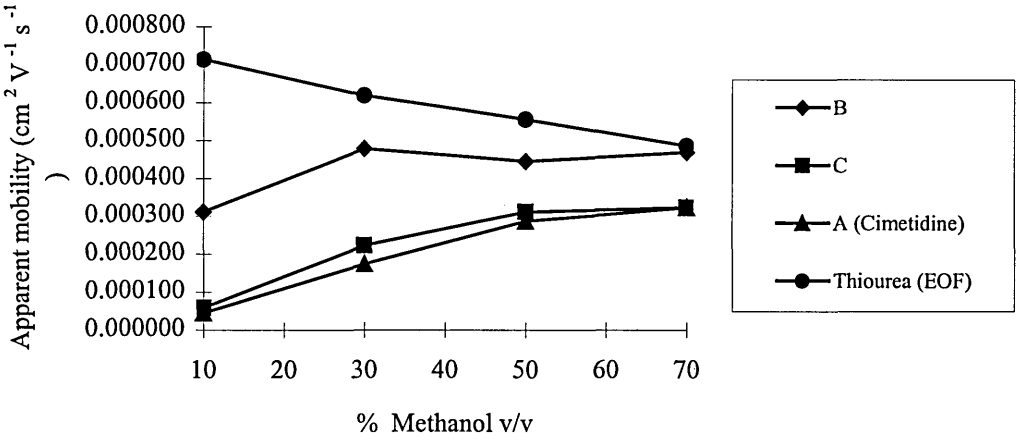

The separation achieved in plain acetonitrile was unclear. The 3 test compounds appeared to co-elute at a migration time equivalent to the EOF (around 2.9 minutes) but the electropherograms contained many spikes and serious current fluctuations and/or total breakdown was experienced during replicate injections. It is possible that these effects were the result of some form of instrumental fault rather than a feature of the non-aqueous medium. The results were not considered to be reliable and were therefore not included in figure 4.1.

The EOF was found to be slower at higher methanol concentrations. Significant overlap between compounds C and A was apparent at all compositions involving methanol at 50 % v/v and above.

A composition of 70/30 % v/v acetonitrile/methanol was found to give the optimum separation in terms of speed, resolution and migration time repeatability. The rapid EOF achieved under these conditions may indicate that a 70/30 % v/v mixture of the two solvents has the lowest viscosity of all possible compositions. Migration time repeatability over 10 replicate injections was better than 0.5% RSD. The current generated under these conditions was 1.0 μA

Further method development was obviously necessary since a slight overlap of the latter two peaks (C and A) was clearly evident. The resolution between this pair was determined to be 1.87 (equation 2.3). A typical separation is presented in figure 4.2.

Figure 4.2 Separation of a simple 3 component test mixture at a solvent composition of 70/30 %v/v acetonitrile/methanol containing 1mM ammonium acetate and 1% v/v acetic acid.

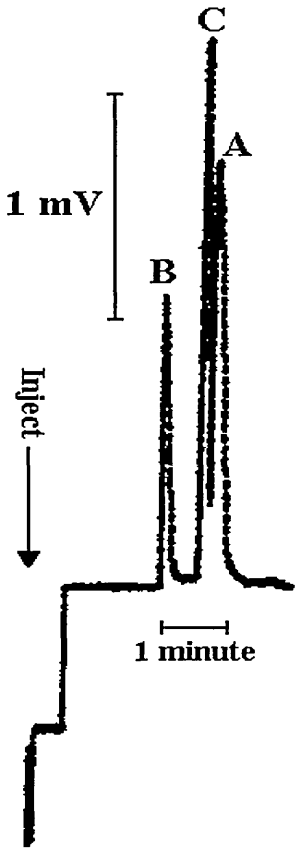

	Average migration time (min)	% RSD (n=10)
B	2.004	0.46
C	2.613	0.42
A	2.777	0.43

4.6.3. Optimisation of electrolyte concentration.

A solvent composition of 70/30 % v/v acetonitrile/methanol was the basis of all subsequent non-aqueous separation media. Increasing the ammonium acetate concentration to 5 mM improved the separation achieved between compounds C and A. The resolution was determined to be 2.81 under these conditions. However this was at the expense of an increased separation time which was a consequence of a reduced EOF. The latter clearly conflicts with the initial studies in non-aqueous media (chapter 3) where the EOF increased with increasing ammonium acetate concentration. The current generated under these conditions was 3.3 μA.

Peak efficiencies were particularly impressive but the repeatability of peak areas was poorer than the USP specification criteria of 2% RSD.

Increasing the ammonium acetate concentration to 10 mM resulted in further enhancement of the separation between compounds C and A. The resolution under these conditions was determined to be 3.17. Peak efficiencies were approximately double those that were achieved at 5 mM ammonium acetate.

Migration time repeatability was particularly impressive being less than 0.2% RSD for all compounds over the 10 replicate injections. Although the repeatability of peak area responses were improved they still did not match the USP requirements of 2% RSD. The current generated under these conditions was 5.2 μA.

Baseline separation (R_s = 3.67) of compounds C and A was achieved in less than six minutes at an electrolyte concentration of 25 mM. However, peak efficiencies along with migration time and peak area reproducibilities were extremely poor. This was surprising since an increase in the ammonium acetate concentration had previously effected significant improvements in all of these parameters. The current generated under these conditions was 10.2 μA. A representative separation is presented in figure 4.3.

Figure 4.3 Separation of a simple 3 component test mixture at a solvent composition of 70/30 %v/v acetonitrile/methanol containing 25 mM ammonium acetate and 1% v/v acetic acid.

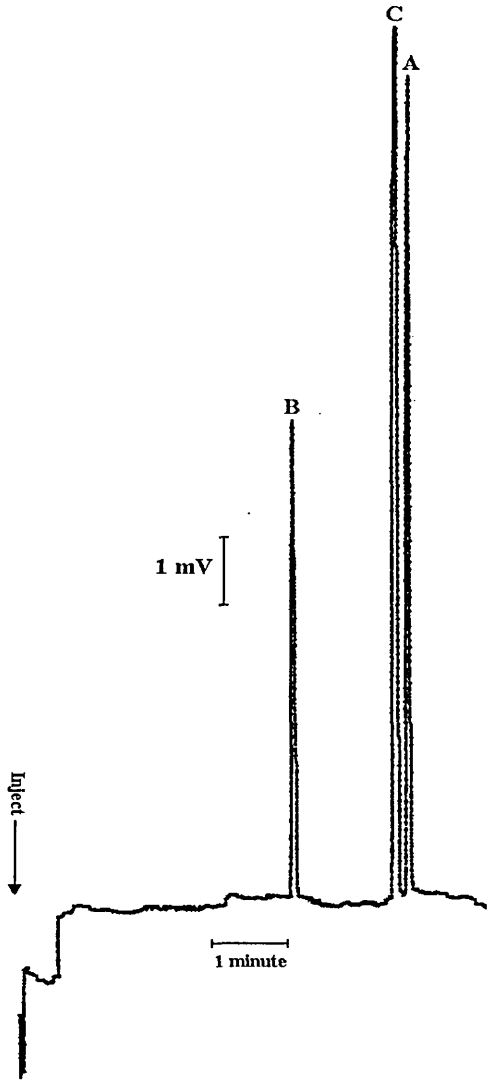

			% RSD (n=10)	
	Average t_m (min)	N (plates/m)	t_m	Peak area
B	3.583	47200	0.99	6.6
C	4.867	65650	1.13	11.4
A	5.026	79000	1.15	8.0

The study was subsequently repeated to confirm the validity of these disappointing results. The migration times obtained are presented in table 4.2

Table 4.2. Repeat study at 20 kV at a solvent composition of 70/30 %v/v acetonitrile/methanol containing 25 mM ammonium acetate and 1% v/v acetic acid.

			% RSD (n=10)	
	Average t_m (min)	N (plates/m)	t_m	Peak area
B	3.628	247250	0.10	3.1
C	5.039	355000	0.05	2.7
A	5. 193	425700	0.05	2.9

These results appeared to invalidate the original study. There was no apparent reason as to why the two apparently identical studies should yield such markedly different results. This raised concerns regarding the day to day reproducibility of the separations.

The migration time repeatabilities achieved in the repeat study were rather impressive. Peak efficiences were again doubled but the repeatability of peak area responses was still greater than 2.0% RSD. The observed current was 10.3 μA which was in good agreement with the original study.

4.6.4. Optimisation of applied voltage.

Five replicate injections of a standard comprising cimetidine (100 mg/l) and thiourea (40 mg/l) were performed using 70/30 %v/v acetonitrile/methanol containing 25 mM ammonium acetate and 1% v/v acetic acid at both 20 and 30 kV (333 and 500 V/cm respectively). The results of this study are presented in table 4.3 below.

Table 4.3 Apparent mobilities of cimetidine and thiourea (EOF marker) at both 20 and 30 kV calculated from averaged migration times (n = 5).

	Cimetidine		Thiourea		
	Mean t_m (min)	% RSD	Mean t_m (min)	% RSD	EOF ($cm^2V^{-1}s^{-1}$)
20 kV	5.164	0.04	5.693	0.04	0.000386
30 kV	3.394	0.06	3.725	0.08	0.000394

This simple study clearly indicated that the separation time would be reduced favourably at an elevated applied voltage. As previously stated, rapid analysis is desirable in the pharmaceutical industry in order to facilitate high sample through-put. The current generated at 30 kV was 15.3 μA.

A separation of the 3 component test mixture was effected at an applied voltage of 30 kV. Efficiencies were found to be lower than had previously been achieved. A representative separation is presented in figure 4.4.

Figure 4.4 Separation of a simple 3 component test mixture at an applied voltage of 30 kV using non-aqueous separation media comprising 70/30 %v/v acetonitrile/methanol containing 25 mM ammonium acetate and 1% v/v acetic acid.

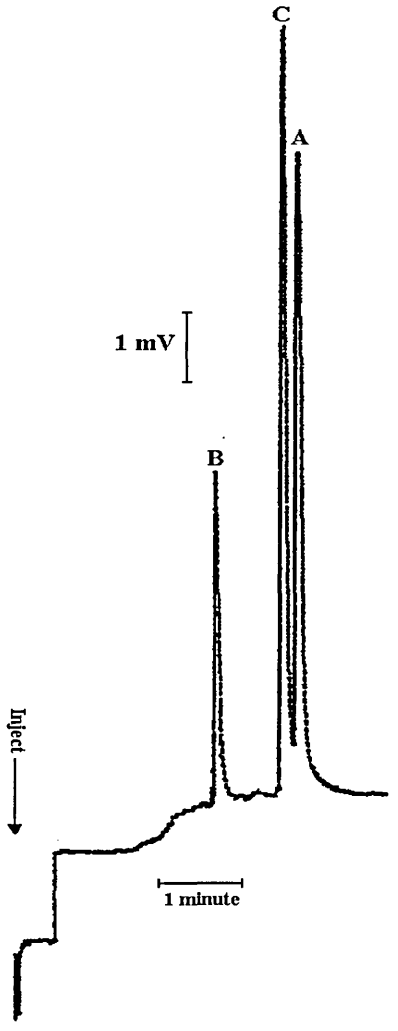

			% RSD (n=5)	
	Average t_m (min)	N (plates/m)	t_m	Peak area
B	2.508	48000	0.31	5.22
C	3.345	85500	0.26	5.40
A	3.535	63500	0.29	4.35

4.6.5. Studies involving the remaining compounds.

The migration times of the remaining 5 compounds (D-H) had previously been determined at an applied voltage of 20 kV. The average migration times for each compound are presented in 4 3. All data were calculated from three replicate injections (25 mbar, 0.2 min).

Table 4.4 Average migration times (n=3) for all compounds at 20 kV.

Compound	Average migration time (mins)
A	5.210
B	3.598
C	5.068
D	4.737
E	5.471
F	5.458
G	5.265
H	4.793

These results indicated that in an analysis of all compounds E would co-elute with F, G would co-elute with A and D would co-elute with H. However, it should be theoretically possible to perform a range of separations each one capable of separating a different permutation of 5 compounds from the total pool of 8.

A new test mixture comprising compounds A, B, C, D and F was injected under the adopted separation conditions as an illustrative example. Unfortunately, serious intermittent problems involving erratic baselines, spikes and variation and/or breakdown of observed current were regularly encountered during this period. It was strongly felt again that these problems were instrumental-based rather than being a function of the non-aqueous media. These difficulties seriously restricted the progress of the investigations. However, 5 replicate injections of sufficient quality were eventually acquired at an applied voltage of 30 kV. A representative separation is presented in figure 4.5.

Figure 4.5. Separation of an active pharmaceutical compound from a series of 4 related manufacturing impurities and degradation compounds at 30 kV using a non-aqueous medium comprising 70/30 %v/v acetonitrile/methanol containing 25 mM ammonium acetate and 1% v/v acetic acid.

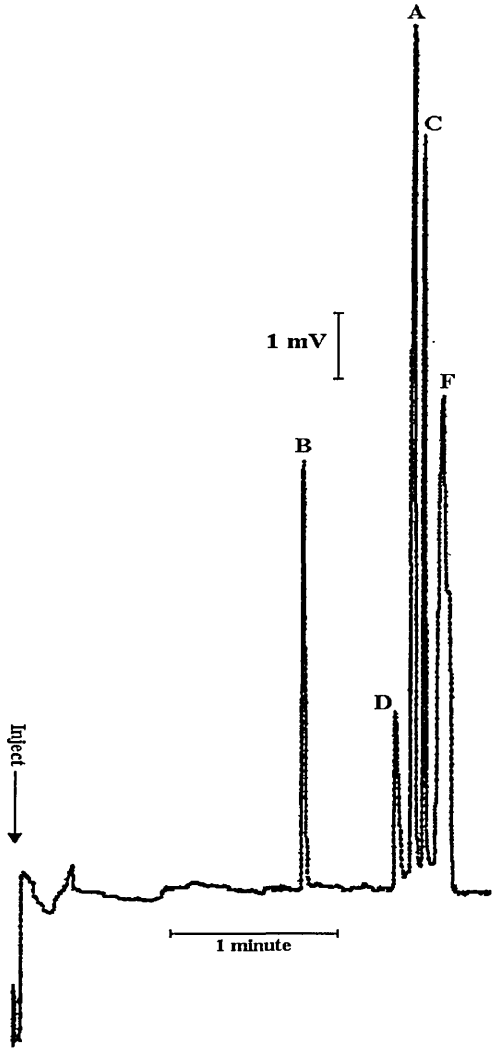

			% RSD (n=5)	
	Average t_m (min)	N (plates/m)	t_m	Peak area
B	2.412	375000	0.25	4.97
D	3.099	1552000	0.28	2.20
C	3.311	520500	0.24	7.82
A	3.405	780000	0.34	5.95
F	3.567	105000	0.43	64.56

The poor peak area repeatability and efficiency associated with compound F appear to have been caused by an overlapping peak introducing errors during integration. This extra peak can clearly be seen as a shoulder on peak F in figure 4.5. The identity of this peak is unknown but it is possible that this may have been compound E which was present either as an impurity in one of the compounds or the result of one or more compounds in the standard degrading during storage. If the method were to be validated the stability of sample and standard solutions would need to be evaluated.

4.6.6. Repeatability of EOF in non-aqueous media.

A brief study was undertaken to assess the day to day reproducibility of the EOF generated in the non-aqueous media. Essentially, 3 replicate injections of a thiourea standard (100mg/l) were performed on five separate occasions that spanned a period of 2 weeks. Separations were effected at 30 kV employing a non-aqueous medium comprising 70/30 %v/v acetonitrile/methanol containing 25 mM ammonium acetate and 1% v/v acetic acid. The results of this study are summarised in table 4.5.

Table 4.5. EOF generated in non-aqueous media monitored over a two week period.

	Mean EOF ($cm^2 V^{-1} s^{-1}$)	Range ($cm^2 V^{-1} s^{-1}$)
1	0.0003645	6.35×10^{-7}
2	0.0003905	7.28×10^{-7}
3	0.0003484	1.90×10^{-6}
4	0.0003938	2.12×10^{-7}
5	0.0004087	2.39×10^{-6}

This brief study confirmed that the magnitude of the EOF generated within the non-aqueous media was highly reproducible over a series of replicate injections but was prone to drift on a day to day basis.

4.6.7. Investigation of alternative background electrolytes.

Sodium acetate and ammonium formate were investigated to determine whether the identity of electrolyte employed had any effect on the separation achieved. Separations using ammonium acetate were performed in parallel with these studies to ensure that accurate comparisons could be made.

Essentially, 5 replicate injections of a test mix comprising compounds A, B and C were performed at an applied voltage of 30 kV in non-aqueous media comprising 70/30 % v/v acetonitrile/methanol containing 25 mM background electrolyte and 1% v/v acetic acid.

The dependence of the apparent electrophoretic mobilities of compounds A, B and C on the identity of the background electrolyte employed is presented in figure 4.6.

Figure 4.6 Dependence of the electrophoretic and electroosmotic mobilities of a simple 3 component test mixture on the identity of the background electrolyte employed in non-aqueous media comprising 70/30 % v/v acetonitrile/methanol containing 25 mM background electrolyte and 1% v/v acetic acid.

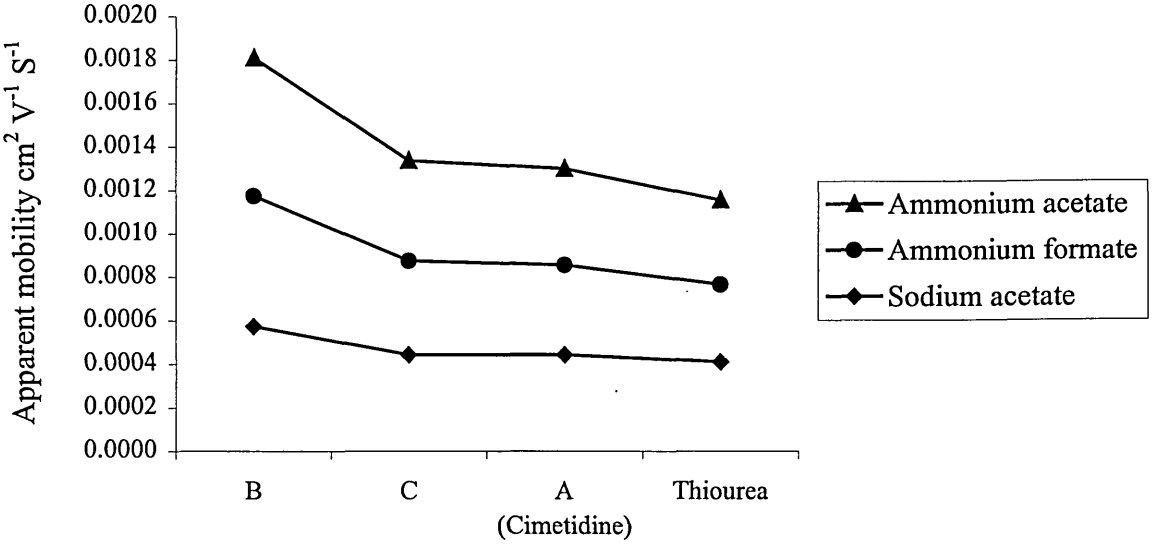

Separation selectivity was found to be unaffected by altering the identity of the background electrolyte. The elution order was determined to be B, C, A using both sodium acetate and ammonium formate. The three test compounds were found to migrate ahead of thiourea in both systems which supported the previously proposed theory that they carried a positive charge in the non-aqueous media. The current generated in the media containing the two alternative electrolytes was found to be slightly higher than when using ammonium acetate as shown in table 4.6.

Table 4.6. Observed current at 30 kV in non-aqueous media comprising comprising 70/30 % v/v acetonitrile/methanol containing 25 mM background electrolyte and 1% v/v acetic acid.

Electrolyte	Ammonium acetate	Ammonium formate	Sodium formate
Observed current (μA)	17.5	18.7	18.5

The slowest EOF was generated in the media that included sodium acetate. Separation was poorest in this system with compounds C and A eluting together as one large peak as shown in figure 4.7.

Figure 4.7. Separation of a simple 3 component test mixture at a solvent composition of 70/30 % v/v acetonitrile/methanol containing 25 mM sodium acetate and 1% v/v acetic acid.

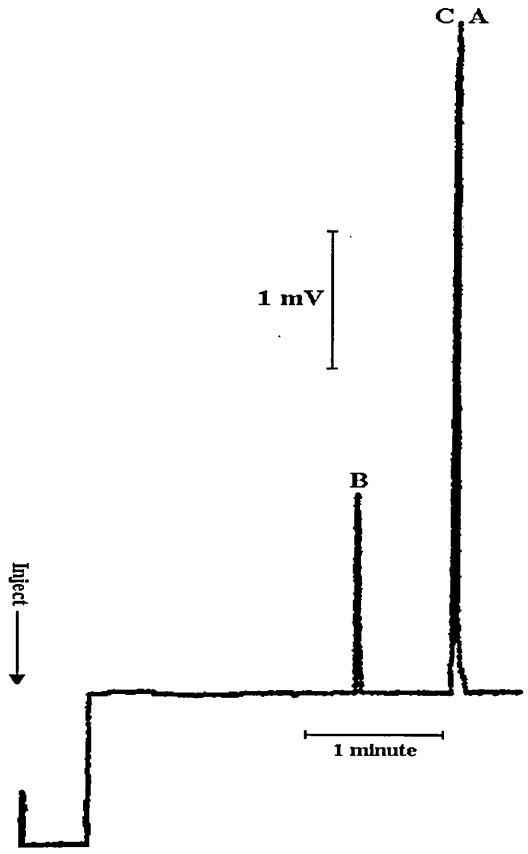

			% RSD (n=5)	
	Average t_m (min)	N (plates/m)	t_m	Peak area
B	2.558	580000	0.09	3.30
C & A	3.311	-	0.14	-

The separation achieved using ammonium formate was remarkably similar to that obtained using ammonium acetate. Separation was slightly faster using ammonium acetate but migration time repeatabilities were similar in both systems. Efficiencies were higher using ammonium formate but peak area repeatability was poor. In contrast, the peak area repeatabilities obtained using ammonium acetate were excellent and passed the USP requirements of 2 % RSD. Representative separations using ammonium acetate and ammonium formate are presented in figures 4.8 and 4.9 respectively

Figure 4.8. Separation of a simple 3 component test mixture at a solvent composition of 70/30 % v/v acetonitrile/methanol containing 25mM ammonium acetate and 1% v/v acetic acid.

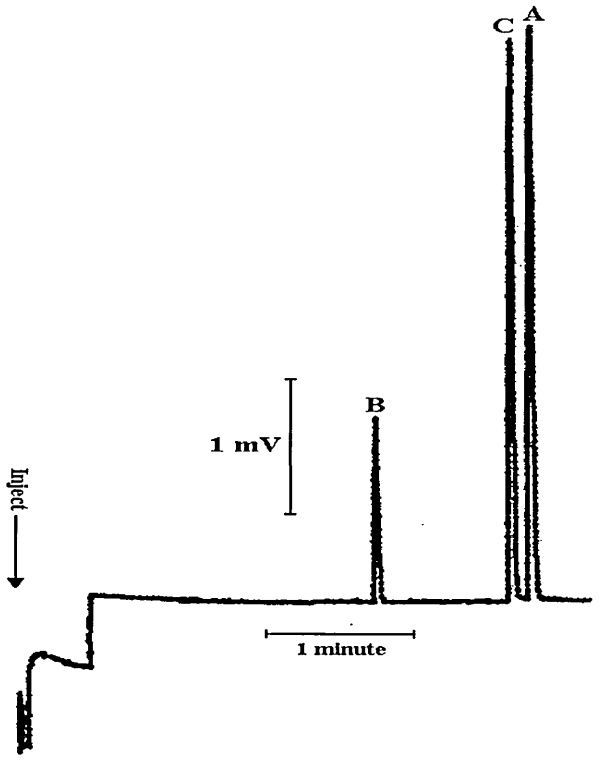

			% RSD (n=5)	
	Average t_m (min)	N (plates/m)	t_m	Peak area
B	2.314	402000	0.12	1.3
C	3.174	423800	0.14	0.9
A	3.297	396000	0.13	1.0

It is interesting to compare the above separation involving ammonium acetate (figure 4.8) with the initial separation that was achieved at 30 kV (figure 4.3). Significant differences are apparent between these separations even though they were effected under apparently identical conditions. Agreement between migration times is fairly poor and associated repeatabilities were poorer in the original separation. However, the greatest inconsistencies are displayed by the achieved peak efficiencies that were 5-8 times lower in the original separation. This comparison provides further evidence to support the belief that the method is not particularly robust.

Figure 4.9. Separation of a simple 3 component test mixture at a solvent composition of 70/30 % v/v acetonitrile/methanol containing 25 mM ammonium formate and 1% v/v acetic acid.

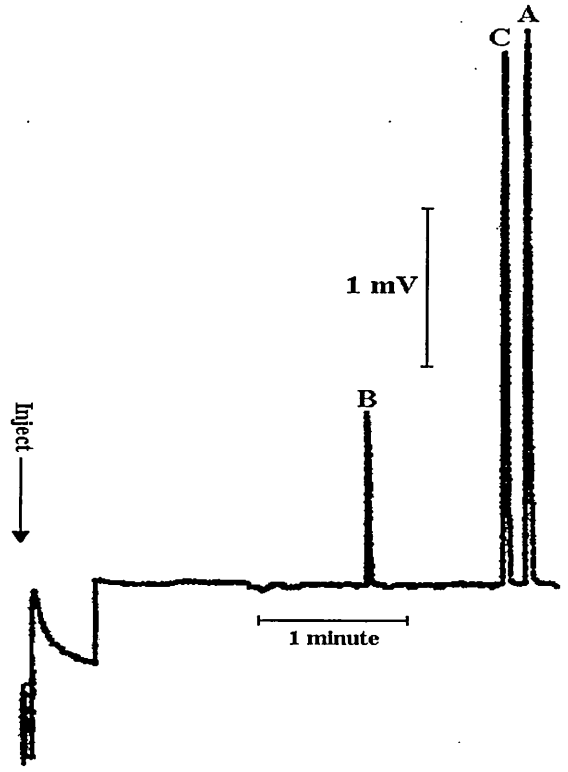

			% RSD (n=5)	
	Average t_m (min)	N (plates/m)	t_m	Peak area
B	2.436	610000	0.13	6.7
C	3.397	650400	0.13	6.4
A	3.556	640000	0.14	4.7

4.7. Critical comparison of separation achieved in non- aqueous media with a comparable separation achieved in typical aqueous-based media.

Luksa and Josic[285] described the CE separation of cimetidine from two metabolites and other compounds in human plasma using a coated capillary at pH 2. Meanwhile, Soini and co-workers[286] described the determination of cimetidine in serum using MEKC at pH 6.4 including an initial electrochromatographic solid phase extraction and preconcentration step. A simple CE separation of the test materials using aqueous-based separation media was developed by a colleague at this institution in parallel with the non-aqueous studies in order to facilitate a comparison of the two modes[48].

A full, systematic method development was performed for the aqueous separation at an applied voltage of 30 kV using a 3 component test mix comprising compounds A, B and C. At pH 7.14 (10 mM phosphate) compound B migrated ahead of compounds C and A which co-eluted at a time equivalent to the EOF. This was not surprising since the pK_a of cimetidine is 6.80[287]. Successive reductions in buffer pH improved resolution until a full separation was achieved at pH 3.14 (10 mM sodium dihydrogenphosphate phosphate). The order of elution was B, C, A and the separation was complete in less than 4 minutes.

When attempting to separate the remaining materials D-H it was found that compounds E and F had extremely poor aqueous solubility. However, a full separation of compounds A, B, C, G and H was achieved in under five minutes using the previously described experimental conditions. The elution order was H, B, C, A, G with the latter two peaks displaying significant tailing. Calculated efficiencies ranged from 47000 to 185000 plates/m with associated RSDs ranging from 1.1 to 23.3% (n=5). The repeatability of migration times over 5 replicate injections was less than 1% for all compounds whilst peak area repeatability ranged from 2.1 to 11.0 % RSD. However, the quoted values for migration time repeatability could only be achieved by removing the outlet buffer vial during the rinsing cycle. This procedure ensured that the rinse solutions did not adversely affect the pH or ionic strength of the buffer in the outlet vial. This would obviously restrict the capability of the method in terms of unsupervised operation. Further development work involving the addition of organic modifiers indicated that the separation could not readily be improved.

4.8. Method transfer.

Staff at the Health and Safety Laboratory kindly allowed time to investigate the non-aqueous separation on their Beckman CE. This gave an excellent opportunity to investigate some of the issues raised during the development of the non-aqueous experiment.

The Beckman instrument employs a liquid cooling system that appears far more efficient than the Thermo-Unicam design[288]. It was therefore anticipated that the repeatability of migration times over a series of replicate injections would be superior and more consistent from day to day using this system. Leung *et al.*.[46] improved repeatability by moving their NACE separation to a different brand of instrument.

The experimental conditions were essentially identical to those that have previously been described. The only significant difference involved reduction of the separation voltage to 23 kV in order to yield an equivalent (500 V/cm) separation. This was necessary due to the different dimensions of the Beckman capillary namely L_d = 40 cm, L_t = 46 cm. All capillaries were prepared from the same batch.

Initial studies involved 5 replicate injections of a thiourea standard (50 mg/l) to determine the repeatability of the EOF generated under the non-aqueous conditions. The results obtained were critically compared with data obtained from an identical study that was performed in parallel using the Crystal model 310 instrument. All results are presented in table 4.7.

Table 4.7. Comparison of the repeatability of the EOF generated at 500 V/cm in non-aqueous media (70/30 %v/v acetonitrile/methanol containing 25 mM ammonium acetate and 1% v/v acetic acid) using two instruments on the same day.

	Crystal 310	Beckman
t_m thiourea (min)	3.584, 3.580, 3.578, 3.575, 3.575	4.258, 4.315, 4.358, 4.396, 4.429
Average t_m (min).	3.578	4.351
Repeatability (% RSD)	0.1	1.4
EOF ($cm^2\ s^{-1}\ V^{-1}$)	0.00041	0.00031

The results in table 4.7 clearly demonstrate that differences existed when attempting to perform equivalent non-aqueous separations on the two instruments. The magnitude of the EOF generated on the Beckman was lower and displayed poorer repeatability over a series of replicate injections. The latter observation was in marked contrast to the expectation that the liquid cooling system would ensure that reproducible migration times were obtained. In addition, the peaks obtained during the Beckman studies appeared to be broader than those obtained using the Crystal 310 instrument. Average peak widths were determined to be 0.11 min and 0.075 min respectively.

It was noted that the migration times in the Beckman study increased over the series of five injections. The study was therefore repeated to ensure that the capillary had been sufficiently equilibrated prior to the acquisition of analytical data. The repeat study was performed soon after the original study. The results are presented in table 4. 8.

Table 4.8. Repeat study on the Beckman instrument to investigate the repeatability of the EOF generated at 500 V/cm in non-aqueous media (70/30 %v/v acetonitrile/methanol containing 25 mM ammonium acetate and 1% v/v acetic acid).

t_m thiourea (min)	9.567, 9.996, 10.175, 10.408, 10.617
Average t_m (min).	10.153
Repeatability (% RSD)	3.5
Magnitude of EOF ($cm^2 s^{-1} V^{-1}$)	0.000131

A minor alteration in the magnitude and repeatability of the EOF between the original and repeat study might have been anticipated. However, the data presented in table 4.8 clearly indicated that significant shifts were apparent in both parameters. An increase in the migration time over the 5 injections was again observed. The fact that the study had been repeated for this reason appeared to eliminate insufficient equilibration of the capillary as an underlying root cause of the differences.

There was obviously some fundamental difficulty associated with transferring the non-aqueous separation media to the Beckman instrument but no immediately obvious explanation could be proposed. Instrumental problems seemed to be an unlikely cause since the instrument had recently been successfully employed to perform routine analysis by staff at the Health and Safety Laboratory.

The only significant difference that was evident between the designs of the two instruments was the size of inlet and outlet buffer vials. The Beckman CE employs identical inlet and outlet vials whereas the outlet vial used by the Crystal 310 instrument is approximately ten times larger than the inlet vial. It is possible that this may have caused some effect. Unfortunately it was impractical to investigate this theory since there was no scope to alter the size of the vials on either instrument. Studies concerning method transfer to the Beckman instrument were abandoned at this stage due to time constraints.

4.9. CONCLUSION.

Development of a separation using non-aqueous CE was found to somewhat of a "black art" when compared with traditional CE or HPLC in which well defined schemes for developing methods are understood and widely available. The starting point in a HPLC or CE method development will typically include a consideration of the analyte materials in terms of their pKa values. This is an obvious disadvantage when attempting non-aqueous separations where the concepts of pH and pKa are not well understood and published values are not readily available. The lack of such fundamental knowledge concerning non-aqueous media inspired a systematic investigation of the area that forms the basis of chapter 6.

The developed method could not separate all compounds it a single run. However, a series of several runs each capable of separating a unique combination of 5 compounds was thought capable of providing a full separation. The use of non-aqueous media allowed the separation of hydrophobic materials that was not possible using traditional aqueous-based buffers. Selectivity was found to be different in the non-aqueous media and a different combination of compounds was separated. The two techniques can therefore be considered to be complimentary. In addition, peak shapes and efficiencies were noticeably better than those achieved under aqueous conditions.

The magnitude of the EOF generated within the non-aqueous media was found to be highly reproducible over a series of replicate injections but was prone to drift on a day to day basis. This would have serious consequences for any acquisition system that relied on a migration time "window" to detect and analyse peaks. For example, when using the HP integrator for a quantitative method it is necessary to specify an absolute migration time for each peak that requires integration. A ± range may also be specified which yields a "window" in which the peak will be detected. Any drift in the method may cause the peak to fall outside of these times and hence not be processed.

It is interesting to evaluate the non-aqueous separations using the USP criteria for the cimetidine HPLC assay that was introduced at the beginning of this chapter. The typical migration time repeatabilities for replicate injections that were routinely achieved during this work easily met the USP monograph criteria of 2% RSD. The efficiencies obtained for the active (cimetidine) peak were significantly in excess of the required n=1000 plates. However, significant differences in migration times and efficiencies were apparent between separations that were performed under identical conditions but on different days.

It is possible that changes in the ambient temperature adversely affected the day to day repeatability of the separations. This is a reasonable theory since changes of even 1-2 ° C would be sufficient to effect significant changes in the viscosity of the non-aqueous media. Such changes would be sufficient to affect the separations achieved. This also presents the opportunity for solvents to evaporate from the buffer vials leading to an alteration of media composition. This phenomenon could also explain the difficulties encountered during the investigations such as current breakdown and spikes obscuring the electropherograms.

An alternative explanation for the variations in peak areas and efficiencies centres on the integrator that was employed to record the electropherograms. A visual inspection of the electropherograms obtained during this work highlighted apparent errors with peak integration. Many peaks that appeared visually identical were found to have wildly different peak widths and areas. In some cases the magnitude of this apparent error was in the order of 50%. The HP 3395 integrator is primarily intended for use with HPLC and GC instrumentation. Separations involving the latter two techniques generate relatively broad gaussian peaks. In contrast, CE, especially when performed in non-aqueous media routinely generates essentially triangular shaped peaks, which are extremely narrow and sharp. It may therefore be possible that the HP3395 integrator was in fact unsuitable for the quantitative aspects of these studies, being unable to reproducibly integrate such sharp peaks with any degree of confidence.

The issue of detection must also be considered when discussing these separations in terms of compatibility to the USP HPLC assay requirements. The amount of active (cimetidine) injected on column in the HPLC separation is 0.5 μg. A similar determination for the non-aqueous separations is outlined below.

The length (mm) and volume (nl) of the sample zone may be determined using equations 4.1 and 4.2 respectively which are specific to hydrodynamic injections performed using the Crystal 310 instrument[289]. The viscosity of the non-aqueous media was approximated using the value for pure acetonitrile (0.37 cP).

$$P.t = \frac{P_{length} \times 3200 \times \eta \times L_t}{d^2} \qquad \textit{Equation 4.1}$$

Where:

P = pressure (mbar).

t = Duration of injection (s).

P_{length} = Sample plug length (mm).

η = Viscosity of medium (cP).

L_t = Total length of the separation capillary (cm)

d = Internal diameter of the separation capillary (μm).

$$V_{samp} = \frac{\pi \times P_{length} \times d^2}{4}$$ *Equation 4.2*

The injection conditions of P = 25 mbar, t = 12 s (0.2 min), η = 0.37 cP, L_t = 60 cm and d = 50 μm would therefore generate a sample plug of around 20 nl which equates to approximately 2 μg on capillary.

The figures calculated above indicate that the solutions employed during the method development would only need to be diluted by a factor of four to be equivalent to those specified in the USP monograph. In the unlikely event of this causing any significant problems it would be feasible to improve detection sensitivity by employing a 75 μM i.d capillary since the generated current would be low compared to a comparable aqueous-based separation. Hence detection does not appear to be an issue in this particular application.

It is perhaps easy to understand the reluctance of some companies to invest time and resources in developing CE assays on the basis of these studies. Although CE was found to be capable of effecting rapid separations with extremely high efficiencies it did not appear able to generate equivalent results to HPLC in terms of the validation criteria set by regulatory agencies. In particular, the inability to replicate data on another instrument in a different laboratory was a significant failing. The cause of this was unclear. Other workers[54, 59] have reported NACE separations using the Beckman P/ACE but did not discuss repeatability in any detail.

Chapter 5.

APPLICATION OF ELECTRICALLY-DRIVEN TECHNIQUES TO THE SEPARATION OF THE PESTICIDE PIRIMICARB FROM RELATED METABOLITES.

5.1. INTRODUCTION.

Critical comparison of the non-aqueous and aqueous-based separations presented in the previous chapter hinted that the various modes of CE could offer tremendous scope when tackling complex separations. This concept was explored using a series of pesticide materials with a high degree of structural similarity. Separations were developed using non-aqueous and aqueous-based CE as well as MEKC.

5.2. BACKGROUND.

Pirimicarb (2-dimethylamino-5,6-dimethyl-4-pyrimidinyl N,N dimethylcarbamate) was developed in the UK by ICI (now Zeneca Agrochemicals) under the assigned code reference PP O62 and marketed as Pirimor[290, 291]. It is a highly selective, fast acting aphicide that is particularly effective against strains of aphid that have developed resistance to organophosphorus pesticides[292].

Pirimicarb undergoes fairly rapid photochemical degradation after spraying to yield compounds R34885 and R34836. Photochemical degradation on surface soil yields compound R31805 as the major product. Extensive chemical and biological hydrolysis of the carbamate functionality occurs in soil to yield the hydroxypyrimidine compounds R34836, R35140 and R31680. The metabolic reactions of pirimicarb are summarised in figure 5. 1.

Figure 5.1. Metabolic fate of pirimicarb[293].

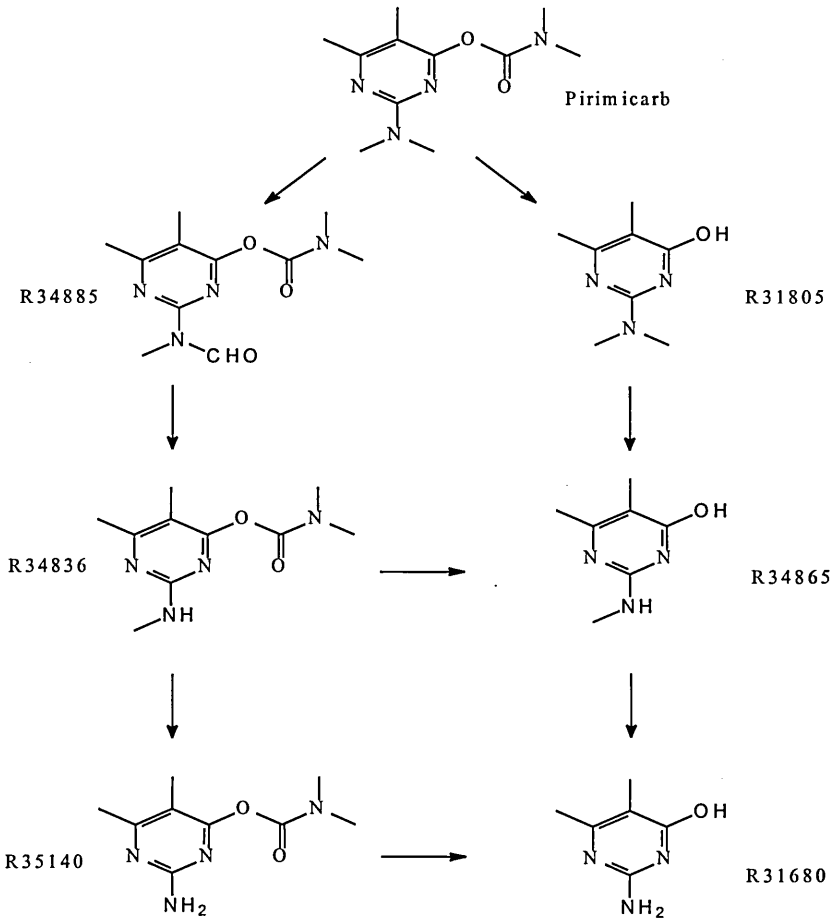

Cabras and co-workers[293] attempted to separate pirimicarb from its full range of metabolites using HPLC. Five of the eight compounds were successfully separated with RP C_8 and C_{18} columns employing an acetonitrile/phosphate buffer mobile phase. Separation was complete in under 10 minutes but the resolution between R34865, R35140 and R31680 was poor. These three highly polar hydroxypyrimidines were subsequently resolved using an amino column employing a water/acetonitrile mobile phase.

CEC separations of these compounds have also been reported[196, 223]. The isocratic CEC separation of pirimicarb and 4 related degradation products was achieved in under 7 minutes by Moffat and co-workers[223]. Meanwhile, Smith and Carter-Finch[196] employed a step gradient to effect the separation of pirimicarb and ten related compounds. However, two of the hydroxypyrimidines involved could not be resolved.

5.3. EXPERIMENTAL.

These investigations employed only a selection of the full range of compounds that were introduced in figure 5.1. Samples of Pirimicarb, R34836, R31805, and R34865 were kindly supplied by Zeneca Agrochemicals (Bracknell, UK). Stock solutions of each compound (1mg/ml) were prepared in methanol and stored in a refrigerator. Sample solutions for injection were prepared when required by diluting the stock solutions with the relevant separation media.

5.3.1. Separation by typical free solution CE.

All electropherograms were acquired using the Beckman P/ACE instrument. Separation capillaries comprised 46 cm lengths of 50 μm i.d. uncoated fused silica capillary. On-capillary UV detection was performed across a wavelength range of 190-300 nm using the in-built diode array detector at a distance of 40 cm from the inlet (L_d = 40 cm). All spectra were displayed at a wavelength of 245 nm.

Separation capillaries were equilibrated at the start of each working day and prior to changing separation media by flushing with sodium hydroxide (0.1 M, 20 PSI) for 5 minutes. Residual sodium hydroxide was removed by flushing with water (20 PSI) for 5 minutes. A two-stage equilibration was performed with the appropriate buffer which was first hydrodynamically pumped (20 PSI) for 5 minutes and then electrically driven (23 kV) for 5 minutes. Capillaries were rinsed using sodium hydroxide (20 PSI) for 2 minutes, water (20 PSI) for 2 minutes and finally air (20 PSI) for 1 minute at the end of each working day prior to careful storage.

Rinsing between replicate separations was accomplished with sodium hydroxide (0.1 M, 20 PSI) for 2 mins, water (20 PSI) for 1 minute and finally the relevant buffer (20 PSI) for two minutes. In addition, the first two separations of all investigation were ignored and not included in any subsequent data analysis.

Samples were hydrostatically injected (0.5 PSI) for 1 second. All separations were effected at an applied voltage of 23 kV (500 V/cm). Replicate injections of thiorea (0.1mg/ml from dilution of 1mg/ml stock with buffer) were performed at each buffer pH to facilitate the determination of the generated EOF.

A batch solution of separation buffer comprising 10mM sodium hydrogen phosphate prepared in purified (Milli-Q) water was filtered through a Whatman (Maidstone, UK) 0.45 μm PTFE filter. Phosphoric acid was added to several aliquots of this solution to yield a series of buffers covering a range of several pH units.

5.3.2. Separation by NACE

Feasibility trials were performed using the Beckman P/ACE instrument. To further explore method development in non-aqueous CE it was necessary to adjust the pH* of the separation media. A pH probe was used to determine such measurements. It is acknowledged that the validity of these measurements was questionable since the concept of pH does not strictly exist in non-aqueous systems as discussed in chapter 1. However, this strategy did provide a crude but effective means of manipulating separations. However, the non-aqueous media was found to corrode the plastic components of the pH probe during the course of these investigations.

The separation capillary was equilibrated at the start of each working day and prior to changing separation media by flushing with acetonitrile (20 PSI) for 5 minutes. A two-stage equilibration was performed with the appropriate buffer that was first hydrodynamically pumped (20 PSI) for 5 minutes and then electrically driven (23 kV) for 5 minutes. The capillary was rinsed using acetonitrile (20 PSI) for 2 minutes followed by air (20 PSI) for 1 minute at the end of each working day prior to careful storage.

The capillary was rinsed between replicate separations with acetonitrile (20 PSI) for 2 mins followed by the relevant buffer (20 PSI) for two minutes. In addition, the first two separations of all investigation were ignored and not included in any subsequent data analysis.

Samples were injected hydrostatically (0.5 PSI) for 3 seconds. All separations were effected at an applied voltage of 23 kV (500 V/cm). Replicate injections of thiorea (0.1mg/ml from dilution of 1mg/ml stock with buffer) were performed at each media pH* to facilitate the determination of the EOF.

5.3.3. Separation by MEKC.

All separations were effected at an applied voltage of 30 kV (500 V/cm) using the Thermo-Unicam instrument using a 60cm length of 50 μm i.d. uncoated fused silica capillary.

A second separation capillary was subsequently prepared in an identical fashion using a 60 cm length of 75μm i.d fused silica capillary. Detection windows for both capillaries were located at a distance of 44 cm from the inlet end (L_d = 44 cm). All UV detection was performed at a wavelength of 245 nm.

The separation capillary was equilibrated at the start of each working day and prior to changing separation media by flushing with sodium hydroxide (0.1 M, 2000 mbar) for 5 minutes. Residual sodium hydroxide was removed by flushing with water (2000 mbar) for 5 minutes. A two-stage equilibration was performed with the appropriate micellar buffer which was first hydrodynamically pumped (2000 mbar) for 5 minutes and then electrically driven (30 kV) for 5 minutes. The capillary was rinsed using sodium hydroxide (2000 mbar) for two minutes followed by water (2000 mbar) for 2 minutes at the end of each working day prior to careful storage.

The capillary was rinsed between replicate separations with sodium hydroxide (0.1 M, 2000 mbar) for 2 mins, water (2000 mbar) for 1 minute and finally the relevant buffer (2000 mbar) for two minutes. In addition, the first two separations of all investigation were ignored and not included in any subsequent data analysis.

The initial micellar buffer comprised 10 mM sodium tetraborate and 50 mM SDS which was adjusted to pH 9.2 (NaOH 0.1 M) and filtered through a Whatman (Maidstone, UK) 0.45 μm PTFE filter prior to use.

5.4. SEPARATION BY CZE.

The test compounds contain basic nitrogen-containing functionalities. It was therefore presumed that a simple CE separation performed at low pH would be capable of effecting a separation. Unfortunately, pKa data were not available for the test compounds.

A partial separation was achieved at pH 3.14. Baseline separation was achieved between the first two compounds whilst the latter two peaks eluted together as a single peak. Comparison of peak spectra with those stored in the spectral library confirmed the elution order as R34865 followed by R31805 and finally pirimicarb eluting with R34836. Migration time repeatability for R34865 and R31805 was comparable with typical HPLC separations (2.0 and 1.7% RSD respectively). A representative separation under these conditions is presented in figure 5.2.

Figure 5.2 Separation of pirimicarb from 3 related metabolites at 23 kV using 10mM sodium hydrogen phosphate (pH 3.14).

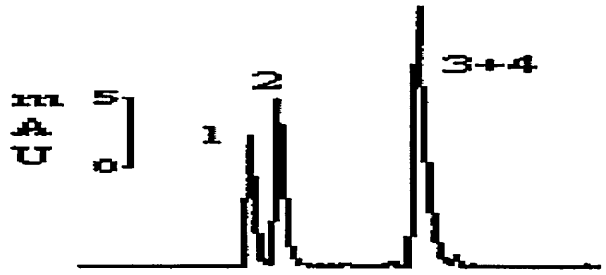

		Average t_m (min)	N (plates/m)	% RSD t_m (n=3)
1	R34865	5.460	60300	2.0
2	R31805	5.740	28000	1.7
3	R34836/ Pirimicarb	6.279	-	-

It was anticipated that pirimicarb and R34836 could be resolved by lowering the pH of the buffer. However, further reduction to pH 2.14 had no effect on the unresolved pair The separation between R31805 and R34865 was poorer than had been achieved at pH 3.14. A representative separation under these conditions is presented in figure 5.3. The expanded view of the electopherogram clearly shows the detrimental effect that lowering the pH had on the separation between R31805 and R34865.

Figure 5.3 Separation of pirimicarb and 3 related metabolites at 23 kV using a buffer comprising 10mM sodium hydrogen phosphate (pH 2.14).

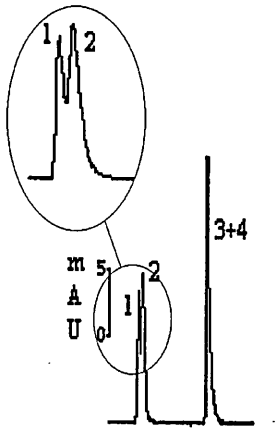

		Average t_m (min)	% RSDt_m (n=3)
1	R34865	6.304	1.8
2	R31805	6.350	1.9
3	R34836/ Pirimicarb	7.200	-

Separation of pirimicarb from R34836 could not be effected by using buffers at intermediate pH values or via the addition of organic modifiers or increasing the electrolyte concentration.

5.5. SEPARATION BY NACE.

The cimetidine separations presented in chapter 3 appeared to be based upon protonation of nitrogen-containing basic functionalities by the non-aqueous media. It was therefore anticipated that a full separation of the pesticide compounds could be effected in a similar fashion.

An initial separation using 70/30 %v/v acetonitrile/methanol containing 25 mM ammonium acetate and 1% v/v acetic acid (pH* 6.93) resulted in an incomplete separation of the four test compounds. The elution order was confirmed as R31805 followed by pirimicarb and R34836 which eluted as a single peak and finally R34865. The latter peak eluted after the EOF marker which was somewhat confusing.

It was anticipated that the initial separation could be improved via systematic reduction of pH* using increased levels of acetic acid. A significant volume of acetic acid was required to effect a notable reduction in pH*. The elution order remained constant over the pH* range studied but no significant improvement in separation was achieved. The dependence of the electrophoretic mobility of each compound on the pH* of the non-aqueous media is presented in figure 5.4.

Figure 5.4 Dependence of the electrophoretic and electroosmotic mobilities of pirimicarb and 3 related metabolites on the pH* of the non-aqueous separation media.

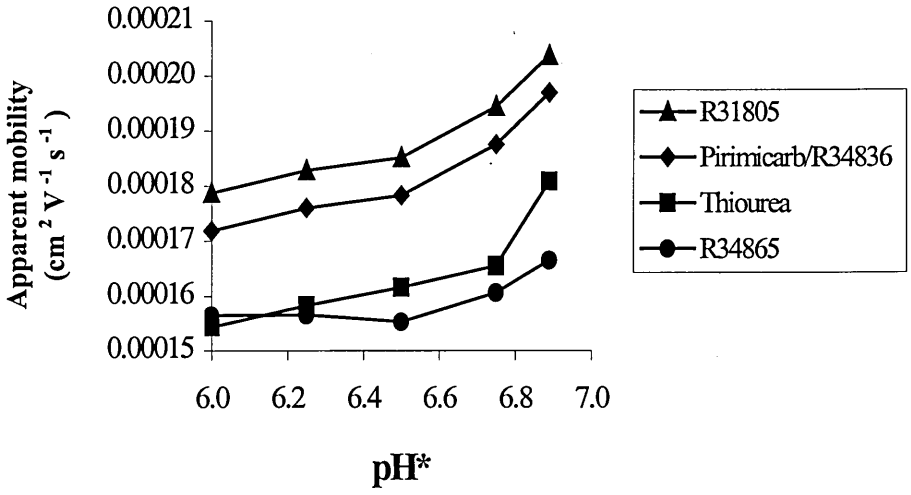

The EOF appeared to reduce in magnitude linearly with decreasing pH* apart from an abrupt drop when the pH* of the initial stock media was first adjusted. The magnitude of the EOF was slower than in the initial media at equivalent pH*. This supports previous findings regarding the EOF reducing with increasing methanol composition. It is interesting to note the behaviour of R34865 as pH* was reduced. In most studies it eluted after the EOF marker as previously discussed. However, at the lower levels of pH* studied it migrated ahead of the EOF. Migration time repeatabilities varied considerably throughout these studies but were better than 1.0% RSD in all cases. Representative separations under all conditions studied are presented in figure 5.5.

Figure 5.5 Separation of pirimicarb and 3 related metabolites at 23 kV using non-aqueous media comprising 70/30 %v/v acetonitrile/methanol containing 25mM ammonium acetate and various levels of acetic acid to yield a series of pH* values.

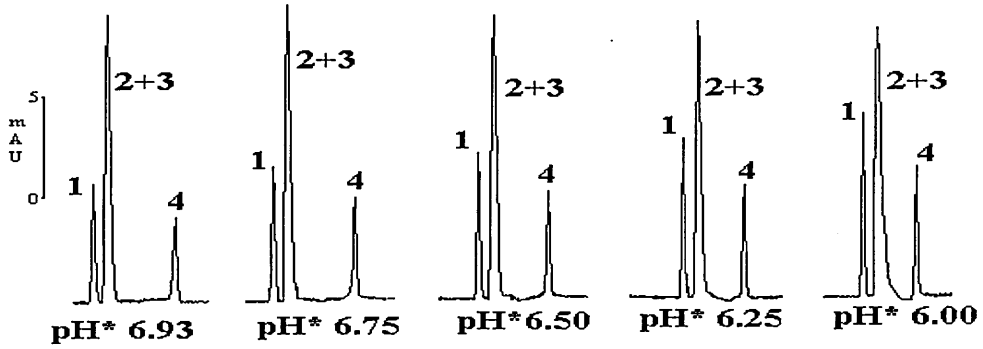

	Average tm (min) and repeatability over 3 replicate injections (%RSD)		
	R31805 1	Pirimicarb & R34836 2+3	R34865 4
6.93	6.547 (0.21)	6.772 (0.20)	8.008 (0.27)
6.75	6.857 (0.88)	7.110 (0.94)	8.301 (1.05)
6.50	7.203 (0.21)	7.482 (0.20)	8.590 (0.24)
6.25	7.296 (0.32)	7.579 (0.29)	8.517 (0.34)
6.00	7.463 (0.41)	7.762 (0.38)	8.525 (0.43)

The influence of solvent composition was studied in a similar fashion using media comprising 50/50 and 90/10 % v/v acetonitrile/methanol. The pH* of the initial (unadjusted) media was found to be dependant on solvent composition. Media comprising a greater proportion of acetonitrile was of higher pH*.

Elution order in 50/50 %v/v media was identical to that in the 70/30 v/v media. The EOF and the apparent mobilities of R31805, pirimicarb and R34836 reduced in a linear fashion with decreasing pH*. In contrast, the apparent mobility of R34865 increased slightly with decreasing pH* whilst still eluting after thiourea. The dependance of the electrophoretic mobility of each compound on the pH* of the non-aqueous media is presented in figure 5.6.

Figure 5.6 Dependence of the electrophoretic and electroosmotic mobilities of pirimicarb and 3 related metabolites on the pH* of the non-aqueous separation media.

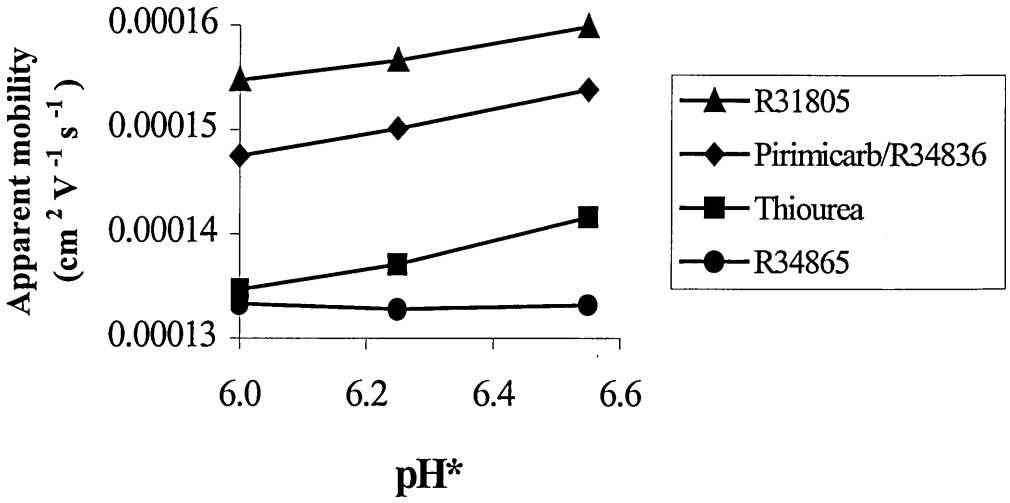

Reduction of pH* did not improve the separation which was poorer than in 70/30 % v/v acetonitrile/methanol. The band comprising pirimicarb and R34836 exhibited significant tailing. This was especially true at the lower values of pH* studied as shown in figure 5.7. However, migration time repeatabilities were more consistent than those achieved in the initial 70/30 % v/v media.

R34865 merged with pirimicarb and R34836 in the 90/10 % v/v acetonitrile/methanol media to yield an extremely broad peak that eluted at a time equivalent to thiourea. A representative separation is presented in figure 5.8. No performance data (repeatabilies etc) were reported since the separation was so poor.

Figure 5.7. Separation of pirimicarb from 3 related metabolites at an applied voltage of 23 kV using non-aqueous media comprising 50/50 % v/v acetonitrile/methanol containing 25mM ammonium acetate and various levels of acetic acid to yield a series of pH* values.

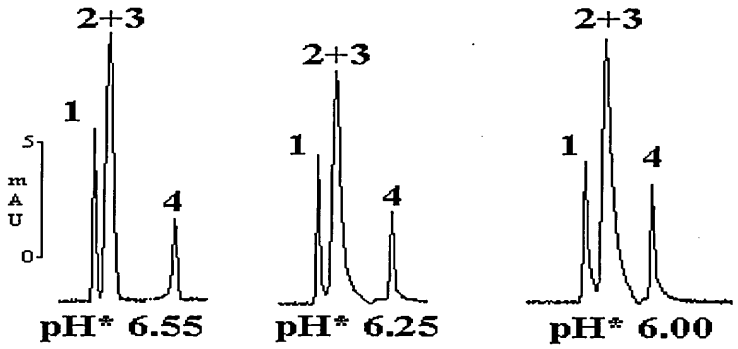

	Average tm (min) and repeatability over 3 replicate injections (%RSD)		
	R31805 1	Pirimicarb & R34836 2+3	R34865 4
6.55	8.337 (0.34)	8.667 (0.29)	9.417 (0.31)
6.25	8.512 (0.28)	8.883 (0.28)	10.042 (0.26)
6.00	8.617 (0.25)	9.042 (0.31)	10.004 (0.29)

Figure 5.8 Separation of pirimicarb from 3 related metabolites at an applied voltage of 23 kV using non-aqueous media comprising 90/10 % v/v acetonitrile/methanol containing 25mM ammonium acetate and various levels of acetic acid to yield a series of pH* values.

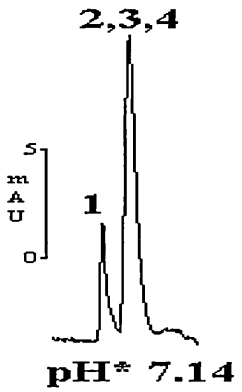

5.6. SEPARATION BY MEKC.

The initial micellar buffer comprised 10 mM sodium tetraborate and 50 mM SDS which was adjusted to pH 9.2 (NaOH 0.1 mol/dm^3). The 4 test compounds eluted in order of increasing hydrophobicity. The elution order was confirmed as R34865 followed by R31805, R34836 and pirimicarb. The separation between R34865 and R31805 was extremely poor. The achieved resolution was estimated to be 0.7 using the peak height valley method that was introduced in chapter 1. These two compounds were barely retained eluting just after t_o (t_o was determined from the baseline disturbance caused by the methanol in the sample solutions). All compounds were eluted in around 5 minutes and migration time reproducibility was found to be better than 0.5% for all 4 compounds. A representative separation under these conditions is presented in figure 5.9.

Figure 5.9 Separation of pirimicarb from 3 metabolites achieved at an applied voltage of 30 kV using a micellar buffer comprising 10 mM sodium tetraborate and 50 mM SDS.

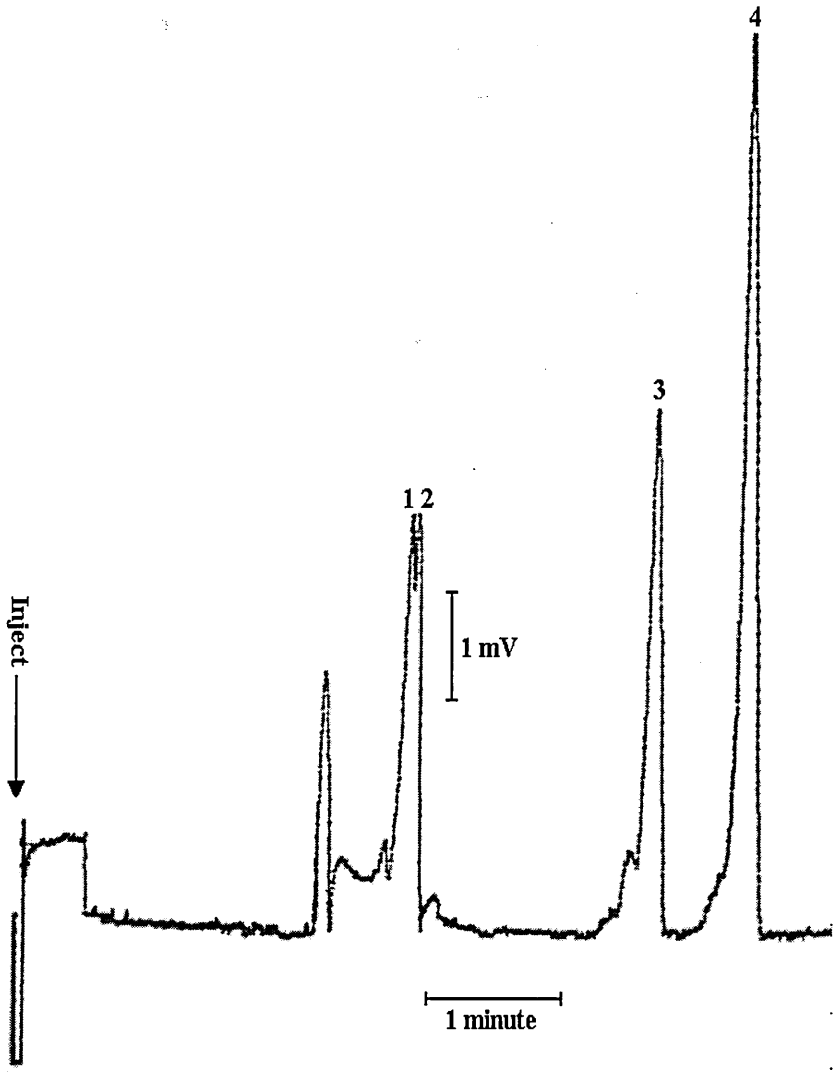

		Average t_m (min)	N (plates/m)	% RSD t_m (n=5)
1	R34865	2.843	-	0.39
2	R31805	2.866	-	0.46
3	R34836	4.542	83000	0.18
4	Pirimicarb	5.191	73000	0.20

The SDS concentration was subsequently increased to 75 mM in order to enhance retention within the micellar phase and improve the separation between R34865 and R31805. The resolution between R34865 and R31805 was enhanced ($R_{estimated}$ = 0.86) but the separation between these two bands was still unsatisfactory.

Migration time reproducibilities were noticeably poorer than those achieved at 50 mM SDS but were still less than 1.0% RSD for all compounds. A representative separation is presented in figure 5.10.

Figure 5.10 Separation of pirimicarb from 3 metabolites achieved at an applied voltage of 30 kV using a micellar buffer comprising 10 mM sodium tetraborate and 75 mM SDS.

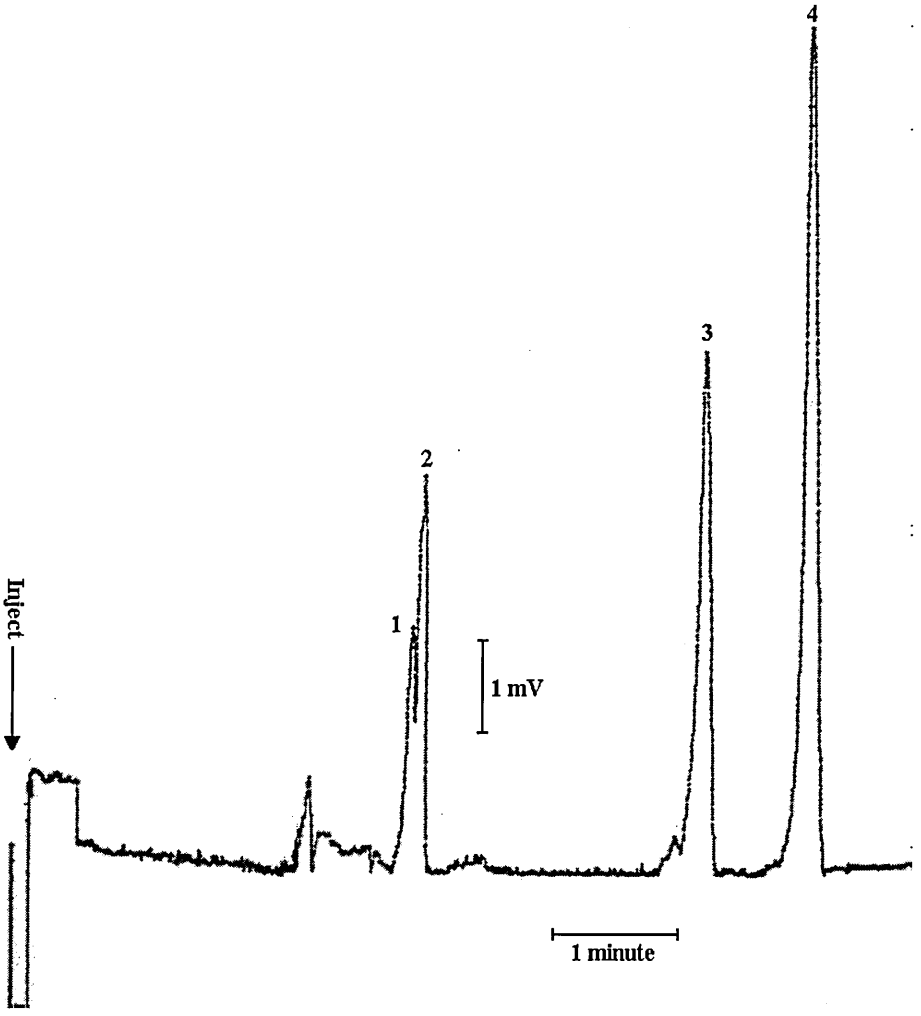

		Average t_m (min)	N (plates/m)	% RSD t_m (n=5)
1	R34865	3.133	-	0.81
2	R31805	3.222	-	0.74
3	R34836	5.416	105000	0.78
4	Pirimicarb	6.224	110000	0.68

The surfactant concentration was further increased to 100 mM. Retention was again increased as was the separation between R34865 and R31805 was further enhanced ($R_{estimated}$ = 0.99). A representative separation obtained under these conditions is presented in figure 5.11.

Figure 5.11. Separation of pirimicarb from 3 metabolites achieved at an applied voltage of 30 kV using a micellar buffer comprising 10 mM sodium tetraborate and 100 mM SDS.

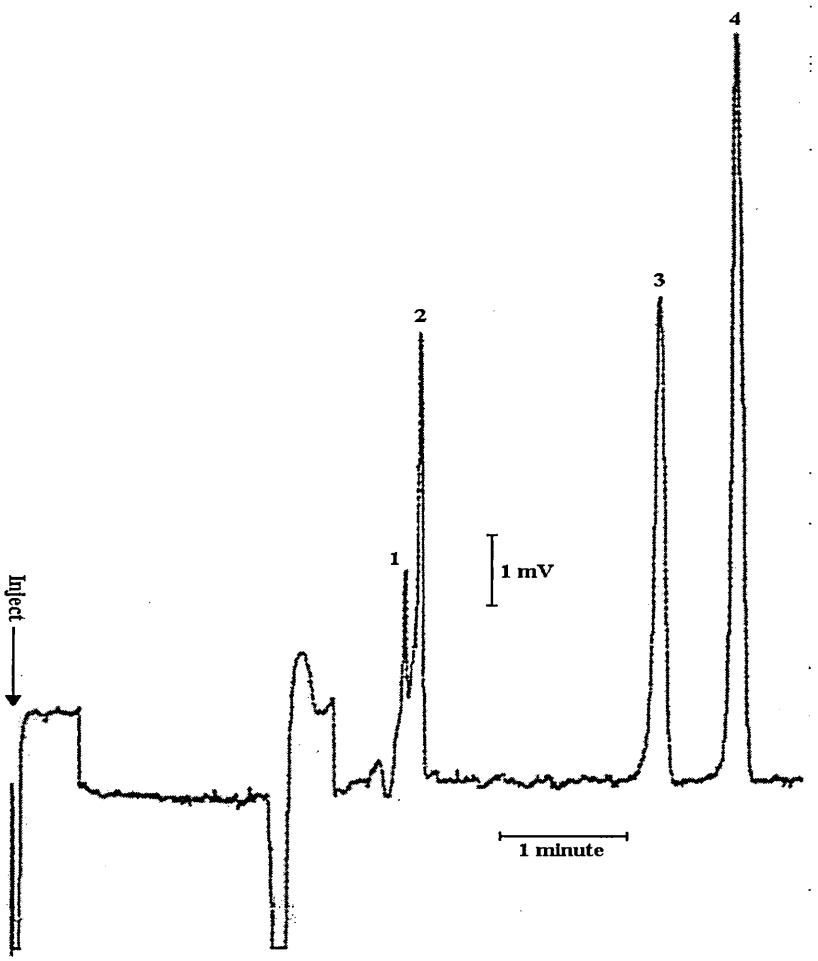

		Average t_m (min)	N (plates/m)	% RSD t_m (n=5)
1	R34865	2.976	-	0.24
2	R31805	3.095	-	0.24
3	R34836	4.893	112000	0.25
4	Pirimicarb	5.457	140000	0.15

Baseline resolution of R34865 and R31805 was accomplished at an SDS concentration of 125 mM. Elution of all compounds was complete in around 7 minutes and the repeatability of elution time was less than 0.5% RSD for all compounds over a series of 5 replicate injections. Peak efficiencies were rather impressive. A representative separation is presented in figure 5.12.

Figure 5.12 Separation of pirimicarb from 3 metabolites achieved at an applied voltage of 30 kV using a micellar buffer comprising 10 mM sodium tetraborate and 125 mM SDS.

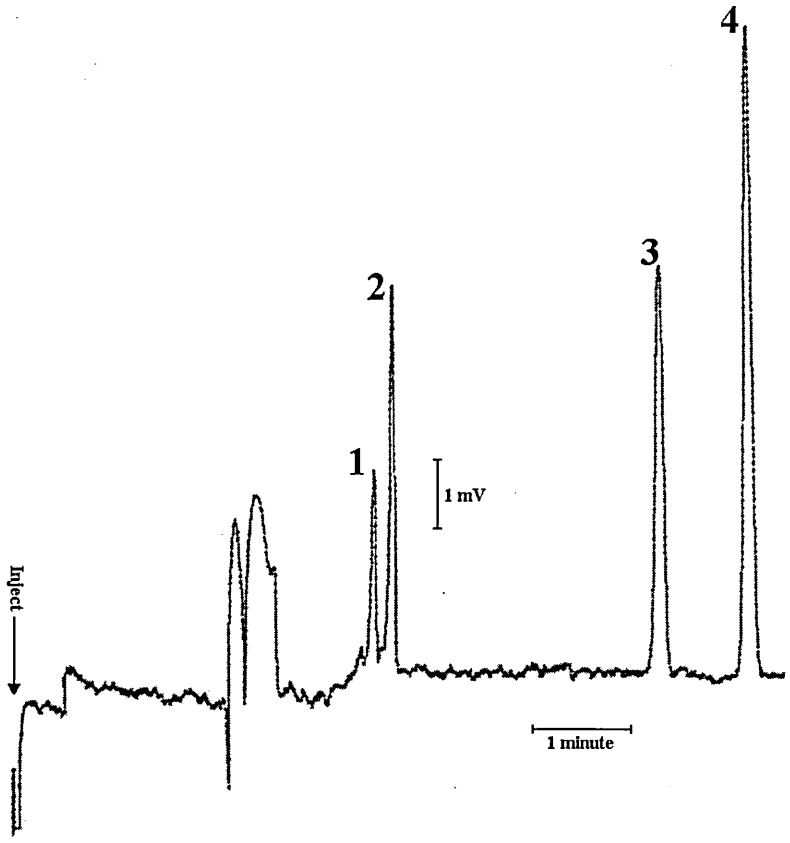

		Average t_m (min)	N (plates/m)	% RSD t_m (n=5)
1	R34865	3.505	298500	0.38
2	R31805	3.687	285000	0.40
3	R34836	6.286	156000	0.34
4	Pirimicarb	7.130	191500	0.40

No fluctuation or breakdown of current was experienced during these investigations. However an Ohms law plot of the measured current at each SDS concentration did display slight curvature as shown in figure 5.13.

Figure 5.13 Ohms law plot of current generated at an applied voltage of 30 kV for each SDS concentration studied.

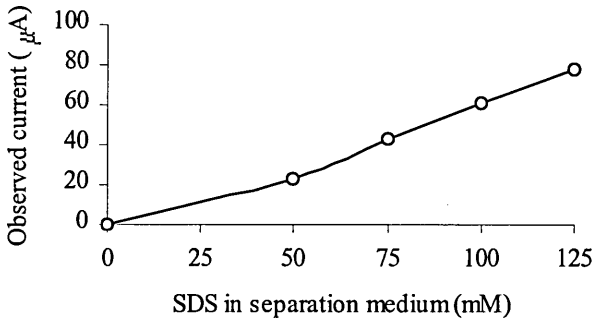

The curvature exhibited by the Ohms law plot may be indicative of Joule heating effects. This would certainly account for the poorer quality baselines that were experienced when employing micellar buffers containing high levels of SDS.

The relatively small peak obtained for R34865 suggested that the detection limits of a routine method based on these investigations would be restricted. A brief attempt was made to enhance detection limits by increasing the internal diameter (and hence detection pathlength) of the capillary to 75 μm. The resulting current was in excess of 200 μm and after several extremely erratic baselines were obtained the investigation was abandoned. It is presumed that a stable baseline could not be acquired due to significant Joule heating produced by the excessive current.

5.7. CONCLUSION.

Simple free solution CE employing typical aqueous-based buffers was incapable of effecting a full separation. Selectivity was again found to be different from the non-aqueous separations. However, a common theme existed in the sense that neither environment was capable of resolving R34836 from pirimicarb but could resolve R31805 from R34865. Both pairs have almost identical structures, differing only by a single methyl group in each case.

The most interesting and intriguing observation in the non-aqueous separation was that R34865 eluted after the EOF marker. This presumably implied either R34865 carried a negative charge or thiourea had become protonated within the non-aqueous media. The former theory seems unfeasible due to the apparently acidic environment involved and the fact that R34865 did not behave in a similar fashion to R31805 which only differs structurally by a methyl group. The latter theory has potentially serious consequences for the use of typical EOF marker compounds in non-aqueous media and possibly invalidates some of the previously presented EOF figures. This area was subsequently investigated in a more thorough and systematic fashion. Experimental details and discussions are presented in chapter 6.

The MEKC method seems extremely promising as it stands and it is unfortunate that the full series of metabolites were not available for further method evaluation. Issues concerning detection limits were not resolved but could presumably be addressed via some form of sample pre-concentration

Chapter 6.

FURTHER INVESTIGATION OF NON-AQUEOUS MEDIA.

6.1. INTRODUCTION.

The studies involving cimetidine (chapter 4) indicated that non-aqueous media offered great potential for CE separations. However, method development had been hindered by a lack of fundamental knowledge. A systematic study was therefore undertaken to determine the interrelationships between method variables and their effect on both the EOF and resulting separation. Additionally, previously encountered incidents of poor day to day repeatability and erratic behaviour when attempting to perform NACE on the Beckman instrument were further explored.

6.2. MATERIALS AND METHODS.

6.2.1. Investigation of day to day repeatability.

The influence of the purity and age of ammonium acetate on the magnitude and repeatability of the EOF generated in non-aqueous media was investigated using three commercially available grades of purity. The grades studied were: 99.999 % and 99.99+ % (both Aldrich, Poole, UK) and HPLC grade Fisons (Loughborough, UK). The latter was nearing the manufacturers expiry date and exhibited a strong odour of acetic acid.

6.2.2. Systematic investigation of the parameters controlling the separation in non-aqueous media.

The ammonium acetate, ammonium formate and sodium acetate employed in these studies was 99.99+ % (Aldrich, Poole, UK).

6.3. EXPERIMENTAL PROCEDURES.

All separations were performed using the Crystal CE system. Separation capillaries comprised 60 cm lengths of 50 μm i.d. uncoated fused silica capillary. Unless otherwise stated, all on-capillary absorbance detection was performed at a wavelength of 254 nm at a distance of 44 cm from the inlet (L_d = 44 cm).

Stock solutions (1000 mg/l) of biphenyl and thiourea were prepared in acetonitrile. Working standards comprising both compounds (each 100mg/l) were prepared as required via dilution of the stock solutions with the non-aqueous media under investigation. All samples were hydrostatically injected (25 mbar) for 0.1 min.

The separation capillary was equilibrated at the start of each working day and prior to changing separation media by flushing with sodium hydroxide (0.1 M, 2000 mbar) for 5 minutes. Residual sodium hydroxide was removed by flushing with acetonitrile (2000 mbar) for 5 minutes. A two-stage equilibration was performed with the appropriate non-aqueous medium which was first hydrodynamically pumped (2000 mbar) for 5 minutes and then electrically driven (20 kV) for 5 minutes. The capillary was rinsed using acetonitrile (2000 mbar) for 5 minutes at the end of each working day prior to careful storage.

The various non-aqueous media studied were prepared via the addition of acetic acid and an electrolyte to mixtures of acetonitrile and methanol. More detailed descriptions of compositions are given in the individual experimental sections.

6.4. INVESTIGATION OF DAY TO DAY REPEATABILITY.

Ammonium acetate is commercially available in a range of grades. It is a hygroscopic material that hydrolyses upon exposure to air. A "wet" appearance and a change from a slight ammonia-like odour to the characteristic smell of acetic acid readily indicate this process. Hydrolysis was identified as a potential root cause of the poor day to day repeatability and breakdown of EOF that had been experienced in previous work.

Separation media comprising 70/30 % v/v acetonitrile/methanol containing 1% v/v acetic acid and 25 mM ammonium acetate was prepared using each of the three grades. The repeatability of the EOF generated in each media was determined via five replicate injections of the thiourea working standard. In addition, the pH* of each media was determined for reference using a pH meter.

The ultrapure 99.999% grade generated the fastest EOF but the repeatability over the five injections was the poorest of the three. The observed current was slightly higher in the HPLC grade which may have been a consequence of the higher level of impurities present. No breakdown of electrical current was experienced during any of the studies. The results are summarised in table 6.1.

Table 6.1 Comparison of non-aqueous media prepared from three different grades of ammonium acetate.

Purity	99.999 %	99.99 %+	HPLC
pH*	6.63	6.50	6.75
Current (μA)	14.6	14.8	16.2
Mean t_m (min)	2.920	3.376	3.701
Apparent mobility ($cm^2 s^{-1} V^{-1}$)	0.000502	0.000435	0.000396
Repeatability (% RSD)	2.39	0.74	0.38

The investigation was repeated a week later with freshly prepared media to assess day to day repeatability. Migration times were higher than those of the original study. The solutions were carefully prepared in an identical fashion and hence analyst error was not considered to be a major contributing factor. In addition, the repeatability of the EOF in the media employing 99.99+ % ammonium acetate had improved significantly as shown in table 6.2.

Table 6.2 Investigation of day to day repeatability.

Purity	99.999%	99.99%+	HPLC
pH*	6.75	6.96	6.60
Current (μA)	14.2	15.3	15.1
Mean t_m (min)	3.049	3.545	3.844
Apparent mobility ($cm^2 s^{-1} V^{-1}$)	0.000481	0.000414	0.000382
Repeatability (% RSD)	2.41	0.09	0.45

Measured pH* values and hence apparent mobilities were noticeably different (particularly the 99.99%+ grade) compared to the original study even though all media was prepared in an identical fashion. There was no obvious relationship between ammonium acetate purity and pH* of the resulting media.

6.5. INVESTIGATION OF THE PARAMETERS CONTROLLING THE SEPARATION IN NON-AQUEOUS MEDIA.

A range of non-aqueous media were prepared in which the identity and concentration of the background electrolyte, pH* and solvent composition were varied. The apparent charged nature of thiourea that was observed during the pirimicarb separations was of great interest. This was further explored by employing a mixed working standard comprising thiourea and biphenyl. The inclusion of biphenyl also ensured that an accurate EOF could be determined for each media studied.

The EOF generated at each composition was determined via five replicate injections of the working biphenyl and thiourea standard. In addition, all values of pH* and generated current were recorded.

6.5.1. Effect of varying the concentration of ammonium acetate.

Five aliquots of non-aqueous media were prepared comprising 70/30 % v/v acetonitrile/methanol containing 1% v/v acetic acid and ammonium acetate (1, 5, 10, 25, 50 mM respectively). The apparent mobilities of both biphenyl and thiourea were found to decrease with increasing ammonium acetate concentration as shown in figure 6.1. This again clearly conflicted with the initial studies in non-aqueous media (chapter 3) where the EOF increased with increasing ammonium acetate concentration.

Figure 6.1 Influence of ammonium acetate concentration on the apparent mobilities of biphenyl and thiourea in 70/30 % v/v acetonitrile/methanol containing 1% v/v acetic acid at an applied voltage of 30 kV.

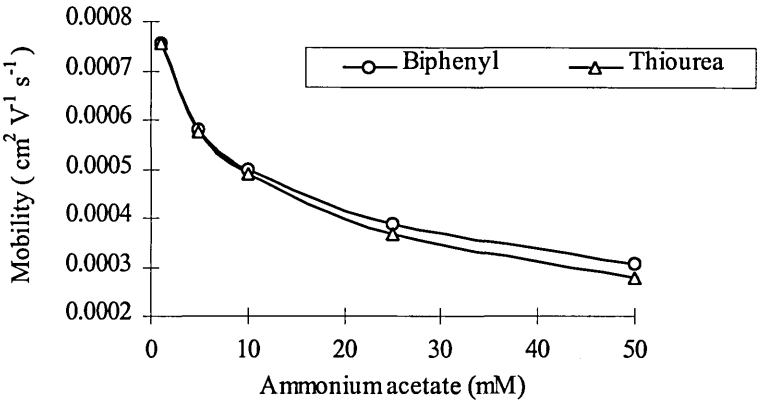

The most interesting observation was the appearance of a split peak at an ammonium acetate concentration of 5 mM. This was more pronounced when the ammonium acetate in the media was increased to 10 mM. At a concentration of 25 mM two overlapping peaks were evident ($R_{estimated}$ = 1.07). Injection of individual working standards confirmed the two peaks to be biphenyl and thiourea respectively. These observations confirmed previous incidents in which thiourea had appeared to carry a negative charge. Baseline separation of the two compounds was effected at an ammonium acetate concentration of 50 mM. The resolution between the pair of peaks was calculated (equation 2.3) to be 4.56. A representative separation is shown in figure 6.2.

Figure 6.2 Separation achieved between biphenyl and thiourea in 70/30 % v/v acetonitrile/methanol containing 50 mM ammonium acetate and 1 % v/v acetic acid at an applied voltage of 30 kV.

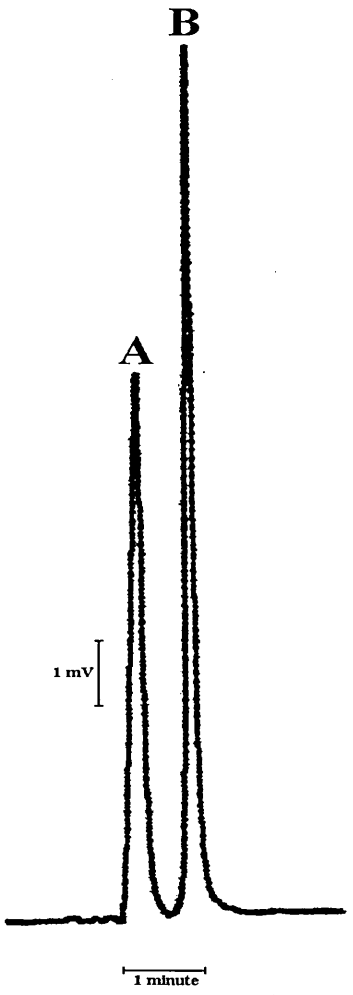

		N (plates/m)
A	Biphenyl	45500
B	Thiourea	133800

Migration time repeatabilities were all below 0.40% RSD and did not exhibit any obvious dependence on the ammonium acetate concentration as shown in table 6.3.

Table 6.3 Average migration times and associated repeatabilities for 5 replicate injections of biphenyl and thiourea.

	Average t_m(min)		Repeatability (%RSD)	
Ammonium acetate (mM)	Biphenyl	Thiourea	Biphenyl	Thiourea
1	1.946	1.946	0.13	0.13
5	2.532	2.551	0.25	0.23
10	2.940	3.001	0.34	0.33
25	3.774	3.980	0.12	0.11
50	4.772	5.278	0.23	0.21

Both the observed current and pH* of the resulting media were found to increase with increasing concentrations of ammonium acetate as illustrated in figures 6.3 and 6.4 respectively.

Figure 6.3 Influence of ammonium acetate concentration on the current generated at an applied voltage of 30 kV.

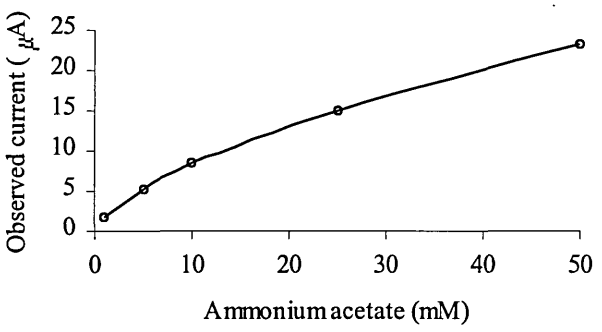

Figure 6.4 Influence of ammonium acetate concentration on the pH* of the resulting non-aqueous media.

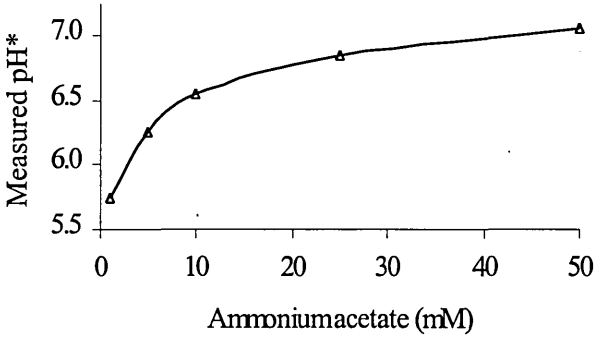

6.5.2. Investigation of the role played by acetic acid in the non-aqueous medium I: Exclusion of acetic acid.

Five aliquots of non-aqueous media were prepared comprising 70/30 % v/v acetonitrile/methanol containing ammonium acetate (1, 5, 10, 25, 50 mM respectively). No acetic acid was added to any of the media.

The apparent mobilities of both biphenyl and thiourea were found to decrease with increasing ammonium acetate concentration in a similar fashion to the previous investigation. However, mobilities and hence migration times were found to be faster than those of equivalent acid-containing media in the first investigation as shown in figure 6.5.

Figure 6.5 Influence of ammonium acetate concentration on the apparent mobilities of biphenyl and thiourea in 70/30 % v/v acetonitrile/methanol at an applied voltage of 30 kV.

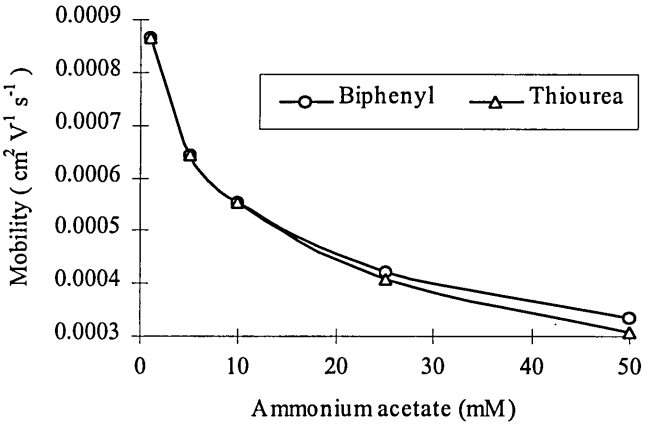

Evidence of the previously described migration behaviour of thiourea was not apparent until an ammonium acetate concentration of 25 mM. The resolution between the two peaks at 50 mM was calculated to be 2.69, approximately half that of the original study. Similarly, peak efficiencies were also approximately half those achieved in equivalent acid-containing media. A representative electropherogram and associated data are provided in figure 6.6.

Figure 6.6 Separation achieved between biphenyl and thiourea in 70/30 % v/v acetonitrile/methanol containing 50 mM ammonium acetate at an applied voltage of 30 kV.

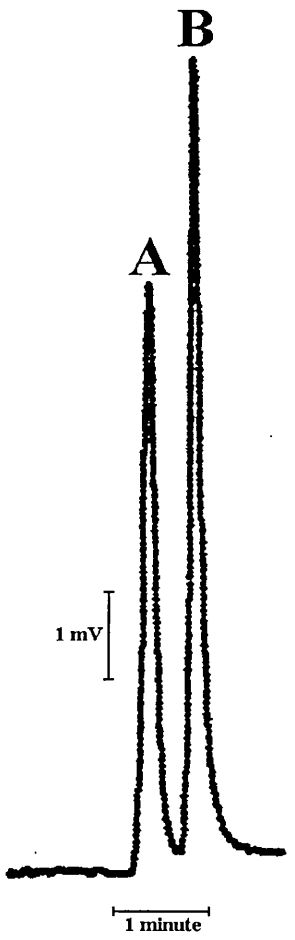

		N (plates/m)
A	Biphenyl	22500
B	Thiourea	75250

As anticipated, the current was again found to increase with increasing ammonium acetate (figure 6.7). Measured currents in this study were lower than equivalent acid-containing media whereas pH* was generally found to be 1-2 units higher. Values varied over a range of 0.25 units with no obvious dependency on the level of ammonium acetate as shown in figure 6.8.

Figure 6.7 Influence of ammonium acetate concentration on the current generated at an applied voltage of 30 kV.

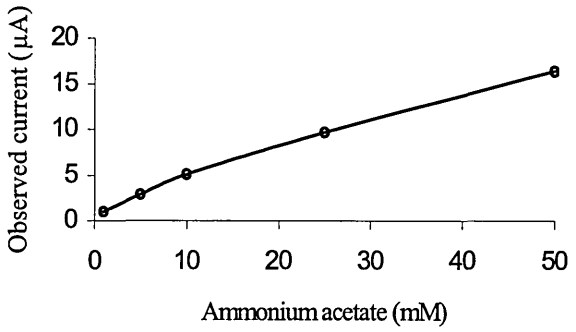

Figure 6.8 Influence of ammonium acetate concentration on the pH* of the resulting non-aqueous media.

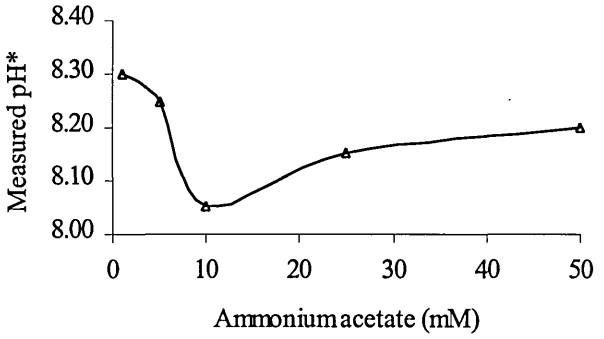

Migration time repeatabilities were found to vary to a greater extent than equivalent acid-containing media but were all below 1% RSD. Again, the data did not exhibit any obvious dependence on the concentration of ammonium acetate as shown in table 6.4.

Table 6.4 Average migration times and associated repeatabilities for 5 replicate injections of biphenyl and thiourea.

	Average t_m(min)		Repeatability (%RSD)	
Ammonium acetate (mM)	Biphenyl	Thiourea	Biphenyl	Thiourea
1	1.696	1.696	0.29	0.29
5	2.277	2.277	0.27	0.27
10	2.654	2.654	0.03	0.03
25	3.467	3.612	0.15	0.15
50	4.398	4.777	0.92	0.84

6.5.3. Investigation of the role played by acetic acid in the non-aqueous medium II: Decreasing pH* via the addition of increased levels of acid.

Six aliquots of non-aqueous media were prepared comprising 70/30 % v/v acetonitrile/methanol containing 25 mM ammonium acetate and acetic acid (1, 2, 3, 4, 5 and 10% v/v respectively).

Apparent mobilities and hence migration times were significantly slower than obtained in the two previous studies as shown in figure 6.9.

Figure 6.9 Influence of acetic acid concentration on the apparent mobilities of biphenyl and thiourea in 70/30 % v/v acetonitrile/methanol containing 25 mM ammonium acetate at an applied voltage of 30 kV.

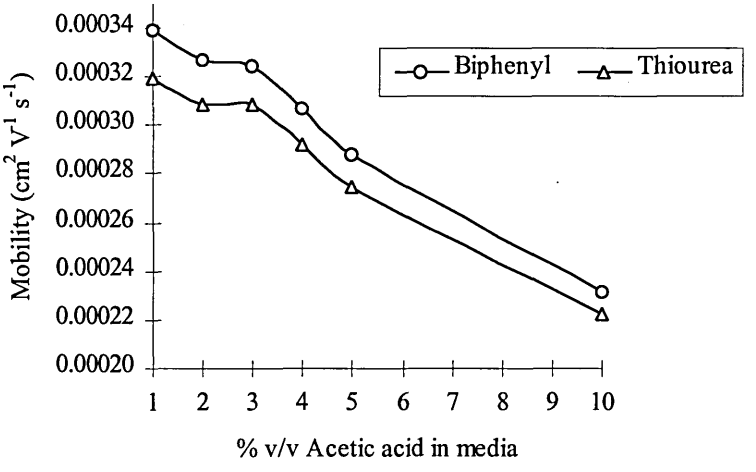

Two overlapping peaks corresponding to biphenyl and thiourea respectively were observed at all acid concentrations studied. The difference in migration times (Δt_m) between these two peaks was essentially constant over the range of acid concentrations studied. A representative electropherogram that was generated at an acid concentration of 10% v/v is shown in figure 6.10. Efficiencies were not determined due to the significant overlap of the two peaks.

Figure 6.10 Separation achieved between biphenyl and thiourea in 70/30 % v/v acetonitrile/methanol containing 50 mM ammonium acetate and 10% v/v acetic acid at an applied voltage of 30 kV.

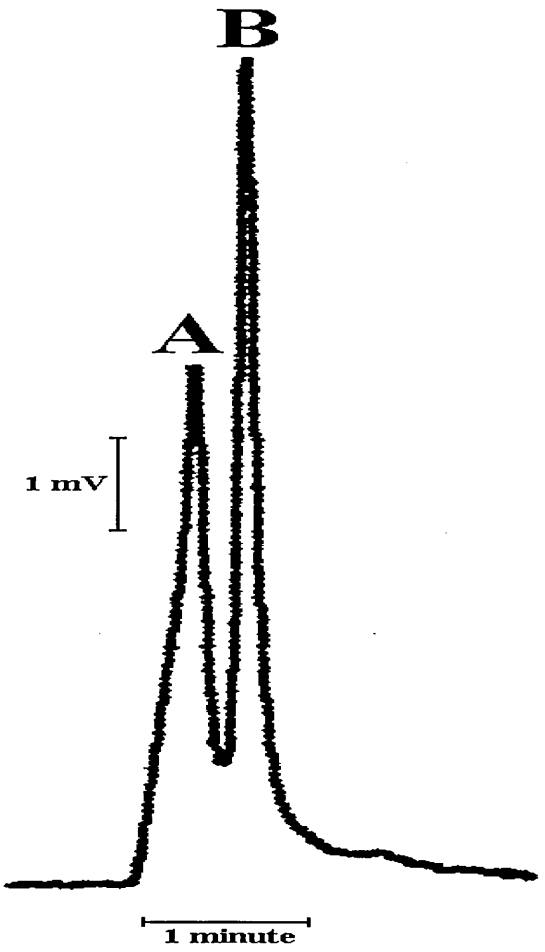

A	Biphenyl
B	Thiourea

The separation between the pair was determined to decrease with increasing acid concentration as shown in figure 6.11. In contrast, peak efficiencies were found to increase at enhanced levels of acidity as shown in figure 6.12.

Figure 6.11 Influence of acetic acid concentration on the resolution achieved between biphenyl and thiourea in 70/30 % v/v acetonitrile/methanol containing 25 mM ammonium acetate at an applied voltage of 30 kV.

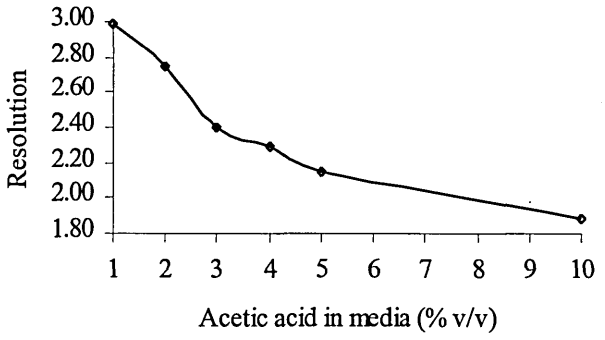

Figure 6.12 Influence of acetic acid concentration on the efficiencies of biphenyl and thiourea in 70/30 % v/v acetonitrile/methanol containing25 mM ammonium acetate at an applied voltage of 30 kV.

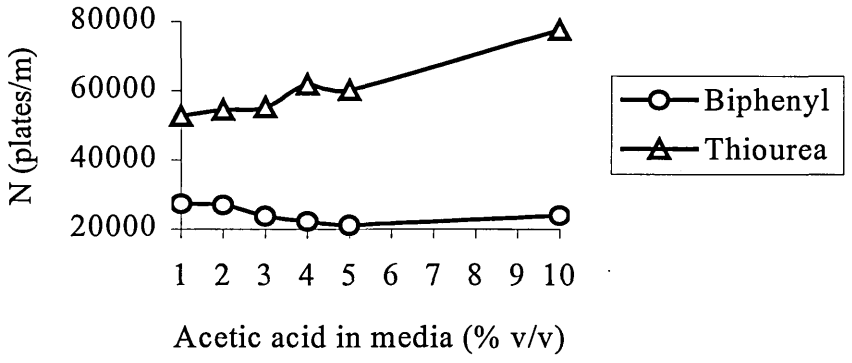

The observed current was first found to increase but then reduce at higher acid concentrations as shown in figure 6.13. As anticipated, the measured pH* was determined to decrease as the concentration of acetic acid in the media was increased as shown in figure 6.14.

Figure 6.13 Influence of acetic acid concentration on the current generated at an applied voltage of 30 kV.

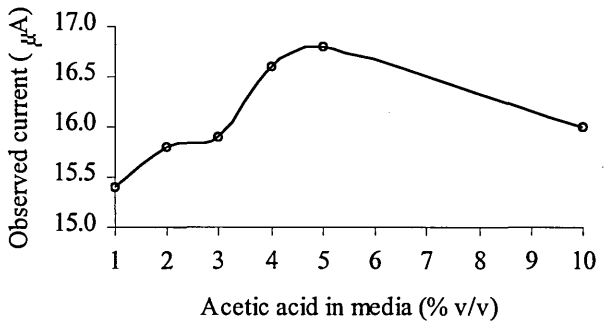

Figure 6.14 Influence of acetic acid concentration on the pH* of the resulting non-aqueous media.

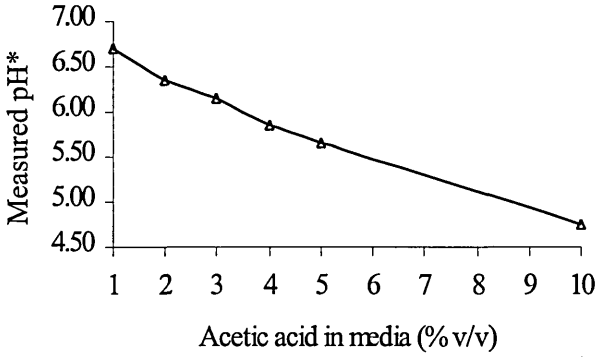

Migration time repeatabilities were all below 0.6 % RSD but showed no dependency on the acid concentration as shown in table 6.5. It is interesting to note that the mean migration times at an acetic acid concentration of 1% v/v were some 0.5 minutes higher than those obtained under apparently identical conditions (table 6.3).

Table 6.5 Average migration times and associated repeatabilities for 5 replicate injections of biphenyl and thiourea.

	Average t_m(min)		Repeatability (%RSD)	
Acetic acid (% v/v)	Biphenyl	Thiourea	Biphenyl	Thiourea
1	4.327	4.604	0.40	0.41
2	4.487	4.749	0.34	0.36
3	4.520	4.758	0.11	0.11
4	4.782	5.022	0.16	0.16
5	5.092	5.336	0.53	0.51
10	6.344	6.588	0.58	0.56

6.5.4 Investigation of an alternative background electrolyte: Ammonium formate.

Five aliquots of non-aqueous media were prepared comprising 70/30 % v/v acetonitrile/methanol containing 1% v/v acetic acid and ammonium formate (1, 5, 10, 25, 50 mM respectively. The apparent mobilities of both biphenyl and thiourea were found to reduce as the concentration of background electrolyte was increased as shown in figure 6.15.

Figure 6.15 Influence of ammonium formate concentration on the apparent mobilities of biphenyl and thiourea in 70/30 % v/v acetonitrile/methanol containing 1% v/v acetic acid at an applied voltage of 30 kV.

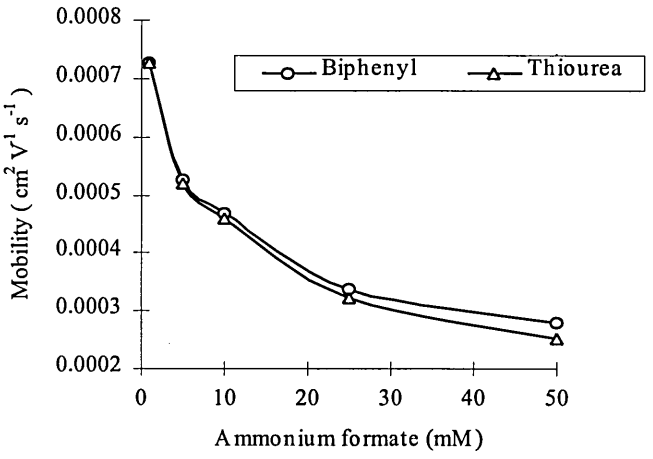

The separation between the two test compounds was first apparent at an electrolyte concentration of 5 mM. Apparent mobilities generated using ammonium formate were found to be slower than with an equivalent concentration of ammonium acetate.

Although baseline separation was achieved at an ammonium formate concentration of 50 mM, the resolution was (R_s = 3.26) than when ammonium acetate had been employed (R_s =4.56). In addition, efficiencies were approximately halved and peak shape was significantly poorer using this alternative electrolyte as illustrated in figure 6.16.

Figure 6.16 Separation achieved between biphenyl and thiourea in 70/30 % v/v acetonitrile/methanol containing 50 mM ammonium formate and 1% v/v acetic acid at an applied voltage of 30 kV.

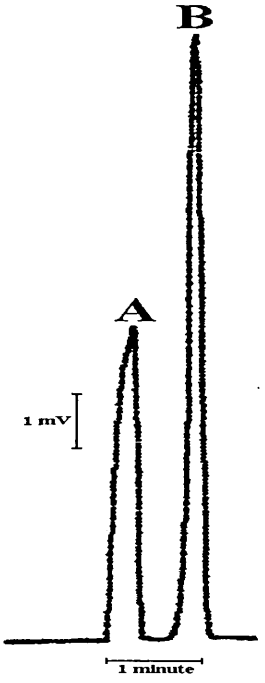

		N (plates/m)
A	Biphenyl	26700
B	Thiourea	78500

Measured currents were of a similar magnitude to those generated with equivalent concentrations of ammonium acetate. No breakdown of current was experienced during these investigations. A plot of observed current versus ammonium formate concentration is given in figure 6.17.

Figure 6.17 Influence of ammonium formate concentration on the current generated at an applied voltage of 30 kV.

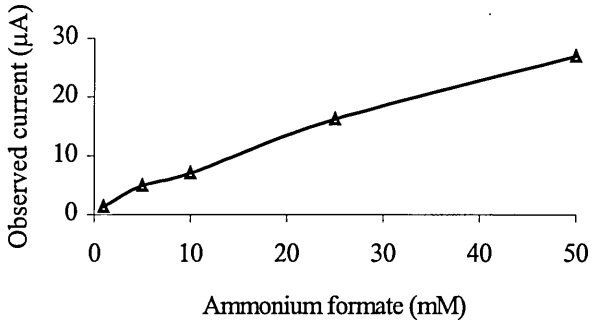

The pH* of the non-aqueous media was determined to rise by approximately 1 unit over the range of electrolyte concentrations studies in a similar fashion to ammonium acetate. However, pH* values were found to be lower in ammonium acetate as demonstrated in figure 6.18.

Figure 6.18 Influence of ammonium formate concentration on the pH* of the resulting non-aqueous media.

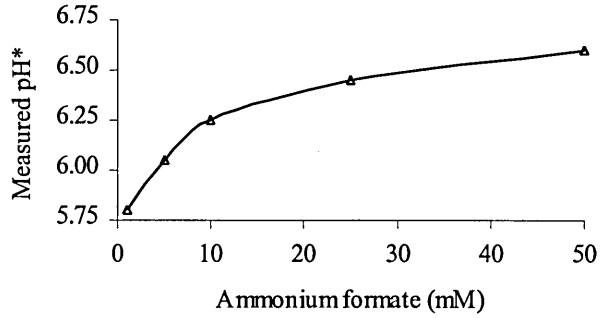

Migration time repeatabilities were below 0.25% RSD apart from at an ammonium formate concentration of 50 mM which were significantly poorer as shown in table 6.6.

Table 6.6 Average migration times and associated repeatabilities for 5 replicate injections of biphenyl and thiourea.

	Average t_m(min)		Repeatability (%RSD)	
Ammonium formate (mM)	Biphenyl	Thiourea	Biphenyl	Thiourea
1	2.014	2.014	0.09	0.09
5	2.794	2.816	0.11	0.09
10	3.144	3.188	0.22	0.21
25	4.338	4.550	0.13	0.12
50	5.273	5.804	1.28	1.16

6.5.5. Investigation of an alternative background electrolyte: Sodium acetate.

Five aliquots of non-aqueous media were prepared comprising 70/30 % v/v acetonitrile/methanol containing 1% v/v acetic acid and sodium acetate (1, 5, 10, 25, 50 mM respectively. The dependency of the apparent mobilities of the test compounds on the concentration of sodium acetate is shown in figure 6.19.

Figure 6.19 Influence of sodium acetate concentration on the apparent mobilities of biphenyl and thiourea in 70/30 % v/v acetonitrile/methanol containing 1% v/v acetic acid at an applied voltage of 30 kV.

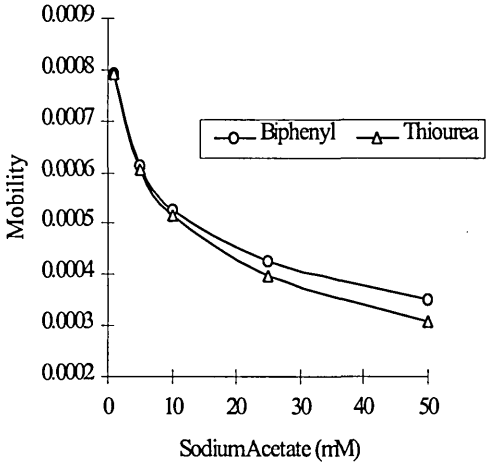

The magnitude of the apparent mobilities was found to be in good agreement with those determined at equivalent concentrations of ammonium acetate. Peak shapes were poorer compared to ammonium acetate but were better than those achieved using ammonium formate. The peak height ratio between biphenyl and thiourea was approximately 1:3 with thiourea being much sharper than had been observed using other electrolytes and the calculated efficiency was around twice that of an equivalent separation using ammonium acetate. A representative electropherogram at a sodium acetate concentration of 50 mM is presented in figure 6.20.

Figure 6.20 Separation achieved between biphenyl and thiourea in 70/30 % v/v acetonitrile/methanol containing 50 mM sodium acetate and 1% v/v acetic acid at an applied voltage of 30 kV.

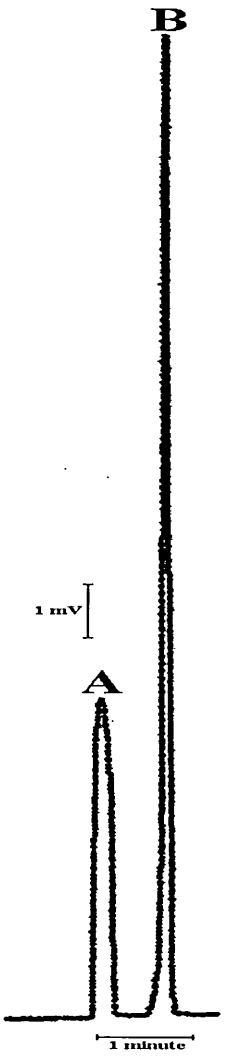

		N (plates/m)
A	Biphenyl	31700
B	Thiourea	261200

Measured currents were of a similar magnitude to those generated with equivalent concentrations of both ammonium acetate and ammonium formate. No breakdown of current was experienced during any of these investigations. Similarly, measured values of pH* were in good agreement with those obtained for ammonium acetate. Current and pH* data for the media prepared using sodium acetate are presented in figures 6.21 and 6.22 respectively.

Figure 6.21 Influence of sodium acetate concentration on the current generated at an applied voltage of 30 kV.

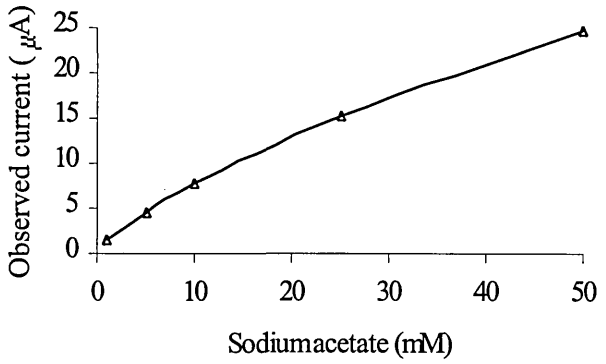

Figure 6.22 Influence of sodium acetate concentration on the pH* of the resulting non-aqueous media.

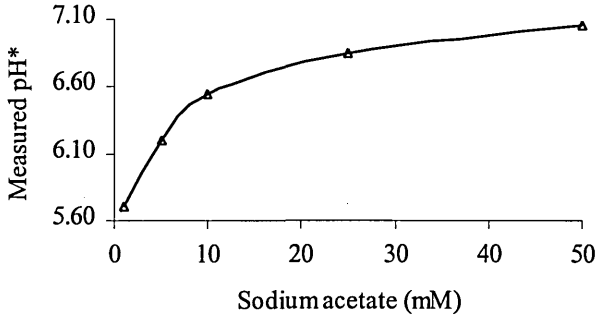

Migration time repeatabilities were particularly impressive as shown in table 6.7.

Table 6.7 Average migration times and associated repeatabilities for 5 replicate injections of biphenyl and thiourea.

	Average t_m(min)		Repeatability (%RSD)	
Sodium acetate (mM)	Biphenyl	Thiourea	Biphenyl	Thiourea
1	1.854	1.854	0.12	0.12
5	2.395	2.419	0.09	0.07
10	2.781	2.842	0.22	0.21
25	3.440	3.684	0.04	0.04
50	4.193	4.746	0.10	0.09

6.5.6. Effect of solvent composition.

Three mixtures of acetonitrile/methanol were prepared namely 0/100 (i.e. pure methanol), 30/70 and 50/50 % v/v. Ammonium acetate (25 mM) and acetic acid (1% v/v) were added to each mixture.

Apparent mobilities were found to decrease as the composition of methanol in the solvent mixture increased which supported the initial work concerning CE in non-aqueous media that was presented in chapter 2. The influence of solvent composition on the apparent mobilities of the test compounds is highlighted in figure 6.23.

Figure 6.23 Influence of non-aqueous solvent composition on the apparent mobilities of biphenyl and thiourea in acetonitrile/methanol containing 25 mM ammonium acetate and 1% v/v acetic acid at 30 kV.

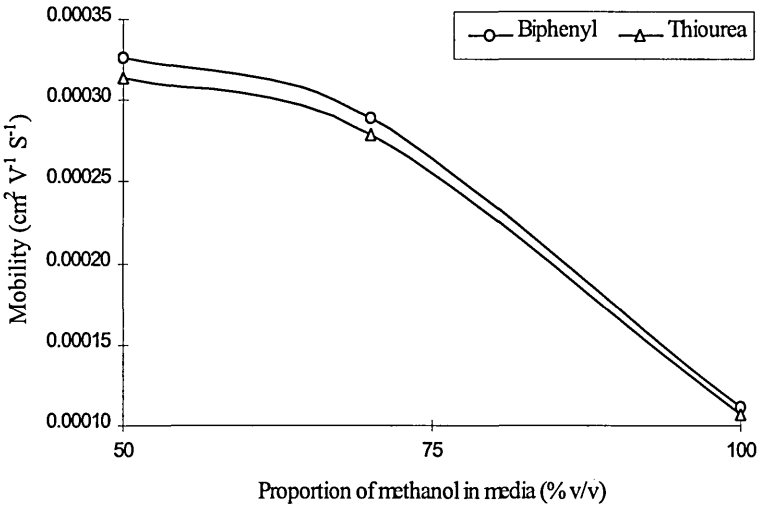

Partial separation of biphenyl and thiourea was apparent at all solvent compositions studied. Peaks were broad. Representative separations at each composition are presented in figure 6.24.

Figure 6.24 Separation achieved between biphenyl and thiourea in various compositions (% v/v) acetonitrile/methanol containing 50 mM ammonium acetate and 1% v/v acetic acid at an applied voltage of 30 kV.

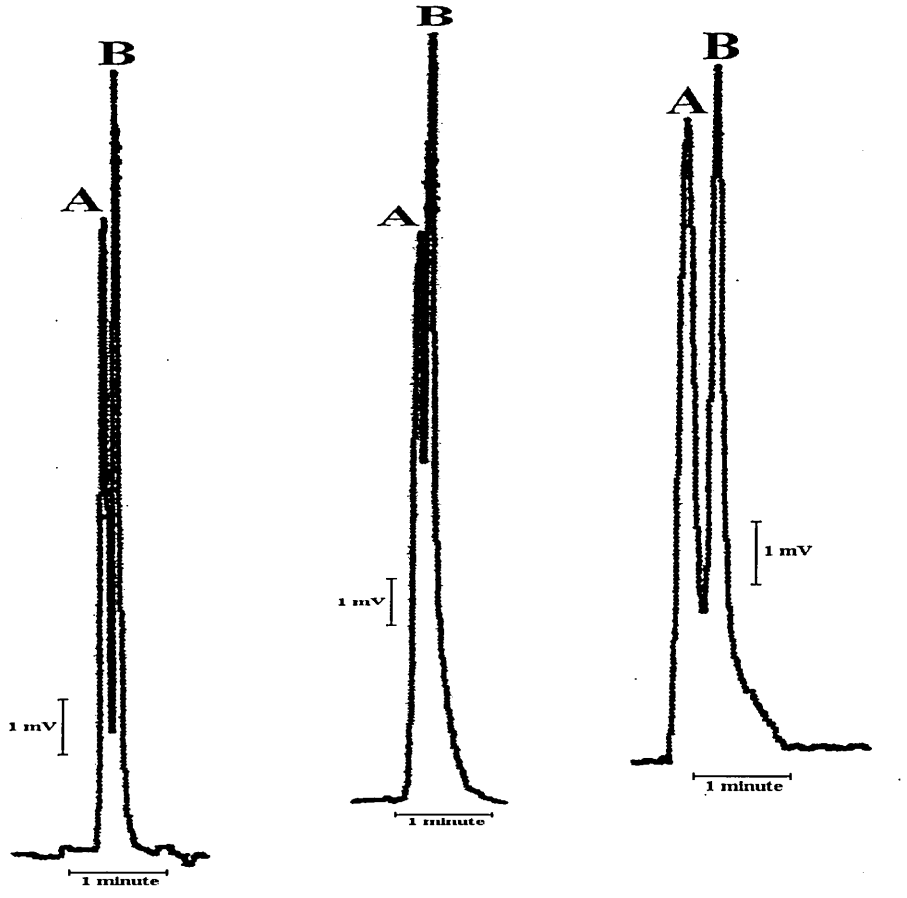

50/50 Acn/MeOH (% v/v) **30/70 Acn/MeOH (% v/v)** **Pure methanol**

(For all compositions A = Biphenyl, B = Thiourea).

The resolution between biphenyl and thiourea at methanol compositions of 50, 70 and 100% v/v was estimated to be 1.07, 0.89 and 1.07 respectively. Again, peak efficiencies were not calculated due the significant overlap of the peaks at all compositions studied.

Figure 6.25 Influence of solvent composition on the current generated at an applied voltage of 30 kV.

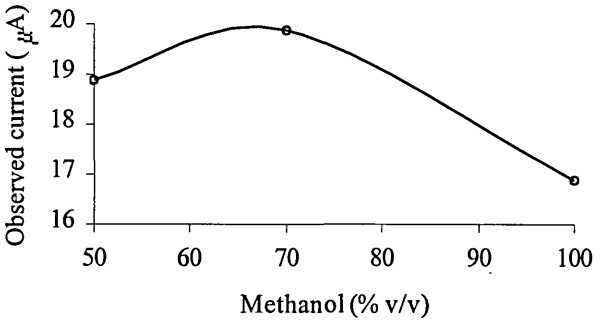

Increasing the percentage of methanol was found to reduce the pH* of the resulting media as shown in figure 6.26.

Figure 6.26 Influence of solvent composition on the pH* of the resulting non-aqueous media.

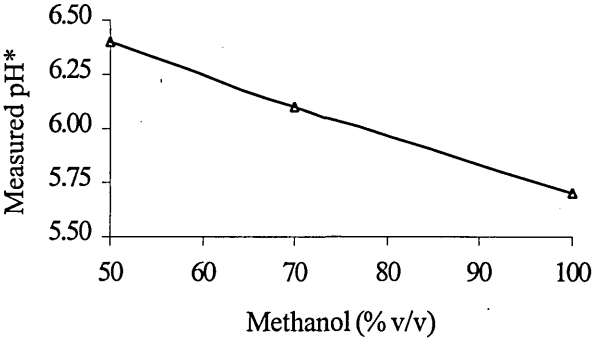

Migration time repeatabilities showed no clear dependency on the composition of the non-aqueous solvent mixture. Repeatabilities were above 1% at methanol compositions of 50 and 100 % v/v as shown in table 6.8.

Table 6.8 Average migration times and associated repeatabilities for 5 replicate injections of biphenyl and thiourea at the methanol compositions studied.

	Average t_m(min)		Repeatability (%RSD)	
Methanol (% v/v)	Biphenyl	Thiourea	Biphenyl	Thiourea
50	4.502	4.702	1.53	1.64
70	5.086	5.257	0.35	0.36
100	13.177	13.686	1.13	1.15

6.5.7. Alternative non-aqueous solvent: N-Methyl Formamide.

N-Methyl Formamide (NMF) was investigated to determine whether thiourea exhibited similar migration behaviour in other non-aqueous solvents. The media studied comprised NMF containing 50 mM ammonium acetate. The pH* of this solution was not adjusted and was determined to be 9.4. The current generated at an applied voltage of 30 kV was 11.6 μA. The EOF was relatively fast and migration time repeatabilities were less than 0.05% RSD as shown in table 6.9.

Table 6.9 Average migration times and associated repeatabilities for 5 replicate injections of biphenyl and thiourea in NMF containing 25 mM ammonium acetate.

Average t_m(min)		Apparent mobility ($cm^2 V^{-1} s^{-1}$)		Repeatability (%RSD)	
Biphenyl	Thiourea	Biphenyl	Thiourea	Biphenyl	Thiourea
3.191	3.203	0.00046	0.000458	0.03	0.04

Two partially resolved peaks again observed. The degree of overlap was far greater than in the previously studied media as shown in figure 6.27.

Figure 6.27 Separation achieved between biphenyl and thiourea in NMF containing 50 mM ammonium acetate at an applied voltage of 30 kV.

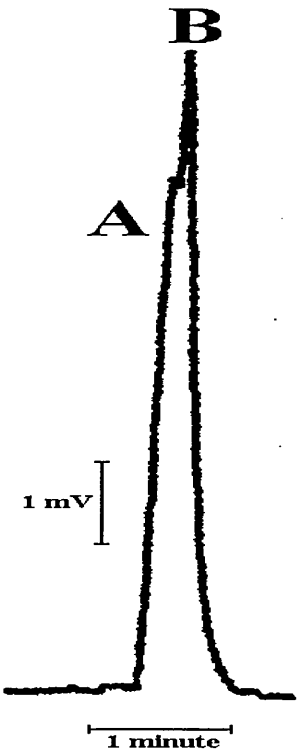

The migration order was confirmed as biphenyl and thiourea by spiking the standard solutions. The ammonium acetate concentration was subsequently increased to 50 mM. The observed current increased to 19.2 μA but the increased electrolyte concentration had no effect on pH* which was determined to be 9.4. Analytical data for thiourea is provided in table 6.10. Calculation of migration time repeatability and apparent mobility for biphenyl was not possible since the integrator could not be made to print details of these peaks.

Table 6.10 Average migration times and associated repeatabilities for 5 replicate injections of biphenyl and thiourea in N-methyl formamide containing 25 mM ammonium acetate.

Thiourea		
Average t_m(min)	Apparent mobility ($cm^2 V^{-1} s^{-1}$)	Repeatability (%RSD)
3.746	0.000392	0.53

6.5.8. Alternative neutral marker: Mesityl oxide.

Essentially, five replicate injections of a mixed standard comprising mesityl oxide (MO) and thiourea were performed to ensure that biphenyl was a true marker of the EOF with thiourea migrating at a slower rate. The non-aqueous media comprised 70/30 % v/v acetonitrile/methanol containing 50 mM ammonium acetate and 1% v/v acetic acid. The resulting electropherogram was similar to the previous investigations, comprising two fully resolved peaks ($R_s = 2.39$).

Injection of individual standards confirmed the migration order to be MO followed by thiourea. The mean migration times and associated repeatabilities of the five replicate injections are presented in table 6.11.

Table 6.11 Average migration times and associated repeatabilities for 5 replicate injections of mesityl oxide and thiourea in 70/30 % v/v acetonitrile/methanol containing 25 mM ammonium acetate at an applied voltage of 30 kV.

Average t_m(min)		Apparent mobility ($cm^2 V^{-1} s^{-1}$)		Repeatability (%RSD)	
MO	Thiourea	MO	Thiourea	MO	Thiourea
3.357	3.564	0.000993	0.000935	0.31	0.22

Five replicate injections of a mixed standard comprising biphenyl and thiourea were subsequently performed for comparison. The average migration times obtained for thiourea were consistent over the two experiments. In addition, the migration times for biphenyl and MO were also found to be in good agreement as shown in table 6.12

Table 6.12 Average migration times and associated repeatabilities for 5 replicate injections of biphenyl and thiourea in 70/30 % v/v acetonitrile/methanol containing 25 mM ammonium acetate at an applied voltage of 30 kV.

Average t_m(min)		Apparent mobility ($cm^2 V^{-1} s^{-1}$)		Repeatability (%RSD)	
Biphenyl	Thiourea	Biphenyl	Thiourea	Biphenyl	Thiourea
3.366	3.547	0.000990	0.000940	0.26	0.17

6.5.9. Confirmation of observations on a second instrument.

The aims of this study were twofold: To discount the possibility that the cause of this phenomenon was the instrumentation and to further investigate the erratic behaviour of non-aqueous CE on the Beckman system.

The capillary that was employed during the investigations in section 6.68 was carefully cut with a ceramic tile to yield dimensions of L_t = 46 cm and L_d = 40 cm. This was subsequently fitted into a Beckman capillary cartridge. Experimental work was essentially a repeat of section 6.68 under identical conditions to provide a comparison between the two instruments. Analytical data for five replicate injections of a working standard comprising MO and thiourea are presented in table 6.13. Equivalent data for five replicate injections of a working standard comprising thiourea and biphenyl are presented in table 6.14.

Table 6.13 Average migration times and associated repeatabilities for 5 replicate injections of mesityl oxide and thiourea in 70/30 % v/v acetonitrile/methanol containing 25 mM ammonium acetate at an applied voltage of 23 kV.

Average t_m(min)		Apparent mobility ($cm^2 V^{-1} s^{-1}$)		Repeatability (%RSD)	
MO	Thiourea	MO	Thiourea	MO	Thiourea
4.225	4.537	0.000605	0.000563	0.88	1.09

Table 6.14 Average migration times and associated repeatabilities for 5 replicate injections of biphenyl and thiourea in 70/30 % v/v acetonitrile/methanol containing 25 mM ammonium acetate at an applied voltage of 23 kV.

Average t_m(min)		Apparent mobility ($cm^2 V^{-1} s^{-1}$)		Repeatability (%RSD)	
Biphenyl	Thiourea	Biphenyl	Thiourea	Biphenyl	Thiourea
4.377	4.677	0.000584	0.000546	0.79	0.80

6.6. CONCLUSION.

These studies have highlighted that the choice of a suitable EOF marker compound may be problematic when developing separations in non-aqueous media. The mechanism by which thiourea migrated was presumably via some form of interaction with the background electrolyte to form a negatively charged species. The possibility of thiourea being protonated in the media was discounted when identical behaviour was obtained in media that did not contain acetic acid. There appeared to be a "threshold" electrolyte concentration at which this process occurred. The age of the ammonium acetate used to prepare the media did not appear to have a detrimental effect since the HPLC grade generated a reproducible EOF.

None of the three electrolytes studied was an obvious best choice in terms of the magnitude and repeatability of the resulting EOF since each behaved in a similar fashion. However, separation quality in terms of resolution, efficiency and peak asymmetry were found to differ significantly with ammonium formate leading to the poorest separation. Such differences were also observed during the cimetidine method development (chapter 3) where sodium acetate generated the poorest separation. These observations could imply that the optimum background electrolyte might be application specific. Investigation of different electrolytes should form part of the method development protocol if this is the case. It is likely that the poor peak shapes obtained when employing ammonium formate could lead to an integration error. This would be particularly significant in any quantitative application.

Non-aqueous media containing a high percentage of methanol was again shown to yield a slow EOF with poor repeatability over several replicate injections. A solvent composition of 70/30 % v/v acetonitrile/methanol appears to yield the best separation and is a suitable starting point when developing a method. However, the optimum procedure for subsequent optimisation of the separation and the intricacies of CE in non-aqueous media are still not fully understood. The inability to measure and manipulate pH* with any degree of certainty was a key limitation.

CHAPTER 7.

DETERMINATION OF ETHYLENEDIAMINE.

7.1. INTRODUCTION.

The work presented in this chapter involved quantification of ethylenediamine (EDA). Method development essentially involved exploring opportunities that were highlighted by previously published studies[294-296] to determine whether a suitable CE-based method could be developed.

7.2. BACKGROUND.

Polyamines such as ethylenediamine (EDA) originate from a variety of industrial processes and are known to cause irritation of the respiratory tract and skin sensitisation. It is extremely difficult to determine EDA directly since it has a tendency to oxidise and does not possess a suitable chromophore. The usual method of overcoming these issues is via the formation of a UV-absorbing derivative. Derivatisation is effected by drawing the test atmosphere through a sample tube containing a sorbent material using a low-flow personal pump[297-300]. The resulting derivative is stable and may be transported and/or stored prior to analysis. The contents of the tube are simply desorbed using solvents when required for analysis. Quantitation requires a method that is capable of separating the EDA-derivative complex from the large excess of unreacted sorbent.

Fluorescein isothiocyanate (FITC), 4-chloro-7-nitrobenzofurazan (NBD-Cl) and 1-napthylisothiocyanate (NIT) have previously been identified as potential derivatising agents for EDA[294, 295]. However, feasibility studies determined that FITC formed a mono-derivative rather the desired di-substituted derivative[294]. This reagent was therefore not included in any subsequent studies. Sample tubes filled with NBD-Cl and NIT are commercially available and hence these were considered suitable choices for further evaluation. An initially promising RP-HPLC method[301] employing NIT had subsequently performed erratically, yielding inconsistent peak areas.

7.3. MATERIALS AND METHODS.

The Health and Safety Laboratory (Sheffield, UK) kindly supplied samples of NIT, EDA-NIT, NBD-Cl and EDA and all other reagents and consumables.

7.4. EXPERIMENTAL PROCEDURES.

7.4.1. NACE separations employing NIT as a derivatising agent.

Initial separations were effected at an applied voltage of 28 kV (500 V/cm) using the Beckman P/ACE 5150 using 56 cm lengths of 50 μm i.d. uncoated fused silica capillary.

On-capillary UV detection was performed across a wavelength range of 190-350 nm using the in-built diode array detector at a distance of 50 cm from the inlet end (L_d = 50 cm).

The separation capillary was equilibrated at the start of each working day and prior to changing separation media by flushing with acetonitrile (20 PSI) for 5 minutes. A two-stage equilibration was performed with the appropriate non-aqueous media that was first hydrodynamically pumped (20 PSI) for 5 minutes and then electrically driven (28 kV) for 5 minutes. The capillary was rinsed using acetonitrile (20 PSI) for 2 minutes followed by air (20 PSI) for 1 minute at the end of each working day prior to careful storage.

The capillary was rinsed between replicate separations with acetonitrile (20 PSI) for 2 mins followed by the relevant non-aqueous media (20 PSI) for two minutes. In addition, the first two separations of all investigations were ignored and not included in any subsequent data analysis. Samples were hydrodynamically injected (0.5 PSI).

Subsequent development work was performed at an applied voltage of 30 kV (500 V/cm) using the Thermo Unicam instrument using a 60 cm length of 50 μm i.d. uncoated fused silica capillary. On-capillary UV absorbance detection was performed at a distance of 44 cm from the inlet end (L_d = 44 cm) at a wavelength of 230 nm.

The separation capillary was equilibrated at the start of each working day and prior to changing separation media by flushing with sodium hydroxide (0.1 M, 2000 mbar) for 5 minutes. Residual sodium hydroxide was removed by flushing with acetonitrile (2000 mbar) for 5 minutes. A two-stage equilibration was performed with the appropriate non-aqueous media which was first hydrodynamically pumped (2000 mbar) for 5 minutes and then electrically driven (20 kV) for 5 minutes. The capillary was rinsed using acetonitrile (2000 mbar) minutes for 5 at the end of each working day prior to careful storage.

The capillary was rinsed between replicate separations with the relevant non-aqueous media (2000 mbar) for two minutes. In addition, the first two separations of all investigation were ignored and not included in any subsequent data analysis. All samples were hydrodynamically injected (25 mbar, 0.2 minutes)

7.4.1. MEKC separations employing NIT as a derivatising agent.

All separations were effected at an applied voltage of 28 kV (500 V/cm) using a Beckman P/ACE 5150. On-capillary UV detection was performed from 190-350 nm using the in-built diode array detector at a distance of 50 cm from the inlet end (L_d = 50 cm). All electropherograms were displayed at a wavelength of 230 nm.

The separation capillary was equilibrated at the start of each working day and prior to changing separation media by flushing with sodium hydroxide (0.1 M, 20 PSI) for 5 minutes. Residual sodium hydroxide was removed by flushing with water (20 PSI) for 5 minutes. A two-stage equilibration was performed with the appropriate micellar buffer which was first hydrodynamically pumped (20 PSI) for 5 minutes and then electrically driven (28 kV) for 5 minutes. The capillary was rinsed using sodium hydroxide (20 PSI) for two minutes followed by water (20 PSI) for 2 minutes and finally air (20 PSI) for 1 minute at the end of each working day prior to careful storage.

The capillary was rinsed between replicate separations with sodium hydroxide (0.1 M, 20 PSI) for 2 mins, water (20 PSI) for 1 minute and finally the relevant buffer (20 PSI) for two minutes. In addition, the first two separations of all investigation were ignored and not included in any subsequent data analysis.

The initial micellar buffer comprised 10 mM sodium tetraborate and 50 mM SDS that was adjusted to pH 9.23 (NaOH 0.1 M/dm^3) and filtered through a Whatman (Maidstone, UK) 0.45 μm filter membrane prior to use. All samples were hydrodynamically injected (0.5 PSI).

7.4.2. MEKC separations employing NBD-Cl as a derivatising agent.

All separations were effected at an applied voltage of 28 kV (500 V/cm) using a Beckman P/ACE 5150. A 56 cm length of 50 μm i.d. uncoated fused silica capillary was flushed with sodium hydroxide (1.0 M, 20 PSI) for 30 minutes to promote the ionisation of surface silanol groups. Residual sodium hydroxide was removed by flushing with water (20 PSI) for 5 minutes.

A detection window was fabricated using a disposable lighter at a distance of 6cm from the outlet end. The effective length was therefore 50 cm. On-capillary UV detection was performed across a wavelength range of 190 to 500 nm using the in-built diode array detector. All electropherograms were displayed at both 340 and 480 nm.

The separation capillary was equilibrated at the start of each working day and prior to changing separation media by flushing with sodium hydroxide (0.1 M, 20 PSI) for 5 minutes. Residual sodium hydroxide was removed by flushing with water (20 PSI) for 5 minutes. A two-stage equilibration was performed with the appropriate micellar buffer which was first hydrodynamically pumped (20 PSI) for 5 minutes and then electrically driven (28 kV) for 5 minutes. The capillary was rinsed using sodium hydroxide (20 PSI) for two minutes followed by water (20 PSI) for 2 minutes and finally air (20 PSI) for 1 minute at the end of each working day prior to careful storage.

The capillary was rinsed between replicate separations with sodium hydroxide (0.1 M, 20 PSI) for 2 mins, water (20 PSI) for 1 minute and finally the relevant buffer (20 PSI) for two minutes. In addition, the first two separations of all investigation were ignored and not included in any subsequent data analysis.

The initial micellar buffer comprised 10 mM sodium tetraborate and 50 mM SDS that was adjusted to pH 9.20 (NaOH 0.1 mol/dm^3).

The reaction between EDA and NDD-Cl was simply performed by mixing solutions of the two compounds in acetonitrile. Optimum reaction conditions were determined using a Thermo Unicam UV/Vis Spectrophotmeter. Samples were hydrodynamically injected (0.5 PSI).

7.5. DEVELOPMENT OF A NACE ASSAY EMPLOYING NIT AS A DERIVATISING AGENT.

Figure 7.1 shows the reaction scheme involved when employing NIT as a derivatising agent for EDA. Essentially, the amino functionalities of EDA react with the isothiocyanate group of NIT to form the stable derivative EDA-NIT.

Figure 7.1 Reaction scheme for derivatisation of EDA with NIT.

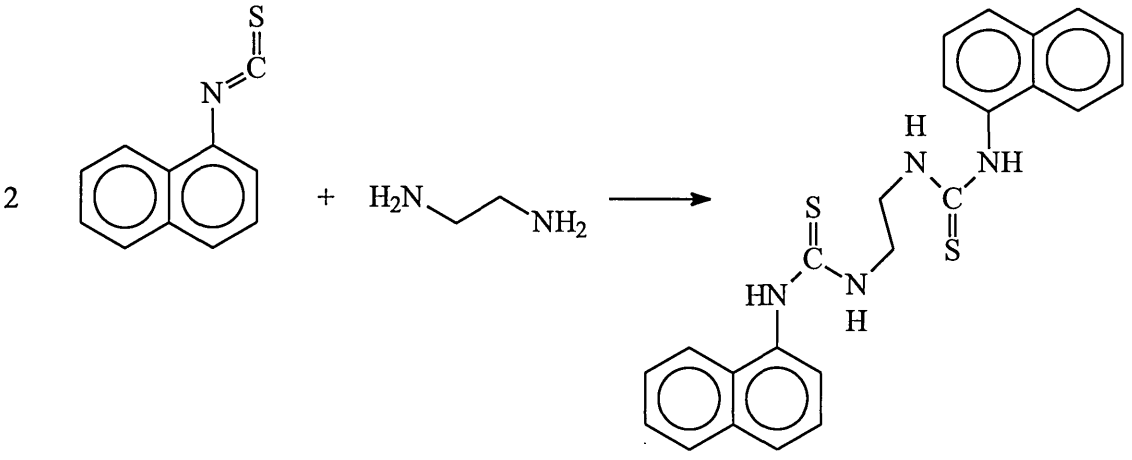

EDA-NIT is extremely hydrophobic and has limited solubility in most organic solvents. However, it is extremely soluble in DMF. Individual standards of EDA-NIT and NIT (1 mg/ml) were prepared in DMF and diluted to a working concentration of 0.1 mg/ml using the non-aqueous media. An initial injection of a NIT standard was made using media comprising 70/30 %v/v acetonitrile/methanol containing 25mM ammonium formate and 1% v/v acetic acid (pH* 6.70). The resulting peak could not be readily identified from its absorbance spectra since DMF swamped the lower half of the diode array scan profile as shown in figure 7.2.

Figure 7.2 Diode array contour map for a 0.1 mg/ml NIT standard (scan range 190-300 nm)

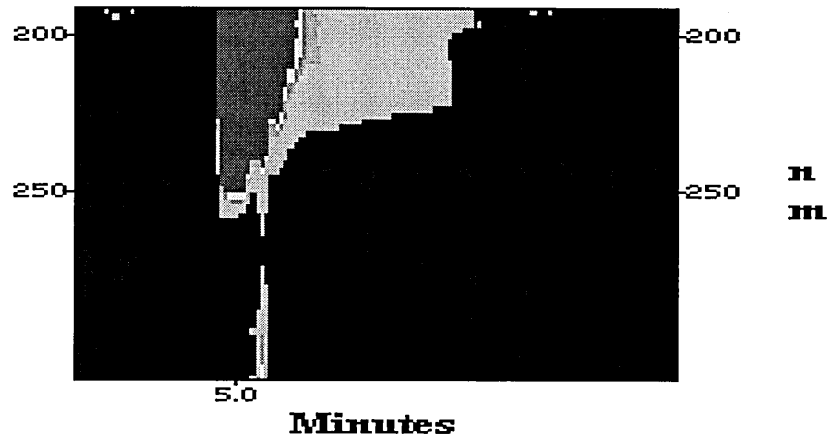

This effect prevented the use of any analysis wavelength less than 260 nm. Figure 7.3 shows electropherograms of the NIT standard displayed at 254 nm and 300 nm respectively.

Figure 7.3 Comparison of a 0.1 mg/ml NIT standard at 2 analysis wavelengths using non-aqueous media comprising 70/30 %v/v acetonitrile/methanol containing 25mM ammonium formate and 1% v/v acetic acid (pH* 6.70)

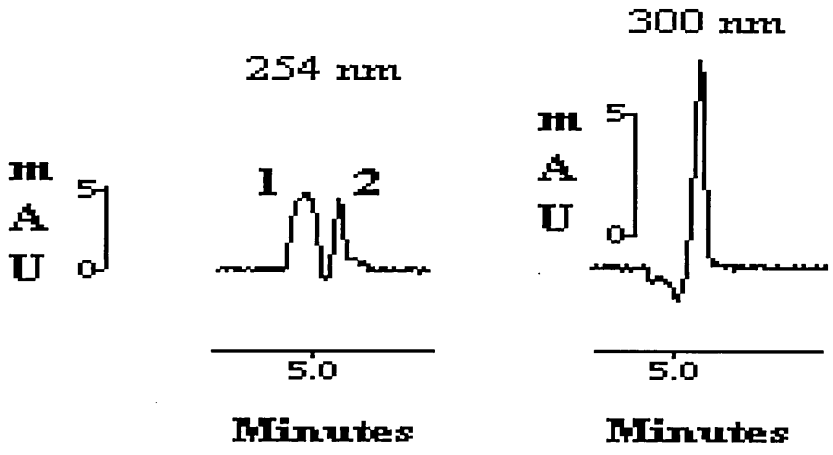

1	Solvent peak
2	Excess NIT

At 254 nm the NIT peak did not appear to be sufficiently resolved from the solvent peak to allow confident quantitation. No solvent peak was observed at 300 nm since this was above the 260 nm UV cut-off of DMF. EDA-NIT was adequately separated from NIT under these conditions and migration time repeatabilities over a series of replicate injections were better than 1% RSD. A representative separation under these conditions displayed at 300 nm is presented in figure 7.4.

Figure 7.4 Separation of EDA-NIT and NIT using non-aqueous media comprising 70/30 % v/v acetonitrile/methanol containing 25 mM ammonium formate and 1% v/v acetic acid (pH* 6.70) at an applied voltage of 28 kV.

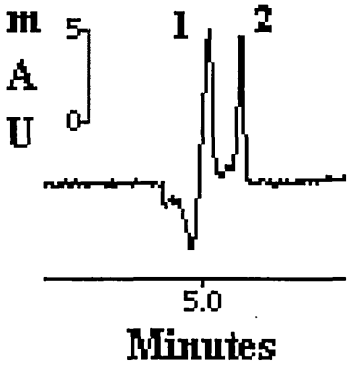

1	EDA-NIT
2	Excess (uncomplexed) NIT

EDA-NIT was also found to be soluble in THF which has a lower (215 nm) UV cut-off than DMF. It was therefore anticipated that detection issues could be resolved using THF-based samples.

Figure 7.5 shows the separation of EDA-NIT from NIT using standards prepared in THF diluted in the non-aqueous media at a wavelength of 240 nm.

Figure 7.5 Separation of EDA-NIT from NIT using standards prepared in THF. Conditions: 70/30 % v/v acetonitrile/methanol containing 25 mM ammonium formate and 1% v/v acetic acid (pH* 6.70) at an applied voltage of 28 kV.

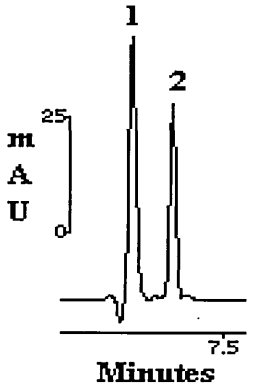

		Average t_m (min)	% RSD t_m (n=3)
1	EDA-NIT	6.825	0.71
2	NIT	7.110	0.73

Injection of a neutral marker compound (biphenyl) indicated that NIT migrated with the EOF whilst EDA-NIT was apparently negatively charged. The latter comment was consistent with previous studies since EDA-NIT contains thiourea-like functionalities.

An equivalent separation was subsequently performed on the Thermo Unicam instrument under identical conditions. Although migration time repeatability was far superior the achieved separation was poorer. The two bands overlapped significantly ($R_{estimated}$ = 0.99). Increasing the electrolyte concentration initially to 50 mM and subsequently to 75 mM had no significant effect on the separation achieved between the two bands.

7.6. DETERMINATION OF EDA BY MEKC EMPLOYING NIT AS A DERIVATISING AGENT.

Initial studies employed a micellar buffer comprising 10 mM sodium tetraborate and 50 mM SDS (pH 9.0) at an applied voltage of 28 kV (500 V/cm). The current generated under these conditions was 30.8 μA.

Individual injections of both NIT and EDA-NIT resulted in sharp peaks that allowed high quality absorbance spectra to be acquired. However, when the pair were injected together they were found to co-migrate as a single band after around 8 minutes.

Addition of 5 % v/v acetonitrile to the micellar buffer (pH* 9.36) achieved a partial separation of the 2 bands ($R_{estimated}$ = 0.75). Separation time was increased to around 11 minutes. A typical separation is shown in figure 7.6, which has been expanded for clarity.

Figure 7. 6 Separation of EDA-NIT from NIT achieved at 28 kV using a micellar buffer comprising 10 mM sodium tetraborate and 50 mM SDS with 5% v/v acetonitrile (pH* 9.36)

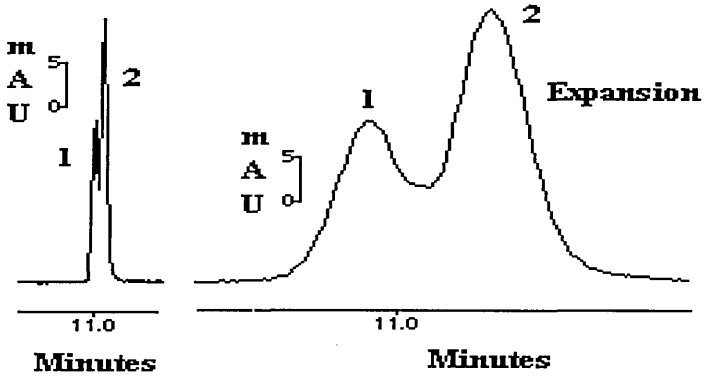

1	EDA-NIT
2	Excess NIT

Peak heights for EDA-NIT were found to vary erratically over a series of replicate injections. This is highlighted in figure 7.7, which shows a repeat of the above separation. Note that the EDA-NIT peak was not observed during this injection.

Figure 7.7 Repeat separation of EDA-NIT from NIT achieved at 28 kV using a micellar buffer comprising 10 mM sodium tetraborate and 50 mM SDS with 5% v/v acetonitrile (pH* 9.36)

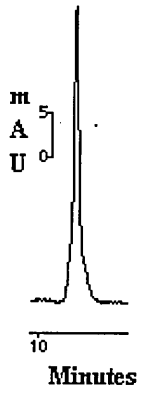

The poor peak height repeatability was presumed to be symptomatic of the limited aqueous solubility of EDA-NIT. A working standard solution of the two compounds was observed to become cloudy on standing.

Increasing the acetonitrile composition to 10% v/v (pH* 9.51) resulted in an improved separation at the expense of analysis time which was further increased to around 15 minutes. Irreproducible peak heights were again observed for EDA-NIT over a series of replicate injections and significant tailing of this band was apparent. Illustrative examples are shown in figure 7.8.

Figure 7. 8 Separation of EDA-NIT from NIT achieved at 28 kV using a micellar buffer comprising 10 mM sodium tetraborate and 50 mM SDS with 10% v/v acetonitrile (pH* 9.51).

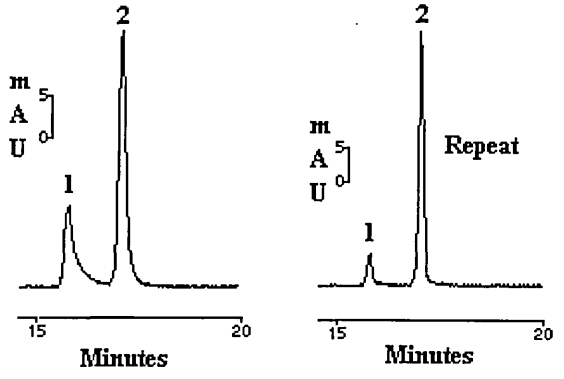

Increasing the acetonitrile composition to 15% v/v (pH* 9.66) significantly increased the analysis time with EDA-NIT eluting after 25 minutes (small peak) and no peak observed for NIT even on a 40 minute run (data not shown). Again, it was observed that standards became cloudy when left to stand.

7.7 DETERMINATION OF EDA VIA DERIVATISATION WITH NBD-CL.

Preliminary studies by Rimmer *et al.*[284] had demonstrated the suitability of NBD-Cl for the derivatisation of primary amines. The unreacted reagent does not absorb between 460-480 nm whereas the derivatives do. A wavelength of 480 nm was therefore employed to monitor only the derivatised EDA. The proposed reaction scheme between NBD-Cl and EDA is given in figure 7.9.

Figure 7.9 Reaction scheme for EDA and NBD-Cl.

Where NBD-Cl is:

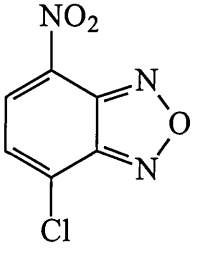

7.7.1. Determination of optimum conditions for the derivatisation reaction.

Investigations were based on a previous study involving primary amines[285] where 500 μL of a 50 μM EDA solution in acetonitrile was added to 1ml of a 16 μM NBD-Cl solution in acetonitrile and left to react at room temperature for 1 hour.

A similar reaction employing the above conditions was monitored at a wavelength of 480 nm. An absorbance plot constructed from this data confirmed that the reaction was complete after 1 hour as shown in figure 7.10.

Figure 7.10 Absorbance plot for reaction between excess NBD-CL and EDA.

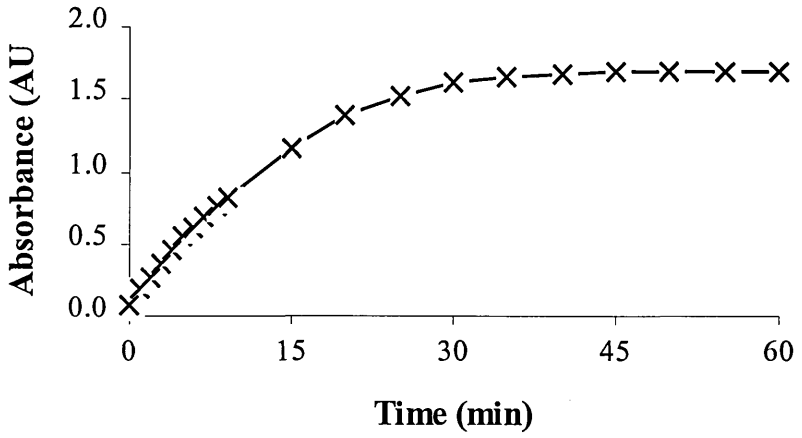

The following reaction conditions were employed in all subsequent separations. Two stock solutions were prepared:

1. 10 mg (1.66×10^{-4} moles) EDA in 10 ml acetonitrile.
2. 160 mg (8.00×10^{-4} moles) NBD-Cl in 10 ml acetonitrile.

(Yields a reaction Ratio of NBD-Cl to EDA approximately 5:1).

1 ml aliquots of each were combined and allowed to react for 1 hour at room temperature.

7.7.2. MEKC separations.

An initial MEKC investigation was performed using a micellar buffer comprising 10 mM sodium tetraborate containing 50 mM SDS (pH 9.18). The separation achieved between the two bands was excellent. However, the size of the NBD-EDA peak was extremely small. A representative separation of a 10 second pressure injection of a five-fold dilution of the reaction mixture is shown at both 340 nm and 480 nm in figure 7.11.

Figure 7.11 Separation of derivatised EDA from unreacted NBD-Cl achieved at 28 kV using a micellar buffer comprising 10 mM sodium tetraborate and 50 mM SDS (pH 9.18).

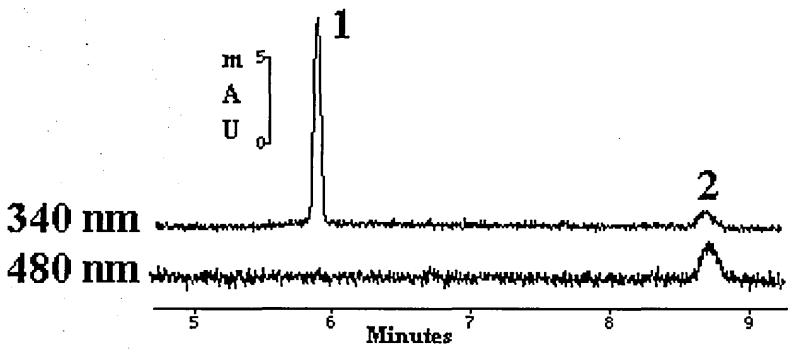

1	Excess NBD-Cl
2	Derivatised NBD-Cl

The magnitude of the derivatised EDA band was enhanced via manipulation of both the injection time and the dilution of the reaction mixture. The band associated with the excess NBD-Cl was extremely broad. A representative example of the separation achieved using an undiluted reaction mixture and an injection time of 5 seconds is shown in figure 7.12.

Figure 7.12 Separation of derivatised EDA from unreacted NBD-Cl achieved at 28 kV using a micellar buffer comprising 10 mM sodium tetraborate and 50 mM SDS.

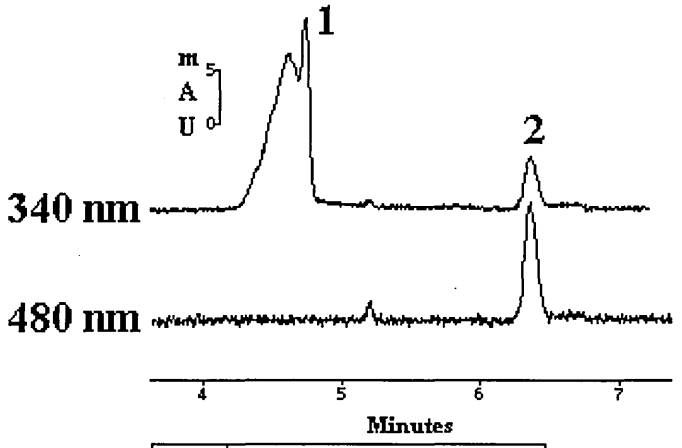

1	Excess NBD-Cl
2	Derivatised NBD-Cl

Employing a 75 μm i.d capillary further enhanced the magnitude of the analyte band. The current generated under these conditions was 79.96 μA. A representative separation obtained via a 2 second injection of an undiluted reaction mixture is shown in figure 7.13.

Figure 7.13 Separation of derivatised EDA from unreacted NBD-Cl achieved at 28 kV using a 75 μm i.d capillary and micellar buffer comprising 10 mM sodium tetraborate and 50 mM SDS.

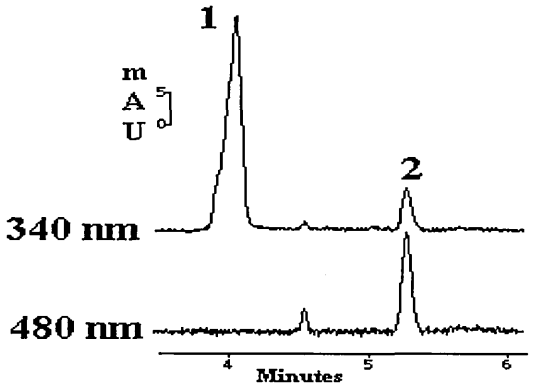

Use of an increased injection time was found to be impractical since it produced an extremely erratic separation involving several unresolved peaks. A representative example is presented in figure 7.14.

Figure 7.14 Separation of derivatised EDA from unreacted NBD-Cl achieved at 28 kV using a 75 μm i.d capillary and micellar buffer comprising 10 mM sodium tetraborate and 50 mM SDS at an increased injection time of 5 seconds.

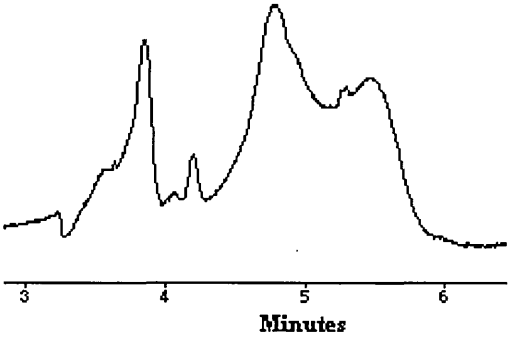

Peak heights were again found to vary over a series of replicate injections and a series of extra, unidentified peaks were noticed on some injections. It was observed that the intensity of standard solutions changed on standing from orange to a dark orange brown colour.

7.8. CONCLUSION.

The NACE separations employing NIT as a derivatising reagent were extremely promising. Non-aqueous media appeared to address the limited aqueous solubility of the derivatives that was apparent during MEKC separations. However, issues concerning the suitability of non-aqueous media on the Beckman P/ACE and transfer of separations between different instruments were again highlighted during method development.

Further evaluation of the NBD-Cl reaction is obviously necessary to elucidate the chemistries involved. The use of diode array detection was shown to yield extremely valuable information but the restricted limit of detection offered by UV detection was highlighted. The achievable limit of quantitation could presumably be significantly enhanced via the use of fluorescence detection since NBD-Cl is non-fluorescent yet yields fluorescent derivatives.

Chapter 8.

APPLICATION OF ELECTRO-MIGRATION TECHNIQUES EMPLOYING NON-AQUEOUS MEDIA TO THE SEPARATION OF TRIALKYLTIN COMPOUNDS.

8.1. INTRODUCTION.

The work undertaken in this chapter involved the application of non-aqueous media to a challenging application provided by the Health and Safety Laboratory. The organotin compounds involved are highly insoluble in aqueous systems and do not possess a suitable chromophore for UV absorbance detection. It was anticipated that certain non-aqueous media might be capable of addressing these issues and allow separation of the test compounds.

8.2. BACKGROUND.

The general formula of organotin compounds is R_nSnX_{4-n} where R comprises either an alkyl or aryl group and X is an anion such as a halide. The chemical nature of the R grouping has a strong influence on the biological properties of the compound whereas X influences both the solubility and volatility.

Alkyltin compounds are extensively employed as agrochemicals, wood preservatives, stabilisers in PVC and in marine anti-fouling coatings. The latter results from the attachment and growth of organisms to surfaces that are immersed in seawater such as ship hulls. The most practical means of treating and/or preventing such growth is to apply an antifouling coating containing a suitable slow-release biocide. Alkyltin compounds, particularly bis(tributyltin) oxide have found extensive use in this area since they are compatible with most organic binders employed in the paints industry.

The published literature concerning the toxicity of organotin compounds is extensive and a detailed discussion is beyond the scope of this thesis. In general, progressive introduction of organic groups at the tin atom produces maximum biological activity when n=3[302]. Toxicity generally decreases as the length of R groups increases with trioctyl species being essentially non-toxic to all living organisms.

The aqueous solubility of alkyl tin species is poor and generally decreases as the number of R groups increase. However, there is a wide variation in published data[302]. Trimethyltin compounds exist primarily as the hydrated trimethyltin cation, $[Me_3Sn(H_2O)_2]^+$ in aqueous solution[303]. The latter exhibits trigonal bypyrimidal geometry.

The eventual fate of organotin compounds is of considerable importance since there are many ways in which they may enter the environment. The degradation process essentially involves the systematic removal of the organic groups from the tin atom thus: $R_4Sn \rightarrow R_3SnX \rightarrow R_2SnX_2 \rightarrow RSnX_3 \rightarrow SnX_4$.

Various strategies have been reported for the speciation and/or quantitation of organotin compounds. GC enables the separation of most species in a single run. However, since most organotin compounds of interest are insufficiently volatile it is necessary to perform time consuming derivatisation procedures prior to separation. Although HPLC methods avoid the necessity of derivatisation steps the resolution achieved is typically poorer. The use of HPLC in this area has been reviewed[304, 305].

The issues associated with traditional chromatographic techniques have led to an interest in capillary electrophoresis. Both Han and co-workers[306] and Whang[132] separated di and trialkylltin species by capillary electrophoresis using indirect UV detection. Meanwhile, Li and Li[307] reported a MEKC separation of trialkytin and trialkyl lead compounds using direct UV absorption at 200 nm.

8.3. MATERIALS AND METHODS

Trimethyltin chloride (TMT), Triethyltin bromide (TET), Tributyltin bromide (TBT) and (bis)tributyltin oxide (TBTO) were kindly supplied by the Health and Safety Laboratory (Sheffield, UK). Individual stock solutions (1mg/ml) of the analytes were prepared in methanol and stored in a refrigerator. Working standards (0.1 mg/ml) were prepared as required via dilution of the stock solutions using the appropriate media.

A stock solution (1mg/ml) of mesityl oxide was also prepared in methanol. This was incorporated into test solutions as neutral marker to determine the magnitude of the EOF generated.

8.4. EXPERIMENTAL PROCEDURES.

The majority of separations were effected using the Beckman P/ACE CE at an applied voltage of 28 kV (500 V/cm) using 56 cm lengths of 50 μm i.d. uncoated fused silica capillary. On-capillary UV detection was performed across a wavelength range of 190-350 nm using the in-built diode array detector at a distance of 50 cm from the inlet end (L_d = 50 cm).

The separation capillary was equilibrated at the start of each working day by flushing with acetonitrile (20 PSI) for 5 minutes. A two-stage equilibration was performed with the appropriate non-aqueous media that was first hydrodynamically pumped (20 PSI) for 5 minutes and then electrically driven (28 kV) for 5 minutes. The capillary was rinsed using acetonitrile (20 PSI) for 2 minutes followed by air (20 PSI) for 1 minute at the end of each working day prior to careful storage.

The capillary was rinsed between replicate separations with the appropriate non-aqueous media (20 PSI) for two minutes. In addition, the first two separations of all investigations were ignored and not included in any subsequent data analysis. All samples were hydrostatically injected (0.5 PSI) for 2 seconds.

The remaining development work was performed at an applied voltage of 30 kV (500 V/cm) using a Thermo Unicam instrument. A 60 cm length of 50 μm i.d. uncoated fused silica capillary was flushed with sodium hydroxide (1.0 M, 2000 mbar) for 30 minutes to promote ionisation of surface silanol groups. Residual sodium hydroxide was removed by flushing with water (2000 mbar) for 5 minutes. A detection window was created at a distance of 16 cm from the outlet using a commercially available frit burner. The effective length was therefore 44 cm. On-capillary UV absorbance detection was performed at a wavelength of 254 nm. The connections from the detector to the integrator were reversed to generate positive peaks.

The separation capillary was equilibrated at the start of each working day and prior to changing separation media by flushing with sodium hydroxide (0.1 M, 2000 mbar) for 5 minutes. Residual sodium hydroxide was removed by flushing with acetonitrile (2000 mbar) for 5 minutes. A two-stage equilibration was performed with the appropriate non-aqueous media which was first hydrodynamically pumped (2000 mbar) for 5 minutes and then electrically driven (20kV) for 5 minutes. The capillary was rinsed using acetonitrile (2000 mbar) for 5 minutes at the end of each working day prior to careful storage.

The capillary was rinsed between replicate separations with the relevant non-aqueous media (2000 mbar) for two minutes. In addition, the first two separations of all investigations were ignored and not included in any subsequent data analysis. All samples were hydrodynamically injected (25mBar) for 0.2 minutes.

8.5. INVESTIGATIONS EMPLOYING 100% NMF.

Since alkyltin compounds are essentially UV transparent it was anticipated that NMF could be used as a separation medium employing indirect UV detection without the requirement of either a background electrolyte or chromophore. A wavelength of 254 nm was arbitrarily chosen for detection.

Initial investigations involved performing five replicate injections of mesityl oxide, (bis)tributyltin oxide and trimethyltin chloride using the Thermo Unicam instrument at an applied voltage of 30 kV (500 V/cm). The resulting data are presented in table 8.1.

Table 8.1 Determination of migration time repeatability for mesityl oxide and two organotin compounds in NMF at an applied voltage of 30 kV.

Compound	Average t_m (mins)	Repeatability (%RSD)
Mesityl oxide	4.293	0.03
(Bis)tributyltin oxide	4.281	0.01
Trimethyltin chloride	4.226	0.03

As anticipated, the migration time of (bis)tributyltin oxide was in good agreement with that of the neutral marker. Trimethyltin chloride migrated slightly before mesityl oxide implying that it may carry a positive charge under these conditions. Although a separation was not achieved it was anticipated that this could be effected via either the manipulation of pH* and/or the addition of a suitable background electrolyte.

A simple non-aqueous titration was performed to investigate the ease by which pH* could be adjusted. Essentially, the pH* of a stirred 10 cm^3 aliquot of NMF was continually measured as 10 µl aliquots of glacial acetic acid were added with an autopipette. The measured pH* of the initial aliquot of NMF was 7.97 which was in good agreement with the data of Janson and Roeraade[43]. It was determined that a reduction in excess of one pH* unit could be achieved via the addition of only 0.1 % v/v glacial acetic acid as shown in figure 8.1.

Figure 8.1. Relationship between pH* and amount of acetic acid added to NMF.

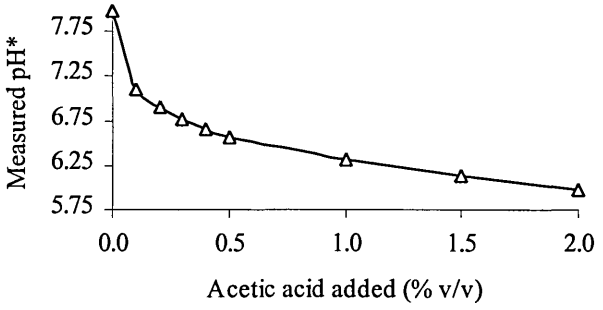

Replicate injections of the mesityl oxide working standard under equivalent conditions on the Beckman instrument gave an average migration times of 3.132 mins for mesityl oxide (equating to an EOF of 0.000532 $cm^2\ V^{-1}\ s^{-1}$) and 3.136 mins for tributyltin chloride. Repeatability was similar for mesityl oxide (0.14% RSD for n=5) but significantly poorer for tributyltin chloride (2.07% RSD). The migration times for the organotin compound were observed to increase over the series of injections. Additionally, the baseline was prone to drift significantly during separations. Injection of a working standard solution comprising mesityl oxide and tributyltin chloride gave rise to only one peak implying that the alkyltin was uncharged under these conditions and migrated at an identical rate to the EOF.

It has been proposed[43] that the low current generated in NMF is due to the presence of hydrolysis products. It was presumed that the addition of an electrolyte would remove the dependency of the separation on the level of any impurities that were present and in turn stabilise the EOF. Addition of 25 mM ammonium acetate improved baseline stability and resulted in a reproducible EOF. Representative data under these conditions are presented in table 8.2.

Table 8.2 Magnitude and repeatability of the EOF generated in NMF containing 25mM ammonium acetate at an applied voltage of 28 kV (500 V/cm).

Mean t_m (mins)	4.300
Repeatability (% RSD)	0.19
Magnitude of EOF ($cm^2 V^{-1} s^{-1}$)	0.000388

Replicate injections of tributyltin chloride gave an average migration time of 4.450 mins However, migration time repeatability was poor (RSD of 2%) involving a 12 second range of observed migration times. Again, injection of a working standard comprising the organotin compounds and the EOF marker resulted in a single peak.

The previously discussed aqueous CE separations[132, 306] were performed under acidic conditions (pH 2.0 and 4.5 respectively). The rationale given for the choice of conditions was that some analytes were prone to adsorbing onto the charged capillary wall resulting in poor peak shapes. Addition of 1% v/v acetic acid resulted in an erratic baseline and poor EOF repeatability as highlighted in table 8.3. The latter involved a 35.5 second migration time range over the replicate injections.

Table 8.3 Magnitude and repeatability of the EOF generated in NMF containing 25mM ammonium acetate and 1% v/v acetic acid at an applied voltage of 28 kV (500 V/cm).

Mean t_m (mins)	6.205
Repeatability (% RSD)	3.94 %
Magnitude of EOF ($cm^2 V^{-1} s^{-1}$)	0.00027

Again, it was demonstrated that tributyltin chloride was uncharged under these conditions. The acid content was subsequently increased to 1M but even under these conditions tributyltin chloride still migrated with the EOF.

Stock solutions of trialkyltin compounds can be prone to rapid degradation[308]. All stock solutions were therefore remade. The plain NMF study was repeated to determine whether all of the previously described investigations had been performed using degraded standards. Injection of a mixed solution of mesityl oxide and tributyltin chloride gave rise to a single peak confirming that the alkyltin compound is uncharged in plain NMF. The interesting observation in this repeat investigation was that an EOF of a comparable magnitude to the original study was observed even though a new bottle of NMF was used (average migration time for mesityl oxide 3.185 compared to 3.132 previously). The latter implied ruggedness/repeatability of separations employing NMF as a separation medium.

8.6. INVESTIGATION OF DIRECT UV DETECTION.

Efforts concentrated on attempting to record the diode array spectra of the analytes over the wavelength range 190-300 nm. It was hoped that a suitable separation medium could be developed that allowed direct absorbance at 200 nm. Identification of unknown peaks could then be effected by comparison of their absorption spectra with those of the standard compounds stored in the library.

Acetonitrile has a low (190 nm) cut-off but requires the addition of acetic acid to effect dissolution of the electrolytes required to yield a stable and reproducible EOF. Acetic acid would result in a significant absorbance at 200 nm.

Methanol has a UV cut-off of approximately 205nm but requires the addition of an electrolyte under acidic or basic conditions to counteract the addition/depletion of protons through electrode processes to yield a stable and reproducible EOF. Sodium acetate is readily dissociated in methanol. The UV absorption spectrum of a 5 mM solution of sodium acetate in methanol was recorded. The resulting scan that is presented in figure 8.2 indicated that this medium would not absorb significantly at 200 nm.

Figure 8.2 UV absorption spectrum of methanol containing 5mM sodium acetate.

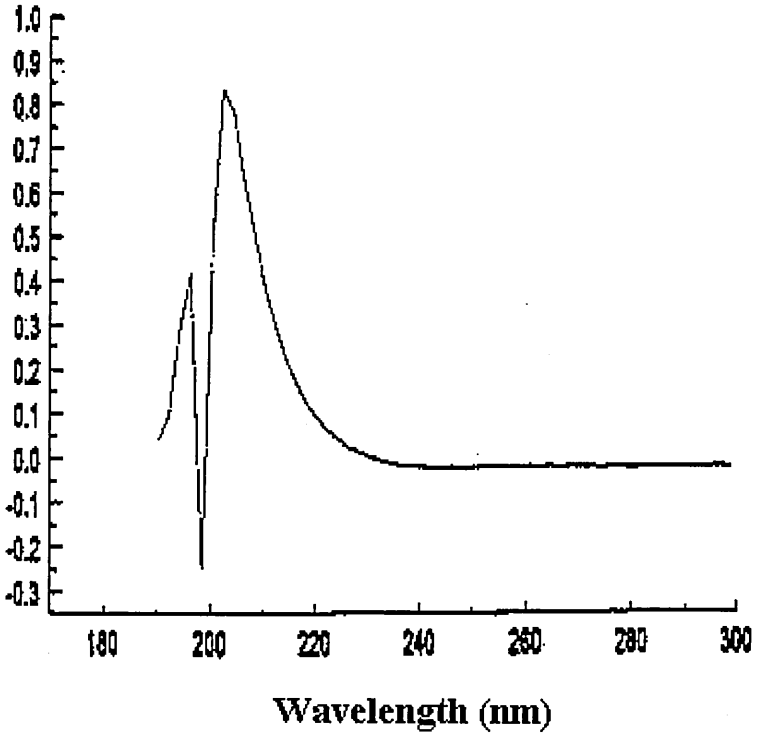

Injection of a working standard comprising all 4 alkyltin compounds resulted in a single peak that was subsequently determined to migrate at an identical rate to the EOF.

Diode array spectra of all 4 test compounds were recorded via the injection of individual compounds. The resulting spectra were essentially featureless as indicated in figure 8.3. Hence, this strategy would be incapable of discriminating between the different analytes if a separation could be effected

Figure 8.3 Diode array spectra of the 4 organotin compounds recorded in non-aqueous media comprising methanol containing 5 mM sodium acetate.

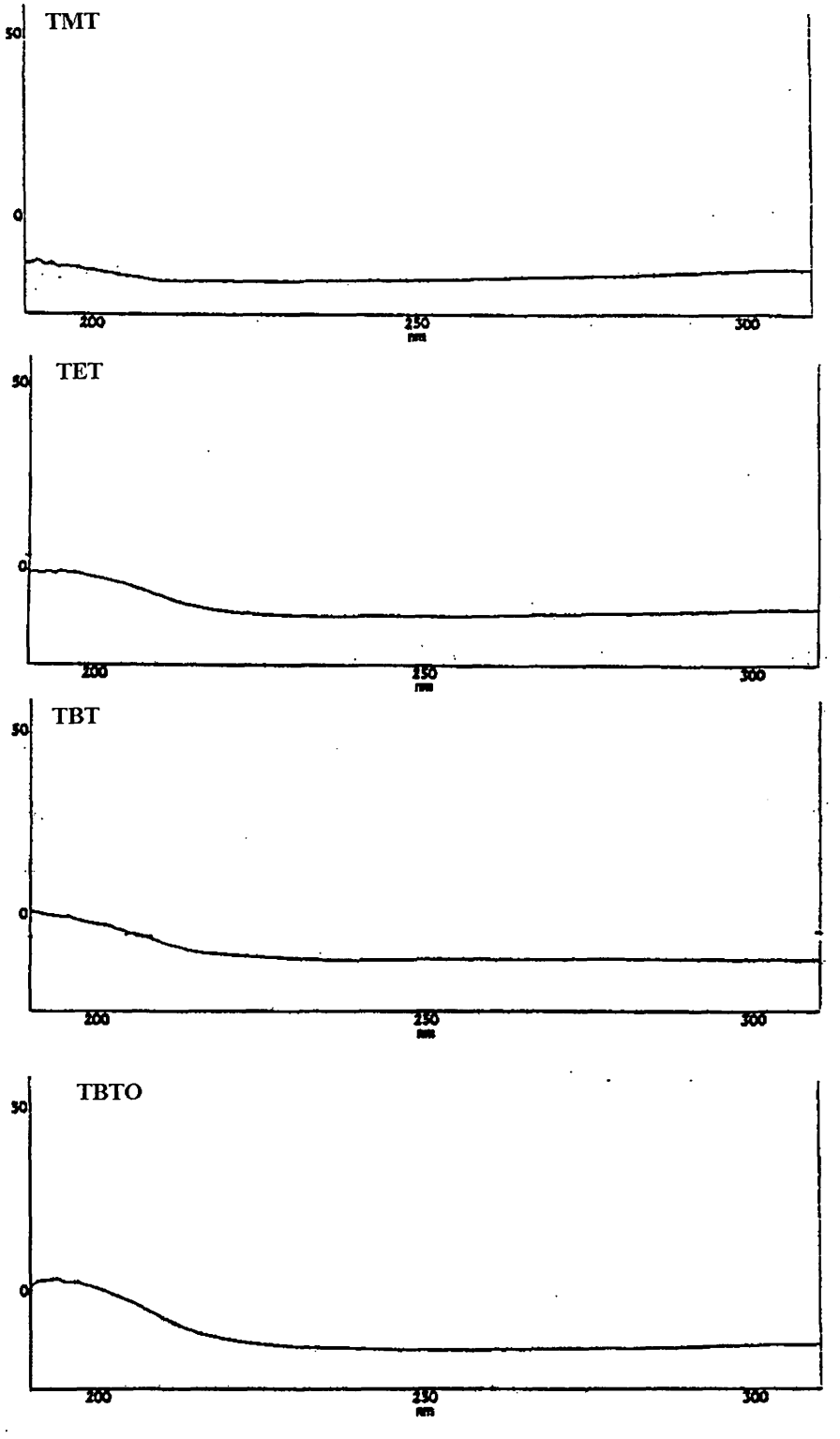

8.7. NON-AQUEOUS CEC.

The majority of reported HPLC methods for organotin species employ either ion exchange materials or cyano phases[304, 305, 309]. The latter typically involves normal phase separation employing non-polar solvents. Unfortunately, ion-exchange packing material was unavailable. Several attempts were made to fabricate a cyano column without success. Columns were prepared but the packed bed was prone to collapse during fabrication or flushing/equilibration.

The failure of the previously reported non-aqueous CEC studies (chapter 8) was frustrating and somewhat puzzling. NMF had consistently generated a repeatable EOF during the course of the experimental work and hence was assessed as a potential eluent for CEC. It was hoped that this would then allow the organotin compounds to be separated. A column was fabricated and equilibrated with NMF (Sherisorb ODS 3 μM batch number 94/262/2). Injection of a mesityl oxide working standard (0.1mg/ml) resulted in a broad peak at a migration time of 18.5 minutes indicating that the desired concept was feasible. Repeatability was extremely poor over a series or replicate injections and hence the column was re-equilibrated. A peak for mesityl oxide was never observed again and due to pressures of time this area of investigation was discontinued.

8.8. CONCLUSION.

Separation of the organotin compounds was not as straightforward as first anticipated. NMF did address the issues concerning detection but the analytes did not appear to be charged in this media. Generation of an EOF in NMF during the CEC investigations was a positive result even if it could not be repeated as it demonstrated the concept of using indirect UV detection using NMF as a separation medium. It would have been interesting to attempt one of the reported HPLC separations by CEC using an ion exchange (SCX) packing.

Chapter 9.

SEPARATION OF PHTHALATE ESTERS: A CRITICAL EVALUATION OF CEC.

9.1. INTRODUCTION.

Phthalate esters were employed to critically assess the performance of CEC in a "real" environmental application. Initial method development was performed using isocratic HPLC to access the ease by which established LC methods could be transferred to CEC. The studies were also intended to determine any advantages offered by electrically-driven separations.

Phthalate esters were identified as a suitable test series from a brief survey of the literature and applications catalogues. Most reported separations employed RP-isocratic elution using a simple acetonitrile/water mobile phase that could easily be adapted to CEC.

9.2. BACKGROUND.

Phthalates are simply the esters of phthalic acid. Their general structure is indicated in figure 9.1.

Figure 9.1. General structure of phthalate esters:

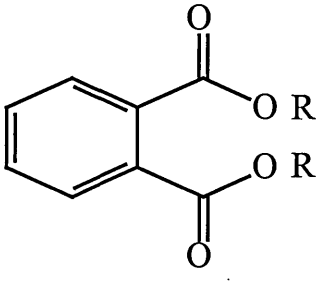

Where R typically represents an alkyl chain. Phthalates in which the two R groups are identical are termed dialkyl (or symmetrical) phthalates.

Phthalates are one of the most abundant artificially made chemicals in the environment. They are well known pollutants[310] and are particularly toxic to aquatic lifeforms[311]. They are widely employed as plasticizers in industrial applications to impart flexibility into high molecular weight polymers such as PVC. Butylbenzyl phthalate is found in vinyl floor tiles and adhesives whilst dibutyl phthalate occurs in food packaging. In these applications the phthalates are not chemically bound to the polymer matrix and hence are able to migrate from the material. This property has obvious implications in applications involving foods and medical products.

Dialkyl phthalate esters are extremely hydrophobic.. The solubility of DEHP in water is particularly limited being only 0.3-0.4 mg/l at 20 °C[312]. Volatility and polarity decrease with increasing molecular weight resulting in increased retention times in chromatographic analyses[313].

9.3. MATERIALS AND METHODS.

The identities and structures of the compounds that were employed in these studies are presented in table 9.1.

Table 9.1 Structures of the dialkyl phthalates employed in this study.

Name	Abbreviation	R
Dimethyl phthalate *	DMP	$-CH_3$
Diethyl phthalate *	DEP	$-C_2H_5$
Dibenzyl phthalate	DBZP	$-CH_2C_6H_5$
Di-n-butyl phthalate *	DNBP	$-C_4H_9$
Bis (2-ethylhexyl) phthalate *	DEHP	$-CH_2CH(C_2H_5)C_4H_9$
Dinonyl phthalate	DNP	$-CH_2(CH_2)_7CH_3$

* Indicates listed as priority pollutant in EPA GC-ECD method no 606.

Individual stock solutions (1mg/ml) of each compound were prepared in acetonitrile. Working standards (0.05mg/ml) were prepared when required via dilution of these stock solutions with the appropriate mobile phase. Elution orders were determined in both HPLC and CEC separations via the injection of individual compounds and/or spiking of standard solutions.

An optimum detection wavelength of 230nm was identified from scans of the phthalate standards in the region 190-300nm using a Thermo Unicam model UV2 spectrometer.

9.4. EXPERIMENTAL PROCEDURES.

9.4.1. Preparation of columns employed for CEC separations.

All of the packing materials that were used to prepare CEC columns were kind gifts. An empty HPLC column of dimensions 100 x 4.6 mm i.d was employed as a reservoir for the packing material slurry. These were packed into fused silica capillaries under a high pressure that was applied using a Shandon column packer (Hypersil, Cheshire, UK).

Columns comprising a packed length of 20 cm (from the inlet side) were prepared using the following slurry method. Minor modifications and improvements were made to the method during the course of the investigations. A diagrammatic summary of the procedure follows in figure 9.2.

1. A 60-70 cm length of 50μm i.d. uncoated fused silica capillary was flushed with sodium hydroxide (1.0 M, 2000 mbar) for 30 minutes to promote the ionisation of surface silanol groups. Residual sodium hydroxide was removed by flushing with water (2000 mbar) for 5 minutes. A temporary retaining frit was formed by tapping 3 μm bare silica (Hypersil, Cheshire, UK) into one end of the capillary and sintering the resultant plug in the flame of a micro Bunsen burner for a few seconds.

2. A packing slurry was prepared by adding a few mg of packing material to approximately 5-10 ml of acetone in a capped CE vial. The resulting solution was placed in an ultrasonic bath for a period of not less than five minutes to ensure homogeneity. The resulting slurry was quickly transferred to the packing reservoir.

3. The capillary was tightly attached to the reservoir and packing against the frit was initiated using acetone at a pressure of 6000 PSI. The whole reservoir assembly was placed into an ultrasonic bath to aid the packing process. It is unlikely that ultrasonic waves penetrated the stainless steel but the vibrational effects induced within the reservoir assembly did appear to enhance the rate of packing. The packing process was monitored with the aid of a microscope.

4. The applied pressure was removed when the packed section length was just greater than the 20 cm required. The pressure remaining within the system was allowed to dissipate without any external interference. This strategy avoided causing any pressure shocks that may have caused inhomogenieties within the packed section. The column was subsequently flushed with water for a period of 1 hour at a pressure of 2000 PSI.

5. The initial bare silica frit was replaced with a permanent inlet frit formed from the packing material. This was achieved by sintering a small section of the packed bed using a commercially available frit burner whilst water still flowed through the column. The burn time required to form a stable retaining frit was found to vary between different packing materials but was typically in the order of two to three minutes.

6. The small section of capillary containing the initial frit was carefully removed with a ceramic cutting tool. An outlet frit was formed in a similar fashion after a period of ten minutes with typical burn times in the order of 30 to 60 seconds. The pressure within the system was again allowed to dissipate naturally to limit the possibility of shocks to either the packed bed or inlet frit.

7. The column was reversed and the excess packing material was removed by flushing with water at a pressure of 2000 PSI. This process typically required ten to fifteen minutes and again was aided by the vibrational effects of an ultrasonic bath.

8. Excess capillary was removed from the outlet side using a ceramic cutting tile to yield a total length of 60 cm. A detection window was created at a distance of 16cm from the outlet end using a commercially available frit burner. The effective length was therefore 44 cm.

Figure 9.2 Packing procedure employed to fabricate columns for CEC separations.

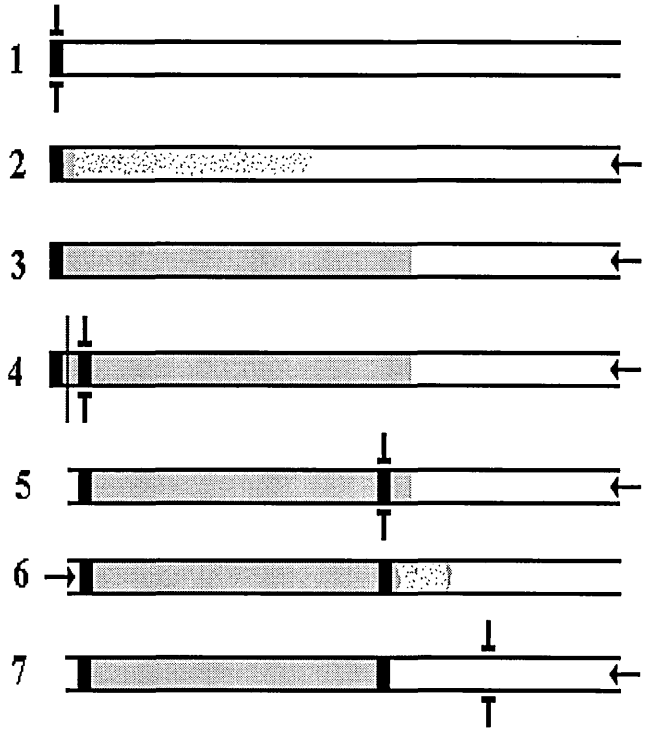

9.4.2. CEC Separation.

All separations were effected at an applied voltage of 30 kV (500 V/cm) using the Thermo Unicam instrument. The current generated under these conditions was typically in the order of 1.0-1.5μA

All mobile phases were degassed prior to use via ultrasonication for a period of 10 minutes. Attempts to repeat the equilibration procedure of Smith and Carter-Finch[196] were unsuccessful. Instead, the separation capillary was flushed with the relevant mobile phase at a pressure of 2000 PSI for 1 hour prior to equilibration on the CE. The latter process initially involved the application of 5 kV. This was subsequently increased in a step-wise fashion to 30 kV over a period of two hours. The column was then allowed to equilibrate at 30 kV for a further hour prior to the acquisition of any analytical data. All samples were electrokinetically injected (30 kV, 0.2 minutes).

9.4.3. Isocratic HPLC separation.

All separations were achieved using a PYE Unicam model PU4015 HPLC system and a model PU4025 UV detector. All samples were manually introduced with a syringe via a 25 μL loop. Chromatograms were acquired using a Hewlett Packard model HP3394 integrator. Mobile phases were freshly prepared prior to analysis and degassed via ultrasonication for a period of 20 minutes.

A Hypersil (Runcorn, Cheshire, UK) column of dimensions 250 x 4.6 mm packed with 5 μm C_{18} ODS particles was employed during method development. This was equilibrated prior to analysis and when changing mobile phase composition by passing 20 column volumes of the appropriate mobile phase. All equilibrations and separations were effected at a flow rate of 1ml/min. The retention time repeatability of triplicate injections of a thiourea working standard (0.05 mg/ml) was used to determine t_o and indicate whether the system was suitably equilibrated prior to commencing separations.

9.4.4. Gradient HPLC

All separations were achieved using a Jasco HPLC system (Essex, UK) comprising a model PU980 pump and model UV975 detector. Sample injections (25 μL) were performed manually using the in-built injector.

Separations were effected using the same 5 μm C_{18} Hypersil column that was employed in the previously described isocratic development work. A flow rate of 1ml/min was again adopted. Chromatograms were acquired using a Hewlett Packard model HP3394 integrator. Mobile phases were freshly prepared prior to analysis and degassed via ultrasonication for a period of 20 minutes.

9.4.5. Open capillary investigations.

All studies were performed at an applied voltage of 30 kV (500 V/cm) using the Thermo Unicam instrument. A 60 cm length of 50 μm i.d. uncoated fused silica capillary was flushed with sodium hydroxide (1.0 M, 2000 mbar) for 30 minutes to promote the ionisation of surface silanol groups. Residual sodium hydroxide was removed by flushing with water (2000 mbar) for 5 minutes. A detection window was created at a distance of 16cm from the outlet using a commercially available frit burner. The effective length was therefore 44 cm. On column UV absorbance detection was performed at a wavelength of 230 nm.

The separation capillary was equilibrated at the start of each investigation by flushing with sodium hydroxide (0.1 M, 2000 mbar) for 5 minutes. Residual sodium hydroxide was removed by flushing with water (2000 mbar) for 5 minutes. A two-stage equilibration was performed with the appropriate mobile phase which was first hydrodynamically pumped (2000 mbar) for 5 minutes and then electrically driven (30 kV) for 5 minutes. The capillary was rinsed using acetonitrile (2000 mbar) for 5 minutes at the end of each working day prior to careful storage.

The capillary was rinsed between replicate separations with the relevant mobile phase (2000 mbar) for two minutes. In addition, the first two separations of all investigation were ignored and not included in any subsequent data analysis. All samples were hydrodynamically injected (25mBar, 0.2 minutes)

9.5. DEVELOPMENT OF A SEPARATION USING HPLC.

Pure (i.e. 100%) acetonitrile was initially employed as a mobile phase. Development of an isocratic separation essentially involved reduction of the initial elution strength in a stepwise fashion via the addition of water.

The first four eluting compounds were hardly retained in 100% acetonitrile, eluting just after t_o. The limited separation made the determination of peak identity and hence elution order extremely difficult. However, the latter two peaks of the six were determined to be DEHP and DNP respectively. All six compounds were eluted in less than six minutes. A representative separation under these conditions is presented in figure 9.3.

Figure 9.3 Initial HPLC separation of 6 phthalates using a mobile phase comprising 100% acetonitrile.

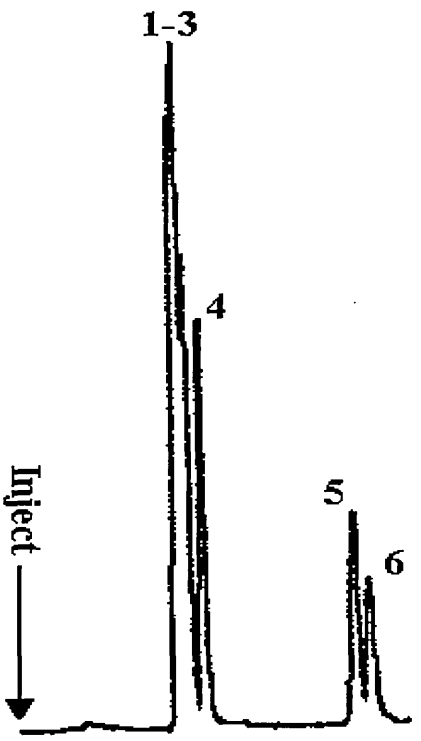

The elution strength of the mobile phase was subsequently reduced via the addition of 10 % v/v water. This resulted in an improved separation between the first four compounds at the expense of analysis time which increased to approximately fourteen minutes. Elution order was based on increasing hydrophobicity namely DMP, DEP, DBZP, DNBP, DEHP and finally DNP. The resolution between DMP and DEP was estimated to be 0.83 (Chapter 2).

Retention time repeatabilities for DMP, DEP, DBZP and DNBP were all below 2.0 % RSD (n=5). However, significantly poorer precision was obtained for the DEHP and DNP bands which displayed extremely erratic behaviour over the five replicate injections. Essentially, retention times for these two compounds increased significantly with each subsequent injection until a point where they were not eluted at all. In this situation they could only be removed from the column by flushing with acetonitrile. A representative separation achieved under these conditions is shown in figure 9.4.

Figure 9.4 Separation of 6 phthalates at a mobile phase composition of 90/10 % v/v acetonitrile/water.

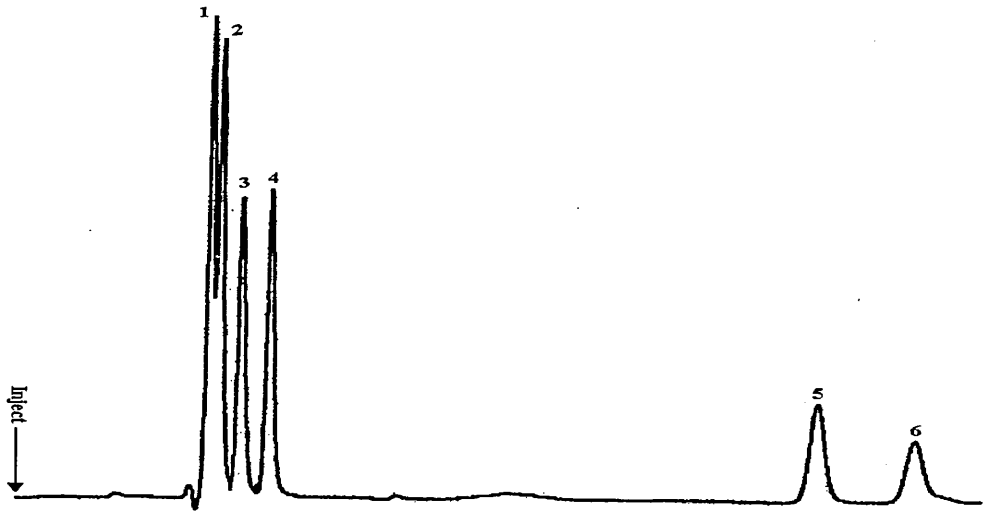

		Average t_r (min)	% RSD (n=5)
1	DMP	3.07	1.66
2	DEP	3.22	1.72
3	DBZP	3.56	1.58
4	DNBP	3.99	1.86
5	DEHP	12.61	-
6	DNP	14.93	-

Further reduction of the mobile phase strength (80/20 v/v acetonitrile/H_2O) resulted in separation of DMP and DEP. However, DEHP and DNP were not eluted under these conditions and could only be removed from the column by flushing with acetonitrile. Retention time repeatabilities were similar to those obtained at higher organic compositions. A representative separation of a working standard comprising DMP, DEP, DBZP and DNBP is presented in figure 9.5.

Figure 9.5 Separation of DMP, DEP, DBZP and DNBP using a mobile phase comprising 80/20 v/v acetonitrile/water.

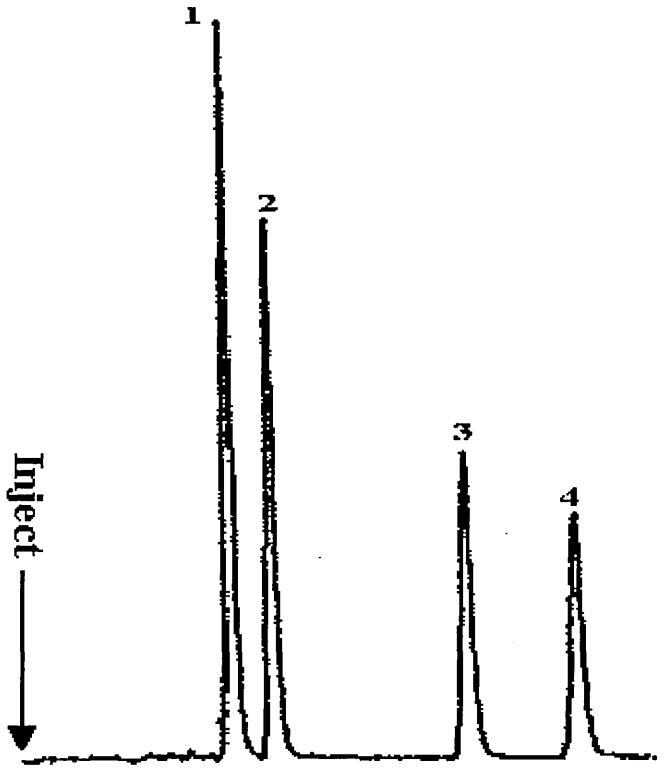

		Average t_r (min)	% RSD (n=5)	N (plates/m)
1	DMP	3.66	1.43	5400
2	DEP	4.31	1.72	7500
3	DBZP	7.39	1.75	12500
4	DNBP	9.14	1.92	19000

These studies implied that it would be necessary to increase the elution strength of the mobile phase during the course of the separation in order to effect a full separation of all six compounds. A full separation was achieved using the simple gradient program given in table 9.2.

Table 9.2 Gradient program for HPLC separation of phthalates.

Time (Min)	% A	% B
0	100	0
5	0	100

Where:

A = 70:30 v/v acetonitrile/water.

B = Acetonitrile.

The final mobile phase composition was held constant for a further 10 minute period to complete the separation.

This simple study adequately illustrated the need to manipulate elution strength in order to effect a full separation and inspired attempts to effect a gradient CEC separation. Hence further method development/optimisation was not undertaken. A representative separation of the six phthalates under these conditions is presented in figure 9.6.

Figure 9.6 Separation of six phthalates using a simple gradient program.

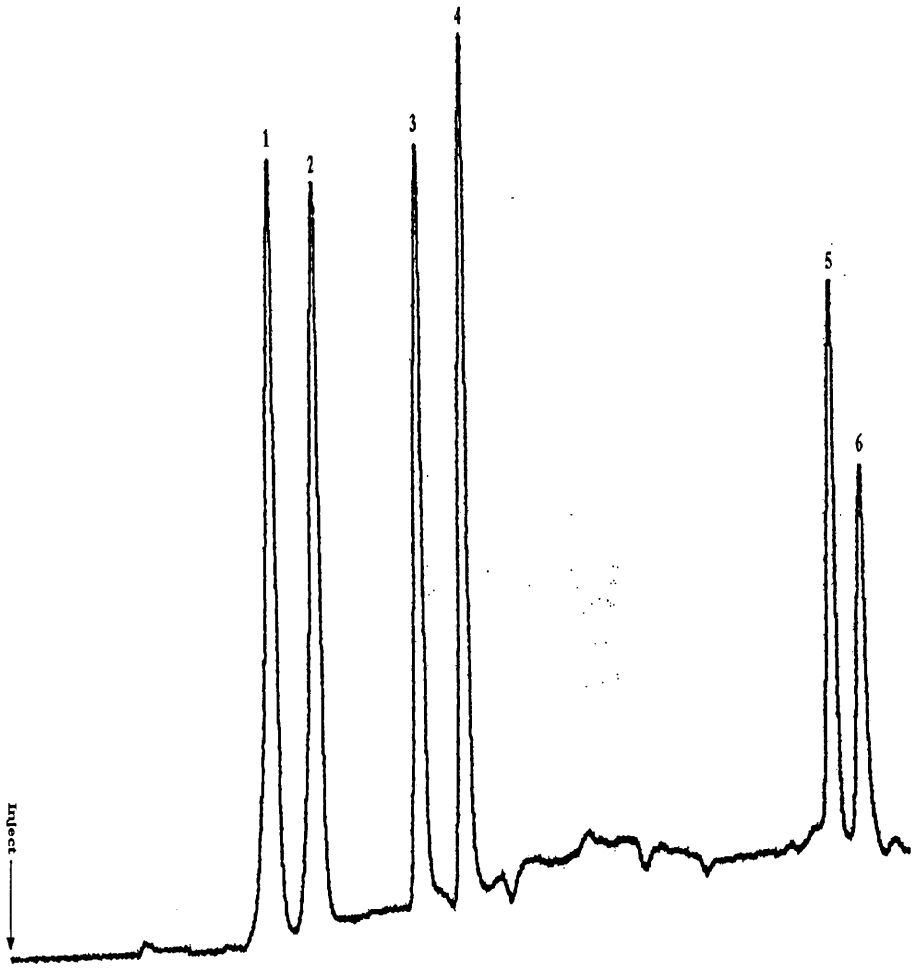

		Average t_r (min)	% RSD (n=5)
1	DMP	4.16	1.84
2	DEP	4.83	1.91
3	DBZP	6.43	1.94
4	DNBP	7.13	2.03
5	DEHP	12.79	1.97
6	DNP	13.24	2.07

9.6. SEPARATION BY CEC.

An initial separation of the six phthalates was performed at 30 kV on a Sherisorb 5 μm ODS column using a background electrolyte comprising 80/20 v/v acetonitrile/4mM sodium tetraborate (pH 9.2). At the time of undertaking this work I believed that no other CEC separation of these EPA phthalates had been presented.

The separation was essentially similar to that achieved by HPLC using 80/20 v/v acetonitrile/water. However, a slight overlap of the DMP and DEP bands was apparent. Conversely, peak efficiencies were significantly higher.

Migration time repeatabilities for the first four phthalates were similar to those that were determined for the HPLC separation. Peaks corresponding to DEHP and DNP were eluted only on the first of the five replicate separations. The investigation was continued regardless to avoid a troublesome and time-consuming column flushing procedure. Elution of these compounds from the CEC column with acetonitrile using the Shandon packer was inconvenient since the buffer had to be flushed from the column before it could be rinsed with acetonitrile to avoid precipitation. No evidence of the two bands was observed during the remaining separations. A copy of the first separation involving all six phthalates is presented in figure 9.7.

Figure 9.7 Separation of 6 phthalates at an applied voltage of 30 kV using a 5 μm ODS capillary and a mobile phase comprising 80/20 v/v acetonitrile/4mM sodium tetraborate (pH 9.2)

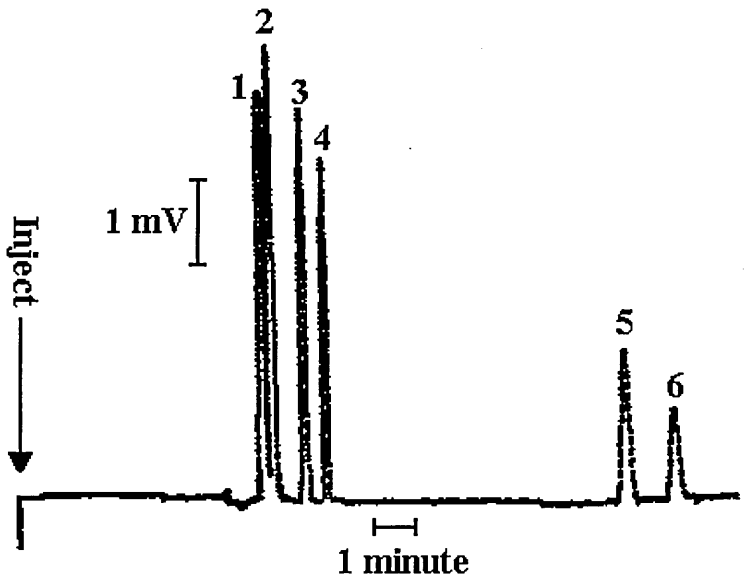

		Average t_m(min)	% RSD (n=5)	N (plates/m)
1	DMP	5.281	1.56	63900
2	DEP	5.480	1.48	90250
3	DBZP	6.172	1.39	141500
4	DNBP	6.546	1.80	175000
5	DEHP	11.887	-	191000
6	DNP	15.508	-	270000

The inlet frit of the column collapsed during flushing and hence the separation could not be repeated. A second study was undertaken using a replacement column that was prepared and equilibrated in an identical fashion. Baseline separation was achieved between DMP and DEP. Mean migration times for DMP, DEP, DBZB and DNBP were similar to those obtained in the initial separation but repeatabilities were poorer. Significant differences were apparent when comparing peak efficiencies with the original study.

Again, peaks corresponding to DEHP and DNP were observed only on the first of the five replicate injections and no evidence of the two bands was observed during the remaining separations. The full separation that was obtained during the first injection is presented in figure 9.8.

Figure 9.8 Separation of 6 phthalates at an applied voltage of 30 kV using a replacement 5 μm ODS capillary and a mobile phase comprising 80/20 v/v acetonitrile/4mM sodium tetraborate (pH 9.2).

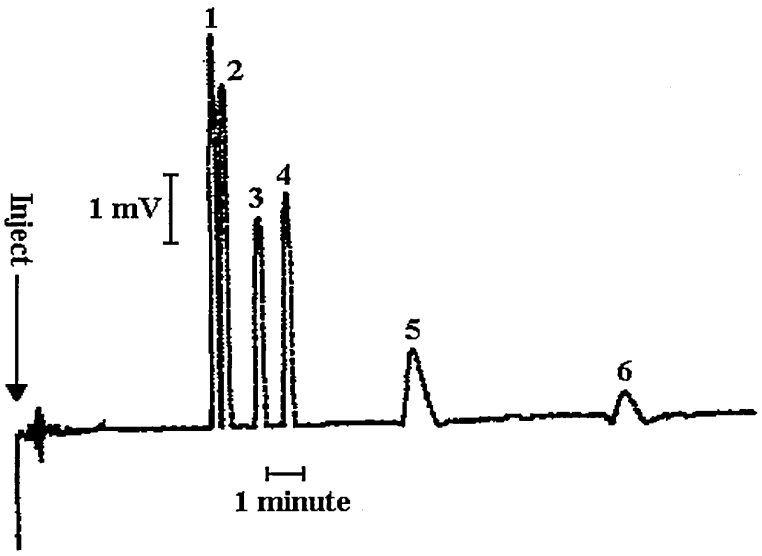

		Average t_r (min)	% RSD (n=5)	N (plates/m)
1	DMP	5.206	1.84	98500
2	DEP	5.436	1.91	107500
3	DBZP	6.172	2.06	34600
4	DNBP	6.776	2.41	41750
5	DEHP	9.481	-	20500
6	DNP	13.801	-	43300

A column was subsequently prepared using 3 μm ODS (Exsil) packing material to determine the improvement in separation that could be achieved by employing smaller particles. Migration time repeatabilities were superior to those that had been achieved using the 5 μm columns. Most surprising was that calculated peak efficiencies were significantly poorer than were obtained using the 5 μm ODS particles. A representative separation using this column is shown in figure 9.9.

Figure 9.9 Separation of 6 phthalates at 30 kV on a 3 μm ODS (Exsil) column employing a mobile phase comprising 80/20 v/v acetonitrile/4mM sodium tetraborate (pH 9.2)

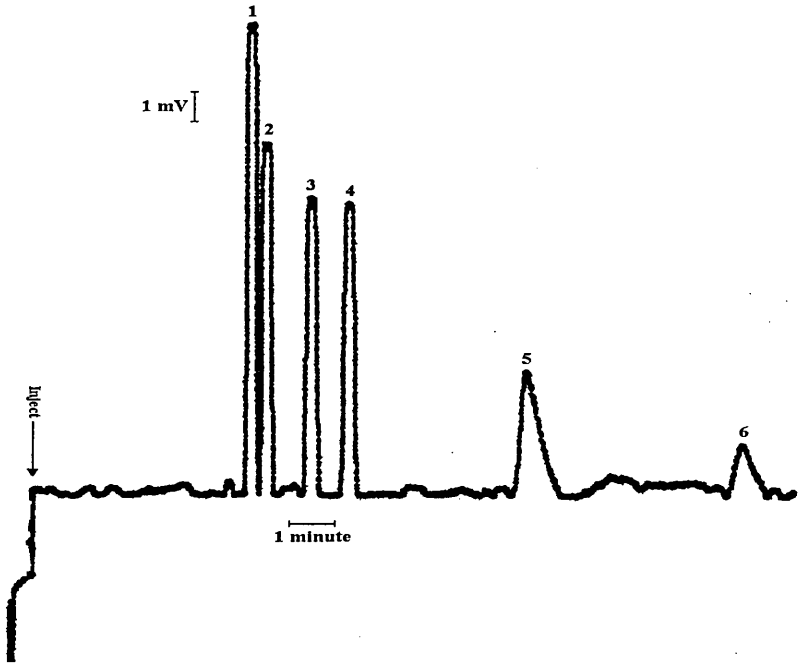

		Average t_r (min)	% RSD (n=5)	N (plates/m)
1	DMP	5.287	0.64	33500
2	DEP	5.614	0.66	21500
3	DBZP	6.658	0.77	27750
4	DNBP	7.454	0.64	35700
5	DEHP	11.237	9.33*	28500
6	DNP	15.508	4.69*	17900

* Note: RSD values for DEHP and DNP calculated for n=2 (not eluted on other injections).

9.6.1. Investigation of DEHP and DNP retention issues using MEKC.

Ong and co-workers[314] experienced similar migration behaviour with DEHP during a MEKC separation of phthalates. They subsequently determined that the high applied separation voltage caused DEHP to undergo hydrolysis yielding phthalic acid. The latter compound appeared as an additional peak that migrated after the analyte compounds due to its electrophoretic attraction towards the anode.

The possibility that this process had affected the CEC separations was investigated. Ten replicate injections of a DEHP working standard (0.05mg/ml) were performed using an open (i.e. unpacked) 50 μm i.d fused silica capillary. All other conditions such as buffer composition, injection procedure and applied voltage were identical to those that were employed for the CEC separations. A summary of the resulting data is presented in table 9.3.

Table 9.3 Migration time repeatability of a DEHP working standard at 30 kV in an open 50 μm fused silica capillary using a mobile phase comprising 80/20 v/v acetonitrile/4mM sodium tetraborate (pH 9.2)

Average DEHP t_m (mins)	3.404
Repeatability (% RSD)	3.39
Range of obtained t_m values (min)	0.284

The DEHP band did not change significantly over the 10 injections and no other evidence to suggest hydrolysis was observed during these investigations. The studies were repeated using a working standard comprising DEHP and thiourea (0.1mg/ml and 0.05mg/ml respectively). DEHP migrated with thiourea resulting in a single peak. Again, no evidence of hydrolysis was apparent over the 10 injections. A summary of the data is presented in table 9.4.

Table 9.4 Migration time repeatability of a working standard containing thiourea and DEHP at 30 kV in an open 50 μm fused silica capillary using a mobile phase comprising 80/20 v/v acetonitrile/4mM sodium tetraborate (pH 9.2)

Average t_m (mins)	3.617
Repeatability (% RSD)	3.14
Range of obtained t_m values (min)	0.270

The issues surrounding DEHP and DNP were presumed to be a result of their limited aqueous solubility causing them to come out of solution. Although the aqueous solubility of these phthalates is extremely low it is surprising that they would be insoluble in 80% acetonitrile. The only other plausible explanation would be adsorption somewhere within the separation system.

9.7. INVESTIGATION OF CEC SEPARATIONS EMPLOYING NON-AQUEOUS MOBILE PHASES.

Further development of the previously discussed CEC separations was restricted due to the limited aqueous solubility of borate and phosphate buffers. Hence, the use of a pseudo-gradient[268] involving replacement of the initial mobile phase with one containing a higher concentration of organic modifier during the separation was unfeasible. Alternative background electrolytes namely TRIS and ammonium acetate were briefly investigated but no useful data were obtained. However, it is possible that the apparent failure of these materials was due to the columns employed in the studies.

The investigation of non-aqueous mobile phases was considered to be a natural progression to the open capillary work that was presented in chapter 3. It was anticipated that non-aqueous media would significantly expand the scope of CEC method development and lead to a successful separation of the hydrophobic phthalates.

Initial studies involved attempting to reproduce the work of Whitaker and Sepaniak[41] who reported a rapid EOF in pure acetonitrile containing no background electrolyte or additives during CEC method development.

A 3 μm ODS (Exsil) column was prepared and flushed with deaerated acetonitrile for 1 hour before being transferred to the CE. Equilibration was initially performed at an applied voltage of 5 kV. This was subsequently increased in increments of 5 kV over the course of an hour and left at 30 kV for a further two hours. No current registered on the instrument during equilibration implying that any current generated was below the measurable limit of 0.1μA. Injection of a thiourea working standard (0.05mg/ml) did not result in a peak after a one hour separation at 30 kV. The column was subsequently removed and inspected under a microscope. No voids or obvious problems were apparent. The column was flushed with acetonitrile to remove the thiourea standard that was presumed to still reside within.

The column was subsequently equilibrated with a mobile phase comprising 80/20 % v/v acetonitrile/4mM sodium tetraborate (pH 9.18). Five replicate injections of a thiourea working standard resulted in repeatable bands indicating that the column was not responsible for the failure of the non-aqueous investigation. Several attempts were made to repeat this work but none were successful even when extensive equilibration regimes and prolonged run times were employed. Unfortunately it was not possible to employ the same column throughout the studies as they were prone to failure during flushing and equilibration.

Whitaker and Sepaniak also demonstrated that separations could be effected and manipulated by varying the composition of a mobile phase comprising acetonitrile and methylene chloride. A mobile phase comprising 80/20 acetonitrile/methylene chloride was investigated in a similar fashion to the pure acetonitrile studies. Again, several studies were performed but a fast EOF was not observed.

The open capillary studies that were presented in chapter 3 implied that the performance of non-aqueous media in CE was enhanced when a background electrolyte was included. It was therefore anticipated that addition of a suitable electrolyte to acetonitrile would generate a fast and reproducible EOF.

A mobile phase comprising acetonitrile containing 1 mM Tris was chosen to investigate this theory. An initial study resulted in a small band that was presumed to be thiourea at a migration time of 17.434 minutes (corresponding to an EOF of 3.1×10^{-8} $cm^2 V^{-1} s^{-1}$). A small current in the region of 0.2-0.3μA was observed during equilibration and the analytical run. However, this work could not be reproduced.

9.8. CONCLUSION.

A significant number of CEC columns were prepared in order to acquire the data presented in this chapter. Column fabrication was found to be an extremely laborious and time consuming task that required a great degree of skill and patience.

The packing process was found to be inconsistent. The time required to yield a 20 cm packed length varied from less than a minute to an hour. Likewise, the time required to flush excess packing material from the column also varied and in some cases the slug of material became stuck and could not be removed rendering the column unusable.

Column lifetime prior to failure was also inconsistent. No obvious cause or pattern was apparent but the main contributing factor appeared to be poor mechanical strength of the inlet frit. Many columns lasted only a few injections before the inlet frit collapsed. Failure was immediately apparent on the CE since it was accompanied by an erratic fluctuation of the separation current. In addition, columns were extremely fragile and a number were broken during installation onto the CE and the Shandon packer. The constant attachment and removal of columns to and from the packer and CE is likely to have contributed to the high failure rate. In addition, columns also failed as a result of the protective polyimide layer dissolving through prolonged exposure to organic solvents.

Bubbles were only formed on one occasion, which was a result of poor deaeration of the mobile phase rather than the CEC process. Alternative techniques such as vacuum filtration or helium sparging were not explored but may have provided more efficient means of mobile phase de-aeration. Hence, these studies did not support the general theory that CEC instrumentation must be pressurised. However, field strengths would be limited under these conditions and it is therefore acknowledged that pressurised systems are beneficial.

The initial section of the packed bed was prone to drying out which resulted in an erratic current and baseline. This was a minor issue in the sense that removing the column and flushing with the appropriate mobile phase easily rectified it. However, as already indicated this was a time consuming process and constant attachment/removal of the capillary may have contributed to a reduced lifespan.

The disappointing column efficiencies obtained during the CEC separations may be indicative that the packing materials employed were not suitable for this technique or that the packing procedure did not yield high quality columns. It is unfortunate that the newer stationary phases that have been specifically designed for CEC applications were not available at the time. The theory concerning the unsuitability of HP integrators for high efficiency techniques that was proposed during the Cimetidine separations may have also have been a contributing factor.

Chapter 10.

DISCUSSION.

Several electrically-driven separation techniques based on CE have been critically evaluated.

The NACE separations involving cimetidine confirmed that significantly higher efficiencies and markedly different selectivities may be achieved using non-aqueous separation media. Furthermore, it was also possible to investigate analytes that were incompatible with typical aqueous-based media.

Despite such advantages NACE was found to be conceptually difficult. Published studies at this time generally involved an empirical approach rather than theoretical understanding. Such studies typically utilised alteration of solvent composition and/or pH* to manipulate selectivity with no clear explanation/justication of the approach used to accomplish the final separation. Additionally, the diversity of conditions and instrumentation employed complicated the comparison of generated data with that reported in the literature.

NACE migration time repeatabilities generally fell well within regulatory specifications for replicate separations even when employing instrumentation that provided poor control of separation temperature. However, day to day repeatability was generally poor. The latter may have been the result of fluctuating ambient temperature or may hint at capillary conditioning issues. The magnitude of the repeatability issue in NACE is currently unclear due the tendency for authors to neglect the inclusion of such data in key publications. Robustness is clearly a key area of investigation when attempting to develop and validate NACE separations and workers in this area are encouraged to share their experiences and data.

The transfer and qualification of methods between laboratories/instruments is a key activity in regulated industries. Instrumental issues involved in transfer of CE methods were found to be subtler and more sensitive compared to comparable HPLC activities. Few published reports have addressed transfer of methods between different brands of CE instrumentation. It is therefore unknown at this time whether other workers have experienced issues when attempting to perform separations in non-aqueous media using Beckman P/ACE instrumentation.

The work in this thesis has clearly demonstrated the potential use of NMF as a "ready made" inverse UV system for both NACE and CEC. Additionally, impressive migration time repeatabilities were demonstrated using non-aqueous solutions of silver nitrate. Both systems show great promise if suitable applications can be found. The investigation of silver nitrate was inspired by reports concerning electrochemistry experiments in the 1930s. Further reviews of this area of the literature may uncover further systems that could be exploited by NACE.

The underlying theory behind NACE separations clearly needs to be understood before key users who can advance its development and usage adopt the technique. In particular, the inability to accurately define and measure pH* and the unavailability of reference data such as pK_a values in non-aqueous media were found to be restrictive when developing separations during these studies. This work also highlighted that the choice of an EOF marker in NACE may not necessarily be a straightforward task. There is clearly a great deal of work that needs to be undertaken in this area before protocols for generic method development can be proposed.

Poor repeatability of peak areas obtained during replicate separations may be attributable to the integration system employed. Data collection rates must be rapid enough to sufficiently describe the peak. Current systems such as the HP integrator employed in this work are intended for the measurement of relatively broad gaussian peaks encountered in GC and HPLC. Such systems may therefore be incapable of adequately describing the sharp triangular peaks resulting from electrically-driven separations. Accurate measurement of extremely narrow peaks will require higher sampling frequencies than current data processors are capable of. However, instrument manufacturers are unlikely to invest heavily in the development of such technology until there is sufficient market demand to generate a return. Faster processors provide associated challenges concerned with noise suppression and data storage.

The mid 1990's witnessed a significant increase in the number of published papers concerning CEC. The majority of reported work utilised C_{18} phases to accomplish separations of neutral model compounds. Although a developed HPLC separation of a "real" application was successfully applied to CEC during this work, numerous issues were encountered.

Critical evaluation of CEC in this laboratory was hindered by the inability to manufacture reliable columns. A diverse range of fabrication methods have been reported in the literature, many with their own quirks and subtleties. Such reports have rarely described the difficulties and frustrations encountered during the preparation of packed capillaries for this work. The fabrication process was found to be extremely variable with a low success rate. Furthermore, the quality of resulting columns in terms of separation performance and lifetime was generally poor and inconsistent.

Although separations were successfully effected overall performance was generally disappointing and could not match the quality of published work. The latter was clearly illustrated the significantly different efficiencies achieved using two apparently identical 5 μm ODS columns. Additionally, peak efficiencies were poorer for a column fabricated using 3 μm ODS which was not expected from theory.

All packing materials were kind gifts and it is possible that they were not particularly well suited to CEC. The commercial availability of appropriate phases is an obvious requirement if the technique is to develop. Furthermore, it will be necessary to develop and commercialise new phases based on ion exchange and mixed mode materials to further enhance selectivity and applicability.

Column lifetimes were found to limited by the mechanical strength of the inlet frits. The latter were prone to collapse during flushing, equilibration or when effecting separations. Structural integrity is likely to have been adversely affected by the cumulative effects of constant removal and attachment of the capillary from both the CE and the column packer. Use of the Beckman cartridge system that is easily fitted and removed from the instrument would possibly reduce failures caused by constant attachment/removal of capillaries. However, this strategy would only be worth pursuing when reliable and robust columns could be routinely fabricated since disassembly of cartridges to investigate potential failures would be a tedious process.

Erosion of the protective polyimide layer via exposure to organic media was also determined to be a key contributor towards column failure. The latter is a key issue and should inspire research into new capillary materials and/or protective coatings.

The commercial availability of CEC capillaries continues to grow. However, the high financial outlay involved restricted their use in this work, especially since few guarantees regarding performance for a given application, lifetime and robustness were provided by vendors. Future efforts must clearly concentrate on the production of robust and reliable columns available in a variety of stationary phases and of various dimensions if the technique is to be applied routinely. Such columns must also be cost-effective since it is not feasible to repair them in the same manner as HPLC columns where it is customary to repack voids.

A major practical issue in CEC is the formation of bubbles that result in loss of EOF and ultimately cessation of sample elution. The latter has implications for the long unsupervised replicate assays that are routinely performed within regulated laboratories. The need to pressurise the separation capillary to avoid bubble formation has been a popular discussion topic in CEC. This work has demonstrated that separations can be achieved under ambient conditions. However, this approach was driven by the inability of the instrumentation to facilitate pressurisation of the capillary and may not be the optimum approach. It will also be prudent to further investigate so-called "fritless" (or monlithic) columns since bubble formation is believed to occur at the interface of the exit frit and unpacked section of the capillary.

The acceptance and development of electrically-driven methods requires the successful resolution of samples in "real" applications. Many pharmaceutical QC applications do not require the high efficiencies that such techniques are capable of and HPLC methods are well established. Electrically-driven techniques must therefore demonstrate advantages over current methods of analysis in terms of speed, expense, improved accuracy/precision and so forth. Crucially, they must also win regulatory approval. The enhanced peak capacity achievable in CEC may drive its development to focus on the resolution of highly complex samples and matrices such as those encountered in environmental and biomedical applications. The resolution of chiral materials also appears be a key area of promise.

Reported CEC separations have utilised modified CE instruments or home-built systems. As previously discussed, the diversity of conditions and instrumentation employed in reported studies complicates comparison of data. There is an obvious need for manufacturers to invest in the technique and commercialise a CEC instrument capable of both isocratic and gradient elution. Amongst the requirements of such a unit would be the need to address poor injection precision compared to HPLC. This is a criticism that is often levelled at electrically-driven techniques. There is no CE equivalent to the well-known Rheodyne injectors that have been so widely and successfully utilised in liquid chromatography. Hydrodynamic injection does not suffer the bias associated with electrokinetic loading but is not suited to packed capillaries used in CEC due to the associated back pressures. Further demonstrations that electrically-driven methods can achieve comparable precision compared to HPLC assays via validated applications is required.

To conclude, CE and related modes were found to be fascinating techniques capable of effecting some impressive separations. However, such niceties do not make a reliable and robust separation technique. On the basis of these relatively brief evaluations electrically-driven separations have some way to go before they can convince key potential users of their ability to perform in "real" environments, particularly regulated industries. However, electrically-driven techniques, particularly CEC are still in their infancy and need time to mature. Several key supporters continue to develop the techniques and research is set to continue.

CITED REFERENCES.

[1] Kemp G. *Biotechnol and Appl Biochem*, 27, (1998), 9.

[2] Altria K. D, Bryant S. M, Clark B. J and Kelly M. A. *LC-GC*, 15, (1997), 34

[3] Boughtflower R. J, Underwood, T and Paterson C. J, *Chromatographia*, 40, (1995), 329.

[4] Vesterberg O. *J. Chromatogr*, 480, (1989), 3.

[5] Tiselius A. *Trans Farad Soc*, 33, (1937), 524.

[6] Mikkers F. E. P, Everaerts F. M and Verhegon Th. P. E. M. *J. Chromatogr*, 169, (1979), 11.

[7] Hjerten S. *Chrom Rev*, 9, (1967), 122.

[8] Virtanen R. *Acta Polytechnica Scandinavica*, 123, (1974), 5.

[9] Jorgenson J. W and Lukacs K. D. *Anal. Chem*, 53, (1981), 1298.

[10] Jorgenson J. W and Lukacs K. D. *Clin Chem*, 27, (1981), 1551.

[11] Jorgenson J. W and Lukacs K. D. *Science*, 222, (1983), 266.

[12] Rice C. L and Whitehead R. *J Phys Chem*, 69, (1965), 4017.

[13] van Orman. B. B, Liversidge G. G, McIntyre G. L, Olefirowicz T. M and Ewing A. G. *J Micro Sep*, 2, (1990), 176.

[14] Altria K. D, Kelly M. A and Clark B. J. *Chromatographia*, 43, (1996), 153.

[15] Blanchin M. D, Baalbaki B, Bosc B and Fabre H. *Anal Chim Acta*, 415, (2000), 67.

[16] Giddings J. C. *Separation Science*, 4, (1969), 181.

[17] van Deemter J. J, Zuiderweg F. J and Klinkenberg A. *Chem Eng Sci*, 5, (1956), 271.

[18] Hjertén S. *Electrophoresis*, 11, (1990), 665.

[19] Lukacs, K.D. and Jorgenson, J.W. *J High Res Chrom and C. C.*, 8, (1985), 407.

[20] Grushka. E, McCormick R. M and Kirkland. J. J. *Anal. Chem*, 61, (1989), 241.

[21] Veraart J. R, Gooijer C and Lingerman H. *Chromatographia*, 44, (1997), 129.

[22] Zare R. N *et al* United States Patent 5,092,973.

[23] Ackermans M. T, Everaerts F. M and Beckers J. L. *J. Chromatogr*, 549, (1991), 345.

[24] Ward V. L and Khaledi M. G. *J. Chromatogr* A, 859, (1999), 203.

[25] Bocek P, Vespalec R and Giese R. W. *Anal. Chem*, 72, (2000), 586A.

[26] Altria K, Kelly T and Clark B. *LC-GC Int*, 9, (1996), 408.

[27] Altria K. D. *LC-GC* Int, 9, (2000), 320.

[28] Valkó I. E, Sirén H and Riekola M-J. *J Micro Sep*, 8, (1996), 421.

[29] Hjertén S and Liao J-L. *et al* United States Patent 5,464,517.

[30] Heiger D. N. High Performance Capillary Electrophoresis – An Introduction. Hewlett-Packard Company, 1992 (2nd ed).

[31] Altria K. D and Simpson C. F. *Chromatographia*, 24, (1987), 527.

[32] Ward T. J. *Anal. Chem*, 72, (2000), 4521.

[33] Guttman A, Brunet S and Cooke N. *LC-GC Int*, 9, (1996), 88.

[34] Valkó I. E, Billiet A, Corstjens H, A. L and Frank J. *LC-GC Int*, 6, (1993), 420.

[35] Kuhn R. *Electrophoresis*, 20, (1999), 2605.

[36] Valkó I. E, Siren H and Riekola M. L. *LC-GC Int*, 10(3), (1997), 190.

[37] Riekola M. L, Jussila M, Porras S. P and Valkó I. E. *J. Chromatogr* A, 892, (2000), 155.

[38] Sarmini K and Kenndler E. *J. Chromatogr A*, 792, (1997), 3.

[39] Kenndler E. in Guzman N. A (Ed), Capillary electrophoresis technology, Marcel Dekker (NY), (1993), 161.

[40] Chipperfield J. R. Non-aqueous solvents, Oxford University Press, (1999).

[41] Whitaker K. W and Sepaniak M. J. *Electrophoresis*, 15, (1994), 1341.

[42] Wright P. B, Lister A. S and Dorsey J. G.. *Anal. Chem*, 69, (1997), 3251.

[43] Jansson M and Roeraade J. *Chromatographia*, 40, (1995), 163.

[44] Lister A. S, Dorsey J. G and Burton D. E. *J High Resol Chromatogr,* 20, (1997), 523.

[45] Espinosa S, Bosch E and Rosés M. *Anal. Chem.* 72, (2000), 5193.

[46] Leung G. N. W, Tang H. P. O,Tso T. S. C and Wan T. S. M. *J. Chromatogr* A, 738, (1996), 141.

[47] Bjørnsdottir I and Hansen S. H. *J. Chromatogr* A, 711, (1995), 313.

[48] Ellis D.R, Palmer M.E, Tetler L.W and Eckers C. *J. Chromatogr* A, 808, (1998), 269.

[49] Senior J, Rolland D, Tolson D, Chantzis S and De Biasi V. *J Pharm Biomed Anal*, 22, (2000), 413.

[50] Cherkaoui S, Mateus L, Christen P and Veuthey J-L. *J Pharm Biomed Anal*, 21, (1999), 165.

[51] Bjørnsdottir I, Tjørnelund J and Hansen S. H. *J Cap Elec*, 3, 1996, 83.

[52] Bjørnsdottir I and Hansen S. H. *J Pharm Biomed Anal*, 15, (1997), 1083.

[53] Hansen S. H, TjØrnelund J and BjØrnsdottir I. *TRAC*, 15, (1996), 175.

[54] Altria K. D and Bryant S. M. *Chromatographia*, 46, (1997), 122.

[55] Fillet M, Bechet I, Piette V and Crommen J. *Electrophoresis*, 20, (1999), 1907.

[56] Tjørnelund J and Hansen S. H. *Chromatographia*, 44, (1997), 5.

[57] Walbroehl Y and Jorgenson J. W. *Anal. Chem*, 58, (1986), 479.

[58] Tjørnelund J and Hansen S. H. *J Chromatogr* A, 792, (1997), 475.

[59] Miller J. L, Shea D and Khaledi M. G. *J. Chromatogr* A, 888, (2000), 251.

[60] Wright P. B and Dorsey J. G. *J High Resol Chromatogr*, 21, (1998), 498.

[61] Piette V, Lammerhofer M, Lindner W and Crommen J. *Chirality*, 11, (1999), 622.

[62] Bjørnsdottir I, Hansen S. H and Terabe S. *J. Chromatogr* A, 745, (1996), 37.

[63] Wang F and Khaledi M. G. *Anal. Chem*, 68, (1996), 3460.

[64] Mori Y, Ueno K and Umeda T. *J. Chromatogr* A, 757, (1997), 328.

[65] Valkó I. E, Porras S. P and Riekkola M-L. *J. Chromatogr* A, 813, (1998), 179.

[66] Palonen J. M, Porras S. P and Riekkola M. L. *Electrophoresis*, 21, (2000), 586.

[67] Rose Jr D. J and Jorgenson J. W. *Anal. Chem*, 60, (1998), 642.

[68] Huang, X, Gordon, M.J. and Zare, R.N. *Anal. Chem*, 60, (1988), 375.

[69] Tsuda T, Mizuno T and Akyama J. *Anal. Chem*, 59, (1987), 799.

[70] Deml M, Foret F and Bocek P. *J. Chromatogr*, 320, (1985), 159.

[71] Altria K. D and Fabre H. *Chromatographia*, 40, (1995), 313.

[72] Mayer B. X and Müller M. *LC-GC*, 18, (2000), 694.

[73] Kutter J and Welsch T. *J High Resol Chromatogr*, 18, (1995), 741.

[74] Zhu T, Sun Y, Zhang C, Ling D and Sun Z, *J High Resol Chromatogr*, 17, (1994), 563.

[75] Shafaati A and Clark B. J. *Anal Proc*, 30, (1993), 481.

[76] Kelly M. A, Altria K. D and Clark B. J. *J. Chromatogr* A, 768, (1997), 73.

[77] Jumanen J. H and Riekkola M-L. *Anal. Chem*, 67, (1995), 1060.

[78] Schwartz H. E, Melera M and Brownlee R. G. *J. Chromatogr* A, 480, (1989), 129.

[79] Yang J, Bose S and Hage D. S. *J. Chromatogr* A, 735, (1996), 209.

[80] Altria K. D. *Chromatographia*, 35(3/4), (1993), 177.

[81] Kurosu Y, Satou Y, Shisa Y and Iwata T. *J. Chromatogr* A, 802, (1998), 391.

[82] Wätzig H and Dette C. *J. Chromatogr*, 636, (1993), 31.

[83] Ohms J. Technical information bulletin TIBC 102, (1990), Beckman Instruments Inc (P Alto, California).

[84] Lloyd D. K, *J. Chromatogr* A, 735, (1996), 29.

[85] Coyler C. L, Oldham K. B and Sorkirko A. V, *Anal. Chem*, 67, (1995), 3234.

[86] Heiger D. N, Kaltenbach P and Sievert H.-J P. *Electrophoresis*, 15, (1994), 1234.

[87] Djordjevic N. M, Widder M and Kuhn R. *J High Resol Chromatogr*, 20, (1997), 189.

[88] Chervert J. P, van Soest. R. E. J and Ursem M. J. *J. Chromatogr*, 543, (1991), 439.

[89] Shihabi Z. K. *J Chromatogr* A, 902, (2000), 107.

[90] Hoyt A. M, Beale S. C, Larmann J. P and Jorgenson J. W. *J Micro Sep*, 5, (1993), 325.

[91] Toulas C and Hernandez. *LC-GC*, 10, (1992), 471.

[92] Olson D. L, Lacey M. E, Webb A. G and Sweedler J. V. *Anal. Chem*, 71, (1999), 3070.

[93] Lord G. A. *CAST*, 15, (2000), 9.

[94] Banks F. J. *Electrophoresis*, 18, (1997), 2255.

[95] Dadoo R, Seto A. G, Colón L. A and Zare R. N. *Anal. Chem*, 66, (1994), 303.

[96] Staller T. D and Sepaniak M. J. *Electrophoresis*, 18, (1997), 229.

[97] Petoney Jr, S.L. and Zare, R.N *Anal. Chem*, 61, (1989), 1642.

[98] Petoney Jr, S.L. and Zare, R.N. *J. Chromatogr*, 480, (1989), 259.

[99] Huang X and Kok W. T. *J. Chromatogr* A, 707, (1995), 335.

[100] Mann S. E, Ringo M. C, Shea-McCarthy G, Penner-Hann J and Evans C. E. *Anal. Chem*, 72, (2000), 1754.

[101] van de Griend C. E. S, Kientz Ch. E and Brinkman U. A. Th. *J Chromatogr* A, 673, (1994), 299.

[102] Haber C and Jones W. R. *Cap Elec*, 3, (1996), 1.

[103] Sutton K, Sutton R. M. C and Caruso J. A. *J. Chromatogr* A, 789, (1997), 85.

[104] Sutton K. L and Caruso J. A. *LC-GC*, 17, (1999), 36.

[105] Swinney K and Bornhop D. J. *Electrophoresis*, 21, (2000), 1239.

[106] Messana I, Rossetti D. V, Cassiano L, Misiti F, Giardina B and Castagnola M. *J. Chromatogr* B, 699, (1997), 149.

[107] Krylov S. N and Dovichi N. J. . *Anal. Chem*, 72, (2000), 111R.

[108] Timberbaev A. R and Shpigun O. A. *Electrophoresis*, 21, (2000), 4179.

[109] Beale S. C. *Anal. Chem*, 70, (1998), 279R.

[110] Smith N. W and Evans M. B. *J Pharm and Biomed Anal*, 12, (1994), 579.

[111] Holland L. A, Chetwyn N. P, Perkins M. D and Lunte S. M. *Pharm Res*, 14, (1997), 372.

[112] Nishi H. *Electrophoresis*, 20, (1999), 3237.

[113] Rabel S R and Stobaugh J F. *Pharm Res*, 10(2), (1993), 171.

[114] Ji W and Zhan J. *J. Chromatogr* A, 868, (2000), 101.

[115] Watzig H, Degenhardt M and Kunkel A. *Electrophoresis*, 19, (1998), 2695.

[116] Yesilada A, Gokhan N, Tozkoparan B, Etran M and Aboul-Enein H. Y. *J. Liq. Chromatogr & Rel. Technol.*, 21, (1998), 2619.

[117] Altria K. D and Rudd D. R. *Chromatographia*, 41, (1995), 325.

[118] Wieglos T, Turner P and Havel K. *J Cap Elec,* 4, (1997), 273.

[119] United States Pharmacopeia XXIV, US Pharmacopeial Convention, Rockville MD <621>, 1923.

[120] Altria K. D and Hindocha D. *LC-GC Int*, 11, 1998, 712.

[121] Altria K. D, Frake P, Gill I, Hadgett T, Kelly M A and Rudd D R. *J Pharm and Biomed Anal*, 13, (1995), 951.

[122] Wynia G. S, Windhorst G, Post P. C and Maris F. A. *J. Chromatogr* A, 773, (1997), 339.

[123] Altria K. D, Elgey J, Lockwood P and Moore D. *Chromatographia*, 42, (1996), 332.

[124] Naylor S, Benson L. M and Tomlinson A. J. *J. Chromatogr* A, 735, (1996), 415.

[125] Chen S-H and Chen Y-H. *Electrophoresis*, 20, (1999), 3259.

[126] Altria K. D, Creasey E and Howells J. S. *J. Liq. Chromatogr & Rel. Technol*, 21, (1998), 1093.

[127] Song X and Budde W. L. *J Amer Soc Mass Spec*, 7, (1996), 981.

[128] Moyano E, Games D. E and Galceran M. T. *Rapid Comm in Mass Spec*, 10, (1996), 1379.

[129] Carneiro M. C, Puignou L and Galceran M. T. *J. Chromatogr* A, 669, (1994), 217.

[130] Pérez-Ruiz T, Martínez-Lozano C, Sanz A and Tomás V. *Chromatographia*, 43, (1996), 468.

[131] Liu X and Frank H. *J High Resol Chromatog*, 21, (1998), 309.

[132] Whang K. S and Whang C. W. *Electrophoresis,* 18, (1997), 241.

[133] Nielson M. W. F. *TRAC*, 12, (1993), 345.

[134] Wehr T, Zhu M and Rodriguez-Diaz R. in Karger B. L and Hancock W. S (eds) Methods in Enzymology, 270, (1996), 358, Academic Press.

[135] Kriváková L, Gebauer P and Bocek P. in Karger B. L and Hancock W. S (eds) Methods in enzymology, 270, (1996), 375, Academic Press.

[136] Kriváková L, Gebauer P and Bocek P. *J. Chromatogr* A, 716, (1995), 35.

[137] Mazereeuw M, Tjaden U. R and Reinhoud N. J. *J. Chrom Sci*, 33, (1995), 686.

[138] Chen S and Lee M. L. *Anal. Chem*, 72, (2000), 816.

[139] Mazereeuw M, Tjaden U. R and Reinhoud N. J. *J. Chromat Sci*, 33, (1995), 686.

[140] Enlund A. M and Westerlund D. *Chromatographia*, 46, (1997), 315.

[141] Terabe S, Otsuka K, Ichikawa K, Tsuchiya A and Ando T. *Anal. Chem*, 56, (1984) 111.

[142] Terabe S, Otsuka K and Ando T. *Anal. Chem*, 57, (1985), 834.

[143] Otsuka K, Terabe S and Ando T. *J. Chromatogr*, 332, (1985), 219.

[144] Sepaniak M. J, Burton D. E and Maskarinec M. P in Hinze and Armstrong (eds) Ordered media in chemical separations. ACS symposium series, 342, (1987), 142.

[145] Matsubara N and Terabe S. in Karger B. L and Hancock W. S (eds) Methods in Enzymology, 270, (1996), 319, Academic Press.

[146] Terabe S. *TRAC*, 8, (1989), 129.

[147] Yang S and Khaledi M. G. *Anal. Chem*, 67, (1995), 499.

[148] Muijselaar P. G, Otsuka K and Terabe S. *J. Chromatogr* A, 780, (1997), 41.

[149] Burton D. E, Sepaniak M. J and Maskarinec M. P. *J. Chromat Sci*, 25, (1987), 514.

[150] Ahuja E. S, and Foley J. P. *Anal. Chem*, 67, (1995), 2315.

[151] Emmer Å, Jansson M and Roeraade J. J Chromatogr, 547, (1991), 544.

[152] Palmer C. P. *J. Chromatogr* A, 780, (1997), 75.

[153] Terabe S, Ozaki H and Tanaka Y. *J Chin Chem Soc*, 41, (1994), 251.

[154] Yang S, Bumgarner J. G and Khaledi M. G. *J. High Resol Chromatogr*, 18, (1995), 443.

[155] Nishi H, Fukuyama T, Matsuo M and Terabe S. *J. Chromatogr*, 498, (1990), 313.

[156] Cole R. O, Sepaniak M. J and Hinze W. L. *J High Resol Chromatogr*, 13, (1990), 579.

[157] Cole R. O, Sepaniak M. J, Hinze W. L, Gorse J and Oldiges K. *J. Chromatogr*, 557, (1991), 113.

[158] Terabe S, Shibata M and Miyashita Y. *J. Chromatogr*, 480, (1989), 403.

[159] Clothier Jr J. G, Daley, J. M and Tomellini S A. *J. Chromatogr* B, 683, (1996), 37.

[160] Otsuka K and Terabe S. *J. Chromatogr*, 515, (1990), 221.

[161] Otsuka K, Kawahara J, Tatekawa K and Terabe S. *J. Chromatogr*, 559, (1991), 209.

[162] Peterson A. G. Ahuja E. S and Foley J. P. *J. Chromatogr* B, 683, (1996), 15.

[163] Issaq H. J, Liang P, Horng P. L. C, Janini G. M and Muschik G. M. *J Liq Chromatogr and Rel Technol*, 20, (1997), 167.

[164] Wiedmer S. K, Riekkola M. J, Nydén M and Söderman O. *Anal. Chem*, 69, (1997), 1577.

[165] Bumgarner J. G and Khaledi M. G. *Electrophoresis*, 15, (1994), 1260.

[166] Esaka Y, Tanaka K, Uno B and Goto M. *Anal. Chem*, 69. (1997), 1332.

[167] Ahuja E. S, Little E. L, Neilsen K. R and Foley J. P. *Anal. Chem*, 67, (1995), 26.

[168] Tanaka N, Iwasaki H, Fukutome T, Hosoya K and Araki T. *J High Resol Chromatogr,* 20, (1997), 529.

[169] Greve K. F, Nashabeh W and Karger B. L. *J. Chromatogr* A, 680, (1994), 15.

[170] Balchunas A. T and Sepaniak. *Anal. Chem*, 60, (1988), 617.

[171] Otsuka K, Higashimori M, Koike R, Karuhaka K, Okada Y and Terabe S. *Electrophoresis*, 15, (1994), 1280.

[172] van Hove E, Szücs R and Sandra P. *J High Resol Chromatogr*, 19, (1996), 674.

[173] Allen D. J, Wall W. E, Denson K. D and Smith J. T. *Electrophoresis*, 20, (1999), 100.

[174] Bütehorn U and Pyell U. *Chromatographia*, 43, (1996), 237.

[175] Terabe S, Miyashita Y, Shibata O, Barnhart E. R, Alexander L. R, Patterson D. G, Karger B. L, Hoosoya K and Tanaka N. *J. Chromatogr*, 516, (1990), 23.

[176] Nishi H and Fukuyama T. *J. Chromatogr*, 553, (1991), 503.

[177] Terabe S, Miyashita Y, Ishihama Y and Shibata O. *J. Chromatogr*, 636, (1993), 47.

[178] Terabe S, Ozaki H, Otsuka K and Ando T. *J. Chromatogr*, 332, (1985), 211.

[179] Terabe T, Ishihama Y, Nishi H, Fukuyama T and Otsuka K. *J. Chromatogr*, 545, (1991), 359.

[180] Otsuka K and Terabe S. *J Micro Sep*, 1, (1989), 150.

[181] Bütehorn U and Pyell U. *Chromatographia*, 40, (1995), 69.

[182] Djordjevic, N. M, Houdiere F, Lerch G and Fitzpatrick F. *J High Resol Chromatogr*, 22, (1999), 443.

[183] Yang L and Lee C. S. *J. Chromatogr* A, 780, (1997), 207.

[184] Nishi H and Terabe S. *J. Chromatogr* A, 735, (1996), 3.

[185] Nishi H and Terabe S. *J Pharm &Biomed Analysis*, 11, (1993), 1277.

[186] Scholl J. P and DeZwaan J. *J. Chromatogr* B, 695, (1997), 147.

[187] Altria K. D and McLean R. *Pharm & Biomed Analysis*, 18, (1998), 807.

[188] Rodrigez delgado M. A, Sànchez M. J, Gonzàlez V and Montelongo G. *J High Res Chromatogr*, 19, (1996), 111.

[189] Cugat M. J, Borrull F and Calull M. *Chromatographia*, 46, (1997), 204.

[190] Penmetsa K. V, Leidy R. B and Shea D. *Electrophoresis*, 18, (1997), 235.

[191] Rossi M and Rotilio D. *J High Res Chromatogr*, 20, (1997), 265.

[192] Farran A and Ruiz S. *Intern J Environ Anal. Chem*, 58, (1995), 121.

[193] Altria K. D, Smith N. W and Turnbull C. H. *Chromatographia*, 46, (1997), 664.

[194] Robson M. M, Cikalo M. G, Myers P, Euerby M. R and Bartle K. D. *J Micro Sep*, 9, (1997), 357.

[195] Colón L. A, Reynolds K. J, Alicea-Maldonado R and Fermier A. M. *Electrophoresis*, 18, (1997), 2162.

[196] Smith N. W and Carter-Finch A. S. *J. Chromatogr* A, 892, (2000), 219.

[197] Dittmann M. M, Wienand K, Bek F and Rozing G. P. *LC-GC*, 13, (1995), 800.

[198] Cikalo M. G, Bartle K. D, Robson M. M, Myers P and Euerby M. R. *Analyst*, 123, (1998), 87R.

[199] Pretorious V, Hopkins B. J and Schieke J. D. *J. Chromatogr,* 99, (1974) 23.

[200] Knox J. H and Grant I. H. *Chromatographia*, 24 (1987), 135.

[201] Knox J. H. *Chromatographia*, 26 (1988), 329.

[202] Knox J. H and Grant I. H. *Chromatographia,* 32 (1991), 317.

[203] Knox J. H and McCormack K. A. *Chromatographia*, 38 (1994), 279.

[204] Knox J. H. *J. Chromatogr* A, 680 (1994), 3.

[205] Jorgenson J. W and Lukacs K. D. *J. Chromatogr* 218, (1981), 209.

[206] Li D and Remcho V. T. *J Micro Sep*, 9, (1997), 389.

[207] Wan Q-H. *J. Chromatogr* A, 782, (1997), 181.

[208] Seifar R. M, Heemstra S, Kok W Th, Kraak J. C and Poe H. *J Micro Sep*, 10, (1998), 41.

[209] Dittmann M. M and Rozing G. P. *J. Chromatogr* A, 744, (1996), 63.

[210] Yamamoto H, Baumann J and Erni F. *J. Chromatogr*, 593, (1992), 313.

[211] Yan C, Schaufelberger D and Erni F. *J. Chromatogr* A, 670, (1994), 15.

[212] Knox J. *Chromatographia*, 26, (1988), 329.

[213] van den Bosch S. E, Heemstra S, Kraak J. C and Poe. J *J. Chromatogr* A, 755, (1996), 165.

[214] Leliévre F, Yan C, Zare R. N, and Gareil P. *J. Chromatogr* A, 723, (1996), 145.

[215] Rebscher H and Pyell U. *Chromatographia*, 38, (1994), 737.

[216] Kitagawa S and Tsuda T. *J Micro Sep*, 6, (1994), 91.

[217] Kitagawa S and Tsuda T. *J Micro Sep*, 7, (1995), 58.

[218] Pyell U, Rebscher H and Banholczer A. *J. Chromatogr* A, 779, (1997), 155.

[219] Zimina T. M, Smith R. M and Myers P. *J. Chromatogr* A, (1997), 191.

[220] Smith N. W and Evans M. B *Chromatographia*, 41, (1995), 197.

[221] Euerby M. R, Gilligan D, Johnson C. M, Roulin S. C. P, Myers P and Bartle K. D. *J Micro Sep*, 9, (1997), 373.

[222] Frame L. A, Robinson M. L and Lough W. J. *J. Chromatogr* A, 798, (1998), 243.

[223] Moffat F, Cooper P. A and Jessop K. M. *Anal. Chem*, 71, (1999), 1119.

[224] Djordjevic N. M, Fitzpatrick F, Houdiere F and Lerch G. *J. High Resol Chromatogr.* 22, (1999), 599.

[225] Yang C and El Rossi Z. *Electrophoresis*, 20, (1999), 18.

[226] Zhang L, Zhang Y, Shi W and Zou H. *J High Resol Chromatogr,* 22, (1999), 666.

[227] Jinno K, Wu J, Sawada H and Kiso Y. *J High Resol Chromatogr,* 21, (1998), 617.

[228] Krause K, Chankvetadze B, Okamoto Y and Blasche G. *Electrophoresis*, 20, (1999), 2772.

[229] Dermaux A, Lynen F and Sandra P. *J High Resol Chromatogr* , 21, (1998), 575.

[230] Roed L, Lundanes E and Greibrokk T. *Electrophoresis*, 20, (1999), 2373.

[231] Pesek J. J and Matyska M. T. *Electrophoresis*, 18, (1997), 2228.

[232] Tsuda T, Nomura K and Nakagawa G. *J. Chromatogr* A, 248, (1982), 241.

[233] Boughtflower R. J, Underwood T and Maddin J. *Chromatographia*, 41, (1995), 398.

[234] Reynolds K. J, Moloney T. D, Fernier A. M and Colón L. A. *Analyst*, 123, (1998), 1493.

[235] Mayer M, Ra E, Marck C and Bruin G. J. M. *Electrophoresis*, 20, (1999), 43.

[236] Chen J, Dulay, M. T and Zare R. N. *Electrophoresis*, 21, (2000), 1430.

[237] Svec F, Peters E. C, Sýkora D, Yu C and Fréchet J. M. J. *J High Resol Chromatogr*, 23, (2000), 3.

[238] Schweitz L, Andersson L. I and Nilsson S. *Anal. Chem*, 69, (1997), 1179.

[239] Dulay M. T, Yan C, Rakestraw D. J and Zare R. N. *J. Chromatogr* A, 725, (1996), 361.

[240] Robson M. M, Roulin S, Shariff S. M, Raynor M. W, Bartle K. D, Clifford P, Euerby M. R and Johnson C. M. *Chromatographia*, 43, (1996), 313.

[241] Dittmann M. M, Rozing G, Unger K. K and Adam T. Column for capillary chromatographic separations and method of producing same. United States Patent 5,858,241.

[242] Dittmann M. M, Rozing G and Zimmermann H-P. Column for capillary chromatographic separations. United States Patent 5,908,552.

[243] Rathore A. S, Wen E and Horváth, *Anal. Chem*, 71, (1999), 2633.

[244] Behnke B, Grom E and Bayer E. *J Chromatogr A*, 716, (1995), 207.

[245] Cortez H *et al* United States Patent 4,793,920.

[246] Smith N. W and Evans M. B. *Chromatographia*, 38, (1994), 649.

[247] Fuchs *et al* United States Patent 5,246,577.

[248] Rebsher H and Pyell U. *Chromatographia*, 42, (1996), 171.

[249] Rathore A. S and Horváth C. *Anal. Chem*, 70, (1998), 3069.

[250] Yan C, Dadoo R, Zhao H, Zare R. N and Rakestraw D. J. *Anal. Chem*, 67, (1995), 2026.

[251] Spikmans V, Smith N.W, Tucker M. G, Horsten R and Mazereeuw M. *LC-GC Int*, 13, (2000), 486.

[252] Rebsher H and Pyell U. *Chromatographia*, 38, (1994), 737.

[253] Carney R. A, Robson M. M, Bartle, K D and Myers P. *J High Resol Chromatogr*, 22, (1999), 29.

[254] Rathore A. S and Horváth C. *Anal. Chem*, 70, (1998), 3069.

[255] Seifer R. M, Kok, W, Krank J. C and Poe H. *Chromatographia*, 46(3/4), (1997), 131.

[256] Euerby M. R, Johnson C. M, Cikalo M and Bartle K. D. *Chromatographia*, 47, (1998), 135

[257] Behnke B and Bayer E. *J. Chromatogr* A, 680, (1994), 93.

[258] Huber, C. G, Choudhary G and Horváth C. *Anal. Chem*, 69, (1997), 4429.

[259] Yan C, Dadoo R, Zare R. N, Rakestraw D. J and Anex D. S. *Anal. Chem*, 68, (1996), 2726.

[260] Euerby M R, Gilligan D, Johnson C. M and Bartle K. D. *Analyst*, 122, (1997), 1087.

[261] Que A. H, Kahle V and Novotny M. V. *J Micro Sep*, 12, (2000), 1.

[262] Gfrörer P, Schewitz J, Pusecker K, Tseng L-H, Albert K and Bayer E. *Electrophoresis*, 20, (1999), 3.

[263] Lane S. J, Boughtflower R, Paterson C and Underwood T. *Rapid Comm Mass Spec*, 9, (1985), 1283.

[264] Euerby M. R, Johnson C. M and Bartle K. D. *LC-GC Int*, 11, (1998), 39.

[265] Angus P. Comparison of CEC and HPLC assays for a neutral drug candidate. Presented at SEARLE Analytical Workshop, Skokie, USA, May 2000.

[266] Gillot N. C, Euerby M. R, Johnson C. M, Barrett D. A and Shaw P. N. *Anal Comm*, 35, (1998), 217.

[267] Lurie I. S, Conver T. S and Ford V. L. *Anal. Chem*, 70, (1998), 4563.

[268] Altria K. D, Smith N. W and Turnbull C. H, *J. Chromatogr B*, 717, (1998), 341.

[269] Li S and Lloyd D. K. *J. Chromatogr* A, 666, (1994), 321.

[270] Wolf C, Spence P. L, Pirkle W. H, Derrico E. M, Cavender D. M and Rozing G. P. *Anal. Sep News*, 1, (1998), 4

[271] Pacakora. V and Stulik. K. *Journal of Chromatography* A, 789, (1997), 169.

[272] Wätzig H, Degenhardt M and Kunkel A. *Electrophoresis*, 19, (1998), 2695.

[273] Rickard E. C, Bo R. J, Skanchy D. J, Chetwyn K. L, Pahlen B, Stobaugh J. F. Chirality, 8, (1996), 108.

[274] Myers, P. *LC-GC Europe*, 13, (2000), 744.

[275] Dolnik V, Liu S and Jovanovich S. *Electrophoresis*, 21(1), (2000), 41.

[276] Convert for Windows™ version 4.08.

[277] Snyder, L. R, Glajch, J. L and Kirkland, J. J. Practical HPLC method development, 22, Wiley Interscience (1988).

[278] Ellis, D. R. *Investigation of short and "equivalent" HPLC columns*. Searle, Morpeth QA internal report QAI001, March 1999.

[279] Vonach B and Schomburg G. *J. Chromatogr*, 149, (1978), 417.

[280] Rules and Guidance for Pharmaceutical Manufacturers ("Orange guide"). HMSO publications (1993).

[281] Brimblecombe R.W, Duncan W.A.M, Durant G.J, Emmett J.C, Ganellin CR and Parsons M.E. *J. Int Med Res* 3, (1975) 86.

[282] Misiewicz J. J. *Drugs* 15, (1978) 89.

[283] Brogden R.N, Heel R.C, Speight T.M and Avery G.S. *Drugs* 15, (1978) 93.

[284] United States Pharmacopeia XXIII, US Pharmacopeial Convention, Rockville MD <621>, 373.

[285] Luksa J and Josic D. J. *J. Chromatogr B*, 667, (1995), 321.

[286] Soini H, Tsuda T and Novotny M. V. *J. Chromatogr B*, 559, (1991), 547.

[287] Newton D.W and Kluza R.B *Drug Intell and Clin Pharm* 12, (1978), 546.

[288] Palmieri R. H. Comparison of air and liquid cooling in CE. Beckman technical note T-1823A

[289] van Asseldonk, B. Prince Technologies. Private communication.

[290] Baranyovits F.L.C and Ghosh R, *Chem Ind,* (1969), 1018.

[291] Bullock D.J.W in Zweig G (ed) Analytical methods for pesticides and plant growth regulators Academic press (Ohio), volume VII, (1973), 399.

[292] Kuhr R.J and Dorough H. W. Carbamate insecticides: Chemistry, Biochemistry and Toxicology. CRC Press (Ohio), 1976, p11.

[293] Cabras P, Spanedda L and Tuberoso C, *J. Chromatogr*, 478, (1989), 250.

[294] Rimmer D, Evans S.G and Patel S. Environmental analysis: Capillary electrophoresis of hazardous industrial and agricultural chemicals. IR/L/IA/95/6 Health and Safety Laboratory, Broad Lane, Sheffield.

[295] Rimmer D, and Patel S. Development of an air monitoring method for the measurement of ethylene diamine. IR/L/IA/95/8. Health and Safety Laboratory, Broad Lane, Sheffield.

[296] Rimmer D, Johnson P, Douglas N and Wassell S. Environmental analysis: Capillary electrophoresis of hazardous industrial and agricultural chemicals final project report. IACS/97/13 Health and Safety Laboratory, Broad Lane, Sheffield.

[297] Andersson. K, Hallgren. C, Levin. O. F and Nilsson. C. A. *Am. Ind. Hyg. Assoc. J.* 46, (1985), 225.

[298] Levin J. O, Andersson K, Fängmark I and Hallgren C. *Am Ind Hyg* 4, (1989), 98.

[299] Levin J.O, Andersson K and Hallgreen C. *Ann. Occup. Hyg.* 38, (1994), 257.

[300] Johnson L, Lagerkvist S, Lindroth P, Ahnoff M and Martinsson K. *Anal. Chem,* 54, (1982), 939.

[301] Possanzini M and Palo V. *Chromaographia*, 29, (1990), 151.

[302] The Industrial Uses of Tin chemicals. Blunden S. J, Cusack P. A and Hill R (eds), The Royal Society of Chemistry, (1985).

[303] Davies A. G and Smith P. J in Wilkinson G. W (ed) Comprehensive Organometallic chemistry: The synthesis, reactions and structures of organometallic compounds (Pergammon Press), Vol 2 (1985), 519.

[304] Harrington C. F, Eigendorf G. K and Cullen W. R. *Am Organomet Chem* 10, (1996) 339.

[305] Ebdon L, Hill S. J and Rivas C. *TRAC*, 17(5), 1998 277.

[306] Han F, Fasching L and Brown P. R. *J Chromatogr B*, 669, (1995), 103.

[307] Li K and Li S. F. Y. *J Chrom Sci*, 33, (1995), 309.

[308] Rogerson V. Private communication.

[309] Praet A, Dewaele C, Verdonck L and Van Der Kelen G. P. *J Chromatogr*, 507, (1990), 427.

[310] Staples C. A, Adams W. J, Parkerton T. F, Gorsuch J. W, Biddinger G. R and Reinert K. H., *Env Toxicol and Chem*, 16, (1997), 875.

[311] Kozumbo W. J, Kroll R and Rubin R. J. *Env Health Pers*, 45, (1982), 103.

[312] Woodward K. N and Smith A. HMSO toxicity review 14, (1986).

[313] Staples C. A, Peterson D. R, Parkerton T. F and Adams W. J. *Chemosphere* 35, (1997), 667.

[314] Ong C. P, Lee H. K and Li S. F. Y. *J. Chromatogr*, 542, (1991), 473.

[315] Jelínek I and Opekar F. *J Chromatogr* A, 802, (1998), 381.

Structural Studies of Phosphine Complexes of Mercury(II) Halides

by

Lorraine Anne March

A Thesis submitted to the Council for National Academic Awards in partial fulfilment of the requirements for the degree of Master of Philosophy.

Sponsoring Establishment: Department of Chemistry
Sheffield City Polytechnic.

Collaborating Establishment: AERE, Harwell,
Materials Development Division.

October 1988

Acknowledgements

The author would like to thank her supervisors Dr. N.A. Bell and Professor I.W. Nowell for their help and interest shown throughout the course of this study.

I would also like to thank Dr. P.T. Moseley (AERE, Harwell, Materials Development Division) for his advice and encouragement.

Special thanks are due to Mrs. S. Etches for her work in typing this thesis.

Contents

Structural Studies of Phosphine Complexes of Mercury(II) Halides by

Lorraine March

ABSTRACT

Previous investigations of the solid-state structures of $(R_3P)_nHgX_2$ (where X = Cl, Br, or I and n = 1 or 2) complexes have been extended by the determination of the structures of the following:

(i) $[(Pr_3P)HgCl_2]_2$

(ii) $[(Pr_3P)HgBr_2]_2$

(iii) $[(\alpha\text{-}Pr_3P)HgI_2]_n$

(iv) $[(\beta\text{-}Pr_3P)HgI_2]_2$

(v) $I_2Cd(\mu\text{-}I)_2Hg(PPr_3)_2$

(vi) $[(NCCH_2CH_2)_3PHgCl_2]_n$

(vii) $[(Ph_3P)HgI_2]_2$

(viii) $[(NCCH_2CH_2)_3P]_2HgCl_2$

(ix) $[(NCCH_2CH_2)_3P]_2HgBr_2Me_2CO$

(x) $[(2\text{-thienyl})_3P]_2HgCl_2$

As with previously solved 1:1 mercury(II) halide tertiary phosphine complexes (i) to (vii) show a wide variety of structures. These vary from symmetrical halogen-bridged dimers (e.g. $[(Pr_3P)HgCl_2]_2$) to a polymeric chain structure for $[(\alpha\text{-}Pr_3P)HgI_2]_n$. Both $[(\beta\text{-}Pr_3P)HgI_2]_2$ and $I_2Cd(\mu\text{-}I)_2Hg(PPr_3)_2$ show the unusual feature for halogen-bridged dimers, of having both phosphine ligands attached to the same metal atom. In the case of $I_2Cd(\mu\text{-}I)_2Hg(PPr_3)_2$ both phosphine groups are attached to the mercury atom, showing mercury to have a stronger affinity than cadmium for phosphorus.

The 2:1 complexes all are distorted monomeric tetrahedral structures, $[(NCCH_2CH_2)_3P]_2HgCl_2$ consisting of two independent monomeric units. However, $[(NCCH_2CH_2)_3P]_2HgBr_2Me_2CO$ which contains a molecule of acetone has a trigonal bipyramidal arrangement due to a weak interaction between the mercury atom and the oxygen atom from the acetone molecule.

The solid-state structures of these complexes have been rationalised in the terms of:

(a) the donor strengths of the R_3P ligands

(b) the donor strengths of the halides

For 2:1 complexes strong σ-phosphine donors give a greater distortion of the structure from the tetrahedral, having large P-Hg-P bond angles and short Hg-P bond lengths. Similarly, for the limited data available, the weaker σ-bonding halides (e.g. Cl) give the predicted trends of short Hg-P bond lengths accompanied by larger P-Hg-P bond angles.

The situation for the 1:1 compounds is more complex with some σ-phosphine donors forming more extended structures. A few of these 1:1 complexes are known to exist in more than one form, for example, Bu_3PHgCl_2 and Pr_3PHgI_2. In both of these cases one form is a halogen-bridged dimer, the other form being a more extended structure; in the former it is tetrameric and in the latter a halogen-bridged chain structure. The expected trend of short Hg-P bond lengths and larger P-Hg-X angles for strong σ-phosphine donors is still apparent in these structures as is the shortening of the Hg-P bonds and increase in the associated X_t-Hg-P angles for weak σ-donor halides.

Objectives

Previous work has shown that a variety of structural types are possible for the 1:1 series of complexes of tertiary phosphines with mercury(II) halides. Additionally, certain molecular parameters found for a limited range of 1:1 and 2:1 complexes appear to be dependent upon the nature of the phosphine ligand. In order to more clearly establish the major factors which influence the type of structure and geometric parameters adopted for $(R_3P)_nHgX_2$ (n = 1 or 2, X = Cl, Br or I) the full X-ray structure has been determined for a much wider range of complexes. The mercury(II) halide-tertiary phosphine complexes have been chosen with varying halogen atoms and phosphine ligands, in order to extend an understanding of both the effect of the halogen atom and of the σ-donor capacity of the phosphine upon the nature of the complex and the geometry adopted.

Contents

1. General Introduction

1.1 General Properties of Zinc, Cadmium and Mercury

Mercury is a member of group IIB along with zinc and cadmium and they all have the general outer electronic configuration $nd^{10}(n+1)s^2$. Although all have the common oxidation state of M(II), mercury also has an oxidation state Hg(I), giving rise to several stable compounds. In contrast, zinc(I) and cadmium(I) compounds are very unstable and are not easily isolated. The melting points of zinc and cadmium are 420 °C and 320 °C respectively but mercury is an unusual metal in that it is liquid at room temperature, having a melting point of -39 °C. X-ray diffraction studies of liquid mercury show that each mercury atom is surrounded by six close atoms at 3.00 Å and six more distant atoms at 3.47 Å[1]. Solid mercury shows similar hexagonal packing,[2] whereas the vapour is shown to be monatomic. Both zinc and cadmium adopt hexagonal structures at room temperature.[3]

In their compounds all three metals show a range of co-ordination numbers varying from two to eight. All three give linear two co-ordination, mercury more commonly than zinc and cadmium. All three also adopt tetrahedral four co-ordination, trigonal bipyramidal five co-ordination and octahedral six co-ordination, often distorted from the regular shapes (Figs. 1.1-1.3). Mercury also shows cubic eight co-ordination.

The covalent radii of zinc, cadmium and mercury atoms decrease with increasing co-ordination number. For example, four co-ordinate compounds of Zn, Cd and Hg are found to have covalent radii of 1.31, 1.48 and 1.48 Å respectively whereas in octahedral six-co-ordinate compounds the covalent radii have decreased to 1.27, 1.45 and 1.45 Å respectively.

1.2 Metal(I) Halides

Of the three metals only mercury forms stable M(I) halides, although

halides of cadmium(I) and zinc(I) have been detected they have not been isolated. Mercury forms all four Hg(I) halides and all have similar dimeric structures.[10] These would appear to be dominated by linear two co-ordination about each mercury, with two mercury and two halogen atoms being colinear (Fig. 1.4). The co-ordination in this dimeric unit is extended to six by weak interaction of four distant halogen atoms (X').

1.3 Metal(II) Halides

Zinc, cadmium and mercury all form the M(II) halides, those of Hg(II) being the most stable. The fluorides are ionic, with that of zinc having a rutile type structure[11] and those of cadmium and mercury adopting a fluorite type structure (Figs. 1.5, 1.6).[1,12] Zinc chloride and bromide have cubic close-packed arrangements while the iodide has a hexagonal close-packed layer structure (Fig. 1.7). Cadmium chloride, bromide and iodide all have layer lattices. The iodide structure is based on a hexagonal close-packing arrangement of iodine atoms (Fig. 1.7) while the other two halide structures involve cubic close-packing arrangements of the halogen atoms.[1] Mercury(II) chloride has a stacked linear structure (Fig. 1.8). The α-form of mercury(II) iodide has a distorted cubic close-packed structure while the β-form adopts a distorted brucite structure also found in mercury(II) bromide.[1]

1.4 Complexes Formed Between Metal(II) Halides and Monodentate Ligands

The halides of all three metals form a range of complexes with monodentate and polydentate neutral ligands having nitrogen, arsenic, sulphur, oxygen or phosphorus as the donor atom. The complexes have a variety of co-ordination numbers, commonly ranging from two to six, but some eight-co-ordinate complexes are also known. The discussion in this section is limited to a discussion of compounds formed between the metal

halides and monodentate ligands; complexes formed with polydentate ligands are not included. A more detailed discussion of complexes formed with tertiary phosphines is included in section 1.5.

1.4.1 Zinc Halide Complexes

Few structures of zinc halide complexes are known with any certainty. A variety of 2:1 complexes L_2ZnX_2 have been prepared and studied mainly by infrared vibrational techniques. Interpretation of infrared data indicates the 2:1 complexes formed between zinc halides and p-toluidine,[13] pyridine and substituted pyridines[14,15] adopt monomeric tetrahedral structures. An X-ray study of (thiourea)$_2$ $ZnCl_2$ shows it to have a simple monomeric structure with slightly distorted tetrahedral co-ordination about zinc (Cl-Zn-Cl, 107.3(2)°; S-Zn-S, 111.5(2)°).[16] The 1:1 phosphine complexes of Zn(II) halides are discussed in section 1.5.1, but few other 1:1 complexes are known.

1.4.2 Cadmium Halide Complexes

Many examples of 1:1 cadmium halide complexes containing neutral monodentate ligands are known and these are usually polymeric. The structures generally consist of a double chain arrangement involving halogen bridging, resulting in a distorted octahedral arrangement about each cadmium atom (Fig. 1.9). A number of 2:1 cadmium complexes (L_2CdX_2) have a halogen-bridged single chain polymeric structure in which cadmium has an octahedral environment, the fifth and sixth positions being occupied by a neutral monodentate ligand (Fig. 1.10). Other 2:1 complexes give rise to monomeric distorted tetrahedral structures (Fig. 1.11).

1.4.3 Mercury(II) Halide Complexes

Many 1:1 mercury(II) halide complexes of monodentate donor ligands form halogen-bridged dimers (Fig. 1.12) although a few complexes, which have oxygen as a donor have been shown to form oxygen-bridged dimers (Fig.

1.13). Some 1:1 complexes have extended five co-ordination resulting in a trigonal bipyramidal structure (Fig. 1.2). For 2:1 complexes (L_2HgX_2) a distorted monomeric tetrahedral structure is common, but some complexes have an effective five co-ordinate trigonal-bipyramidal arrangement (Fig. 1.14). Some 2:1 complexes as for example $(pyridine)_2HgCl_2$[27,28] and $(methanol)_2HgCl_2$[29] adopt polymeric structures in which mercury occupies a distorted octahedral arrangement (Fig. 1.15).

Bis(o-ethylthiocarbamate)mercury chloride [4]

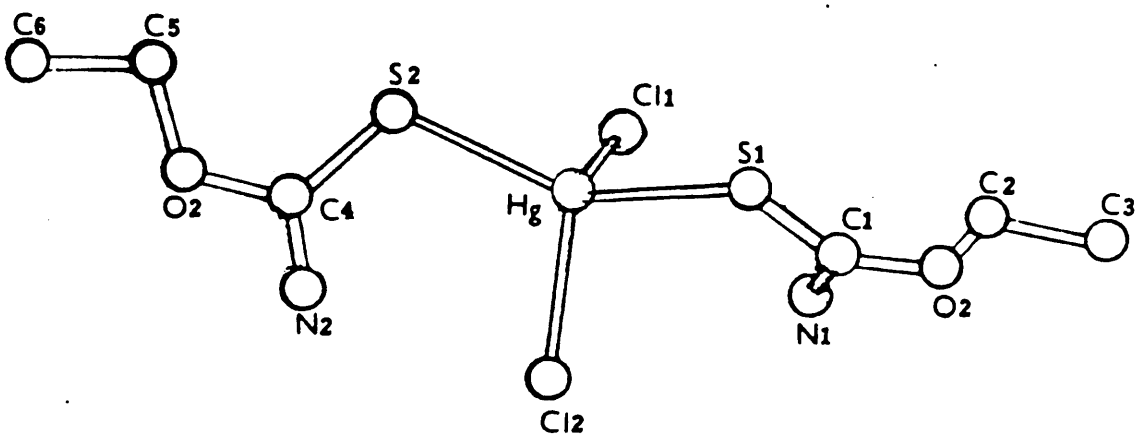

Bond lengths (Å)		Bond angles (°)			
Hg-S1	2.62(1)	S1-Hg-S2	96.2(2)	S2-Hg-Cl1	103.2(2)
Hg-S2	2.58(1)	S1-Hg-Cl1	103.2(2)	S2-Hg-Cl2	112.4(2)
Hg-Cl1	2.45(1)	S1-Hg-Cl2	106.5(2)	S2-Hg-Cl2	129.9(2)
Hg-Cl2	2.43(1)				

Bis(triphenylphosphine)cadmium chloride [5]

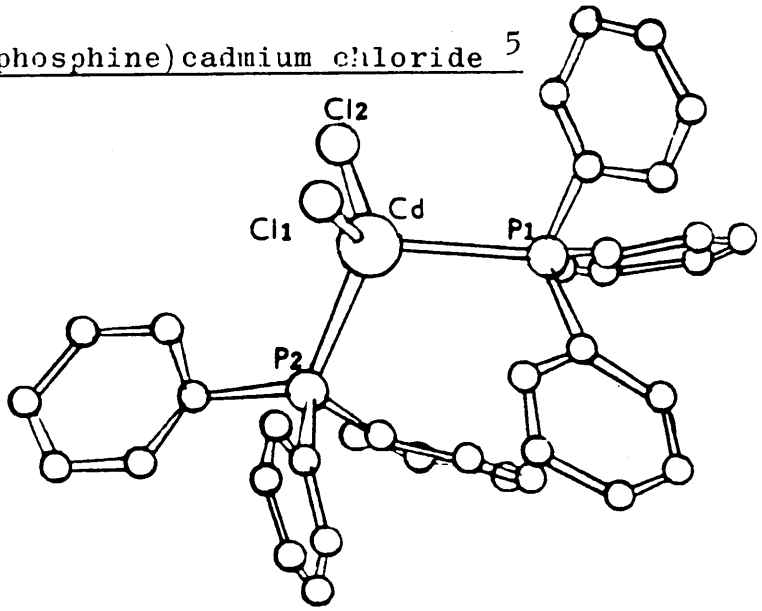

Bond lengths (Å)		Bond angles (°)			
Cd-Cl1	2.504(6)	Cl1-Cd-Cl2	113.9(2)	Cl2-Cd-P1	105.7(2)
Cd-Cl2	2.440(6)	Cl1-Cd-P1	104.5(2)	Cl2-Cd-P2	112.1(2)
Cd-P1	2.635(6)	Cl1-Cd-P2	112.2(2)	P1-Cd-P2	107.6(2)
Cd-P2	2.632(6)				

Fig. 1.1 Tetrahedral Four Co-ordination

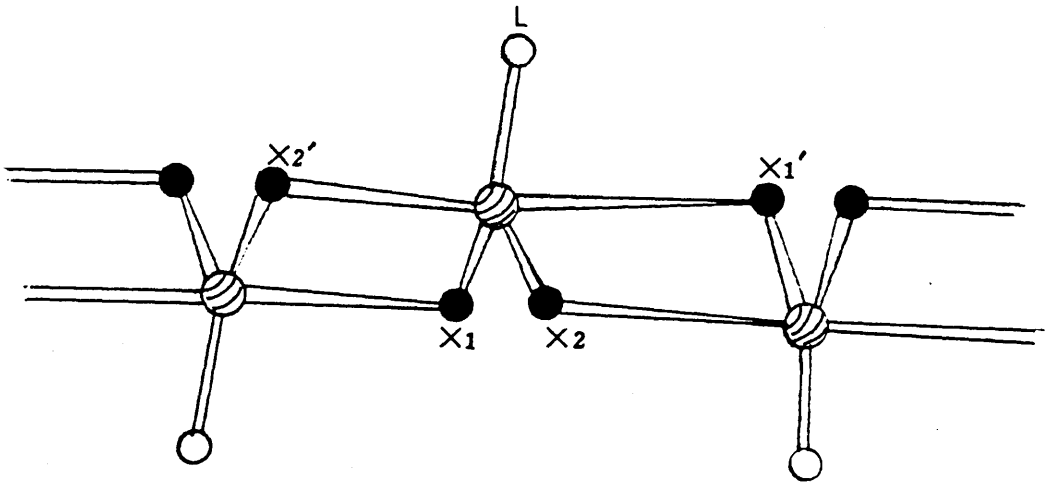

	(2,4-Dimethylpyridine)$HgBr_2$ [6]	(Collidine)$HgCl_2$ [7]
Bond lengths (Å)		
Hg-Br1 / Hg-Cl1	2.621(3)	2.455(18)
Hg-Br2 / Hg-Cl2	2.486(4)	2.542(18)
Hg-Br1′ / Hg-Cl1′	2.911(3)	2.956(18)
Hg-Br2′ / Hg-Cl2′	3.548(4)	2.948(18)
Hg-N	2.21(2)	2.181(18)
Bond angles (°)		
Br1-Hg-Br1′ / Cl1-Hg-Cl1′	92.4(2)	85.8
Br1-Hg-Br2 / Cl1-Hg-Cl2	122.2(2)	110.1
Br1-Hg-Br2′ / Cl1-Hg-Cl2′	83.5(2)	93.3
Br1-Hg-N / Cl1-Hg-N	106(1)	122.5
Br1′-Hg-Br2 / Cl1′-Hg-Cl2	100.8(2)	94.7
Br1′-Hg-Br2′ / Cl1′-Hg-N	164.9(3)	89.3
Br1′-Hg-N / Cl2-Hg-Cl2′	90(1)	84.3
Br2-Hg-Br2′ / Cl2 Hg-N	93.6(2)	128.4
Br2-Hg-N / Cl2′-Hg-N	129(1)	92.1
Br2′-Hg-N	77(1)	

Fig 1.2 Trigonal Bipyramidal Five Co-ordination

(Bisformamide)$CdCl_2$ [8]

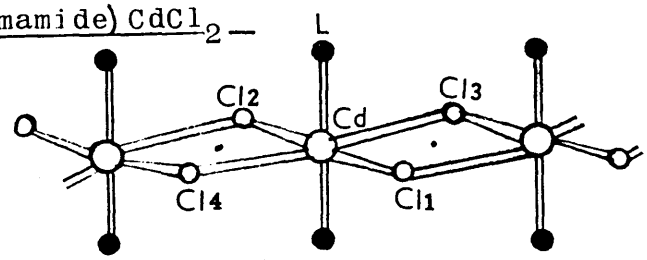

Bond lengths (Å)		Bond angles (°)	
Cd-Cl1	2.383(8)	Cl1-Cd Cl3	90.1(2)
Cd-Cl2	2.912(8)	Cl2-Cd-O	83.0(1)
Cd-Cl3	2.910(8)	Cl2-Cd-Cl4	89.8(3)
Cd-Cl4	2.379(8)	Cl3-Cd-Cl4	180 (-)
Cd-O	2.34 (3)	Cl3-Cd-Cl2	89.9(-)

(Tetrahydrofuran)$HgBr_2$ [9]

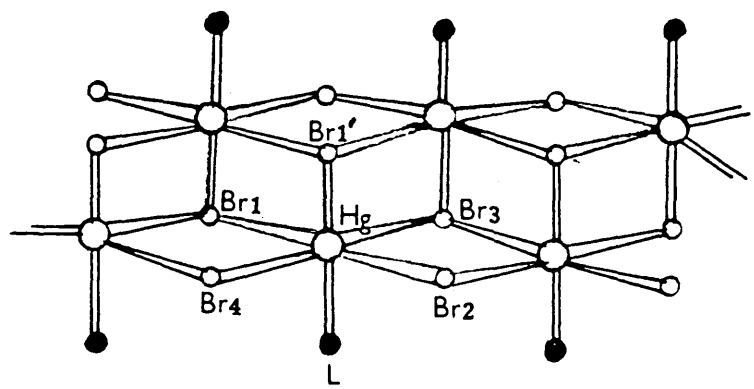

Bond lengths (Å)				Bond angles (°)	
Hg-Br	2.475(10)	Hg-Br4	3.27(1)	Br1-Hg-Br2	174.6(4)
Hg-Br2	2.480(10)	Hg-O	2.67(8)	Br1'-Hg-O	180(-)
Hg-Br3	3.15(1)	Hg-Br1'	3.47(1)	Br1 Hg Br4	90(-)

Fig 1.3 Octahedral Six Co-ordination

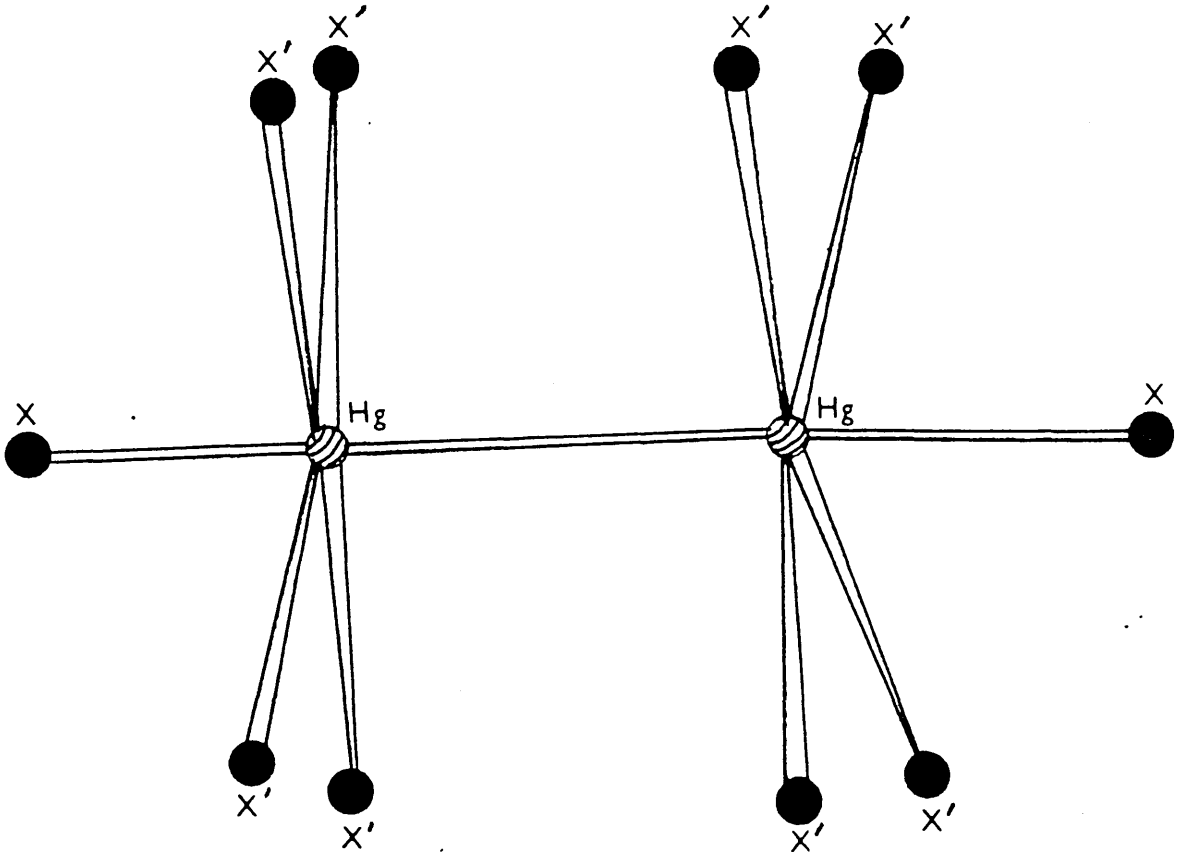

Bond Distances (Å)

	F	Cl	Br	I
Hg-Hg	2.42	2.53	2.58	2.69
Hg-X	2.31	2.53	2.57	2.69
Hg-X'	2.69	3.17	3.32	3.51

Fig. 1.4 Structures of the Mercury (I) Halides Hg_2X_2 (X=F,Cl,Br,I).[10]

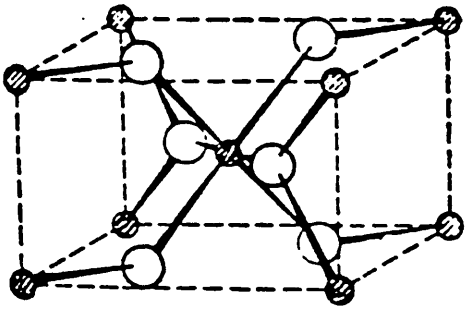

Fig 1.5 Rutile Structure of ZnF_2 [1]

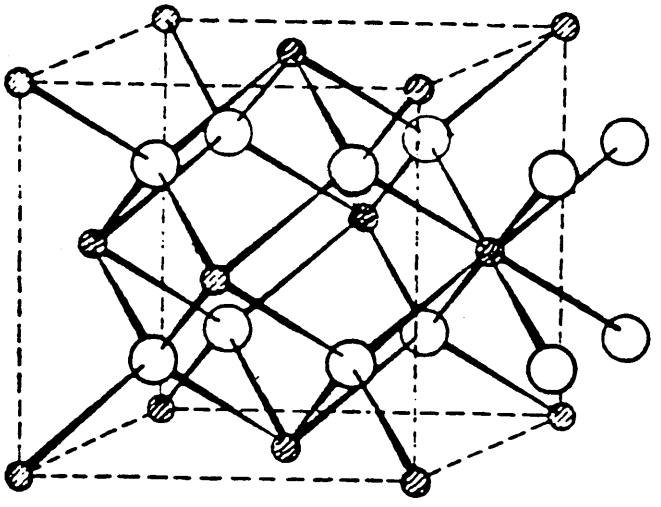

Fig 1.6 Fluorite Structure of MF_2 ,(M=Cd,Hg)[1]

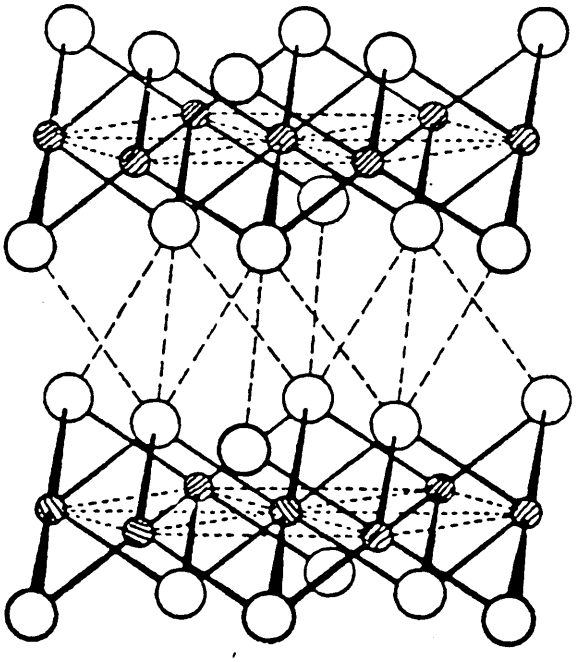

Fig 1.7 Layer Structure of MI_2(M=Cd,Zn) [1]

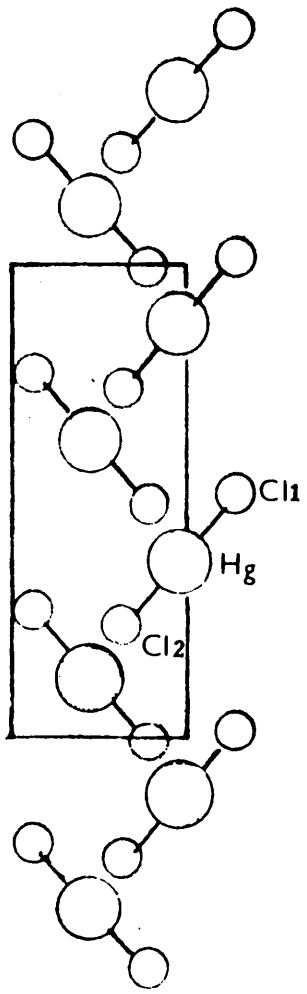

Fig 1.8 Structure of $HgCl_2$ [1]

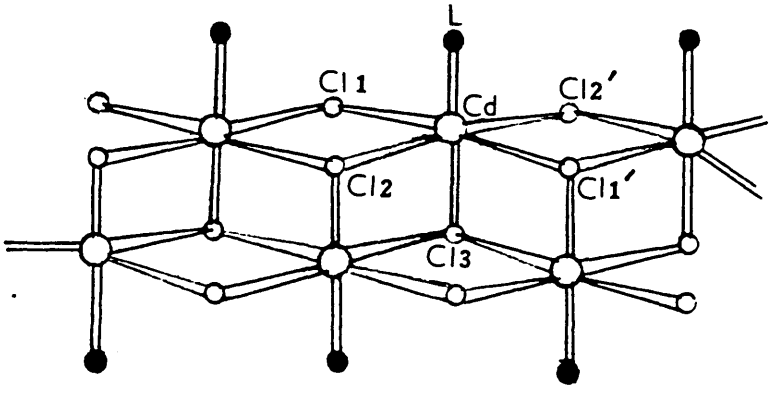

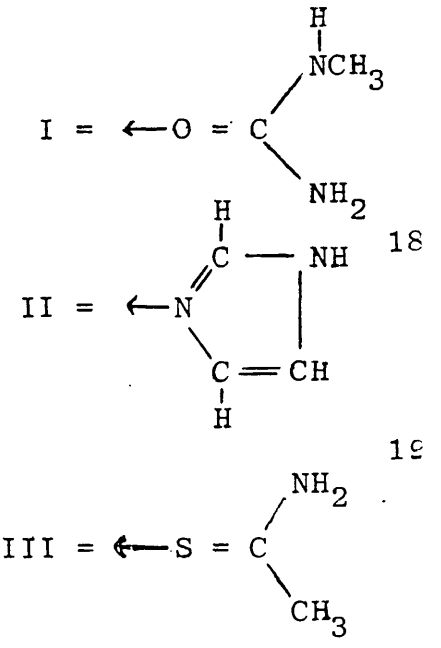

Bond lengths (Å)

L	Cd-Cl1	Cd-Cl2	Cd-Cl3	Cd-Cl1′	Cd-Cl2′	Cd-L
I	2.62(-)	2 67(-)	2.66(-)	2.58(-)	2.67(-)	2.18(-)
II	2.729(3)	2.604(4)	2.676(3)	2.728(3)	2.601(4)	2.243(5)
III	2.57(2)	2.89(2)	2.63(1)	2.76(2)	2.89(2)	2.55(1)

Bond angles (°)

L	Cl1-Cd-Cl2	Cl1-Cd-Cl1′	Cl1-Cd-Cl3	Cl1-Cd-L
I	87(-)	172(-)	88(-)	99(-)
II	87.5(1)	173.5(1)	90.8(1)	94.1(2)
III	86.1(5)	171.4(4)	90.6(4)	98.2(7)
L	Cl2-Cd-Cl3	Cl2-Cd-L	Cl2-Cd-Cl1′	Cl2-Cd-Cl1
I	88(-)	106(-)	89(-)	91(-)
II	83.1(1)	90.5( )	89.4(2)	95.0(1)
III	79.3(4)	81.7(6)	88.4(5)	97.7(5)

Fig. 1.9. Structure of Selected $LCdCl_2$, Complexes (L=Monodentate Ligand).

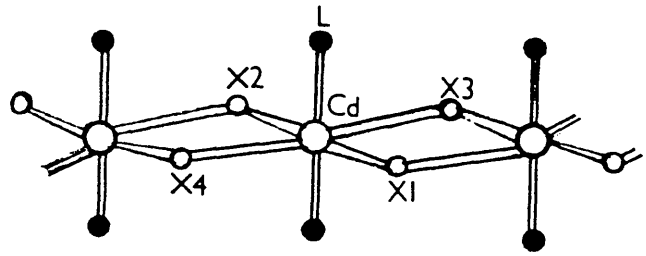

Bond lengths (Å)

L	X	Cd-X1	Cd-L	Cd-X3	Cd-X2
NH_3	Cl	2.71(-)	2.1(-)	2.71(-)	2.71(-)
NH_3	Br	2.86(-)	2.1(-)	2.86(-)	2.86(-)
pyridine	Cl	2.35(4)	2.46(-)	2.35(4)	2.35(4)

Bond angles (°)

L	X	X1-Cd-X3	X1-Cd-L
pyridine	Cl	89.5(-)	90.4(-)

Fig. 1.10. Structures of Selected Octahedral L_2CdCl_2 Complexes (L=NH_3 [20] or Pyridine [21]; X=Cl or Br).

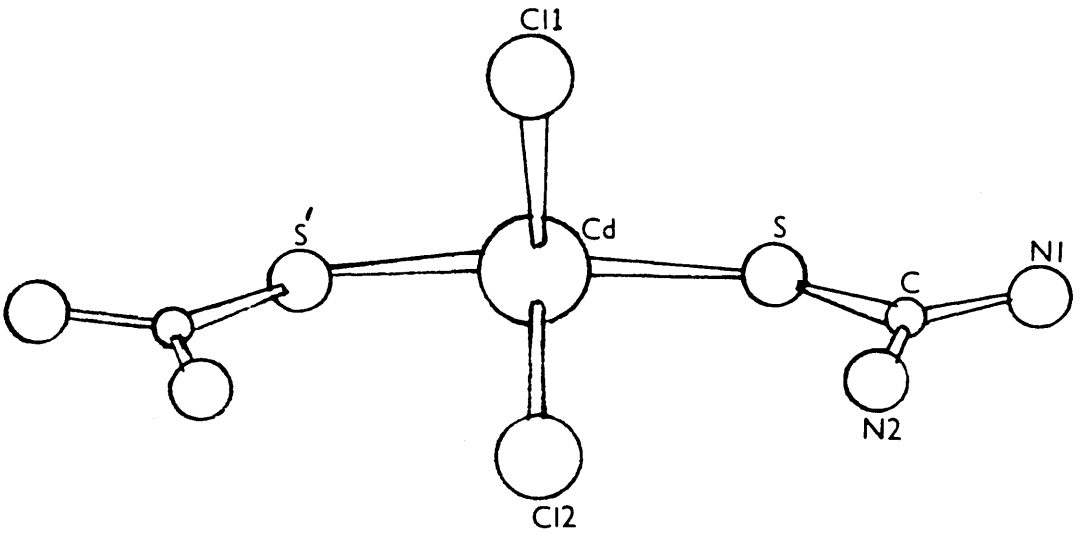

Bond lengths (Å)	
Cd-Cl1	2.51(-)
Cd-Cl2	2.50(-)
Cd-S	2.45(-)

Bond Angles (°)	
Cl1-Cd-Cl2	103(-)
Cl1-Cd-S	106(-)
Cl2-Cd-S	105(-)
S-Cd-S′	129(-)
Cd-S-C	113(-)

Fig 1.11 Structure of Bis(thiourea)Cadmium (II)Chloride [22]

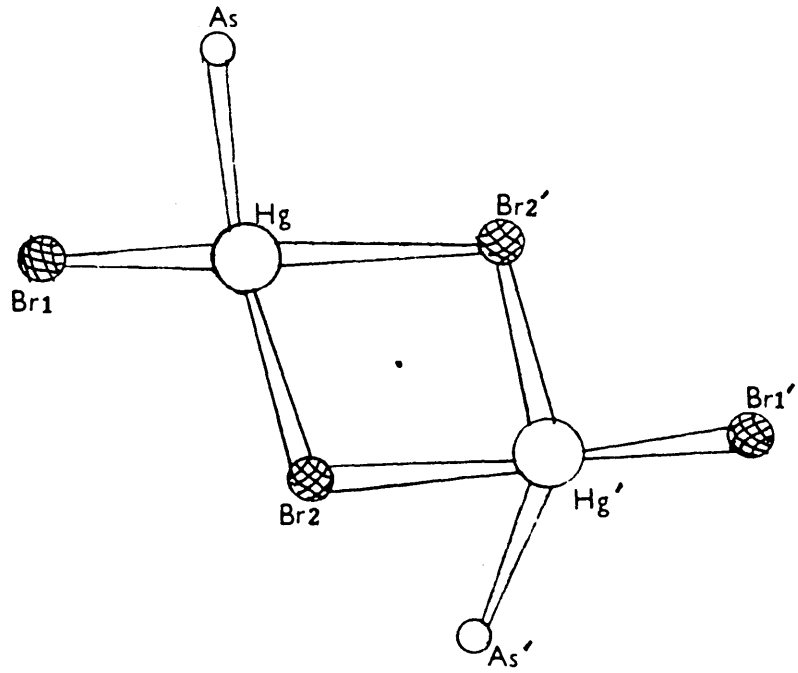

Bond lengths (Å)

Hg-Br1	2.25(-)	Hg-Br2′	2.90(-)
Hg-As	2.25(-)		
Hg-Br2	2.60(-)		

Bond angles (°)

As-Hg-Br1	135(-)	Br1-Hg-Br2	102(-)
As-Hg-Br2′	94(-)	Br2-Hg-Br2′	87(-)
As′-Hg′-Br2	94(-)	Hg-Br2-Hg′	93(-)

Fig. 1.12. Structure of $(Bu_3As)HgBr_2$ [24]

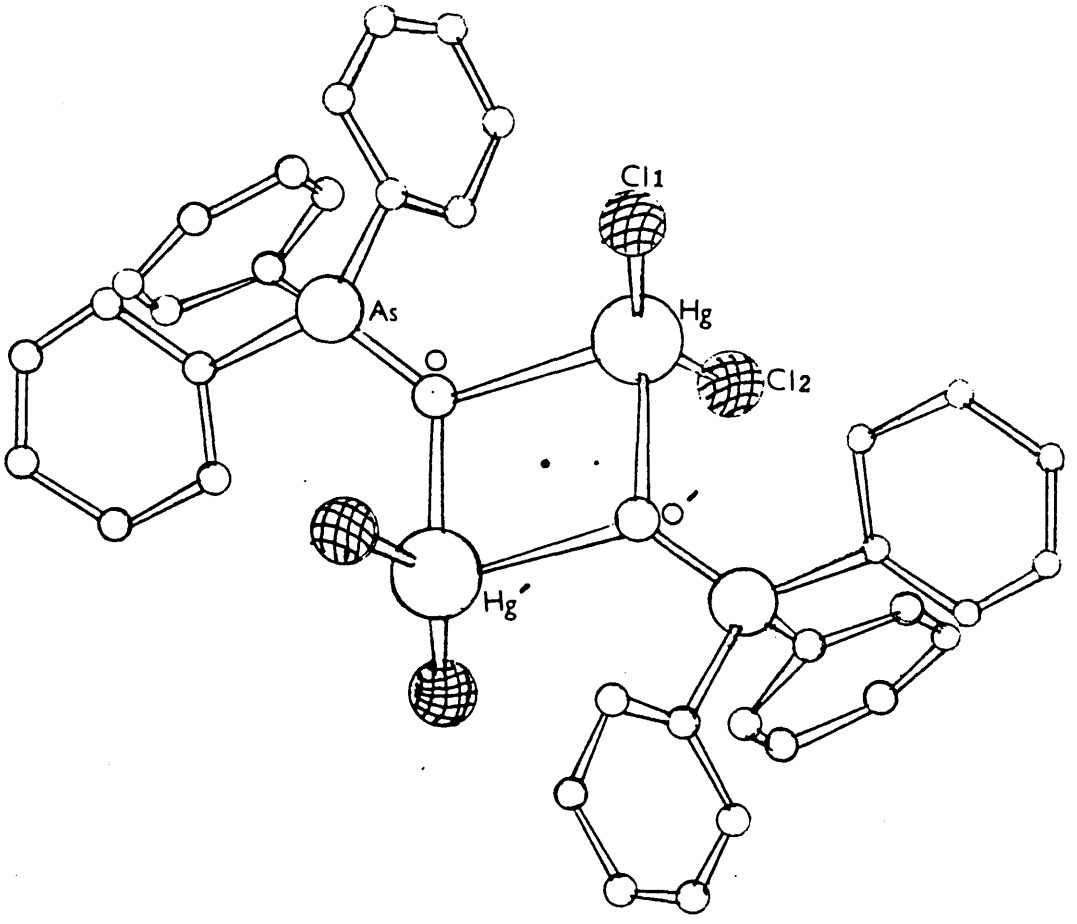

Bond lengths (Å)

Hg-Cl1	2.32(1)	Hg-O'	2.46(2)
Hg-Cl2	2.32(1)	As-O	1.66(2)
Hg-O	2.48(2)		

Bond angles (°)

Cl1-Hg-Cl2	144.8(4)	Cl2-Hg-O'	104.8(7)
Cl1-Hg-O	105.8(7)	O-Hg-O'	78.7(9)
Cl1-Hg-O'	105.4(7)	As-O-Hg	129.3(13)
Cl2-Hg-O	97.6(7)	As-O-Hg'	122.4(13)

Fig. 1.13. Structure of $(Ph_3AsO)HgCl_2$ [25]

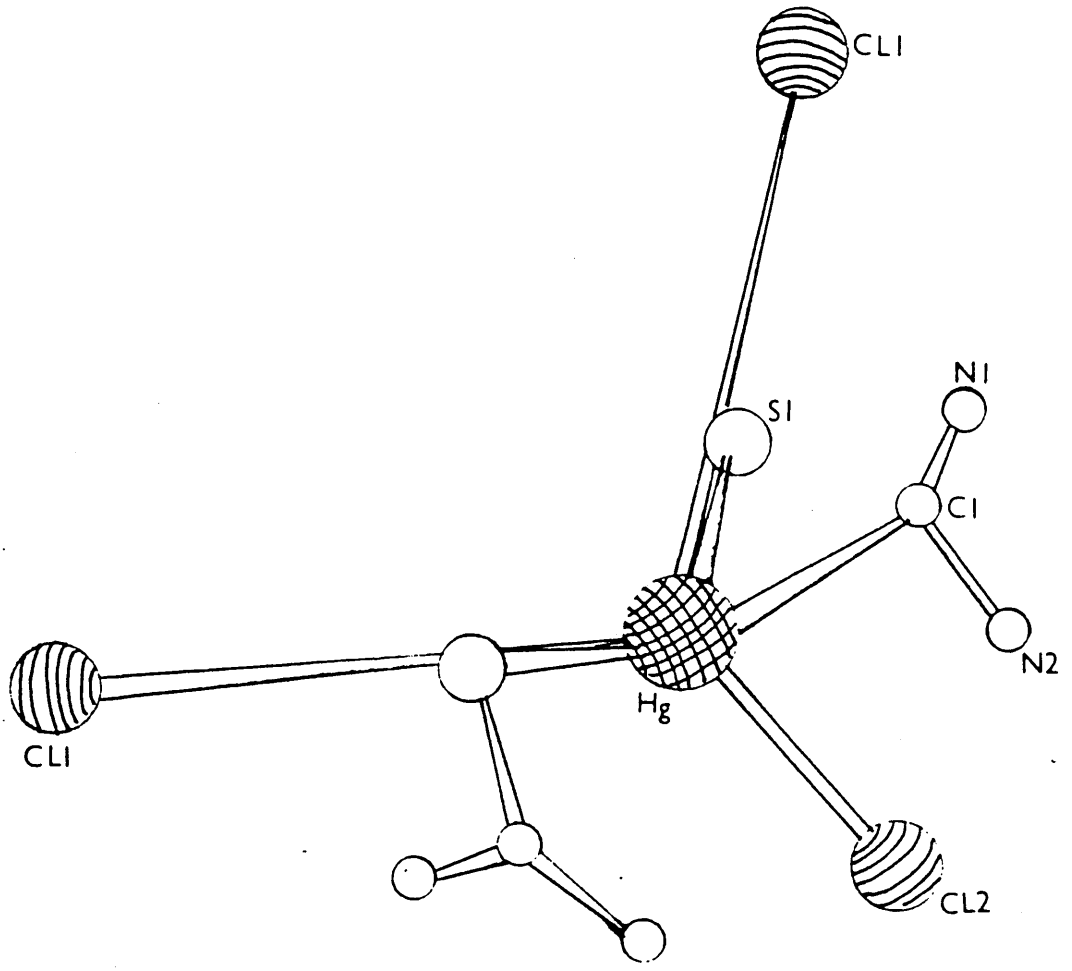

Bond lengths (Å)		Bond angles (°)	
Hg-S1	2.416(6)	S1-Hg-Cl2	110.8(2)
Hg-Cl2	2.57(1)	S1- Hg-S1	138.6(2)
Hg-Cl1	3.22(1)	Hg-S1-C11	110.0(9)
Hg-Cl1	3.22(1)		

Fig. 1.14. Structure of $(NH_2CSNH_2)_2HgCl_2$ [26]

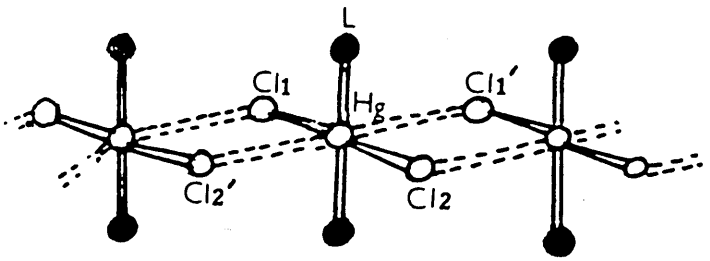

Bond lengths (Å)

L	Hg-Cl1	Hg-L	Hg-Cl1	Hg-Cl2	Hg-Cl2
CH_3OH	2.31(3)	2.82(5)	3.07(3)	2.31(3)	3.07(3)
pyridine	2.754(2)	2.266(6)	2.765(2)	2.754(2)	2.765(2)

Bond angles (°)

L	Cl1-Hg-L	Cl1-Hg-Cl2	Cl1-Hg-Cl1	Cl1-Hg-Cl2
CH_3OH	80(1)	180(1)	86(1)	129(1)
pyridine	88.5(2)	180(–)	90.21(6)	-

	L-Hg-Cl1	Hg-Cl1-Hg
pyridine	90.6(2)	90.21(7)

Fig. 1.15. Structures of the 2:1 Complexes L_2HgCl_2 (L=CH_3OH [27] or pyridine [28,29])

1.5 Phosphine Complexes of Zinc, Cadmium and Mercury

Mercury(II) halides form tertiary phosphine complexes having a wide variety of stoichiometries:

$$(R_3P)MX_2,\ (R_3P)_2(MX_2),\ (R_3P)(MX_2)_2,\ (R_3P)_3(MX_2)_2.$$

Zinc and cadmium halides, in contrast, give rise to a limited range of complexes and the moxt extensively studied are the 2:1 and the 1:1 adducts, L_nMX_2 (n = 1,2). These complexes are generally prepared by the reaction of the metal(II) halide with the tertiary phosphine in a suitable solvent.

1.5.1 Complexes Formed by Zinc Halides and Tertiary Phosphine Monodentate Ligands

Few zinc halide tertiary phosphine complexes have been prepared. The complexes $(R_3P)ZnX_2$ (X = Cl, Br or I:R = t-butyl, cyclohexyl) have been studied using infrared and ^{31}P NMR techniques. All these complexes are reported to be halogen-bridged dimers.[30,31] The 2:1 complexes formed with triphenylphosphine, $(Ph_3P)_2ZnX_2$ (X = Cl, Br or I), have been prepared and infrared studies indicate that they have monomeric tetrahedral structures.[32]

1.5.2 Complexes Formed by Cadmium Halides and Tertiary Phosphine Monodentate Ligands

Many cadmium halide 1:1 complexes have dimeric halogen-bridged structures with distorted tetrahedral co-ordination about cadmium. However, $(PhMe_2P)CdCl_2$ adopts a polymeric structure in which cadmium has unusual five co-ordination (Fig. 1.16).[33] The 2:1 complexes appear to be monomeric, $(Ph_3P)_2CdCl_2$ having a distorted tetrahedral structure (Fig. 1.1).[5]

1.5.3 Complexes formed by Mercury Halides and Tertiary Phosphine Monodentate Ligands

Although the literature contains many reports of phosphine complexes

$(R_3P)_nHgX_2$ (n = 1, 1.5, 2), the earlier papers gave little unambiguous evidence for the structure of such complexes. Assignment of far-infrared frequencies of mercury-halogen bands appear to be consistent with a halogen-bridged dimeric arrangement. Indeed, preliminary X-ray analysis confirmed this arrangement for $(Pr_3P)HgBr_2$.[24] A programme of work has been undertaken at Sheffield City Polytechnic to rationalize the range of structures adopted by complexes formed between mercury(II) halides and monodentate tertiary phosphines.[6,34-37]

(A) 3:2 Complexes $(R_3P)_3(HgX_2)_2$

The existence of 3:2 mercury(II) halide complexes was reported by Evans et al.[24] Crystallographic data are available for only one complex $(EtMe_2P)_3(HgCl_2)_2$ which is found to have an extended chain structure with the mercury atoms having alternating co-ordination numbers of four and five[35] (Fig. 1.17).

(B) 1:1 Complexes $(R_3P)HgX_2$

In the series of complexes $(R_3P)HgCl_2$ (R = Me, Et, Bu, Ph, cyclohexyl) and (R_3P = 1,2,5-triphenylphosphole) halogen-bridging is observed as shown in (Figs. 1.18-1.24).[34,36,38,39] Full X-ray structural data are available for these complexes, the structural types being indicated in Table 1.1. Structures have been proposed for several of their bromide and iodide analogues using far-infrared vibrational spectroscopy and from preliminary X-ray photographs. In some cases the availability of ^{31}P NMR data has been used to reinforce these structural assignments.

Although many of the complexes are centrosymmetric dimers they show a wide range of structural arrangements. X-ray studies show that $(Cy_3P)HgCl_2$[39] contains two independent dimers within the unit cell. Though the Hg-P distances are almost identical 2.416(3) and 2.412(3) $\mathring{A}$ for

dimers 1 and 2 respectively, other bond distances and angles vary considerably (Table 1.2). $(Me_3P)HgCl_2$ and $(Et_3P)HgCl_2$[36] are both polymeric, with the mercury atoms in distorted trigonal bipyramidal environments, but the details of the structures differ markedly. $(Et_3P)HgCl_2$ is regarded as an extended chlorine-bridged chain (Fig. 1.19) while $(Me_3P)HgCl_2$ (Fig. 1.20) which has a large P-Hg-Cl angle of 162.1(1)°, is ionic in nature (Table 1.2).

Both $(TPP)HgCl_2$ and $(Ph_3P)HgCl_2$ are centrosymmetric dimers in which the ligands are mutually trans (Figs. 1.21-1.22), but the relative Hg-Cl bridging distances differ considerably. For $(TPP)HgCl_2$ the bridging is very asymmetric, $Hg-Cl_{br}$ distances being 2.54(1) and 2.75(1) Å, whilst for $(Ph_3P)HgCl_2$ the $Hg-Cl_{br}$ values are almost equal, being 2.623(8) and 2.658(8) Å.[34]

$(Bu_3P)HgCl_2$ exists in two different forms, the α-form[34] contains a tetrameric unit with mercury in both tetra-co-ordinate and penta-co-ordinate environments. The tetramer comprises two unsymmetrical dimeric units (Fig. 1.23) which are linked by weak chlorine bridges (Hg-Cl, 3.38(3) Å). The terminal mercury atoms have an extremely distorted tetrahedral environment, the angles ranging from 92.6(7) to 147.8(7)°. The angles about the central mercury vary even more, ranging from 78.7(6) to 150.6(7)°. The β-form of $(Bu_3P)HgCl_2$[38] is a centrosymmetric halogen-bridged dimer similar to that found in $(Ph_3P)HgCl_2$[34] and shows no evidence of any further interaction of the dimers (Fig. 1.24).

Preliminary photographic evidence indicates that $(TPP)HgBr_2$,[34] $(Me_3P)HgBr_2$,[36] and $(Ph_3P)HgX_2$ (X = Br or I)[34] may be isostructural with their corresponding chlorides. In contrast $(Me_3P)HgI_2$[34] is not isostructural with its chloride analogue.

(C) 2:1 Complexes $(R_3P)_2HgX_2$

The $(R_3P)_2HgX_2$ series of complexes (R = Et, Bu, Ph; X = Cl, Br or I) have been characterised as four co-ordinate monomers, with varying degrees of distortion from regular tetrahedral geometry. $(Ph_3P)_2HgI_2$[40] has an almost regular tetrahedral geometry about the mercury with an I-Hg-I angle of 110.43(8)° and a P-Hg-P angle of 108.15(4)° (Fig. 1.25) In contrast, the complexes $(R_3P)_2HgCl_2$ (R = Bu,[41] Et[42] and Ph[43]) all show a greater distortion from tetrahedral geometry (Table 1.3) (Figs. 1.26-1.28). This distortion may be attributed in the ethyl and butyl complexes to the phosphines having high pKa values of 8.69 and 8.64 respectively. Such high pKa values indicate a higher donor strength than for triphenylphosphine (pKa 2.73). For $(Ph_3P)_2HgCl_2$ the greater distortion from its iodide analogue must be caused by the effect of the halogen atoms. Iodide is a stronger donor than chloride to mercury so that the P-Hg-P angle is less in the iodide (108.15(4)°)[40] than in the chloride (135.2(4)°).[43]

Initial results for $(Ph_3P)_2HgBr_2$ have been reported.[43] These indicate a distorted tetrahedral structure; the P-Hg-P angle being 113.0(5)° in accord with the above results for the iodide and chloride.

NMR data is available for several 2:1 complexes and coupling constants have been determined for $(R_3P)_2HgX_2$[49] complexes (X = Cl, Br or I and R = Et, Bu or Ph). Table 1.3 compares bond distances, angles and coupling constants for these complexes. The factors which influence the degree of distortion of 1:1 and 2:1 complexes are discussed in detail in Section 2.

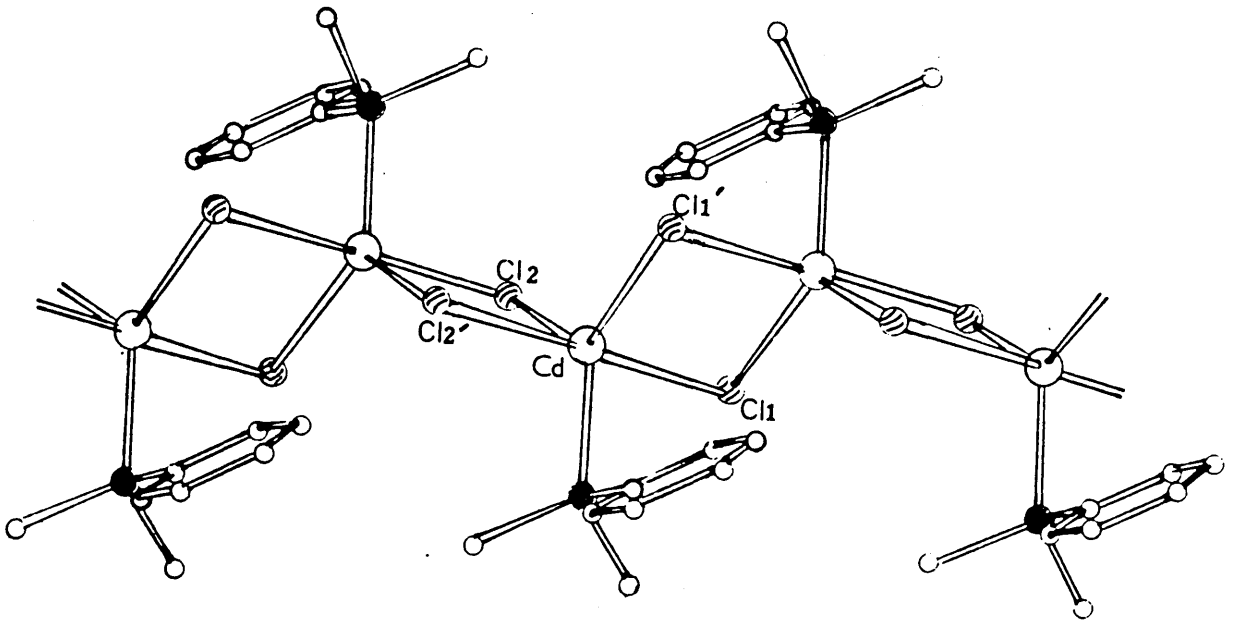

Bond lengths (Å)

Cd-Cl1	2.481(1)	Cd-Cl2′	2.734(1)
Cd-Cl2	2.497(1)	Cd-P	1.825(5)
Cd-Cl1	2.745(1)		

Bond angles (°)

Cl1-Cd-Cl2	110.50(2)	Cl2-Cd-Cl2′	87.10(2)
Cl1-Cd-Cl1′	86.00(2)	Cl2-Cd-P	119.50(5)
Cl1-Cd-Cl2′	92.60(2)	Cl1′-Cd-Cl2′	178.60(4)
Cl1-Cd-P	130.00(4)	Cl1′-Cd-P	88.70(4)
Cl2-Cd-Cl1′	93.40(2)	Cl2′-Cd-P	92.20(2)

Fig 1.16 Structure of $(PhMe_2P)CdCl_2$ [33]

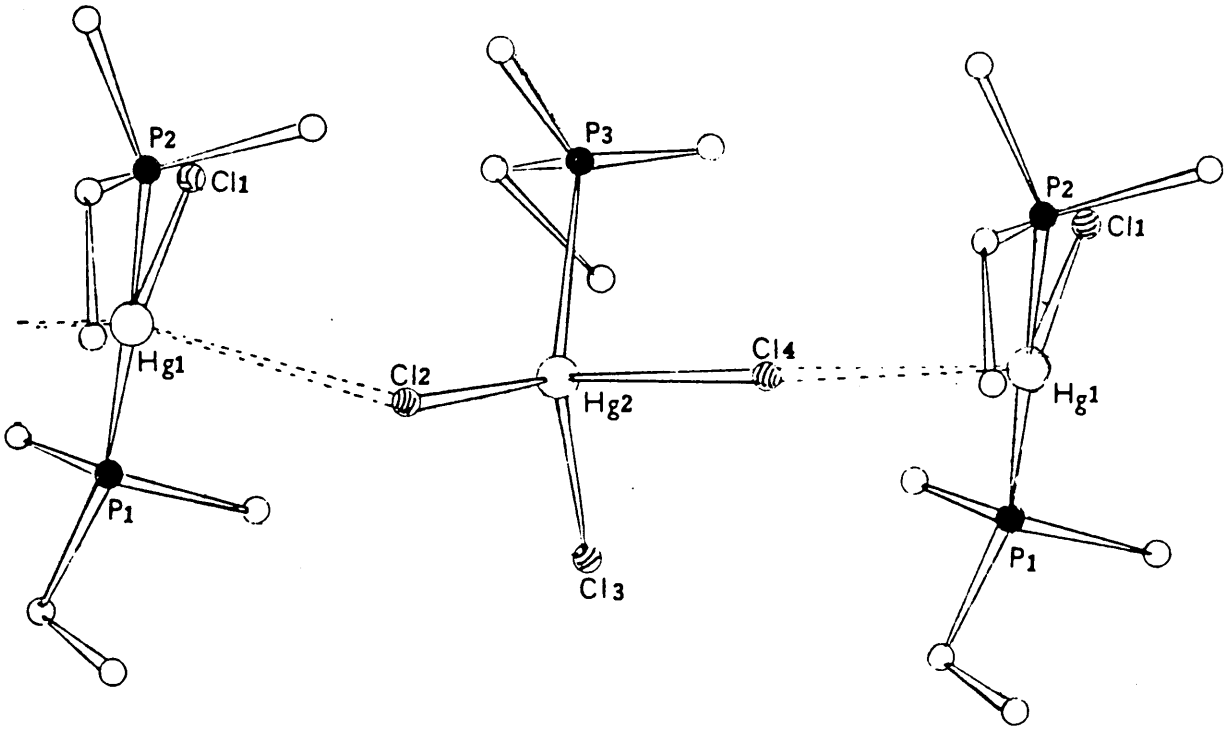

Bond lengths (Å)

Hg1-Cl1	2.69(1)	Hg1-P2	2.40(1)	Hg2-P3	2.40(1)
Hg1-Cl2	3.07(1)	Hg2-Cl2	2.62(1)		
Hg1-Cl4	3.25(2)	Hg2-Cl3	2.52(1)		
Hg1-P1	2.40(1)	Hg2-Cl4	2.45(1)		

Bond angles (°)

C-l1Hg1-P1	97.6(5)	Cl2-Hg-Cl3	98.2(5)
Cl1-Hg-P2	90.1(5)	Cl2-Hg2-Cl4	104.1(5)
Cl4-Hg1-Cl2	149.1(4)	Cl3-Hg2-Cl4	98.5(5)
P1-Hg1-P2	172.3(5)	Cl2-Hg2-P3	101.0(5)
Cl3-Hg2-P3	117.2(5)	Hg1-Cl2-Hg2	133.1(5)
Cl4-Hg2-P3	132.9(6)	Hg1-Cl4-Hg2	107.1(5)

Fig 1.17 Structure of $(EtMe_2P)_3(HgCl_2)_2$ [35]

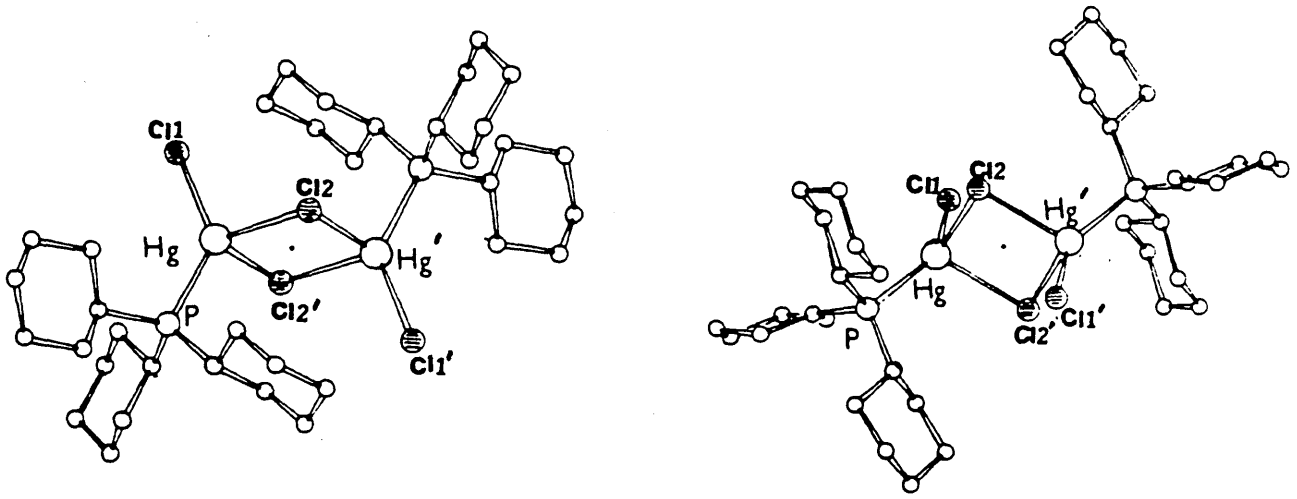

Fig. 1.18 Structure of $(Cy_3P)HgCl_2$ [39]

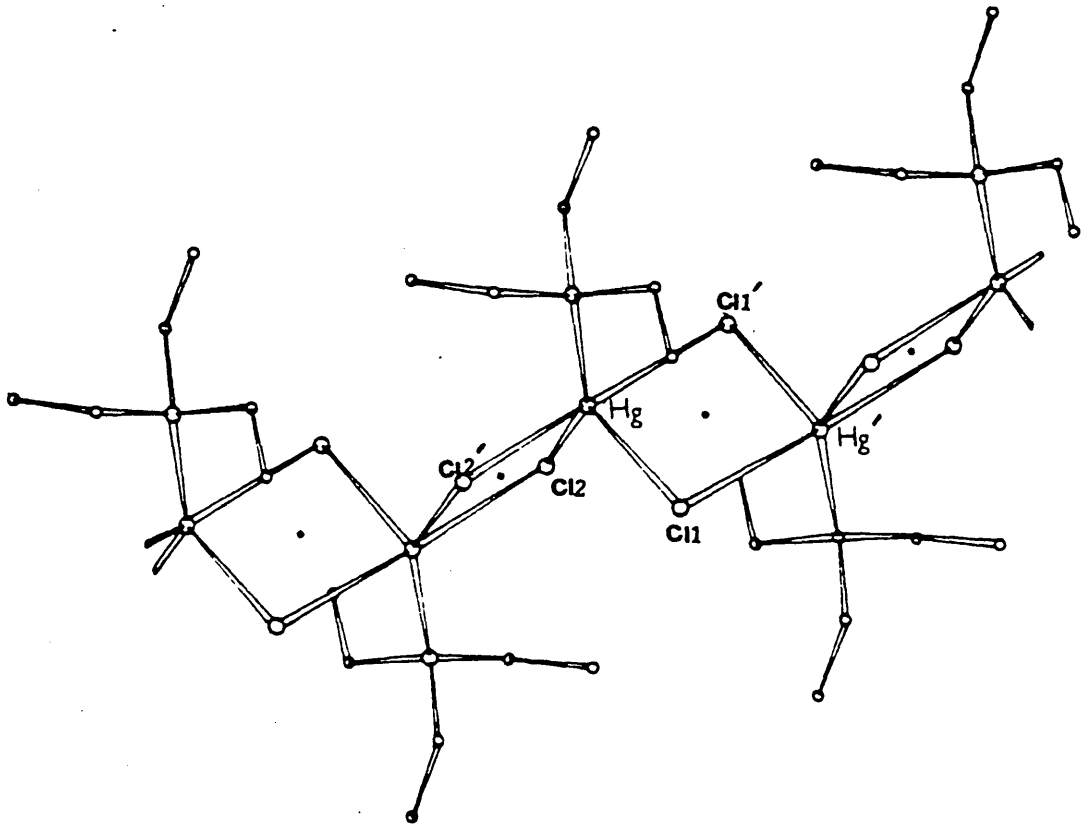

Fig. 1.19 Structure of $(Et_3P)HgCl_2$ [36]

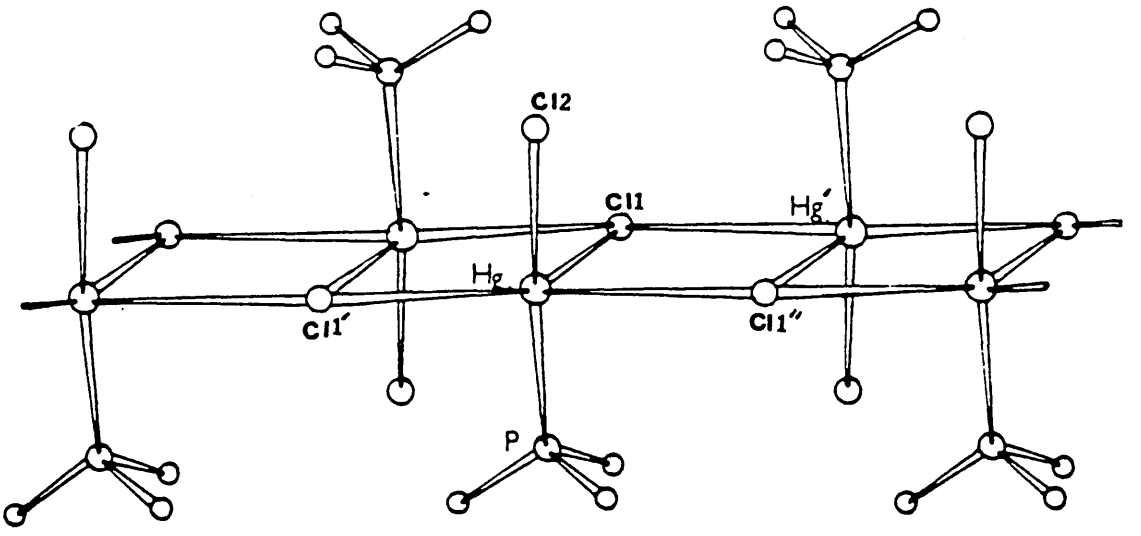

Fig. 1.20 Structure of $(Me_3P)HgCl_2$ [36]

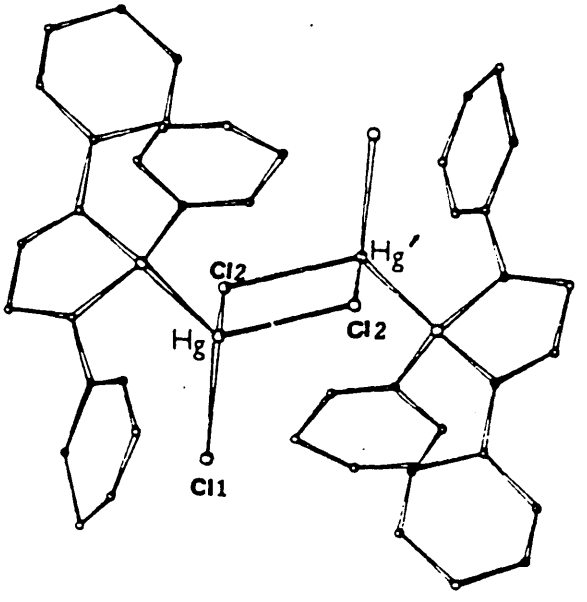

Fig. 1.21 Structure of $(TPP)HgCl_2$ [34]

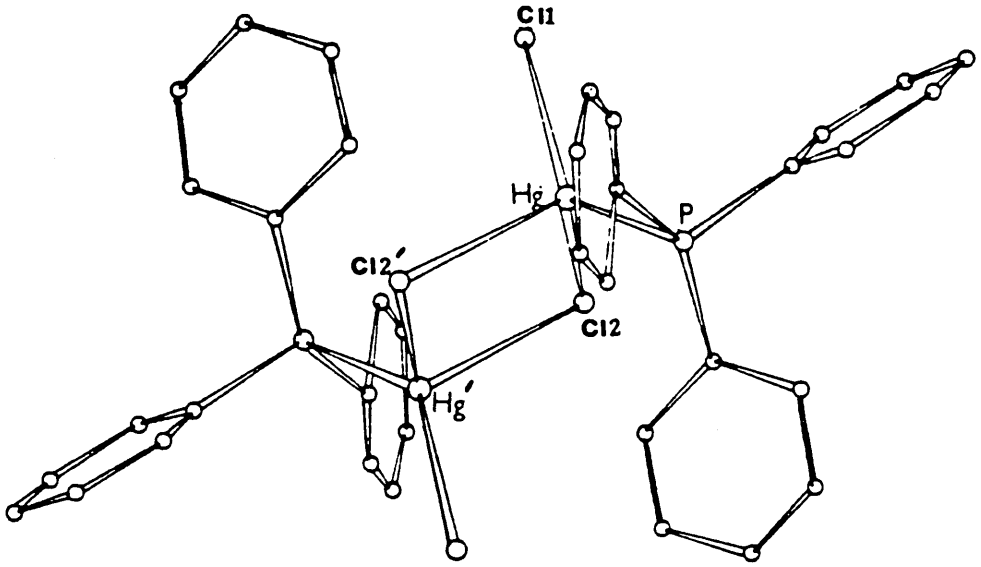

Fig. 1.22. Structure of $(Ph_3P)HgCl_2$ [34]

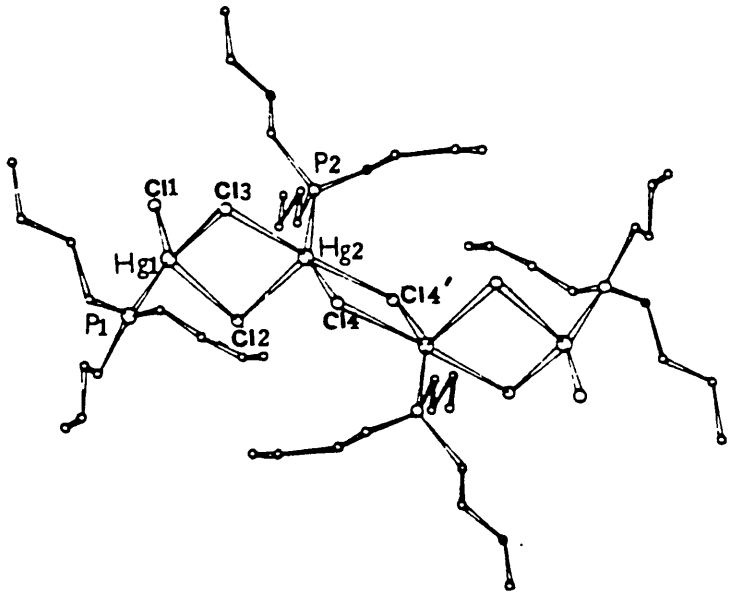

Fig. 1.23 Structure of α-$(Bu_3P)HgCl_2$ [34]

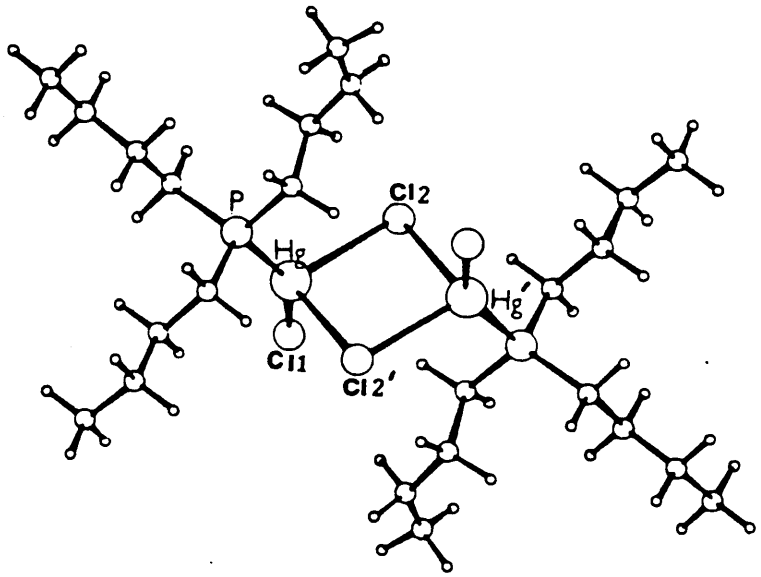

Fig. 1.24. Structure of β-$(Bu_3P)HgCl_2$ [38]

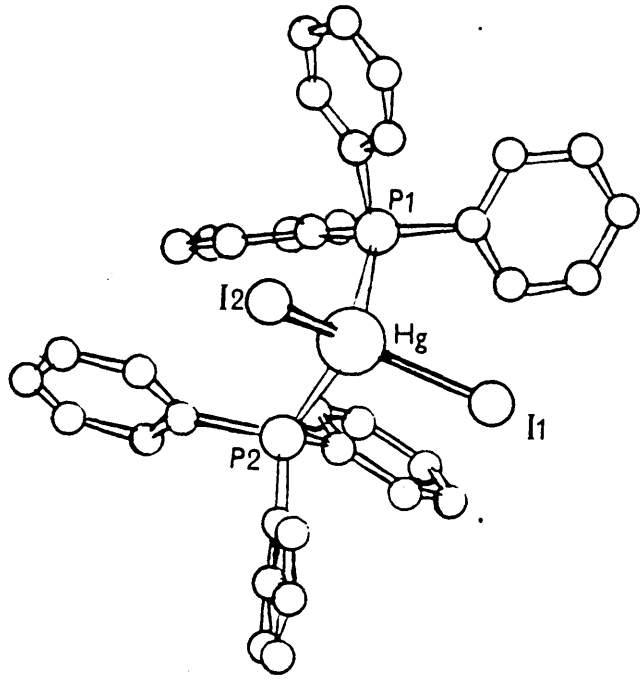

Fig 1.25 Structure of $(Ph_3P)_2HgI_2$ [40]

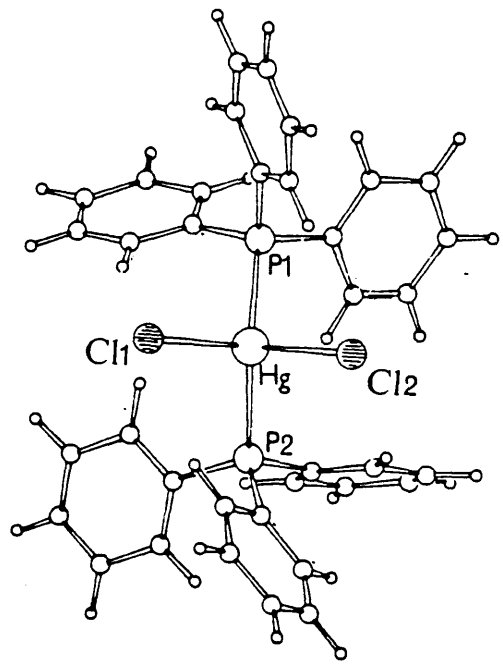

Fig 1.26 Structure of $(Ph_3P)_2HgCl_2$ [43]

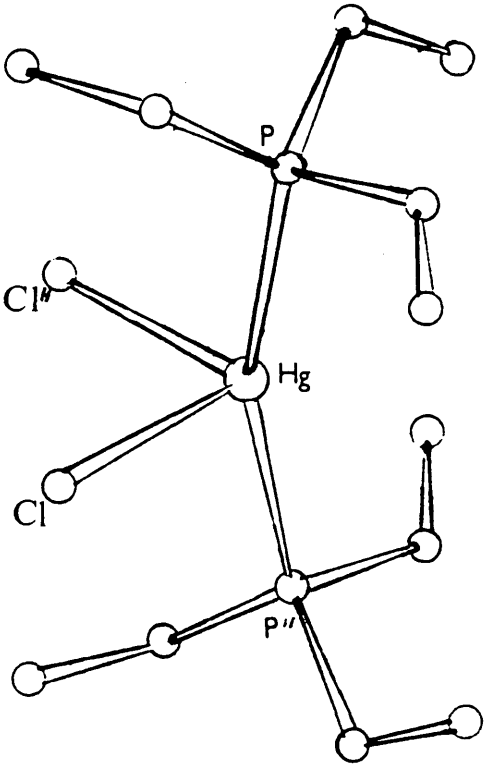

Fig 1.27 Structure of $(Et_3P)_2HgCl_2$ [42]

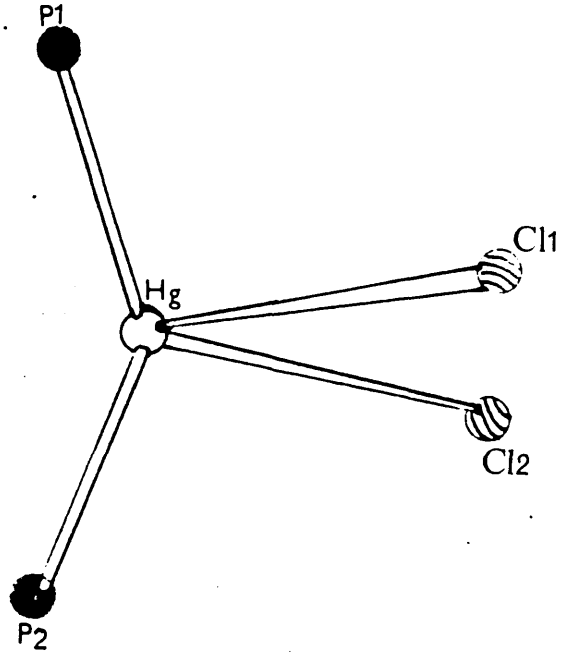

Fig 1.28 Structure of $(Bu_3P)_2HgCl_2$ [41]

TABLE 1.1 Known Structures of $(R_3P)HgX_2$ Complexes

Complex	Structure	Evidence	Ref.
$(Ph_3P)HgCl_2$	Centrosymmetric dimer	Full X-ray structure	34
$(Ph_3P)HgBr_2$	Centrosymmetric dimer	Preliminary X-ray photographs	34
$(Ph_3P)HgI_2$	Centrosymmetric dimer	Preliminary X-ray photographs	34
$(TPP)^{+}HgCl_2$	Centrosymmetric dimer	Full X-ray structure	34
$(TPP)^{+}HgBr_2$	Centrosymmetric dimer	Preliminary X-ray photographs	34
α-$(Bu_3P)HgCl_2$	'Tetramer'	Full X-ray structure	34
β-$(Bu_3P)HgCl_2$	Centrosymmetric dimer	Full X-ray structure	38
$(Cy_3P)^{\ddagger}HgCl_2$	Two independent centrosymmetric dimers	Full X-ray structure	39
$(Et_3P)HgCl_2$	Chain polymer	Full X-ray structure	36
$(Me_3P)HgCl_2$	'Ionic' polymer	Full X-ray structure	36
$(Me_3P)HgBr_2$	'Ionic' polymer	Preliminary X-ray structure	36

$^{+}$TPP = 1,2,5-triphenylphosphole

‡Cy = cyclohexyl

TABLE 1.2 Selected Bond Angles and Bond Lengths of 1:1 $(R_3P)HgCl_2$ Complexes

Ligand	Hg-P(Å)	Hg-Cl_t(Å)	Hg-Cl_{br}(Å)	P-Hg-Cl_t(°)	Cl_1-Hg-Cl_2(°)
PMe_3[36]	2.365(3)	2.355(4)	2.782(4) 2.941(4) 3.489(4)	162.1(1)	98.2(1)
PEt_3[36]	2.35(1)	2.42(1)	2.56(1) 3.04(1) 3.21(1)	145.4(3)	98.7(3)
PBu_3[34] (α-form)	2.363(21) 2.337(19)	2.289(21)	2.709(20) 2.626(19)	147.8(7)	92.6(6)
PBu_3[38] (β-form)	2.377(6)	2.348(8)	2.720(6) 2.736(6)	150.9(3)	89.0(3)
PPh_3[34]	2.406(7)	2.370(10)	2.658(8) 2.623(8)	128.7(4)	84.4(3)
PCy_3[39] mol (1)	2.416(3)	2.391(5)	2.641(4) 2.665(4)	139.6(2)	95.2(2)
mol (2)	2.412(3)	2.413(3)	2.602(4) 2.779(4)	132.0(1)	101.5(1)
TPP[34]	2.438(10)	2.404(11)	2.542(13) 2.747(14)	127.8(5)	86.5(4)

br = bridging
t = terminal

TABLE 1.3

Bond Distances, Angles and Coupling Constants with Estimated Standard Deviations for $(R_3P)_nHgX_2$ (n = 1, 2 and X =Cl, Br or I)

$(R_3P)_n$	X	P-Hg (Å)	P-Hg-P (°)	$J(^{199}Hg-^{31}P)$ Hz	pKa	ref.
$(Ph_3P)_2$	Cl	2.462(2) 2.478(2)	134.1(1)	4740	2.73	50
	Br	2.54(3) 2.53(2)	113.0(5)	4178	"	"
	I	2.574(3)	109.0(1)	3073	"	"
$(Ph_3P)_1$	Cl	2.406(7)		7431	"	"
	Br			6464	"	"
	I			4700	"	"
$(Bu_3P)_2$	Cl	2.34(6) 2.64(6)	139.0(2)	5078	8.64	49
	Br			4741	"	"
	I			4110	"	"
$(Bu_3P)_1$	Cl	2.34(3) 2.35(2)		7446		"
	Br			6624		"
	I			5127		"
$(Et_3P)_2$	Cl	2.39(1) 2.39(1)	158.5(1)	5095	8.69	42
	Br			4792	"	"
	I			4004	"	"

Contents

2. Factors which Influence the Solid State Structure of Mercury(II) Halide Complexes

The following factors are believed to influence the solid state structures of mercury(II) halide complexes with monodentate neutral donor ligands:

(i) type of donor atom;

(ii) electronic effect of the substituents attached to the donor atom;

(iii) steric effect of the substituents attached to the donor atom;

(iv) nature of the halogen atom;

(v) entropy effects.

2.1 Influence of the Donor Atom

Hg^{2+} and Cd^{2+} ions are classed as 'soft acids' or 'Class b' metal ions but Zn^{2+} is a 'harder acid' than either Hg^{2+} or Cd^{2+}.[51] Mercury(II) will therefore form strong interactions with 'soft' bases such as sulphur, phosphorus and arsenic but nitrogen, being a harder base, is less likely to form strong interactions. The strong interactions cause distortion of the X-Hg-X unit from a linear arrangement and an increase in the length of the Hg-X bond. Oxygen which is classed as a 'hard' base, only interacts weakly with mercury resulting in polymeric structures with only a slight distortion from linearity of the X-Hg-X units. For $(C_4H_8O)HgBr_2$[9] the Br-Hg-Br angle is 174.6(4)° while the Hg-Br bond distance is 2.475(10) Å. In contrast $(Ph_3P)_2HgBr_2$[43] shows a larger degree of distortion from linearity, having a Br-Hg-Br angle of 106.9(3)° and Hg-Br distances of 2.633(6) and 2.626(8) Å.

The advent of the modern Fourier Transform NMR spectrometer has enabled the ^{31}P and ^{199}Hg spectra of complexes to be studied, the main areas of interest being the chemical shifts and coupling constants.

A clear correlation has been found between the coupling constants and

the σ-donor strengths of the ligands (Table 1.3). The stronger donor ligands tend to give larger coupling constants, for example, $(Et_3P)_2HgCl_2$[42] has a larger coupling constant ($J(^{199}Hg-^{31}P)$) than $(Ph_3P)_2HgCl_2$.[50] The 2:1 complexes have smaller coupling constants than the corresponding 1:1 complexes, probably as the donor ability of the ligand is affected by the competition of a second ligand about the mercury atom. This would mean that in the case of the 1:1 complexes the ligand is a stronger donor atom, hence having a larger coupling constant.

2.2 The Electronic Effect of the Substituents Attached to the Donor Atom

The extent of the interaction between mercury and the donor is also dependent on the ability of the donor atom to act as a "Lewis Base". Thus the σ-donor ability of the ligand is dependent on the substituents attached to the donor atom. A considerable amount of work has been carried out on tertiary phosphine complexes,[52] much of which relates the basicity of the phosphine to the Hg-P bond lengths and to the bond angles about Hg. In general, complexes formed with ligands of a high pKa are found to have shorter Hg-P bonds which may reflect a strong mercury-phosphorus interaction.

The 1:1 and 2:1 complexes show an increase in the length of the Hg-Cl bond and a corresponding decrease in the Hg-P distance from Ph_3P to Et_3P. These data appear to support the idea that Ph_3P, with a pKa of 2.73, has a weaker interaction with the mercury atom than Et_3P, which has a pKa of 8.69. For the 1:1 complexes the Cl_t-Hg-P angle increases, while for the 2:1 complexes the P-Hg-P angle increases from Ph_3P to Et_3P (Table 2.21).

2.3 The Steric Effect of the Substituents Attached to the Donor Atoms

The steric requirements of a ligand have been defined by the use of the term 'cone angle'. The cone angle for a symmetric ligand PR_3 (R=R=R) is the apex angle of a cylindrical cone centred 2.28 Å from the centre of the

TABLE 2.21

A Comparison of Some Bond Lengths and Angles of $(R_3P)_nHgCl_2$ Complexes

(n = 1 or 2, R = Ph or Et)

n = 1				n = 2				
R_3P	Hg-P(Å)	Hg-Cl(Å)	P-Hg-Cl_t(°)	R_3P	Hg-P(Å)	Hg-Cl(Å)	P-Hg-P(°)	pKa[52]
Et_3P[36]	2.35(1)	2.56(1)	145.4(3)	Et_3P[42]	2.39(1)	2.68(1)	158.5(5)	8.69
		2.42(1)			2.39(1)	2.68(1)		
Ph_3P[34]	2.406(7)	2.370(10)	128.7(4)	Ph_3P[43]	2.478(2)	2.559(2)	134.1(1)	2.73
		2.623(8)			2.462(2)	2.545(3)		

Cl_t = terminal chlorine atom

phosphorus atom which touches the Van der Waals' radii of the outermost atoms (Fig. 2.1). For an unsymmetrical ligand the angles are calculated[47] by the equation $\theta = \frac{2}{3}\Sigma_{i=1}^{3} \theta i/2$

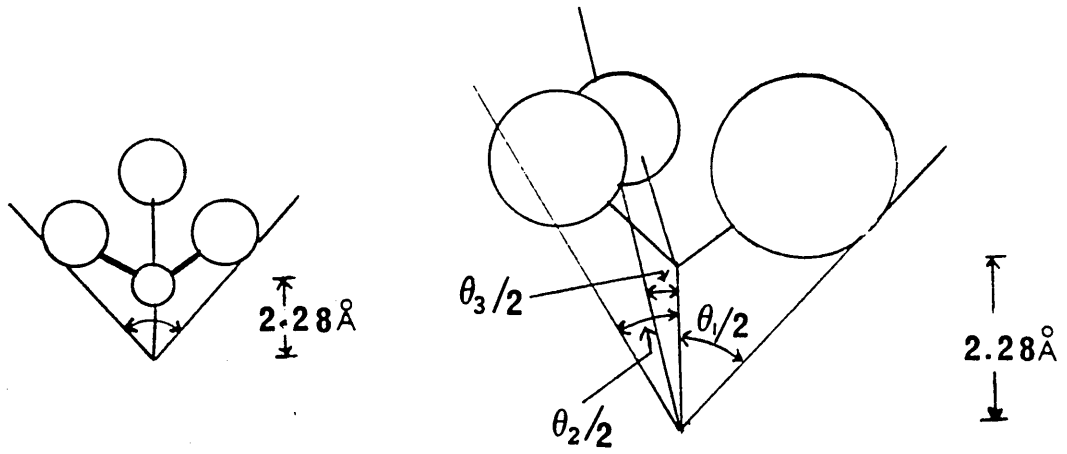

(a) (b)

FIGURE 2.1

(a) Cone Angle Measurement for Symmetrical Ligand (b) Cone Angle Measurement for Unsymmetrical Ligands[47]

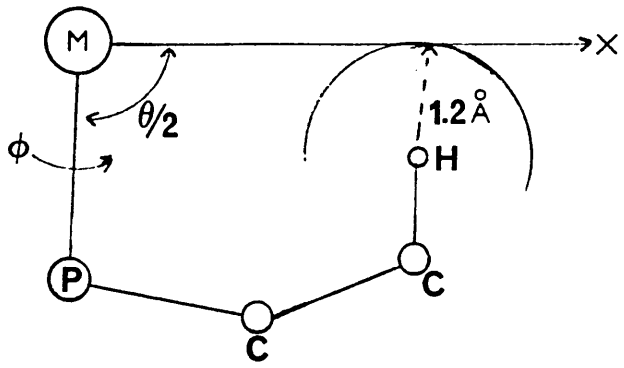

FIGURE 2.2 Details of the Calculation of the Maximum Semicone Angle $\theta/2$[53]

The cone angle is defined as a steric parameter which is a measure of the degree of congestion around the bonding face of phosphorus. Very bulky phosphines such as Cy_3P and $Bu^t{}_3P$ do not behave as solid cones but are described as irregular 'conic cogs'.[53] The concept of 'ligand profile' has been developed to obtain precise maximum cone angle data and information on the gaps between moieties in a ligand (the depth of the tooth of the conic cog). To obtain a 'ligand profile', a plot is made of the maximum semicone angle, $\theta/2$, as a function of the angle ϕ through which the M → X vector is rotated about the M-P bond (Fig. 2.2). Cone angles measured for some phosphines are as follows:

$$Me_3P = 118°,\ Cy^{\dagger}{}_3P = 170°,\ Bu^t{}_3P = 180°,\ Et_3P = 132°$$[47]

Cy_3P is a "bulky" ligand (cone angle = 170°) but it is known to be a stronger donor than Et_3P and Me_3P ligands. The pKa values are Cy_3P = 9.70, Et_3P = 8.69, and Me_3P = 8.65.[52] It would be expected that Cy_3P complexes would have shorter Hg-P bonds and larger X_t-Hg-P angles than the Et_3P and Me_3P complexes.[36] However, the X_t-Hg-P angles for Cy_3P are 132.0(1) and 139.6(2)° while the Hg-P distances are 2.412(3) and 2.416(3) Å.[39] The corresponding angles for the complexes of Et_3P are 145.4(3) and for Me_3P, 162.1(1)° while the Hg-P bonds are 2.35(1) and 2.365(3) Å.[36] This would indicate that the 'bulky' nature of Cy_3P ligand and the inflexibility of the cyclohexyl rings sterically inhibit the opening up of the Cl_t-Hg-P angle beyond 139.6°.

2.4 The Nature of the Anion in $(R_3P)_nHgX_2$ (n = 1, 2 X = anion)

In the halide complexes the halogen atoms compete with the phosphorus for bonding around the mercury atom. The relative donor strength of halides (Cl^-, Br^- and I^-) towards mercury increases with decreasing

---

†Cy = Cyclohexyl

electronegativity of the halogen, chloride being the weakest. This is indicated by comparison of the $\log K_1$ values (where K_1 = first stepwise formation constant) calculated from equation 2.41.

$$Hg^{2+} + X^- \rightleftharpoons HgX^+ \qquad 2.41$$

$$K_1 = \frac{[HgX^+]}{[Hg^{2+}][X^-]}$$

$\log K_1$ (25 °C)[60] for $[HgCl]^+ = 6.74$

$[HgBr]^+ = 9.05$

$[HgI]^+ = 12.87$

In general for anions, when X is strongly σ-bonding, the X-Hg-X grouping tends towards linearity with longer Hg-P bonds than are found in complexes involving weaker anions. This trend has been illustrated by both X-ray and NMR techniques in the series $(Ph_3P)_2HgX_2$ (X = Cl, Br, I, CF_3, CN, SCN and ONO_2)[42] (Table 2.41). This table shows that for strong σ-donors, for example, where X = CF_3, an X-Hg-X angle of 146.6(9)° and an Hg-P bond length of 2.91 Å are found. In marked contrast for X = ONO_2, which forms a weaker σ-bond, a much smaller X-Hg-X angle of 70.0° and significantly shorter Hg-P bond length of 2.45 Å results. The NMR measurements show weaker σ-bonding groups have larger coupling constants and this has also been illustrated by the series $(EtMe_2P)_2P)_2HgX_2$ (X = Cl, Br, I, CN and SCN),[42] $(Et_3P)_2HgX_2$ and $(Bu^n{}_3P)_2HgX_2$ (X = Cl, Br, I and ONO_2)[42] (Table 2.42).

2.5 Entropy Effects

Entropy is a measure of the disorder of a system; for this reason entropy measurements can give some indication of the number of molecules present in a structure. The higher the entropy of a system the greater the number of independent molecules it contains. Systems tend towards higher

entropies and hence the most possible number of independent molecules allowed after consideration of the other factors involved.

TABLE 2.41 Bond Lengths and Interbond Angles in Some Crystalline $(Ph_3P)_2HgX_2$ Complexes (X = CF_3, CN, I, SCN, ONO_2, Br and Cl)[42]

X	(Hg-P)(Å)	(Hg-X)(Å)	P-Hg-P(°)	X-Hg-X(°)	J(^{199}Hg-^{31}P)Hz
CF_3	2.91(2)	2.12(2)	94.8(1)	146.6(9)	-
CN	2.515(7)	2.234(26)	108.9(2)	108.5(15)	2617
I	2.565(3)	2.748(1)	108.95(9)	110.43(4)	3074
SCN	2.488(3)	2.571(3)	118.1(1)	96.7(1)	3725
Br	2.533(15)	2.629(7)	113.0(5)	106.9(3)	4156
Cl	2.47(2)	2.552(2)	134.1(1)	110.7(1)	4675
ONO_2	2.451(1)	2.507(4)	131.8(1)	70.0(2)	5925

TABLE 2.42 Coupling Constants (J(^{199}Hg-^{31}P)Hz) for $R_3P)_2HgX_2$ (X = Cl, Br, I, CN, SCN and ONO_2)[42]

X	$(EtMe_2P)_2HgX_2$	$(Et_3P)_2HgX_2$	$(Bu^n{}_3P)_2HgX_2$
Cl	5606	5095	5125
Br	5436	4792	4829
I	4702	4033	4089
CN	3225	-	-
SCN	5084	-	-
ONO_2	-	5221	5212

Contents

3. General Introduction to Crystal Structure Analysis

3.1 Single Crystal X-ray Diffraction

A single crystal can be considered as a three-dimensional lattice, with each lattice point occupied by an atom or group of atoms. It is, therefore, possible for a crystal to act as a three-dimensional diffraction grating for X-rays. The conditions required to produce a diffraction maximum from a regular three-dimensional array of scattering atoms are given by the three Laue equations.[54] These may be derived from Figure 3.1.

For a row of scattering atoms of regular spacing b along the y axis, where X-rays are incident at an angle $\emptyset_2$, and are scattered at an angle ψ_2 the path difference (δ_2) between scattered rays is given by

δ_2 = AQ - BP or δ_2 = b (Cos ψ_2 - Cos $\emptyset_2$)

For reinforcement of the scattered rays, the path difference must be an integral number of wavelengths.

$$\delta_2 = b\ (\text{Cos}\ \psi_2 - \text{Cos}\ \emptyset_2) = k\lambda \qquad 3.1$$

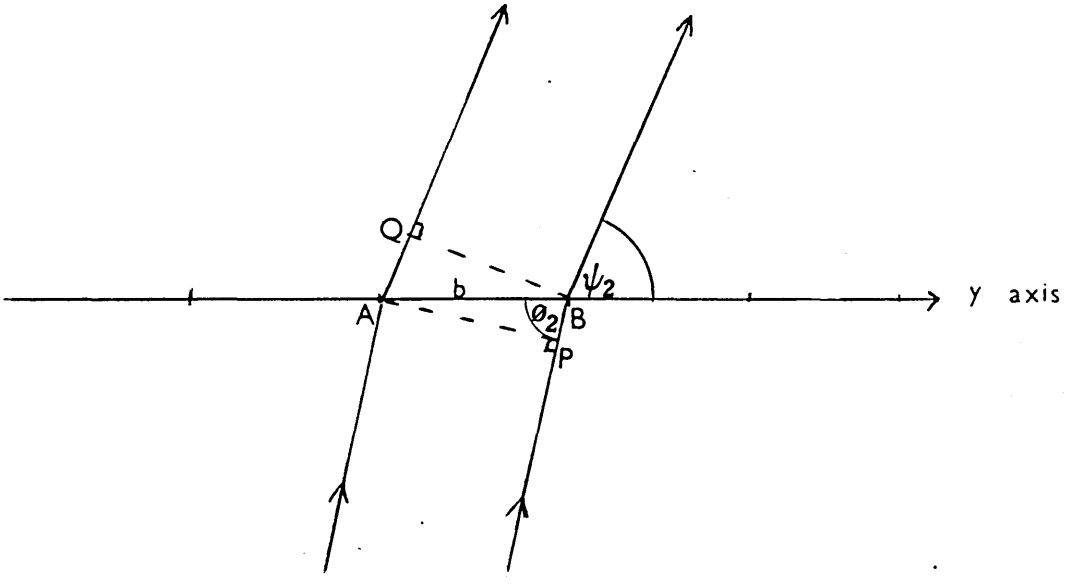

FIGURE 3.1 Diffraction from a Row of Atoms

Equation 3.1 is satisfied by the generators of a cone which is coaxial with the line of scattering atoms and has a semi-vertical angle of ψ_2. For a series of values $\emptyset_2$, there are a number of cones each corresponding to an order of diffraction k and a semi-vertical angle ψ_{2k}. This theory when extended to the x-axis (spacing a) gives the equation

$$a(\text{Cos } \psi_2 - \text{Cos } \emptyset_2) = h\lambda \qquad 3.2$$

For three-dimensional systems a third equation corresponding to the third axis of spacing c can be generated.

$$c(\text{Cos } \psi_2 - \text{Cos } \emptyset_2) = l\lambda \qquad 3.3$$

Bragg[55] considered diffraction to be analogous to 'reflection' from a set of lattice planes. The waves are 'reflected' only under certain conditions. The length of path between the waves scattered from successive planes must have an integral number of wavelengths (i.e. $n\lambda$).

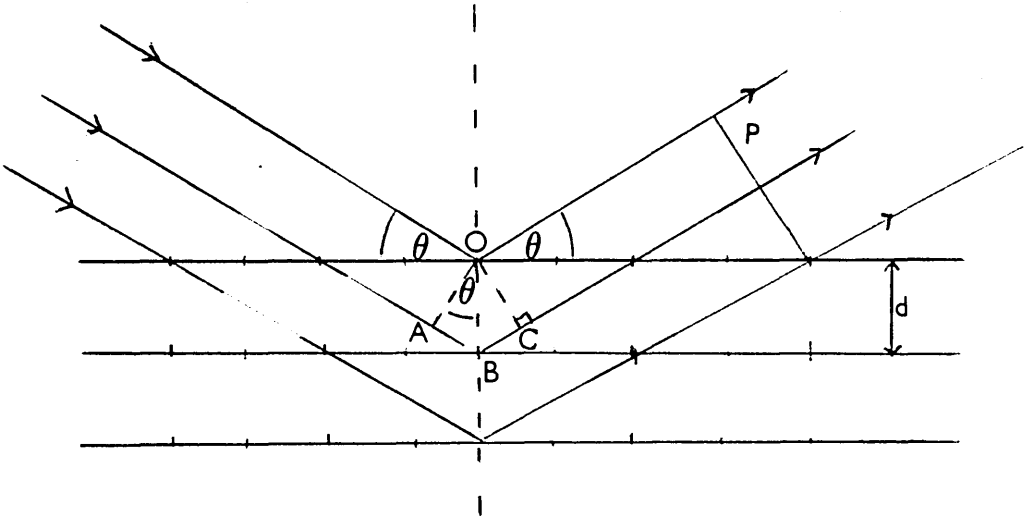

FIGURE 3.2 Diffraction of X-Rays by a Set of Lattice Planes

The path difference δ between successive waves is given by:

$$\delta = AB + BC$$

As AB = BC

$$\delta = 2AB$$

$$\therefore \delta = 2d \sin\theta$$

where d is the interplanar spacing

For reinforcement of the scattered waves the difference δ must be a whole number of wavelengths.

$$n\lambda = 2d \sin\theta \qquad 3.4$$

This expression is often referred to as 'Braggs Law'.

3.2 The Phase Problem

The phase problem arises from the difficulty in the direct determination of the phase angle associated with each structure factor. While the structure amplitude $|F|$ may be derived directly from the intensity of each reflection (Equation 3.5) the phase angle may not.

$$I_{hkl} = k\,|F_{hkl}|^2(Abs)(LP)(Th) \qquad 3.5$$

I_{hkl} is the intensity of the diffraction from the set of planes hkl and may be determined experimentally.

k - scale factor associated with $|F_{hkl}|$, which may be approximated using Wilson's method.[56]

Abs - the absorption factor and is dependent upon the number and type of the atoms present in the unit cell.

L - correction for Lorentz effect which arises as the time required for a reciprocal lattice to pass through the sphere of reflection varies with its position in reciprocal space. The exact nature of the effect depends upon the type and nature of the data collection. For data collected on a Stöe Stadi-2 two circle diffractometer the collection is given by

$$L = \sin\theta/[\sin 2\theta(\sin^2\theta - \sin^2\mu)^{1/2}] \qquad 3.6$$

P - correction for the polarization of the X-rays. The incident X-ray beam loses intensity due to polarization by both the graphite monochromator crystal and by the crystal under investigation.

Correction for polarization (P) by the data crystal is given by

$$P = \frac{1}{2}(1 + \text{Cos}^2\ 2\theta) \qquad 3.7$$

The electron density (p) at a point x, y, z in a unit cell of volume V_c is given by equation 3.8 where α_{hkl} is the phase angle and must be evaluated before the map can be computed.

$$p(x,y,z) = \frac{1}{V_c}\ \Sigma_h\Sigma_k\Sigma_l\ |F|\ \text{Cos}[2\pi\ (hx + ky + lz) - \alpha_{hkl}] \qquad 3.8$$

A plot of p(x,y,z) for appropriate values of x, y and z gives a three-dimensional electron density map from which electron density and hence the atomic positions may be elucidated. Evaluation of the phase angles, i.e. overcoming the phase problem, is normally achieved by one of the following approaches:

Patterson synthesis

Direct methods

3.2.1 Patterson Synthesis

The Patterson function P(uvw) may be calculated without the knowledge of phase angles (equation 3.9). The resulting three-dimensional map gives rise to positive peaks representing vectors between all possible pairs of atoms in the unit cell. The heights of the vectors are proportional to the product of the atomic numbers of the two atoms. Hence, if one or more heavy atoms are present, then their associated vectors may be readily located on the map.

$$P(uvw) = \frac{1}{V_c}\ \Sigma_{-\infty}^{\infty}{}_h\ \Sigma_k\ \Sigma_l\ |F_{hkl}|^2\ \text{Cos}\ 2\pi(hu + kv + lw) \qquad 3.9$$

The value for $|F_{hkl}|$ is obtained from the measured intensities I_{hkl} using the equation 3.5.

3.2.2 Direct Methods

While this technique has been widely used for organic molecules it has also proved to be useful in locating heavy atoms in, for example, organometallic compounds. These methods were developed assuming that if a structure can be derived from a Fourier synthesis of the measured intensities, such as in the Patterson function, it should be possible to derive the structure directly from the intensities themselves. An initial development of "direct methods" was the derivation of inequalities which expressed the phases of the structure factors in terms of observed structure amplitudes $|F_o|$, where $I \propto |F_o|^2$. Using the general structure factor expression the trivial result

$$|F_{hkl}|^2 < F_{ooo}^2 \qquad 3.10$$

may be extended by centrosymmetric requirements to give

$$F_{hkl}^2 < F_{ooo}\,(\tfrac{1}{2}F_{ooo} + \tfrac{1}{2}F_{2h,2k,2l}) \qquad 3.11$$

$$\text{If } U_{hkl} \text{ is defined as } = F_{hkl}/F_{ooo} \text{ then } U_{hkl}^2 < \tfrac{1}{2} + \tfrac{1}{2}U_{2h,2k,2l} \qquad 3.12$$

As the magnitude and sign (+) of U_{hkl}^2 are known, only the phase of $U_{2h,2k,2l}$ is unknown. In centrosymmetric systems the phase angle may only take one of two values, 0° or 180°, corresponding to the signs + and - in the structure factor expression. For non-centrosymmetric crystals, however, the phase angle may take any value between 0° and 360°.

Inequalities proved to be of limited use as often it was not possible to determine sufficient phases from which the structure could be solved. This limitation led to the development of 'probability methods' for the determination of phases which could be used for structural analysis. Karle and Hauptmann found the normalized structure factor $|E_{hkl}|$ to be more suitable for use in probability functions.[64]

$$|E_{hkl}|^2 = \frac{|F_{hkl}|^2}{\varepsilon N \Sigma_j f_j^2} \qquad 3.13$$

ε is an integer dependent upon the reflection and upon the space group symmetry.

The distribution of $|E|$ values is independent of the size and content of the unit cell but is dependent whether or not there is a centre of symmetry in the space group.

The tabulated distribution of $|E|$ values are:

Mean Values	Centrosymmetric crystal	Non-centrosymmetric crystal
$\|E\|^2$	1.00	1.00
$\|\|E\|^2 - 1\|$	0.97	0.74
$\|E\|$	0.80	0.89
% $\|E\| > 1$	32.00	36.80
% $\|E\| > 2$	5.00	1.80
% $\|E\| > 3$	0.30	0.01

The most commonly used expression to predict the phases of reflections in centrosymmetric crystals is the Sayre relationship.[57]

$$\text{sign } F_h \simeq \text{sign } (F_k F_{h-k}) \qquad 3.14$$

or in a more general form

$$\text{sign } E_{\underline{h}} \simeq \text{sign } \underset{\underline{k}}{\Sigma} E_{\underline{k}} E_{\underline{h}-\underline{k}} \qquad 3.15$$

where $\simeq$ means 'is probably equal to'.

Equation 3.15 is known as the Σ_2 formula but this formula cannot be used for non-centrosymmetric crystal analysis. The phase angle, ϕ_h, for such systems may be derived from the 'tangent formula'.

$$\tan \phi_{\underline{h}} \quad \frac{\Sigma_{\underline{k}} |E_{\underline{k}} E_{\underline{h}-\underline{k}}| \text{Sin}(\phi_{\underline{k}} + \phi_{\underline{h}-\underline{k}})}{\underset{\underline{k}}{\Sigma} |E_{\underline{k}} E_{\underline{h}-\underline{k}}| \text{Cos}(\phi_{\underline{k}} + \phi_{\underline{h}-\underline{k}})} \qquad 3.16$$

A measure of the reliability of the predicted phases $\alpha_{\underline{h}}$ is given by equation 3.17. The higher the $\alpha_{\underline{h}}$ value the better the reliability of the phase prediction.

$$\alpha^2_{\underline{h}} = [\sum_{\underline{k}} \kappa_{\underline{hk}} \cos(\phi_{\underline{k}} + \phi_{\underline{h}-\underline{k}})]^2 + [\sum_{\underline{k}} \kappa_{\underline{hk}} \sin(\phi_{\underline{k}} + \phi_{\underline{h}-\underline{k}})]^2 \qquad 3.17$$

where $\kappa_{\underline{hk}} = 2\sigma_3\sigma_{\frac{2}{-3}}^{-2}|E_{\underline{h}}E_{\underline{k}}E_{\underline{h}-\underline{k}}|$

being calculated from equation 3.18

$$\sigma n = \sum_{j=1}^{n} Z_j^n \qquad 3.18$$

Z_j is the atomic number of the j atom

Initially $\phi_{\underline{k}}$ and $\phi_{\underline{h}-\underline{k}}$ are unknown, so an estimated value of $\alpha_{\underline{h}}$ must be used and this is given by

$$\langle\alpha^2_{\underline{h}}\rangle_e = \sum_{\underline{k}} \kappa^2_{\underline{hk}} + 2\sum\sum_{\underline{kk}'} \kappa_{\underline{hk}}\kappa_{\underline{hk}'} \cdot \frac{I_1(\kappa_{\underline{hk}})I_1(\kappa_{\underline{hk}'})}{I_0(\kappa_{\underline{hk}})I_0(\kappa_{\underline{hk}'})} \qquad 3.19$$

Where I_1 and I_0 are modified Bessel functions.

The expression (3.19) is often modified to the approximate formula

$$\langle\alpha^2_{\underline{h}}\rangle^{1/2}_e = \sum_{\underline{h}} \kappa_{\underline{hk}} \frac{I_1(\kappa_{\underline{hk}})}{I_0(\kappa_{\underline{hk}})} \qquad 3.20$$

Before these expressions may be used, the phases of some of the reflections must be fixed (usually at 0°) in order to determine the position of the origin in the unit cell. The number and type of reflections used depend on the space group. Some reflections have their phases fixed by the structure, and these structure semi-invariants may not be altered. For non-centrosymmetric crystals a further reflection is given fixed values for its phase to distinguish between the two possible enantiomorphous forms of the crystal.

3.3 Refinement of a Trial Structure

Having deduced the initial structure by Patterson or direct methods techniques, further atoms may be located by the successive use of Fourier

maps. This method makes use of the fact that the electron density at any point in the unit cell is given by equation 3.8. The structure amplitude, $|F_c|$ may be calculated:

$$|F_{hkl}| = (A^2_{hkl} + B^2_{hkl})^{1/2} = |F_c| \qquad 3.21$$

where

$$A_{hkl} = \Sigma_j f_j \text{Cos}2\pi(hx_j + ky_j + lz_j)$$

$$B_{hkl} = \Sigma_j f_j \text{Sin}2\pi(hx_j + ky_j + lz_j)$$

f_j is the atomic scattering factor of the j^{th} atom

x_j, y_j, z_j, is the position of j atoms in the unit cell, and the phase angle is given by

$$\phi_{hkl} = \tan^{-1}\left(\frac{B_{hkl}}{A_{hkl}}\right) \qquad 3.22$$

The resulting observed Fourier map displays areas of electron density corresponding to the initially located atoms plus other unknown atoms in the structure. In the later stages of analysis, a difference Fourier synthesis is normally employed in which the $|F_o|$ coefficients are replaced by $(|F_o| - |F_c|)$ this reveals atoms other than those used to determine $|F|$, providing the calculated phases are close to the observed ones.

3.4 Least-Squares Refinement

When the positions of atoms have been located it is possible to calculate the phase and $|F_c|$ for all observed reflections. These phases and the $|F_o|$ values may be used to obtain further Fourier maps (equation 3.8) from which the positions of further atoms may be located. New values for $|F_c|$ and ϕ_{hkl} may then be calculated which, since they are based on more atoms, should give a closer approximation to the experimentally determined structure amplitudes and phases. The measure of agreement between $|F_c|$ and $|F_o|$ is given by the reliability or residual index (the R-value) which is calculated from equation 3.23.

$$R = \Sigma_{hkl} \frac{||F_o|-|F_c||}{\Sigma_{hkl}|F_o|} \qquad 3.23$$

The better the agreement between $|F_o|$ and $|F_c|$ the lower the R-value. A least-squares technique is used to refine the atomic positional parameters (x_j, y_j, z_j), thermal parameters (U or U_{ij} etc.), the overall scale factor, K, and the non-unit population factors.

3.5 Thermal Parameters

The atomic scattering factor as used to calculate $|F_c|$ (equation 3.21), assumes the atoms to be point atoms. However, in practice atoms vibrate and hence a correction for thermal motion needs to be made:

$$f = f_o \exp \frac{[-8\pi^2 U \sin^2\theta]}{\lambda^2} \qquad 3.24$$

where U is the isotropic temperature factor and is the mean square amplitude of the atomic vibration. For anisotropic vibration the correction to f_o is given by:

$$f = f_o \exp[-2\pi^2(U_{11}h^2a^{*2} + U_{22}k^2b^{*2} + U_{33}l^2c^{*2} + 2U_{12}hka^*b^* + 2U_{13}hla^*c^* + 2U_{23}klb^*c^*] \qquad 3.25$$

Where U_{ij} describes the direction and magnitude of a vibrational elipsoid and are taken as anisotropic thermal factors.

3.6 Weighting Scheme

Unit weights are applied in the early stages of the least squares analysis but a non-unit weighting scheme is introduced in the later stages. If a non-unit weighting scheme is applied then a weighted R - value R_W or R' may be calculated:

$$R_W = \frac{\Sigma_{hkl}|K|F_o| - |F_c||(W_{hkl})^{1/2}}{\Sigma_{hkl}K|F_o|(W_{hkl})^{1/2}} \qquad 3.26$$

Where W is the non-unit weight as calculated using equation 3.27.

$$W = a/[\sigma|F_o|^2 + b|F_o|^2] \qquad 3.27$$

a and b are refined to give the best consistency of $W\Delta^2$

($W\Delta^2 = |F_o| - |F_c|$) over ranges of F_o and $\sin\emptyset/\lambda$

3.7 Anomalous Dispersion

When the scattering factor of an atom is calculated as a real number it is assumed that the frequency of the incident radiation is different from the natural absorption frequency of the atom. Although this may be true for light atoms and the radiations used for X-ray diffraction, it is generally not so for heavier atoms which may absorb the incident radiation. If such absorption occurs there will be an anomalous change in phase of the radiation scattered by the electrons associated with the absorption. This effect, anomalous scattering or anomalous dispersion, causes the scattering factor to become a complex number represented by:

$$f_j^{anom} = f_j + \Delta f'_j + i\Delta f''_j \qquad 3.28$$

where f_j is the normal scattering factor

$\Delta f'_j$ is a real correction term usually negative

$\Delta f''_j$ is an imaginary correction term

For a centrosymmetric structure the effect of the anomalous dispersion is to alter the phases of certain reflections so they are no longer restricted to 0° and 180°, but for such cases Friedel's law still holds. For non-centrosymmetric crystal systems Friedel's law no longer holds as the phases and magnitudes of the reflections are altered.

Contents

4. Crystallographic Studies of Selected $(R_3P)_nHgX_2$ Complexes

4.1 Crystallographic Methods

The methods used for structure solution and refinement are similar for all the crystals studied and a general description of these is outlined below.

4.1.1 Space Group Determination

The space groups were determined by the examination of oscillation, Weissenberg and precession photographs for:

(i) Symmetry

(ii) Systematic absences

4.1.2 Density Determination and Relative Mass Evaluation

The density D_m of the crystals under examination may be measured by suspending them in a liquid. The density of the liquid is altered until the crystals neither float to the surface of the liquid nor fall to the bottom. At this point the density of the crystals is assumed to be the same as the density of the liquid.

If the crystal contains Z molecules in the unit cell then:

$$D_m = \frac{ZM}{V \times 0.6022 \times 10^{24}} \quad (g\ cm^{-3}) \qquad 4.1$$

Where M is the relative molecular mass

V is the unit-cell volume expressed as cm^3

0.6022×10^{24} is the Avogadro constant

The value of Z is related to the number of molecules in the asymmetric unit and the space group. Knowing D_m and M, Z may be calculated, from which the number of molecules in the asymmetric unit can be established. Alternatively, knowing the space group, the value for Z may be assumed, from which the relative molecular mass may be evaluated.

4.1.3 Unit Cell Measurements

The unit cell dimensions, used for alignment of the crystal on the diffractometer, were obtained from measurements of precession photographs and subsequently refined using the diffractometer.

4.1.4 Data Collection

All data were collected using a Stöe Stadi-2 two-circle diffractometer with Mo-K_α radiation (λ = 0.71069 Å), and the background-ω-scan-background technique. By this method the counter remains stationary and the crystal is rotated by small steps in ω (0.01° per second). The scan range, $\Delta\omega$ selected, is dependent upon the equi-inclination angle μ, and upon θ as given in equation 4.2.

$$\Delta\omega = A + \frac{B \sin \mu}{\tan \theta} \qquad 4.2$$

Values are found for A and B step scanning several reflections before data collection proceeds.

The intensity of a reflection, I_{hkl}, is given by equation 4.3.

$$I_{hkl} = T - \frac{(B_1 + B_2)c}{2t} \qquad 4.3$$

Where T is the scan count, B_1 and B_2 are background counts at beginning and end of the scan, c is the scan time and t is the time taken for the background measurements. (For all data collected t = 30 seconds). The standard deviation in the intensity measurement $\sigma(I_{hkl})$ is given by equation 4.4.

$$\sigma(I_{hkl}) = [T - \frac{(B_1 + B_2)^2}{4t^2}]^{1/2} \qquad 4.4$$

Reflections included in the final stages of analysis were those having $I_{hkl}/\sigma(I_{hkl}) \geqslant 3.0$

Corrections were applied to the data for Lorentz and polarisation effects

for all complexes but an absorption correction also for $(Pr_3P)HgI_2$ and $[(NCCH_2CH_2)_3P]HgCl_2$.

4.1.5 Structure Solution and Refinement

The mercury co-ordinates for all the structures were determined from a three-dimensional Patterson map. The remaining atoms were located from successive difference electron-density maps. All non-carbon atoms were assigned anisotropic thermal parameters and wherever possible carbon atoms were all given anisotropic thermal parameters. However, for $(Pr_3P)_2HgI_2$ and $[(NCCH_2CH_2)_3P]_2HgCl_2$ only isotropic temperature factors were applied. Where included, hydrogen atoms have been assigned ideal positions (C-H 1.08 Å). Non-unit weighting schemes have been applied to all structures and all calculations were carried out on an IBM 4341 computer using the SHELX (15) computing package.[58]

4.2 The Crystallographic Studies of Some 2:1 Complexes $(R_3P)_2HgX_2$

4.2.1 Crystallographic Examination of the 2:1 Complex $[(2\text{-thienyl})_3P]_2HgCl_2$

TABLE 4.2.1 Crystal Data

Crystal Size	0.30 x 0.23 x 0.40 mm
Crystal System	Monoclinic
	a = 9.556(6), b = 18.280(10), c =16.609(9) Å, β = 102.14(5)°
V	2836.4 $Å^3$
M_r	832.2
D_c	1.95 g cm^{-3} D_m 1.93 g cm^{-3} Z = 4
Systematic Absences	h0l h + l = 2n + 1
	0k0 k = 2n + 1
Space Group	$P2_1/n$ (a non-standard setting of $P2_1/c$)
μ(Mo-Kα)	59.2 cm^{-1}
F(000)	1608 electrons

Data Collection and Structural Analysis

The crystal was mounted with its c-axis coincident with the ω-axis of the Stöe Stadi-2 two-circle diffractometer. 4774 unique reflections were measured, 4067 had $(I/\sigma(I)) \geq 3.0$ and were subsequently used for refinement. The initial co-ordinates of the independent mercury atom in the asymmetric unit were determined using the Patterson function:

For $P2_1/n$ there are four equivalent positions of the mercury atoms in the unit cell, viz.

x, y, z; -x, -y, -z; $\frac{1}{2}$+x, $\frac{1}{2}$-y, $\frac{1}{2}$+z; $\frac{1}{2}$-x, $\frac{1}{2}$+y, $\frac{1}{2}$-z.

These four mercury atoms in the unit cell give rise to sixteen vectors of which four occur at the origin and represent the vector between the atom and itself.

		Hg1	Hg2	Hg3	Hg4
		x,y,z	-x,-y,-z	$\frac{1}{2}+x,\frac{1}{2}-y,\frac{1}{2}+z$	$\frac{1}{2}-x,\frac{1}{2}+y,\frac{1}{2}-z$
Hg1	x,y,z	0,0,0	-2x,-2y,-2z	$\frac{1}{2},\frac{1}{2}-2y,\frac{1}{2}$	$\frac{1}{2}-2x,\frac{1}{2},\frac{1}{2}-2z$
Hg2	-x,-y,-z	2x,2y,2z	0,0,0	$\frac{1}{2}+2x,\frac{1}{2},\frac{1}{2}+2z$	$\frac{1}{2},+2y,\frac{1}{2}$
Hg3	$\frac{1}{2}+x,\frac{1}{2}-y,\frac{1}{2}+z$	$-\frac{1}{2},-\frac{1}{2}+2y,-\frac{1}{2}$	$-\frac{1}{2}-2x,-\frac{1}{2},-\frac{1}{2}-2z$	0,0,0	-2x,2y,-2z
Hg4	$\frac{1}{2}-x,\frac{1}{2}+y,\frac{1}{2}-z$	$-\frac{1}{2}+2x,-\frac{1}{2},-\frac{1}{2}+2z$	$-\frac{1}{2},-\frac{1}{2}-2y,-\frac{1}{2}$	2x,-2y,2z	0,0,0

Many of the remaining 12 vectors are related by the symmetry allowed in a monoclinic crystal system. Thus, the vectors 2x, 2y, 2z and -2x, -2y, -2z are related by a centre of symmetry while in turn to the vectors at -2x, 2y, -2z and 2x, -2y, 2z by a mirror plane perpendicular to b. These are three unique vectors:

$\frac{1}{2}$, $\frac{1}{2}-2y$, $\frac{1}{2}$; 2x, 2y, 2z; $\frac{1}{2}-2x$, $\frac{1}{2}$, $\frac{1}{2}-2z$

Examination of the three-dimensional Patterson map generated using the 4067 reflections having $I/\sigma(I) \geq 3.0$ enabled the co-ordinates of the independent mercury to be established:

Vector	Fractional Co-ordinate of Peak located on Patterson Map	Height of Vector
$\frac{1}{2},\frac{1}{2}-2y,\frac{1}{2}$	0.5, 0.1906, 0.5	368
	y = 0.1547	
$\frac{1}{2}-2x,\frac{1}{2},\frac{1}{2}-2z$	-0.3830, 0.5, 0.0008	363
	x = 0.4415 z = 0.2496	
2x,2y,2z	x = 0.8830 y = 0.3094 z = 0.4992	166

This gives a consistent set of co-ordinates (x, y, z) for the mercury atom of (0.4415, 0.1547, 0.2496). Least-squares refinement of these co-

ordinates (together with the refinement of the overall scale factor and the isotropic temperature factor of the mercury) gave an R-value of 0.33 after four cycles of refinement. The difference Fourier map, using phases derived from the refined position of the mercury atom, enabled the chlorine and phosphorus atoms to be located, together with a number of sulphur and carbon atoms. The remaining atoms were then located from successive difference electron-density maps. Full matrix refinement gave a final R value of 0.049 and R' value of 0.058.

Two of the six thienyl units were found to exhibit rotational disorder. The disordered groups are related to each other by a pseudo two-fold axis about the P2-Cnl (n = 4 or 6) bonds. Each disordered 2-thienyl group was given an ideal geometry and included in the least-squares refinement with common isotropic temperature factors applied to each atom related by pseudo symmetry. The population parameters applied to each pair of thienyl units were refined, giving final occupancy values of 45% for [C(41), S(42A) -C(45A)], 55% [C(41), S(42B) -C(45B)] and 50% for each of the disordered units associated with C(61). The hydrogen atoms were located for the ordered 2-thienyl groups, and a common isotropic temperature factor applied which refined to a final value of 0.059(13) $\mathring{A}^2$. The weighting scheme $W = 1.000/[\sigma^2(F_o) + 0.0078(F_o)^2]$ was adopted. Final positional parameters are given in the appendix tables 1 and 2, bond distances and angles in Table 4.2.2.

Results and Discussion

The X-ray study of $[(2\text{-thienyl})_3P]_2HgCl_2$ shows it to be a distorted tetrahedral monomer (Fig. 4.2.1) with two of the six thienyl groups showing disorder as discussed in the structural analysis section. The angles about the mercury vary from 99.6(1) to 128.6(1)°. The angles about the phosphorus atoms are less distorted with angles ranging from 110.4(3) to

115.8(3)°. The Hg-Cl bond distances are 2.539(2) and 2.519(2) Å, while the Hg-P bonds are 2.472(2) and 2.513(2) Å in length respectively. A full comparison of the data for this complex with available parameters for other 2:1 structures is made in section 4.2.3.

Fig. 4.2.1 The Molecular Structure of $[(2\text{-thienyl})_3P]_2HgCl_2$

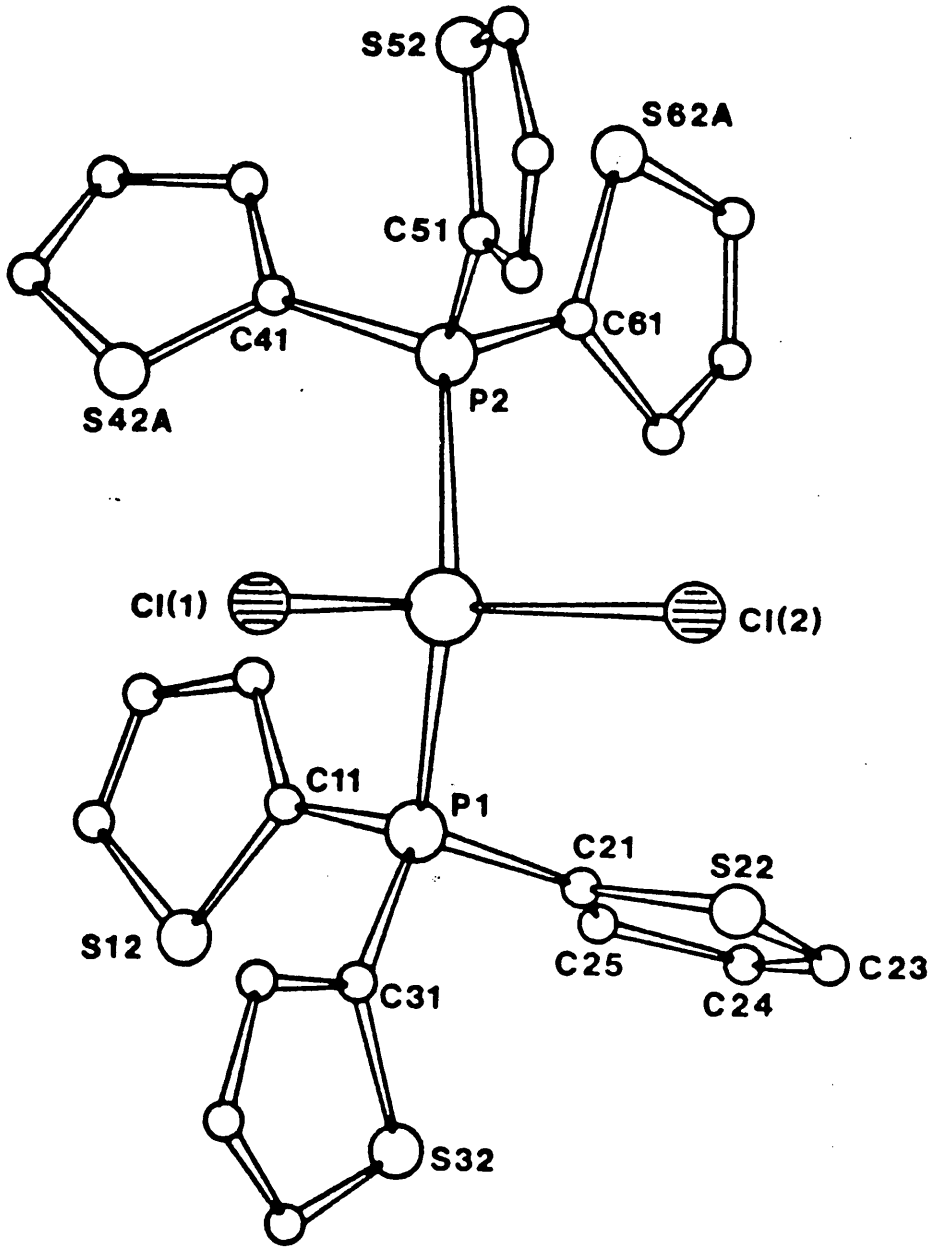

Table 4.2.2 Bond Lengths (Å) and Angles (°) for $[(2\text{-thienyl})_3P]_2HgCl_2$ with Estimated Standard Deviations in Parentheses.

Distances (Å)			
Hg -Cl(1)	2.539(2)	Hg -Cl(2)	2.519(2)
Hg -P(1)	2.472(2)	Hg -P(2)	2.513(2)
P(1) -C(11)	1.803(9)	P(2) -C(41)	1.804
P(1) -C(21)	1.785(9)	P(2) -C(51)	1.779(9)
P(1) -C(31)	1.787(9)	P(2) -C(61)	1.795
C(11)-S(12)	1.686(11)	C(41) -S(42A)	1.611
C(11) -C(15)	1.385(14)	C(41) -C(45A)	1.407
S(12) -C(13)	1.726(12)	S(42A) -C(43A)	1.701
C(13) -C(14)	1.285(20)	C(43A) -C(44A)	1.318
C(14) -C(15)	1.395(17)	C(44A) -C(45A)	1.414
C(21) -S(22)	1.717(9)	C(41) -S(42B)	1.631
C(21) -C(25)	1.442(12)	C(41) -C(45B)	1.406
S(22) -C(23)	1.676(12)	S(42B) -C(43B)	1.700
C(23) -C(24)	1.385(16)	C(43B) -C(44B)	1.299
C(24) -C(25)	1.457(13)	C(44B) -C(45B)	1.485
C(31) -S(32)	1.682(10)	C(51) -S(52)	1.720(10)
C(31) -C(35)	1.434(12)	C(51) -C(55)	1.355(12)
S(32) -C(33)	1.708(12)	S(52) -C(53)	1.692(10)
C(33) -C(34)	1.350(17)	C(53) -C(54)	1.346(16)
C(34) -C(35)	1.406(16)	C(54) -C(55)	1.439(15)
C(61) -S(62A)	1.664	C(61) -S(62B)	1.624
C(61) -C(65A)	1.415	C(61) -C(65B)	1.404
S(62A)-C(63A)	1.700	S(62B)-C(63B)	1.701
C(63A)-C(64A)	1.321	C(63B)-C(64B)	1.336
C(64B)-C(65A)	1.444	C(64B)-C(65B)	1.555

Table 4.2.2 (cont.)

Angles (°)

P(1)	-Hg -Cl(1)	109.3(1)	P(2)	-Hg -Cl(1)	101.6(1)
P(1)	-Hg -Cl(2)	108.6(1)	P(2)	-Hg -Cl(2)	99.6(1)
P(1)	-Hg -P (2)	128.6(1)	C (1)	-Hg -Cl(2)	107.3(1)
Hg	-P(1)-C (11)	111.1(3)	Hg	-P(2)-C(41)	113.1
Hg	-P(1)-C (21)	113.0(3)	Hg	-P(2)-C(51)	110.4(3)
Hg	-P(1)-C (31)	115.8(3)	Hg	-P(2)-C(61)	112.4
P(1)	-C(11) -S(12)	122.7(6)	P(2)	-C(41) -S(42A)	122.6
P(1)	-C(11) -C(15)	128.0(9)	P(2)	-C(41) -C(45A)	126.2
S(12)	-C(11) -C(15)	109.3(8)	S(42A)	-C(41)-C(45A)	110.6
C(11)	-S(12) -C(13)	91.5(6)	C(41)	-S(42A)-C(43A)	92.2
S(12)	-C(13) -C(14)	112.9(9)	S(42A)	-C(43A)-C(44A)	114.1
C(13)	-C(14) -C(15)	112.6.(11)	C(43A)	-C44A) -C(45A)	107.8
C(11)	-C(15) -C(14)	113.6(12)	C(41)	-C(45A)-C(44A)	112.3
P(1)	-C(21) -S(22)	121.3(5)	P(2)	-C(41) -S(42B)	126.1
P(1)	-C(21) -C(25)	125.8(7)	P(2)	-C(41) -C(45B)	122.4
S(22)	-C(21) -C(25)	112.9(7)	S(42B)	-C(41) -C(45B)	110.7
C(21)	-S(22) -C(23)	91.8(5)	C(41)	-S(42B)-C(43B)	92.3
S(22)	-C(23) -C(24)	114.6(8)	S(42B)	-C(43B)-C(44B)	117.0
C(23)	-C(24) -C(25)	112.2(9)	C(43B)	-C(44B)-C(45B)	106.7
C(21)	-C(25) -C(24)	108.4(8)	C(41)	-C(45B)-C(44B)	112.5
P(1)	-C(31) -S(32)	124.0(5)	P(2)	-C(51) -S(52)	124.9(5)
P(1)	-C(31) -C(35)	123.9(7)	P(2)	-C(51) -C(55)	125.7(8)
S(32)	-C(31) -C(35)	111.7(7)	S(52)	-C(51) -C(55)	109.4(7)
C(31)	-S(32) -C(33)	92.6(5)	C(51)	-S(52) -C(53)	92.8(5)
S(32)	-C(33) -C(34)	111.6(9)	S(52)	-C(53) -C(54)	112.8(8)

Table 4.2.2. (cont.)

C(33)-C(34) -C(35)	114.6(10)	C(53) -C(54) -C(55)	110.7(9)
C(31)-C(35) -C(34)	109.5(9)	C(51) -C(55) -C(54)	114.3(9)
P(2) -C(61) -S(62A)	123.0	P(2) -C(61) -S(62B)	120.7
P(2) -C(61) -C(65A)	122.0	P(2) -C(61) -C(65B)	123.2
S(62A)-C(61)-C(65A)	115.0	S(62B)-C(61) -C(65B)	116.1
C(61)-S(62A)-C(63A)	92.2	C(61) -S(62B)-C(63B)	92.3
S(62A)-C(63A)-C(64A)	110.4	S(62B)-C(63B)-C(64B)	113.1
C(63A)-C(64A)-C(65A)	117.6	C(63B)-C(64B)-C(65B)	109.1
C(61) -C(65A)-C(64A)	104.7	C(61) -C(65B)-C(64B)	104.1

4.2.2 Crystallographic Examination of the 2:1 Complexes $[(NCCH_2CH_2)_3P]_2HgX_2$ (X = Cl or Br)

TABLE 4.2.3 Crystal Data

	(I) $[(NCCH_2CH_2)_3P]_2HgCl_2$	(II) $[(NCCH_2CH_2)_3P]HgBr_2.(CH_3)_2CO$
Crystal Size (mm)	.08 x .48 x .04	.44 x .20 x .13
Crystal System	Monoclinic	Monoclinic
a (Å)	25.728(8)	9.174(6)
b (Å)	8.627(7)	15.795(9)
c (Å)	24.482(8)	20.741(11)
β (°)	115.14(1)	93.01(5)
V(Å^3)	4919.49	3001.4
M_r	657.9	821.1
D_c(gcm^{-3})	1.78	1.82
D_m(gcm^{-3})	1.80	1.84
Systematic Absences	h0l l = 2n + 1	h0l h + l = 2n + 1
	0k0 k = 2n + 1	0k0 k = 2n + 1
Z	8	4
Space group	$P2_1/c^+$	$^‡P2_1/n$
μ(Mo-Kα)(m^{-1})	63.6	76.6
F(000)	2544	1544

+Two independent molecules in the asymmetric unit.

‡Non-standard setting of $P2_1/c$.

Data Collection and Structural Analysis

Details of data collection are given in Table 4.2.4 and both structures were solved using the Patterson method and refined by full-matrix least squares techniques.

TABLE 4.2.4 Details of the Data Collection

	(I)	(II)
Axis crystal mounted about	b	a
No. layers collected	9	11
No. unique reflections	4241	4700
+No. observed reflections	2522	2511
Final R value	0.062	0.043
Final R' value	0.064	0.045
$W = a/[\sigma^2(F_o) + b(F_o)^2]$		
a	1.0000	1.0000
b	0.001296	0.0040

+No. of reflections with $I/\sigma(I) \geqslant 3.0$

The data were corrected for Lorentz and polarisation effects, but absorption corrections were not applied. Hydrogen atoms were included for (II) in ideal positions (C-H, 1.08 Å) and were given a common isotropic temperature factor. All other atoms in (II) were assigned anisotropic thermal parameters. In the chloride complex, (I), there is some degree of disorder in the cyanoethyl groups and it proved difficult to resolve this satisfactorily resulting in high errors and widely varying C-N and C-C bond lengths (Table 4.2.5). Hence, anisotropic temperature factors were only applied to mercury, phosphorus and chlorine atoms, and all the remaining atoms were treated isotropically. The degree of disorder made it impossible to include any hydrogen atoms for structure (I).

Results and Discussion

$[(NCCH_2CH_2)_3P]_2HgCl_2$ consists of two independent monomeric units (Fig. 4.2.2). Both units are highly distorted from a regular tetrahedral arrangement, the angles about mercury varying from 92.3(3) to 153.9(3)°.

All the cyanoethyl chains are disordered to some degree, the widest variations being found in the bond lengths for C(A2)-C(A3) and C(A3)-N(A3) (where A = 1-6). The carbon-carbon bonds vary from 1.04(7) to 1.63(7) Å while the carbon-nitrogen bonds have wider variations, 1.08(3) to 1.95(8) Å. There is a weak interaction between the nitrogen atom of three of the cyanoethyl groups, one in one of the units, two in the other. In monomer I the Hg-N distances are 3.51(3) and 3.52(3) Å and for monomer II the Hg-N distance is 3.74(3) Å, these distances being longer than the sum of the van der Waals' radii (3.30 Å). The Hg-N bond distances found for monomer I are very similar to those found for $[(NCCH_2CH_2)_3]PHgCl_2$ 3.51(3) and 3.47(3) Å. Selected bond angles and bond lengths for $[(NCCH_2CH_2)_3P]_2HgCl_2$ are given in Table 4.2.5. The torsion angles (appendix table 16) show that three of the cyanoethyl chains are twisted from their expected geometry of 180° (to 49, 57 and 87° respectively). This allows the nitrogen atoms in these groups to take up positions near the mercury atom.

$[(NCCH_2CH_2)_3P]_2HgBr_2(CH_3)_2CO$ also adopts a monomeric arrangement but with a trigonal bipyramidal polyhedral arrangement about mercury, the oxygen atom of the acetone molecule occupying an equatorial position. The bond angles about the mercury atom vary from 151.3(1)° for P(1)-Hg-P(2) to 75(1)° for P(1)-Hg-O. Further bond lengths and angles are given in Table 4.2.6. The length of the Hg...O bond (3.91(2) Å) is greater than the sum of the van der Waals radii (3.25 Å) and indicates that the mercury-acetone interaction is extremely weak. However, the infrared and thermal studies[59] indicate that the interaction between the mercury and acetone is significant and the presence of the acetone may, at least in part, be responsible for the enlargement of the P-Hg-P angle (151.3(1)°).

Final positional and thermal parameters for both complexes are given in

the appendix (tables 3-6). Torsion angles are given in the appendix table 2.1.

Fig. 4.2.2(a) The Molecular Structure of $[(NCCH_2CH_2)_3P]_2HgCl_2$, Molecule I

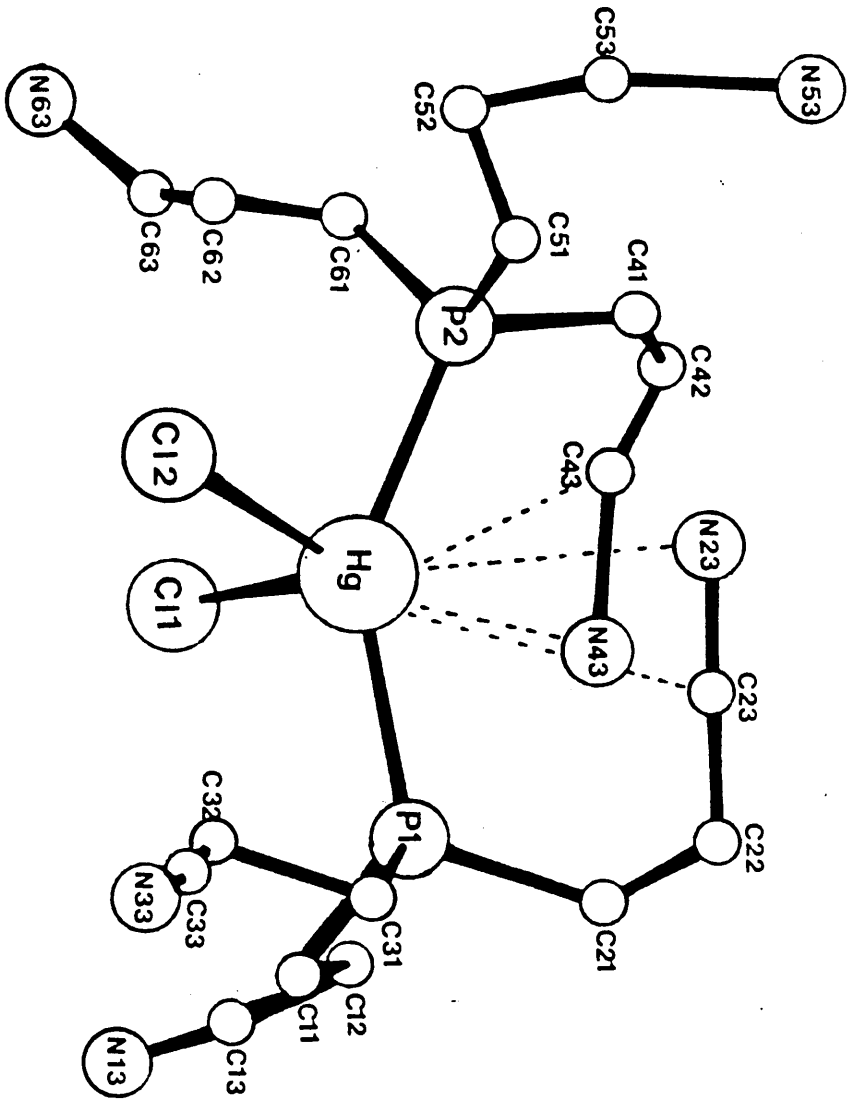

Fig. 4.2.2(b) The Molecular Structure of $[(NCCH_2CH_2)_3P]_2HgCl_2$, Molecule II

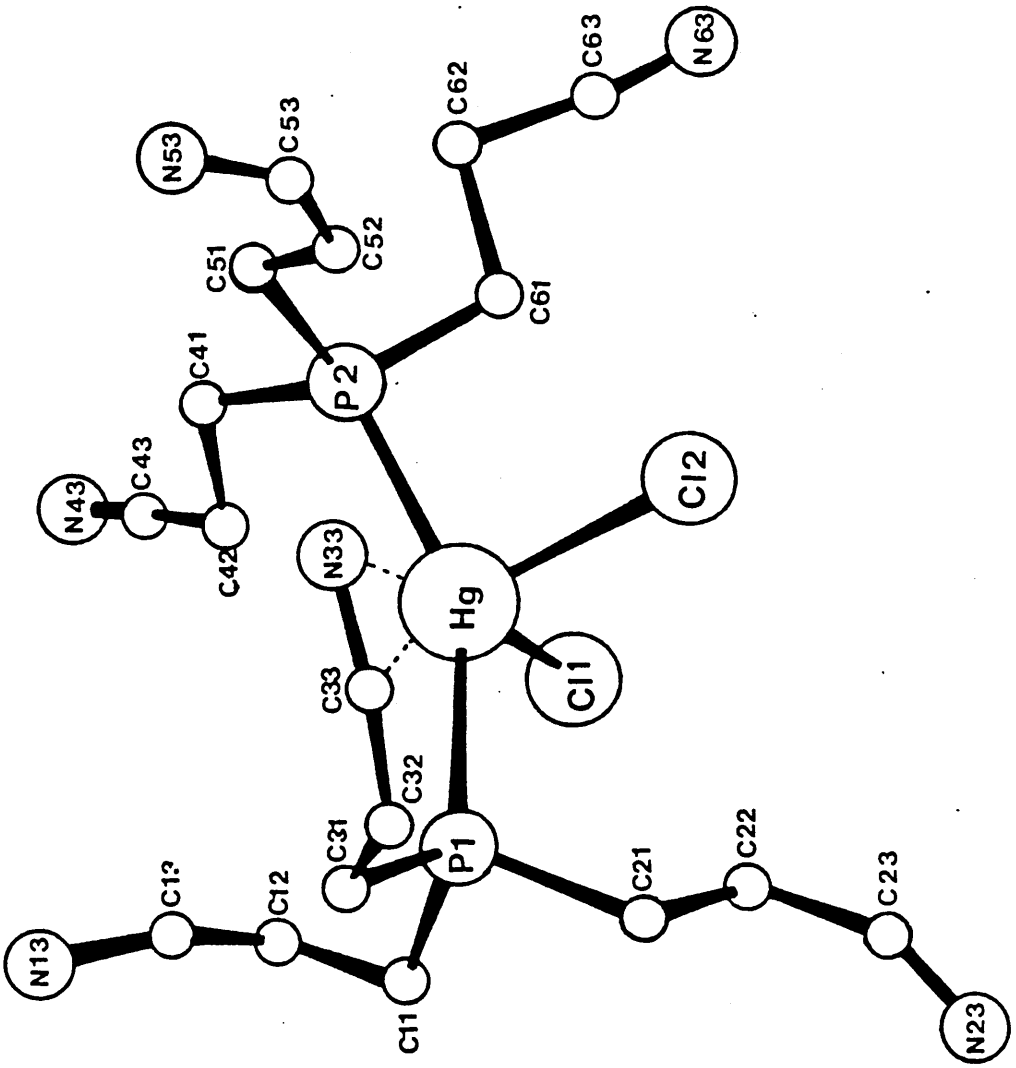

Fig 4.2.3 The Molecular Structure of $[(NCCH_2CH_2)_3P]_2HgBr_2.OC(CH_3)_2$

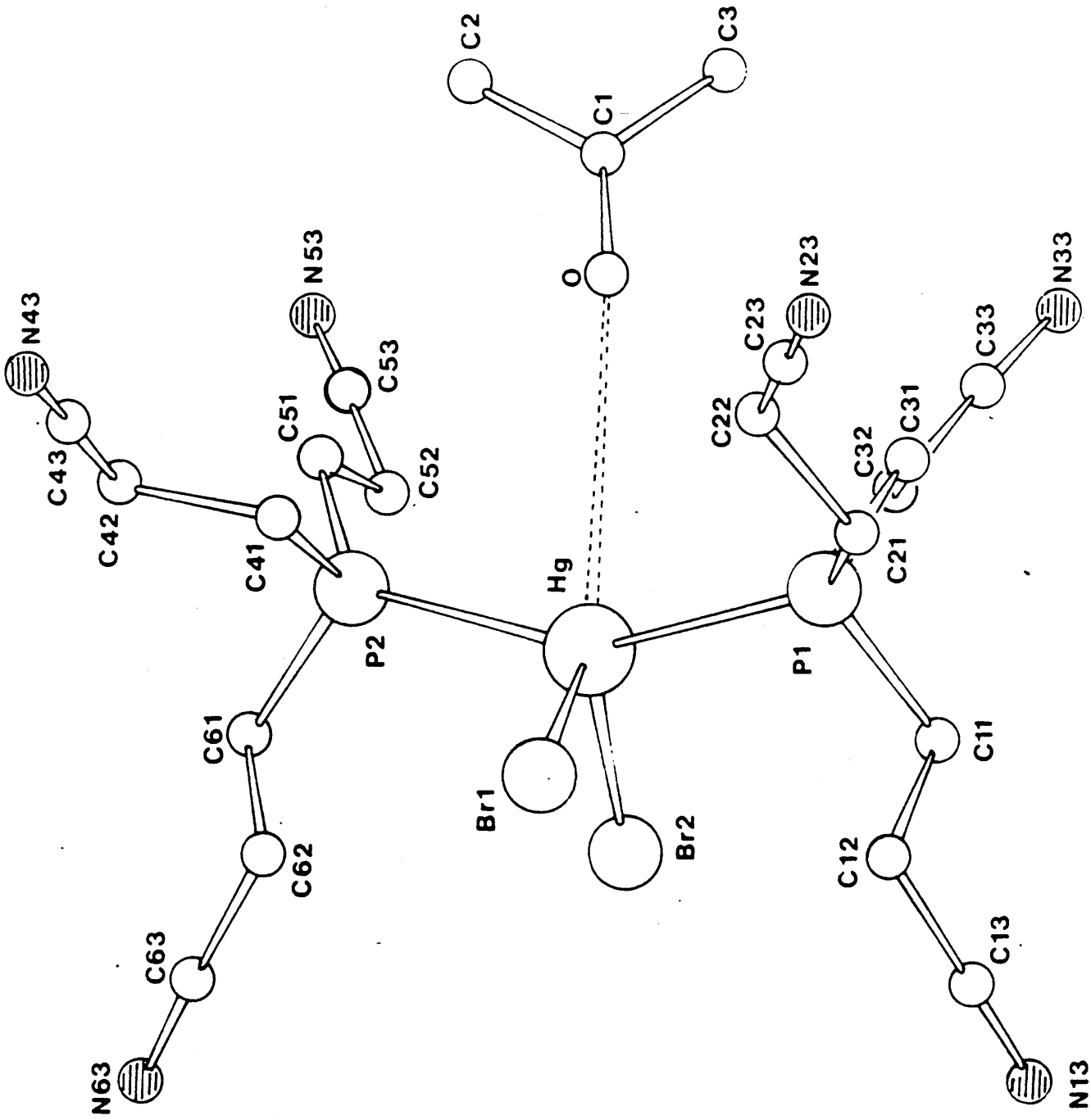

Table 4.2.5 Bond Lengths (Å) and Angles (°) for $[(NCCH_2CH_2)_3P]_2HgCl_2$ with Estimated Standard Deviations in Parentheses

Distances (Å)	Molecule 1	Molecule 2		Molecule 1	Molecule 2
Hg-Cl(1)	2.608(10)	2.669(11)	Hg-Cl(2)	2.622(1)	2.603(10)
Hg-P(1)	2.450(12)	2.411(7)	Hg-P(2)	2.452(11)	2.450(6)
P(1)-C(11)	1.86	1.84	P(2)-C(41)	1.80	1.80
P(1)-C(21)	1.87	1.87	P(2)-C(51)	1.99	1.85
P(1)-C(31)	1.76	1.80	P(2)-C(61)	1.78	1.85
C(11)-C(12)	1.50	1.51	C(41)-C(42)	1.57	1.49
C(12-C(13)	1.30	1.20	C(42)-C(43)	1.04	1.45
C(13)-N(13)	1.36	1.42	C(43)-N(43)	1.59	1.08
C(21)-C(22)	1.44	1.46	C(51)-C(52)	1.25	1.37
C(22)-C(23)	1.33	1.42	C(52)-C(53)	1.34	1.40
C(23)-N(23)	1.28	1.26	C(53)-N(53)	1.95	1.30
C(31)-C(32)	1.63	1.34	C(61)-C(62)	1.46	1.57
C(32)-C(33)	1.51	1.28	C(62)-C(63)	1.04	1.50
C(33)-N(33)	1.15	1.29	C(63)-N(63)	1.62	1.18

Angles (°)

	Molecule 1	Molecule 2		Molecule 1	Molecule 2
Cl(1)-Hg-Cl(2)	95.0(3)	98.1(3)	P(1)-Hg-P(2)	146.6(3)	153.9(3)
Cl(1)-Hg-P(1)	101.2(4)	95.4(3)	Cl(2)-Hg-P(2)	92.3(3)	96.1(3)
Cl(1)-Hg-P(2)	100.0(4)	94.1(3)	Cl(2)-Hg-P(1)	111.2(3)	106.6(3)
Hg-P(1)-C(11)	113(2)	113(2)	Hg(1)-P(2)-C(41)	120(1)	118(1)
Hg-P(1)-C(21)	116(2)	114(1)	Hg(1)-P(2)-C(51)	105(1)	116(1)
Hg-P(1)-C(31)	118(2)	120(1)	Hg(1)-P(2)-C(61)	114(2)	102(1)
C(11)-P(1)-C(21)	103	99	C(41)-P(2)-C(51)	96	99
C(11)-P(1)-C(31)	103	104	C(41)-P(2)-C(61)	103	108
C(21)-P(1)-C(31)	103	105	C(51)-P(2)-C(61)	119	114
P(1)-C(11)-C(12)	109	115	P(2)-C(41)-C(42)	122	114
C(11)-C(12)-C(13)	93	107	C(41)-C(42)-C(43)	98	115
C(12)-C(13)-N(13)	164	161	C(42)-C(43)-N(43)	158	176
P(1)-C(21)-C(22)	119	111	P(2)-C(51)-C(52)	119	111
C(21)-C(22)-C(23)	114	110	C(51)-C(52)-C(53)	78	124
C(22)-C(23)-N(23)	178	155	C(52)-C(53)-N(53)	159	140
P(1)-C(31)-C(32)	108	114	P(2)-C(61)-C(62)	100	113
C(31)-C(32)-C(33)	107	123	C(61)-C(62)-C(63)	92	103
C(32)-C(33)-N(33)	168	158	C(62)-C(63)-N(63)	150	173

Table 4.2.6 Bond Lengths (Å) and Angles for $[(NCCH_2CH_2)_3P]_2HgBr_2.OC(CH_3)_2$ with Estimated Standard Deviations in Parentheses

Bond lengths (Å)			
Hg - Br(1)	2.750(2)	Hg - Br(2)	2.703 (2)
Hg - P (1)	2.441(3)	Hg - P(2)	2.440 (3)
P(1)-C(11)	1.824(14)	P(2)-C(41)	1.806 (15)
P(1)-C(21)	1.795(16)	P(2)-C(51)	1.808 (16)
P(1)-C(31)	1.812(17)	P(2)-C(62)	1.828 (13)
C(11)-C(12)	1.511(26)	C(41)-C(42)	1.551 (20)
C(12)-C(13)	1.465(21)	C(42)-C(43)	1.455 (28)
C(13)-N(13)	1.122(21)	C(43)-N(43)	1.146 (29)
C(21)-C(22)	1.544(20)	C(51)-C(52)	1.518 (22)
C(22)-C(23)	1.426(24)	C(52)-C(53)	1.482 (25)
C(23)-N(23)	1.118(24)	C(53)-N(53)	1.126 (26)
C(31)-C(32)	1.535(25)	C(61)-C(62)	1.518 (24)
C(32)-C(33)	1.448(28)	C(62)-C(63)	1.459 (25)
C(33)-N(33)	1.146(31)	C(63)-N(63)	1.134 (25)
Hg---O	3.91 (2)		

TABLE 4.2.6 (cont.)

Bond angles (°)

Br(1)-Hg-Br(2)	107.3(1)	P(1)-Hg-P(2)	151.3(1)
Br(1)-Hg-P (1)	97.2(1)	Br(2)-Hg-P(1)	99.3(1)
Br(1)-Hg-P (2)	95.2(1)	Br(2)-Hg-P(2)	101.5(1)
Hg-P(1)-C(11)	110.9(5)	Hg-P(2)-C(41)	109.1(4)
Hg-P(1)-C(21)	112.3(5)	Hg-P(2)-C(51)	117.1(5)
Hg-P(1)-C(31)	118.5(5)	Hg-P(2)-C(61)	111.3(4)
C(11)-P(1)-C(21)	104.5(7)	C41-P(2)-C(51)	106.0(7)
C(11)-P(1)-C(31)	103.9(7)	C41-P(2)-C(61)	107.5(7)
C(21)-P(1)-C(31)	105.4(7)	C51-P(2)-C(61)	105.2(7)
P(1)-C(11)-C(12)	111.0(11)	P(2)-C(41)-C(42)	115.2(11)
C(11)-C(12)-C(13)	113.2(15)	C(41)-C(42)-C(43)	111.9(14)
C(12)-C(13)-N(13)	176.2(19)	C(42)-C(43)-N(43)	179.3(24)
P(1)-C(21)-C(22)	112.1(11)	P(2)-C(51)-C(52)	111.9(10)
C(21)-C(22)-C(23)	112.2(15)	C(51)-C(52)-C(53)	109.4(13)
C(22)-C(23)-N(23)	178.6(19)	C(52)-C(53)-N(53)	177.7(19)
P(1)-C(31)-C(32)	114.7(11)	P(2)-C(61)-C(62)	112.3(10)
C(31)-C(32)-C(33)	106.7(16)	C(61)-C(62)-C(63)	112.2(15)
C(32)-C(33)-N(33)	174.5(22)	C(62)-C(63)-N(63)	177.1(22)
P(1)-Hg-O	78(1)	P(2)-Hg-O	75(1)
Br(1)-Hg-O	137(1)	Br(2)-Hg-O	116(1)

4.2.3 A Comparison of 2:1 Mercury(II) Halide Complexes

In this section selected parameters for the 2:1 structures presented in this thesis, together with data from previously established structures are rationalised in terms of the factors believed to influence solid state structures of mercury(II) halide complexes (Section 2). Some of the relevant bond lengths and bond angles are given in Table 4.2.7. All complexes have distorted monomeric tetrahedral structures with the exception of $[(NCCH_2CH_2)_3P]_2HgBr_2.OC(CH_3)_2$ which adopts a trigonal bipyramidal polyhedral structure. In this case the oxygen atom of the acetone molecule of crystallisation occupies an equatorial position in the trigonal bipyramidal polyhedron. The complexes $(EtMe_2P)_2HgBr_2$ and $[(NCCH_2CH_2)_3P]_2HgCl_2$, in contrast to the other 2:1 complexes studied, each contains two independent monomeric units. Studies of the $(R_3P)_2HgX_2$ complexes indicate that the structures adopted in the solid state are influenced by (i) the electronic strength and steric requirement of the phosphine ligand, (ii) the nature of the halogen, and (iii) the tendency of mercury(II) to adopt linear two co-ordination. The present comparison of the 2:1 complexes seeks to investigate these influences and tries to establish the key factors and their relative importance. A study of the bond lengths and bond angles about the mercury atoms, given in Table 4.2.7, indicates $[(NCCH_2CH_2)_3P]_2HgCl_2$ and $(Et_3P)_2HgCl_2$ have similar interactions with mercury(II) halides. Triethylphosphine has a high pKa value (8.69), and its 2:1 complex with mercury(II) chloride has a large P-Hg-P angle (158.5(5)°) and short Hg-P bonds (2.39(1) Å) in comparison to some other 2:1 tertiary phosphine mercury(II) chlorides (see below). This indicates a strong interaction of the tertiary phosphine with the mercury(II) halide and as such this phosphine is considered to be a strong σ-donor.

Tris(2-cyanoetnyl)phosphine, whose 2:1 mercury(II) chloride complex has comparable bond lengths and bond angles to the triethylphosphine analogue is also considered to be a strong σ-donor to mercury(II) halides, even though the phosphine has a much lower pK_a value (1.37) than Et_3P. This indicates that the electron-withdrawing properties of the cyano groups, while lowering the pK_a value does not appear to reduce the co-ordinating ability of the substituted phosphine to mercury(II) halides. However, a comparison of the parameters of $[(2\text{-thienyl})_3P]_2HgCl_2$ with those of $(Et_3P)_2HgCl_2$ indicates the σ-donor ability of tris(2-thienyl)phosphine to be considerably weaker than that of triethylphosphine. The Hg-P and Hg-Cl bond distances for the heterocyclic phosphine complex are similar to those found in the triphenylphosphine and tributylphosphine 2:1 complexes. The P-Hg-P bond angle found for di(tris(2-thienyl)phosphine) mercury(II) chloride (128.6(1)°) is the smallest of the 2:1 chloride complexes for which data are available which indicates that tris(2-thienyl)phosphine is the weakest σ-donor.

A comparison of the mercury(II) bromide complexes shows a similar trend; in this case the di(tris2-cyanoethyl)phosphine mercury(II) bromide has longer Hg-Br bonds (2.725 Å) and a larger P-Hg-P angle (151.3(1)°) than the complex of the weak σ-donor triphenylphosphine (2.628 Å and 113.0(5)°). The bond lengths and bond angles for $(EtMe_2P)_2HgBr_2$ are comparable to those of $[(NCCH_2CH_2)_3P]_2HgBr_2OC(CH_3)_2$.

From Table 4.2.7 it is clear that the phosphines with the higher pK_a values have the larger P-Hg-P angles and shorter Hg-P bonds in their complexes, i.e. they are the stronger σ-donors to mercury(II), the exception being tris(2-cyanoethyl)phosphine (pK_a 1.36). The pK_a of tris(2-thienyl)phosphine is not available for comparison.

Using the criteria of relative Hg-P distances and P-Hg-P angles, σ-donor

strengths to mercury(II) halides vary in the order:

$Et_3P > (NCCH_2CH_2)_3P > EtMe_2P > Bu_3P > Ph_3P >$ (2-thienyl)$_3P$.

A comparison of the P-Hg-P angles for the $(Ph_3P)_2HgX_2$ (X = Cl, Br, I) shows that these decrease from X = Cl to Br to I. This may be related to the relative electronegativity of the halogens (Cl > Br > I) which affords greatest Hg-P interaction in the chlorocomplex, thereby leading to the larger P-Hg-P angle. The presence of a molecule of acetone in $[(NCCH_2CH_2)_3P]_2HgBr_2$ prevents a simple comparison with the chloride complex.

From the NMR shifts and coupling constants given in Table 4.2.8 the stronger σ-donors, Et_3P and $(NCCH_2CH_2)_3P$, have the greater chemical shifts and coupling constants. The complex $[(2\text{-thienyl})_3P]_2HgI_2$ has the smaller chemical shifts and coupling constant than the triphenylphosphine analogue giving further evidence that the heterocyclic phosphine is an extremely weak σ-donor as suggested by the small P-Hg-P angle and long Hg-P bonds. The chemical shifts and coupling constants show a marked decrease from Cl to Br to I following the trend of decreasing P-Hg-P angle size observed in the $(Ph_3P)_2HgX_2$ (X = Cl, Br or I) complexes. These trends are apparent from the data given in Table 4.2.8 in spite of the effects of varying solvents and temperatures.

TABLE 4.2.7. Selected Molecular Parameters for $(R_3P)_2HgX_2$ (X=Cl, Br, I) Complexes

	Hg-P (Å)		PHgP (°)	Hg-X (Å)		XHgX (°)	pK_a for R_3P [52]
$(Et_3P)_2HgCl_2$ [a]	2.39(1)	2.39(1)	158.5(5)	2.68(1)	2.68(1)	105.5(5)	8.69
$((NCC_2H_4)_3P)_2HgCl_2$ (I) [b]	2.450(12)	2.452(11)	146.6(3)	2.608(10)	2.622(10)	95.0(3)	1.36
(II)	2.411(7)	2.450(6)	153.9(6)	2.669(11)	2.603(10)	98.1(3)	
$((NCC_2H_4)_3P)_2HgBr_2.Me_2CO$ [b]	2.441(3)	2.440(3)	151.3(1)	2.750(2)	2.703(2)	107.3(1)	1.36
$(EtMe_2P)_2HgBr_2$ [c] (I)	2.44(6)	2.50(5)	147(2)	2.72(2)	2.79(2)	101.7(8)	8.61
(II)	2.39(5)	2.48(6)	150(2)	2.79(3)	2.88(2)	106.9(8)	
$(Bu_3P)_2HgCl_2$ [c]	2.3(6)	2.6(6)	139(2)	2.55(5)	2.66(5)	105(2)	8.43
$(Ph_3P)_2HgCl_2$ [d]	2.478(2)	2.462(2)	134.1(1)	2.559(2)	2.545(3)	110.7(1)	2.73
$(Ph_3P)_2HgBr_2$ [d]	2.535(15)	2.540(16)	113.0(5)	2.633(6)	2.626(8)	106.9(3)	2.73
$(Ph_3P)_2HgI_2$ [e]	2.557(3)	2.574(3)	108.95(9)	2.733(1)	2.763(1)	110.43(4)	2.73
$((2\text{-}C_4H_3S)_3P)_2HgCl_2$ [b]	2.472(2)	2.513(2)	128.6(1)	2.539(2)	2.519(2)	107.3(1)	-

a Ref. 42

b Ref. This Work

c Ref. 41

d Ref. 43

e Ref. 40

TABLE 4.2.8. ^{31}P NMR Data for some $(R_3P)_2HgX_2$ Complexes

Complex	δ(ppm)	$J(^{199}Hg-^{31}P)$	Solvent	Temp (°C)
$(Et_3P)_2HgCl_2$ [a]	38.0	5095	$CDCl_3$	27
$(Et_3P)_2HgBr_2$ [a]	32.2	4792	$CDCl_3$	27
$(Et_3P)_2HgI_2$ [a]	16.9	4033	$CDCl_3$	27
$((NCC_2H_4)_3P)_2HgCl_2$ [d]	44.4		$(CD_3)_2CO$	26
$((NCC_2H_4)_3P)_2HgBr_2$ [d]	17.6		$(CD_3)_2CO$	26
$((NCC_2H_4)_3P)_2HgI_2$ [d]	2.6		$(CD_3)_2CO$	26
$(EtMe_2P)_2HgCl_2$ [a]	16.0	5606	$CDCl_3$	-30
$(EtMe_2P)_2HgBr_2$ [a]	13.1	5560	$CDCl_3$	-30
$(EtMe_2P)_2HgI_2$ [a]	2.5	4778	$CDCl_3$	-40
$(Bu_3P)_2HgCl_2$ [b]	28.9	5125	$CDCl_3$	27
$(Bu_3P)_2HgBr_2$ [b]	23.9	4829	$CDCl_3$	27
$(Bu_3P)_2HgI_2$ [b]	9.3	4089	$CDCl_3$	27
$(Ph_3P)_2HgCl_2$ [c]	28.1	4740	CH_2Cl_2	-43
$(Ph_3P)_2HgBr_2$ [c]	21.7	4178	CH_2Cl_2	-43
$(Ph_3P)_2HgI_2$ [c]	7.3	3073	CH_2Cl_2	-43
$((2\text{-}C_4H_3S)_3P)_2HgI_2$ [d]	-26.0	2722	CH_2Cl_2	-90
$((2\text{-}C_4H_3O)_3P)_2HgCl_2$ [d]	-37.5	4322	CH_2Cl_2	-90
$((2\text{-}C_4H_3O)_3P)_2HgBr_2$ [d]	-44.2	3540	CH_2Cl_2	-90

a Ref. 42

b Ref. 49

c Ref. 50

d This Work

4.3 Crystallographic Studies of Selected 1:1 Complexes $(R_3P)HgX_2$

4.3.1 Crystallographic Examination of the 1:1 Complex $[(NCCH_2CH_2)_3PHgCl_2]_n$

TABLE 4.3.1 Crystal Data

Crystal Size	0.04 x 0.08 x 0.52 mm		
Crystal System	Orthorhombic		
a = 20.871(6)	b = 7.853(9)	c = 8.518(8) Å	
V 1396.4 $Å^3$			
M_r 472.8			
D_c 2.25 g cm^{-3}	D_m 2.23 g cm^{-3}	Z = 4	
Systematic Absences	h00 h = 2n + 1		
	0k0 k = 2n + 1		
	00l l = 2n + 1		
Space Group	$P2_12_12_1$		
μ (Mo-Kα)	110.6 cm^{-1}		
F(000)	864 electrons		

Data Collection and Structural Analysis

The crystal was mounted with its c-axis coincident with the ω-axis of a Stöe Stadi 2 two-circle diffractometer. 1725 unique reflections were measured; 1121 had $I/\sigma(I) \geq 3.0$ and were subsequently used for refinement. The structure was solved via the Patterson function and refined by full-matrix least squares techniques. Hydrogen atoms were included in ideal positions (C-H 1.08 Å) and given a common isotropic temperature factor, all other atoms except one nitrogen and three carbons were assigned anisotropic thermal parameters. Complex neutral-atom scattering factors were used throughout the refinement. The weighting scheme $W = a/[\sigma^2(F_o) + b(F_o)^2]$ was adopted in the final stages of refinement (where a = 0.1965 and b = 0.03781), the final R value being 0.063 and R', 0.068. The final atomic positional and thermal parameters are given in the appendix, tables 7 and 8,

and bond distances and angles are listed in Table 4.3.2. A correction for absorption effects was applied for the complex (appendix A2).

Results and Discussion

The complex $[(NCCH_2CH_2)_3PHgCl_2]$ is found to be polymeric with almost linear Cl-Hg-PR_3 units bridged by further chlorine atoms (Fig. 4.3.1), resulting in single chains running parallel to the b-axis. The angles about the mercury atom are highly distorted from tetrahedral, varying from 89.7(2)° to 162.3(4)°. However, there is a weak π-interaction between one of the cyanoethyl groups and the mercury atom. From Fig. 4.3.1 it can be seen that C23, N23 and the symmetry related C(23''') and N(23''') lie in positions close to the mercury atom (Table 4.3.2). These distances (3.51, 3.47 Å respectively) are longer than the sum of the van der Waals' radii which is 3.05 Å, indicating a weak interaction. A similar weak bonding between three cyanoethyl groups is found in the 2:1 cyanoethylphosphine complex (Section 4.2.2). A comparison of the Hg-C and Hg-N bond lengths is given in Table 4.3.3. The P-C-C-CN torsion angles for two of the cyanoethyl groups lie close to the expected 180° (173° and 177°), but that for the P-C(21)-C(22)-C(23) is only 81°, allowing N to take up a position near the mercury atom. The resulting co-ordination polyhedron about mercury is distorted octahedral with the two cyano-groups (C(23)-N(23), C(23''')-N(23''')) occupying positions trans to each other, the other four positions being occupied by three chlorine atoms and one phosphorus atom. The angles about the phosphorus are slightly distorted from the tetrahedral, varying from 116.2(10)° to 103.8(10)°.

Fig. 4.3.1 Molecular Structure of $[(NCCH_2CH_2)_3PHgCl_2]_n$

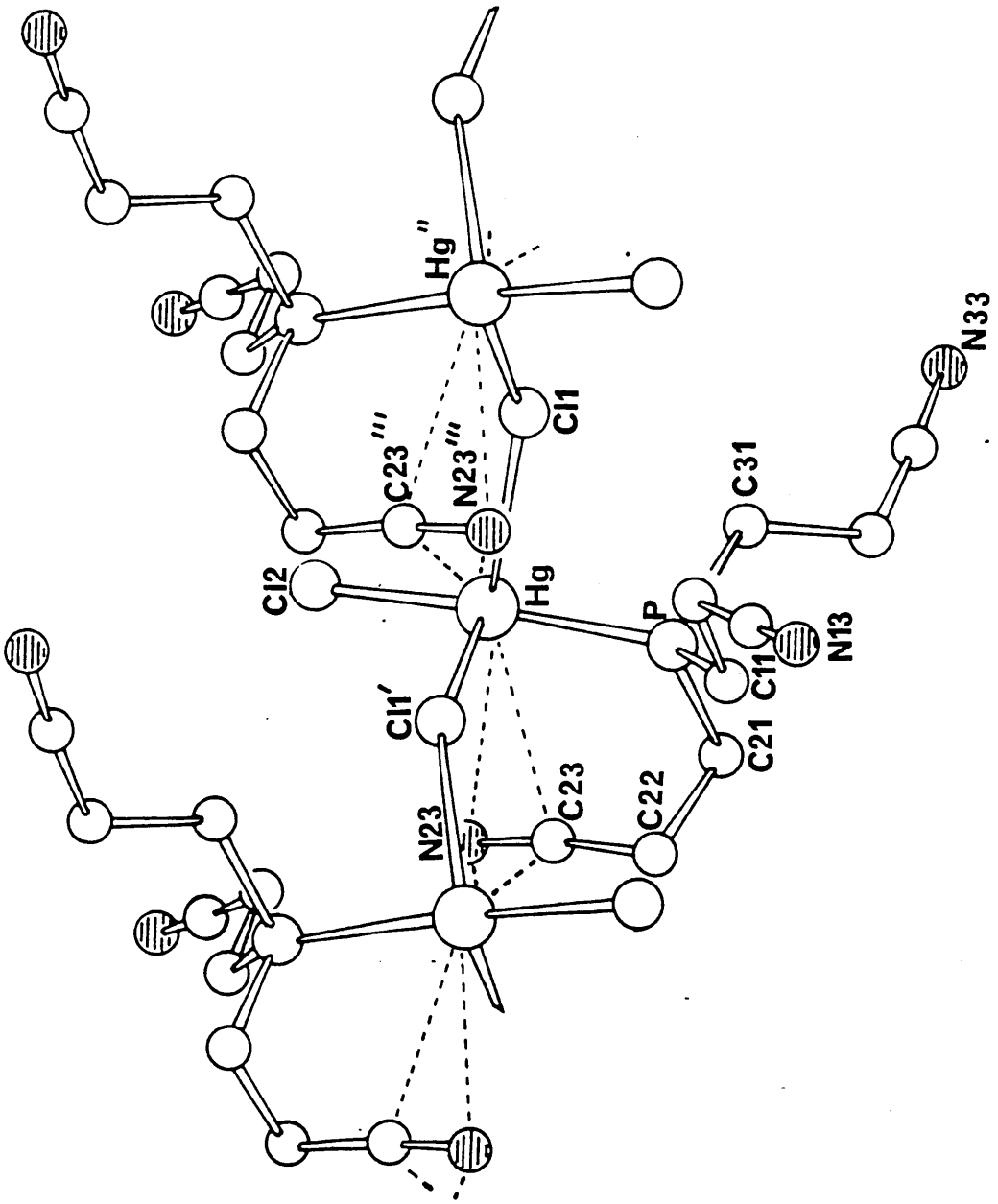

Table 4.3.2 Bond Lengths (Å) and Angles (°) for $[(NCCH_2CH_2)_3PHgCl_2]_n$ with Estimated Standard Deviations in Parentheses

Bond Lengths (Å)

Hg-Cl(1)	2.762(9)	Hg...C(23)	3.44(3)
Hg-Cl(1')	2.754(9)	Hg...N(23)	3.51(3)
Hg-Cl(2)	2.336(7)	Hg...C(23''')	3.61(3)
Hg-P	2.387(6)	Hg...N(23''')	3.47(3)
P-C(11)	1.71(3)		
P-C(21)	1.92(2)		
P-C(31)	1.84(2)		
C(11)-C(12)	1.63(3)		
C(12)-C(13)	1.48(3)		
C(13)-N(13)	1.07(4)		
C(21)-C(22)	1.52(3)		
C(22)-C(23)	1.48(4)		
C(23)-N(23)	1.09(4)		
C(31)-C(32)	1.56(3)		
C(32)-C(33)	1.40(3)		
C(33)-N(33)	1.16(4)		

Bond Angles (°)

Cl(1)-Hg-Cl(1')	99.2(4)	P-C(11)-C(12)	114(2)
Cl(1)-Hg-Cl(2)	99.9(4)	P-C(21)-C(22)	111(2)
Cl(1)-Hg-P	89.7(2)	P-C(31)-C(32)	115(2)
Cl(1')-Hg-Cl(2)	97.3(4)	C(11)-C(12)-C(13)	111(2)
Cl(1')-Hg-P	95.7(2)	C(12)-C(13)-N(13)	177(3)
Cl(2)-Hg-P	162.3(4)	C(21)-C(22)-C(23)	107(2)
Hg-Cl(1)-Hg''	141.4(2)	C(22)-C(23)-N(23)	164(4)
Hg-P-C(11)	116.2(10)	C(31)-C(32)-C(33)	110(2)
Hg-P-C(21)	114.2(8)	C(32)-C(33)-N(33)	174(3)

Table 4.3.2 cont.

Hg-P-C(31)	107.7(7)
C(11)-P-C(21)	103.8(10)
C(11)-P-C(31)	108.8(11)
C(21)-P-C(31)	105.6(11)

symmetry operations

'-x, -0.5 + y, 0.5 - z

''-x, 0.5 + y, 0.5 - z

'''-x, 0.5 + y, -0.5 - z

TABLE 4.3.3 A Comparison of Hg-C and Hg-N Bond Lengths ($\mathring{A}$) for $[(NCCH_2CH_2)_3P]_nHgCl_2$, where (n = 1 or 2)

$[(NCCH_2CH_2)_3P]HgCl_2$		$[(NCCH_2CH_2)_3P]_2HgCl_2$(a)		
			Monomer I	Monomer II
Hg...C(23)	3.44(3)	Hg...(C23)	3.600	-
Hg...N(23)	3.51(3)	Hg...N(23)	3.510	-
Hg...C(23''')	3.61(3)	Hg...C(33)	-	3.894
Hg...N(23''')	3.47(3)	Hg...N(33)	-	3.740
		Hg...C(43)	3.703	-
		Hg...N(43)	3.518	-

(a) Section 4.2.2

4.3.2 Crystallographic Examination of the 1:1 Complex $[(Ph_3P)HgI_2]_2$

TABLE 4.3.4 Crystal Data

Crystal Size	0.125 x 0.45 x 0.037 mm			
Crystal System	Monoclinic			
a = 19.299(4)	b = 11.130(3)	c = 19.102(2) Å	β = 90.50(1)°	
V 4103.1 Å^3				
M_r 1432.8				
D_c 2.32 g cm^{-3}	D_m 2.41 g cm^{-3}	Z = 4		
Systematic Absences	h0l l = 2n + 1			
	0k0 k = 2n + 1			
Space Group	$P2_1/c$			
μ(Mo-Kα)	101.06 cm^{-1}			
F(000)	2592 electrons			

Data Collection and Structural Analysis

The crystal was mounted with its b-axis coincident with a Stöe Stadi 2 two-circle diffractometer. Fourteen layers h0l → h13l were collected; 4444 unique reflections were measured of which 2984 had $I/\sigma(I) \geq 3.0$ and were subsequently used for refinement. All non-hydrogen and carbon atoms were assigned anisotropic thermal parameters. All carbon atoms except C(24), C(25), C(26), C(61), C(62), C(63) and C(64) were also assigned anisotropic thermal parameters, these seven carbon atoms could only be assigned isotropic thermal parameters. Hydrogen atoms associated with the anisotropic carbon atoms, were included in ideal positions (C-H 1.08 Å) and were given a common isotropic temperature factor. Complex neutral atom scattering factors were employed throughout the refinement; the weighting scheme $W = 1.000/[\sigma^2(F_o) + 0.0175(F_o)^2]$ was adopted in the final cycles. Full matrix refinement gave a final R value of 0.094 and R' value of

0.091. The final atomic and thermal parameters are given in the appendix, tables 9 and 10. Bond angles and distances are listed in Table 4.3.5a.

Results and Discussion

The complex is found to be an asymmetrical halogen bridged dimer (Fig. 4.3.2). The terminal iodine atoms are trans to each other. The mercury atoms are four co-ordinate with the distortion from the tetrahedral being similar for each atom, the angles vary from 94.8(1)° to 128.4(2)°. The geometry about the phosphorus atom is only slightly distorted from the tetrahedral with the angles varying from 104.9(11)° to 112.7(10)°. The Hg-I bridging distances are unequal, being 2.990(2), 2.960(2), 2.860(2) and 2.846(2) Å while the Hg-I terminal bond lengths are similar, 2.671(2) and 2.684(2) Å and are shorter. The Hg-P bond lengths have similar values of 2.461(8) and 2.483(8) Å. The phenyl rings are planar. The angles between the associated mean planes are given in Table 4.3.5b.

Fig. 4.3.2 Molecular Structure of $[Ph_3PHgI_2]_2$

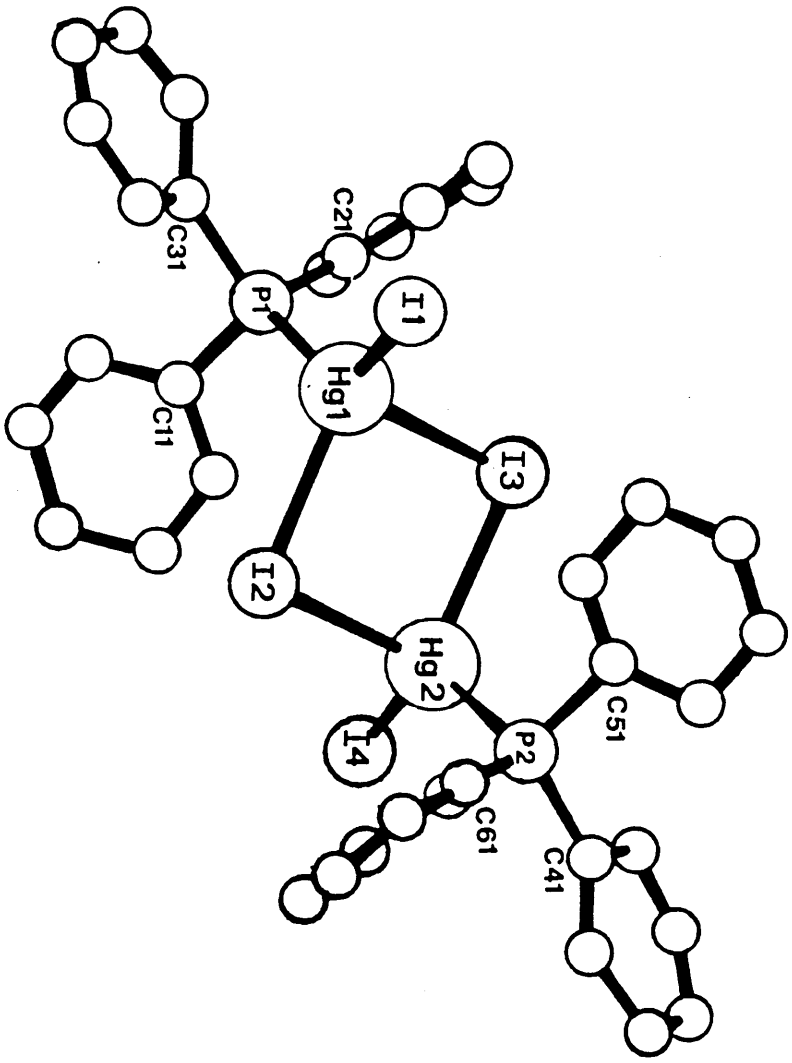

Table 4.3.5a Bond Lengths (Å) and Bond Angles (°) for $[Ph_3PHgI_2]_2$ with Estimated Standard Deviations in Parentheses

Bond Lengths (Å)

Hg(1)-I(1)	2.671(2)	Hg(2)-I(4)	2.684(2)
Hg(1)-I(2)	2.860(2)	Hg(2)-I(2)	2.960(2)
Hg(1)-I(3)	2.990(2)	Hg(2)-I(3)	2.846(2)
Hg(1)-P(1)	2.461(8)	Hg(2)-P(2)	2.483(8)
P(1)-C(11)	1.85(3)	P(2)-C(41)	1.85(3)
P(1)-C(21)	1.80(4)	P(2)-C(51)	1.80(2)
P(1)-C(31)	1.76(2)	P(2)-C(61)	1.75(3)

Bond Angles (°)

I1-Hg1-I2	106.9(1)	I3-Hg2-I4	116.2(1)
I1-Hg1-I3	107.9(1)	I2-Hg2-I4	106.4(1)
I1-Hg1-P1	128.4(2)	I4-Hg2-P2	126.6(2)
I2-Hg1-I3	94.8(1)	I2-Hg2-I3	95.8(1)
I2-Hg1-P1	112.8(2)	I3-Hg2-P2	110.0(2)
C(11)-P1-C(21)	112.0(15)	C(41)-P(1)-C(51)	108.8(11)
C(11)-P(1)-C(31)	104.9(11)	C(41)-P(2)-C(61)	108.0(14)
C(11)-P(1)-Hg(1)	111.2(12)	C(41)-P(2)-Hg(2)	112.7(10)
C(21)-P(1)-C(31)	109.3(14)	C(51)-P(2)-C(61)	108.0(14)
C(21)-P(1)-Hg(1)	109.3(10)	C(51)-P(2)-Hg(2)	108.8(10)
C(31)-P(1)-Hg(1)	110.1(10)	C(61)-P(2)-Hg(2)	110.3(10)
Hg1-I3-Hg2	84.6(1)	Hg2-I2-Hg1	84.9(1)

Table 4.3.5b Angles between mean planes for $(Ph_3P)HgI_2$

Mean Planes	Complexed Ligand	
	1	2
A-B	83.7	89.9
B-C	76.8	78.5
C-A	81.4	82.2

Plane A - ring A (1) C(11), C(12), C(13), C(14), C(15), C(16)

$-0.5384X + 0.1962Y - 0.8196Z + 18.3945 = 0$

(2) C(41), C(42), C(43), C(44), C(45), C(46)

$-0.1830X - 0.9817Y - 0.0534Z + 3.2129 = 0$

Plane B - ring B (1) C(21), C(22), C(23), C(24), C(25), C(26)

$0.8217X - 0.3080Y - 0.4795Z - 1.0119 = 0$

(2) C(51), C(52), C(53), C(54), C(55), C(56)

$-0.5969X + 0.1523Y - 0.7877Z + 20.8931 = 0$

Plane C - ring C (1) C(31), C(32), C(33), C(34), C(35), C(36)

$0.0932X + 0.9956Y - 0.0048Z - 4.5725 = 0$

(2) C(61), C(62), C(63), C(64), C(65), C(66)

$0.8526X - 0.2730Y - 0.4455Z - 8.8718 = 0$

4.3.3 Crystallographic Examination of the 1:1 Complexes $[Pr_3PHgX_2]_2$ (where X = Cl, Br or I)

TABLE 4.3.6 Crystal Data

	(I)	(II)	(III)
	$[Pr_3PHgCl_2]_2$	$[Pr_3PHgBr_2]_2$	$[\beta\text{-}Pr_3PHgI_2]_2$
Crystal System	Monoclinic	Monoclinic	Monoclinic
Dimension (mm)	0.32x0.44x0.6	0.12x0.84	0.4x0.25x0.16
a (Å)	18.474(5)	11.777(5)	10.707(3)
b (Å)	11.328(1)	8.758(5)	13.766(5)
c (Å)	13.891(6)	16.761(1)	22.399(8)
β (°)	101.17(5)	116.18(8)	96.5(1)
V ($Å^3$)	2852.3	1551.5	3280.3
M_r	863.4	1041.0	1229.6
D_c (g cm^{-3})	2.02	2.23	2.49
D_m (g cm^{-3})	2.00	2.25	2.50
Systematic Absences			
	hkl h+l=2n+1	h0l l=2n+1	h0l l=2n+1
	0k0 k=2n+1	0k0 k=2n+1	0k0 k=2n+1
	0hl h=2n+1		
Z	4	4	4
Space Group	$B2_1/a^{\ddagger}$	$P2_1/c$	$P2_1/c$
μ(Mo-Kα)(cm^{-1})	108.2	146.8	126.3
F(000) electrons	1632	1920	2208

‡A non-standard setting of $P2_1/c$.

Data Collection and Structural Analysis

Details of data collection are given in Table 4.3.7 and all three structures were solved using the Patterson method and refined by full-

matrix least squares techniques.

TABLE 4.3.7 Details of the Data Collection

	(I)	(II)	(III)
Axis mounted about	c	b	a
No. layers collected	15	11	11
No. unique reflections	1876	2285	2620
No. observed reflections	1446	1431	1638
Final R value	0.069	0.052	0.103
Final R' value	0.070	0.039	0.103
$W = a/[\sigma^2(F_o) + b(F_o)^2]$			
a	1.0000	1.00000	1.00000
b	0.09116	0.000162	0.016547
$I/\sigma(I) \geq$	3	2	4

The data were corrected for Lorentz and polarisation effects, but an absorption correction was only applied for (III). For (I) and (II) hydrogen atoms were included in ideal positions (C-H, 1.08 Å) and were given a common isotropic temperature factor. All other atoms in (I) and (II) were assigned anisotropic thermal parameters. In complex (III) only the mercury, iodine and phosphorus atoms were assigned anisotropic thermal parameters; it was also impossible to include hydrogen atoms in this structure. This is probably due to the presence of so many heavy atoms. The application of the absorption correction for this complex did not significantly improve the R value or reduce the errors.

Results and Discussion

All three compounds are halogen bridged dimers with varying degrees of distortion about the mercury atoms. Tripropylphosphine mercury iodide differs from the other two complexes in that both phosphine groups are

attached to the same mercury atom (Fig. 4.3.3). In this complex the geometry about the Hg(1) atom to which both phosphine groups are attached is highly distorted from a tetrahedral arrangement with the angles varying from 89.5(1)° to 149.1(5)°. The distortion is less about Hg(2), these angles varying from 93.9(1)° to 123.6(2)°. A full list of bond angles and bond lengths are given in Table 4.3.8, the final positional and thermal parameters are given in the appendix, table (11). Around the phosphorus atom there is significant deviation from the expected tetrahedral arrangement with the bond angles ranging from 104(3)° to 121(2)°, but there is little deviation apparent in the carbon chains.

In tripropylphosphine mercury(II) chloride (Fig. 4.3.4) the distortion from the regular tetrahedral arrangement about the mercury atom is considerable, with angles ranging from 96.5(2)° to 148.7(2)°. Around the phosphorus atom there is only slight deviation from tetrahedral with the angles ranging from 106.4(8)° to 113.6(7)°. A full list of bond angles and bond lengths are given in Table 4.3.9, the final positional and thermal parameters are given in the appendix table (12).

The degree of distortion about the mercury atom in tripropylphosphine mercury(II) bromide (Fig. 4.3.5) is considerable, the angles ranging from 102.5(1) to 135.9(1)°. There is, however, only a slight degree of distortion from tetrahedral about the phosphorus atom, with the angles varying from 112.8(4) to 107.3(7)°. The terminal and bridging mercury-halogen bond lengths for this complex are similar (2.507(2) and 2.667(2) $\overset{o}{A}$ respectively). The structure is very unsymmetrical as the bridging bond lengths differ markedly (Hg-Br_{br}* = 2.667(2) and Hg-Br_{br}* = 3.051(2) $\overset{o}{A}$). A full list of bond lengths and bond angles are given in Table 4.3.10 and the final positional and thermal parameters are given in the appendix table (13).

Fig. 4.3.3 Molecular Structure of $[\beta\text{-}Pr_3PHgI_2]_2$

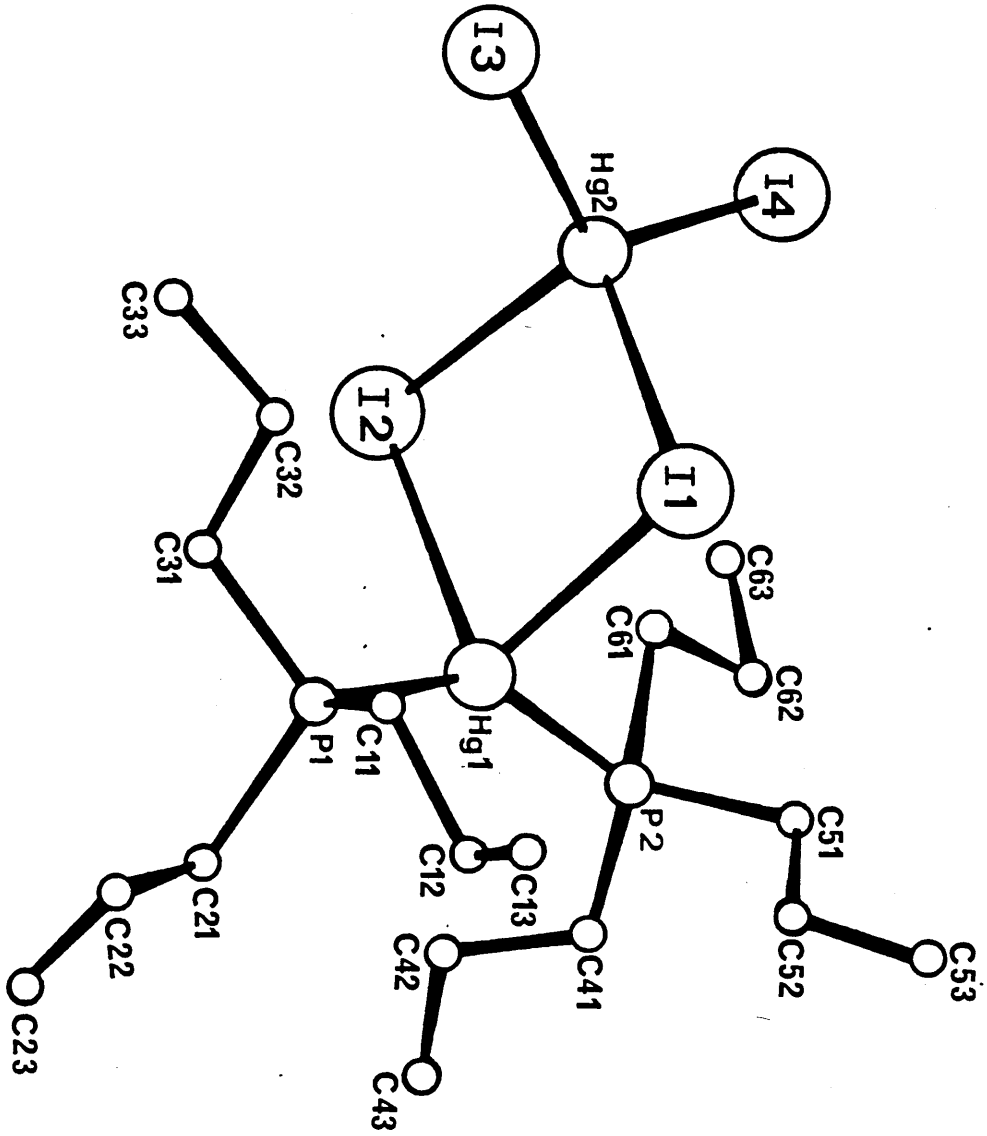

Fig. 4.3.4 Molecular Structure of $[Pr_3PHgCl_2]_2$

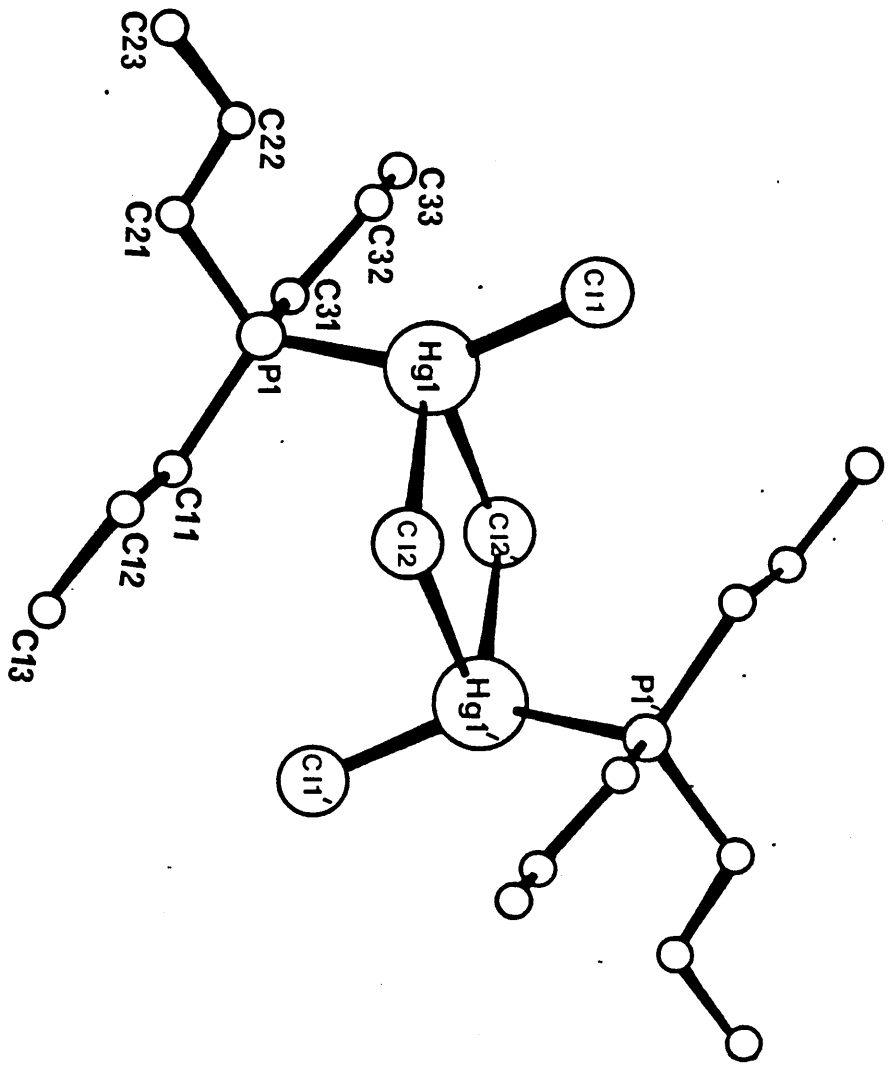

Fig. 4.3.5 Molecular Structure of $[Pr_3PHgBr_2]_2$

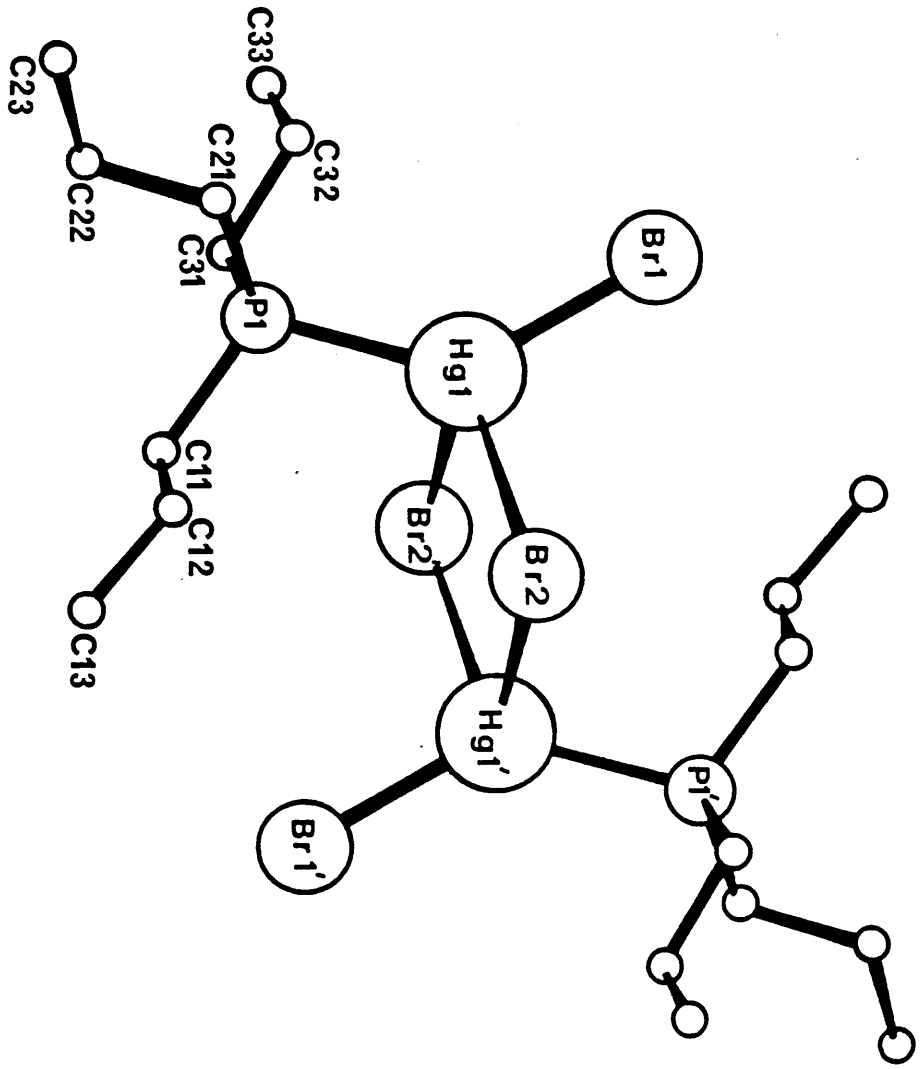

Table 4.3.8 Bond Lengths (Å) and Bond Angles (°) for $[\beta\text{-}Pr_3PHgI_2]_2$ with Estimated Standard Deviations in Parentheses

Bond Distances (A)

Hg1 - I1	3.027(4)	P2 - C61	2.09(9)
Hg1 - I2	3.050(5)	C11 - C12	1.63(9)
Hg1 - P1	2.457(14)	C12 - C13	1.36(11)
Hg1 - P2	2.421(15)	C21 - C22	1.53(8)
Hg2 - I1	2.937(5)	C22 - C23	1.54(9)
Hg2 - I2	2.921(4)	C31 - C32	1.64(8)
Hg2 - I3	2.694(4)	C32 - C33	1.58(8)
Hg2 - I4	2.685(5)	C41 - C42	1.50(9)
P1 - C11	1.91(6)	C42 - C43	1.50(12)
P1 - C21	1.84(5)	C51 - C52	1.45(7)
P1 - C31	1.81(6)	C52 - C53	1.35(9)
P2 - C41	1.84(9)	C61 - C62	1.47(11)
P2 - C51	1.65(6)	C62 - C63	1.65(11)

Bond Angles (°)

I1 - Hg1 - I2	89.5(1)	C21 - P1 - C31	105(3)
I1 - Hg1 - P1	100.8(4)	Hg1 - P2 - C41	113(3)
I1 - Hg1 - P2	98.0(4)	Hg1 - P2 - C51	121(2)
I2 - Hg1 - P1	102.2(4)	Hg1 - P2 - C61	104(3)
I2 - Hg1 - P2	102.4(4)	C41 - P2 - C51	105(3)
P1 - Hg1 - P2	149.1(5)	C41 - P2 - C61	106(4)
I1 - Hg2 - I2	93.9(1)	C51 - P2 - C61	107(3)
I1 - Hg2 - I3	106.3(2)	P1 - C11 - C12	106(4)
I1 - Hg2 - I4	109.6(2)	C11 - C12 - C13	105(7)
I2 - Hg2 - I3	109.5(1)	P1 - C21 - C22	110(4)
I2 - Hg2 - I4	109.8(2)	C21 - C22 - C23	105(5)
I3 - Hg2 - I4	123.6(2)	P1 - C31 - C32	106(4)
Hg1 - I1 - Hg2	88.1(1)	C31 - C32 - C33	104(4)
Hg1 - I2 - Hg2	88.0(1)	P2 - C41 - C42	113(6)
Hg1 - P1 - C11	109(2)	C41 - C42 - C43	108(7)
Hg1 - P1 - C21	109(2)	P2 - C51 - C52	113(4)
Hg1 - P1 - C31	112(2)	C51 - C52 - C53	108(6)
C11 - P1 - C21	105(2)	P2 - C61 - C62	111(6)
C11 - P1 - C31	116(3)	C61 - C62 - C63	103(7)

Table 4.3.9 Bond Lengths (Å) and Bond Angles (°) for $[Pr_3PHgCl_2]_2$ with Estimated Standard Deviations in Parentheses

Bond Lengths (Å)

Hg-Cl1	2.348(5)	C11-C12	1.45(3)
Hg-Cl2	2.638(4)	C12-C13	1.51(3)
Hg-P	2.358(4)	C21-C22	1.45(3)
Hg-Cl2'	2.780(4)	C22-C23	1.58(3)
P-C11	1.815(16)	C31-C32	1.46(3)
P-C21	1.795(17)	C32-C33	1.47(3)
P-C31	1.827(17)	Hg---Hg'	3.813

Bond Angles (°)

Cl2-Hg-Cl1	96.5(2)	P-C11-C12	111.1(15)
P-Hg-Cl1	148.7(2)	P-C21-C22	115.1(14)
P-Hg-Cl2	111.2(2)	P-C31-C32	115.3(16)
Hg-P-C11	112.4(6)	C11-C12-C13	113(2)
Hg-P-C21	110.1(6)	C21-C22-C23	113(2)
Hg-P-C31	113.6(7)	C31-C32-C33	115(2)
C11-P-C21	106.4(8)	C11-Hg-Cl2'	103.6(2)
C11-P-C31	107.2(9)	Cl2-Hg-Cl2'	90.6(2)
C21-P-C31	106.6(10)	P-Hg-Cl2'	90.8(2)
		Hg-Cl2-Hg'	89.4(1)

', -x, 1-y, -z

Table 4.3.10 Bond Lengths (Å) and Bond Angles (°) for $[Pr_3PHgBr_2]_2$ with Estimated Standard Deviations in Parentheses

Bond Lengths (Å)			
Hg-Br1	2.507(2)	C11-C12	1.507(18)
Hg-Br2	2.667(2)	C12-C13	1.499(20)
Hg-P	2.408(4)	C21-C22	1.514(17)
Hg-Br2'	3.051(2)	C22-C23	1.507(18)
P-C11	1.794(14)	C31-C32	1.553(17)
P-C21	1.806(14)	C32-C33	1.521(19)
P-C31	1.796(14)	Hg---Hg'	4.022
Bond Angles (°)			
Br2-Hg-Br1	102.5(1)	P-C11-C12	114.6(11)
P-Hg-Br1	135.9(1)	C11-C12-C13	114.4(15)
P-Hg-Br2	119.7(1)	P-C21-C22	113.1(10)
Hg-P-C11	108.4(5)	C21-C22-C23	111.2(13)
Hg-P-C21	112.8(4)	P-C31-C32	113.8(11)
Hg-P-C31	112.7(5)	C31-C32-C33	110.8(14)
C11-P-C21	107.7(7)	Br1-Hg-Br2'	105.6(1)
C11-P-C31	107.7(7)	Br2'-Hg-Br2	90.9(1)
C21-P-C31	107.3(7)	Br2'-Hg-P	87.2(1)
		Hg-Br2-Hg'	89.1(1)

', -x, 1-y, 1-z

4.3.4 Crystallographic Examination of the Mixed Metal Complex $(Pr_3P)_2Hg(\mu\text{-}I)_2CdI_2$

TABLE 4.3.11 Crystal Data

Crystal Size	0.21 x 0.19 x 0.25 mm			
Crystal System	Monoclinic			
a = 10.694(6)	b = 13.794(7)	c = 22.415(9) Å	β = 96.25(5)°	
V	3286.7 Å^3			
M_r	1141.1			
D_c	2.31 g cm^{-3}	D_m	2.29 g cm^{-3}	Z = 4
Systematic Absences	h0l l = 2n + 1			
	0k0 k = 2n + 1			
Space Group	$P2_1/c$			
μ(Mo-Kα)	86.2 cm^{-1}			
F(000)	2080 electrons			

Data Collection and Structural Analysis

The crystal was mounted with its a-axis coincident with a Stöe Stadii 2 two-circle diffractometer. Twelve layers 0kl → 11kl were collected; 4159 unique reflections were measured of which 5053 had $I/\sigma(I) \geq 3.0$ and were subsequently used for refinement. Hydrogen atoms were included in ideal positions (C-H, 1.08 Å) and were given a common isotropic temperature factor. All other atoms were assigned anisotropic thermal parameters. Complex neutral-atom scattering factors were employed throughout the refinement; the weighting scheme $W = 1.7507/[\sigma^2(F_o) + 0.0009(F_o)^2]$ was adopted in the final cycles. Full matrix refinement gave a final R value of 0.048 and R' value of 0.052. The final atomic parameters and thermal parameters are given in the appendix, tables 14 and 15 and bond distances and angles are listed in Table 4.3.12.

Results and Discussion

The complex is found to be an unsymmetrical halogen bridged dimer (Fig. 4.3.6) in the solid state with, surprisingly, both phosphine ligands being bonded to the mercury atom. The four-membered ring is approximately planar, the angles within the ring ranging from 87.2(1)° to 96.3(1)°. Each metal atom is four co-ordinate and the distortion from a tetrahedral arrangement for the cadmium is not large, the angles varying from 108.3(1)° to 118.6(1)°. However, the tetrahedral arrangement of the mercury is highly distorted, the angles ranging from 88.6(1)° tO 152.8(1)°. The arrangement of the propyl groups about the phosphines is little distorted from the tetrahedral, with the angles varying from 106.3(7)° to 108.2(7)°.

The unsymmetrical structure of this complex was further confirmed by ^{199}Hg NMR studies.[62] The spectra showed a 1:2:1 triplet with a chemical shift of -621 ± 2 ppm which confirmed the bonding of two equivalent phosphine ligands to mercury. The ^{31}P spectrum gave a single sharp peak with a chemical shift of 17.5 ± 0.1 ppm with a coupling constant J(^{199}Hg-^{31}P) of 4340 ± 2.5 Hz.

Fig. 4.3.6 Molecular Structure of $(Pr_3P)_2Hg(\mu\text{-}I)_2CdI_2$

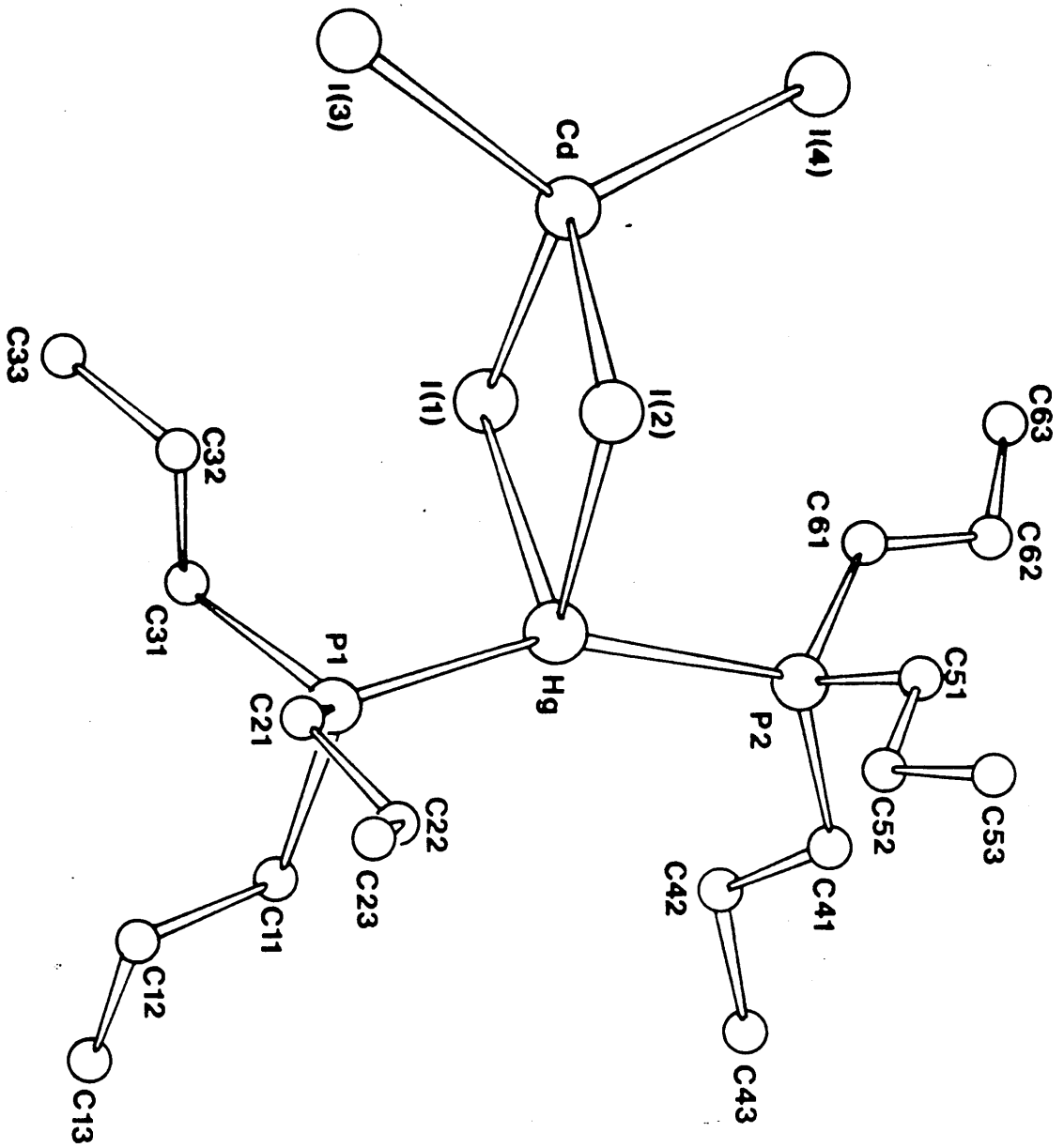

Table 4.3.12 Bond Lengths (Å) and Bond Angles (°) for $(Pr_3P)_2Hg(\mu\text{-}I)_2CdI_2$ with Estimated Standard Deviations in Parentheses

(a) Bond lengths (Å)

Hg-I(1)	3.077(1)	Cd-I(4)	2.705(2)
Hg-I(2)	3.056(1)	P(1)-C(11)	1.829(16)
Hg-P(1)	2.424(4)	P(1)-C(21)	1.790(14)
Hg-P(2)	2.410(4)	P(1)-C(31)	1.850(17)
Cd-I(1)	2.866(1)	P(2)-C(41)	1.819(18)
Cd-I(2)	2.882(1)	P(2)-C(51)	1.805(20)
Cd-I(3)	2.705(2)	P(2)-C(61)	1.826(25)

(b) Bond angles (°)

I(1)-Hg-I(2)	88.6(1)	Hg-I(2)-Cd	87.3(1)
I(1)-Hg-P(1)	100.6(1)	Hg-P(1)-C(11)	111.4(5)
I(1)-Hg-P(2)	101.4(1)	Hg-P(1)-C(21)	111.6(5)
I(2)-Hg-P(1)	99.9(1)	Hg-P(1)-C(31)	111.5(5)
I(2)-Hg-P(2)	96.4(1)	C(11)-P(1)-C(21)	107.6(7)
P(1)-Hg-P(2)	152.8(1)	C(11)-P(1)-C(31)	108.2(7)
I(1)-Cd-I(2)	96.3(1)	C(21)-P(1)-C(31)	106.3(7)
I(1)-Cd-I(3)	110.3(1)	Hg-P(2)-C(41)	113.2(6)
I(1)-Cd-I(4)	110.9(1)	Hg-P(2)-C(51)	113.6(7)
I(1)-Cd-I(4)	110.9(1)	Hg-P(2)-C(51)	113.6(7)
I(2)-Cd-I(3)	108.3(1)	Hg-P(2)-C(61)	108.3(8)
I(2)-Cd-I(4)	110.0(1)	C(41)-P(2)-C(51)	107.0(10)
I(3)-Cd-I(4)	118.6(1)	C(41)-P(2)-C(61)	107.8(12)
Hg-I(1)-Cd	87.2(1)	C(51)-P(2)-C(61)	106.6(12)

4.3.5 Crystallographic Examination of the 1:1 Complex $[\alpha\text{-Pr}_3\text{PHgI}_2]_n$

TABLE 4.3.13 Crystal Data

Crystal Size	0.30 x 0.05 x 0.10 mm		
Crystal System	Monoclinic		
	a = 8.670(8)	b = 13.174(9)	c = 14.893(8) Å β = 106.57(5)°
V	1630.7 Å^3		
M_r	614.5		
D_c	2.50 g cm^{-3}	D_m 2.47 g cm^{-3}	Z = 8
Systematic Absences	hkl h + l = 2n + 1		
	0k0 k = 2n + 1		
	h0l h = 2n + 1		
Space Group	$B2_1/a$‡		
μ(Mo-Kα)	127.1 cm^{-1}		
F(000)	2208 electrons		

‡A non-standard setting of $P2_1/c$

Data Collection and Structural Analysis

The crystal was mounted with its a-axis coincident with the ω-axis of the Stoe Stadi 2 two-circle diffractometer. Ten layers 0kl → 9kl were collected; 1032 unique reflections were measured of which 582 had $I/\sigma(I) \geq 2$ and were subsequently used in the refinement. It was impossible to assign positions for the carbon atoms and this was probably due to the small number of reflections available and the presence of a large proportion of heavy atoms. The mercury, iodine and phosphorus atoms were assigned anisotropic thermal parameters. Complex neutral-atom scattering factors were employed throughout the refinement; the final weighting scheme adopted was $W = 2.6953/(\sigma^2|F_o| + 0.002123|F_o|^2)$ and interlayer scaling was applied. Full matrix refinement gave a final R value of 0.092 and R' value of 0.097.

The final atomic parameters and thermal parameters are given in the appendix, table 16 and bond distances and angles are listed in table 4.3.14.

Results and Discussion

The complex is found to consist of a single $(HgI_2)_n$ polymeric chain with each mercury atom co-ordinated to four iodine and one phosphorus atoms (fig. 4.3.7). The mercury atom lies in a distorted trigonal bipyramidal environment with the bond angles varying from 85.8(2)° to 169.7(2)°. The complex has two Hg-I bonds of 2.726(5) Å and 2.715(5) Å and an Hg-P bond of 2.406(17) Å in an approximately planar arrangement (sum of angles is 359.7°). The five co-ordination is completed by bonding of the mercury atom to iodine atoms from two adjacent molecules approximately perpendicular to this HgI_2P plane. These Hg-I bond lengths (3.617 Å and 3.579 Å) are longer than the sum of the van der Waals' radii (3.45 Å) and are considered to be weak interactions.

Fig. 4.3.7 Molecular Structure of $[\alpha\text{-}Pr_3PHgI_2]_n$

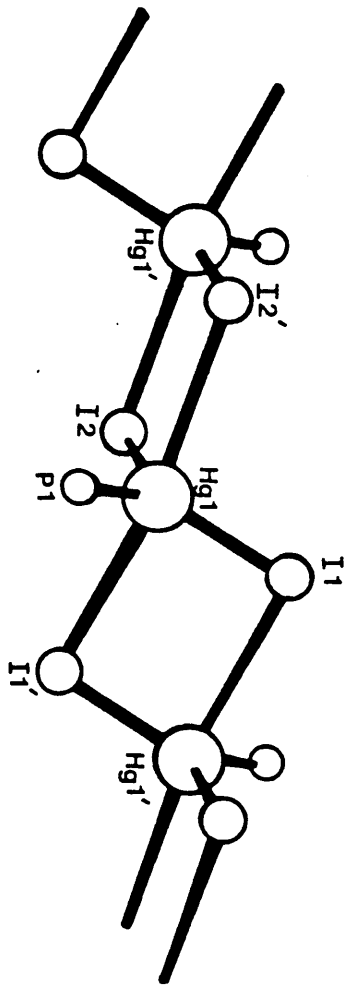

Table 4.3.14 Bond Lengths (Å) and Bond Angles (°) for $[\alpha\text{-}Pr_3PHgI_2]_n$ with Estimated Standard Deviations in Parentheses

Bond Lengths (Å)

Hg-I1	2.726(5)	Hg---Hg'	4.501(4)
Hg-I1'	3.627(5)	Hg---Hg''	4.501(4)
Hg-I2	2.715(5)	symmetry code	
Hg-I2''	3.579(5)	' 1-x, 1-y, -z	
Hg-P	2.406(17)	'' -x, 1-y, -z	

Bond Angles (°)

I2-Hg-I1	112.2(2)	I2''-Hg-I1'	169.7(2)
P-Hg-I2	126.1(5)	Hg-I1-Hg'	89.3(2)
P-Hg-I1	121.4(5)	Hg-I2-Hg''	94.2(2)
I1-Hg-I1'	90.7(2)	P-Hg-I1'	89.0(5)
I2''-Hg-I1	99.1(2)	P-Hg-I2''	88.7(5)
I2-Hg-I2''	85.8(2)		
I1'-Hg-I2	87.4(2)		

4.3.6 A Comparison of 1:1 Mercury(II) Halide Complexes

Although not strictly one of this category, the structure of $(Pr_3P)_2Hg(\mu\text{-}I)_2CdI_2$ is included in this section due to its great similarity to $[\beta\text{-}Pr_3PHgI_2]_2$. All the 1:1 mercury(II) halide complexes studied in this work fig. 4.3.8 $(R_3P)HgX_2$ (X = Cl, R = $NCCH_2CH_2$ (e), C_3H_7 (a) and C_6H_5 (f); X = Br, R = C_3H_7 (a); X = I, R = C_3H_7 (b and c) and C_6H_5 (f)) are halogen-bridged dimers with varying degrees of distortion about the mercury atom except for $[(NCCH_2CH_2)_3PHgCl_2]_n$ (e) and $[\alpha\text{-}Pr_3PHgI_2]_n$ (c) which have halogen-bridged polymeric structures. In $[\alpha\text{-}Pr_3PHgI_2]_n$ (c) the mercury atom has a penta-coordinate environment, resulting in an extended distorted trigonal bipyramidal structure. The structure of polymeric tris(2-cyanoethyl)-phosphine mercury(II) chloride (e) shows the mercury atom to be six-coordination though two of these bonds result from weak CN...Hg π-interactions. Tripropylphosphine mercury(II) iodide exists in two forms; the α-form (c), as reported above, is polymeric whereas $[\beta\text{-}Pr_3PHgI_2]_2$ (b) is unique among all the 1:1 mercury(II) halide phosphine complexes known having both phosphine ligands coordinated to the same mercury atom. The only bromo mercury(II) complex studied is $(Pr_3PHgBr_2)_2$ (a) which is a halogen bridged dimer similar to its chloro-analogue. Apart from $[Pr_3PHgCl_2]_2$ which has a symmetrical bridged arrangement, all the dimers studied in this work fig. 4.3.8 (a-l) have asymmetrical bridged structures. The structural types established for 1:1 mercury(II) halide complexes with tertiary phosphines from this work and from earlier studies are given in table 4.3.15.

It has been suggested[65] that strong donor ligands give rise to less extended structures. The structures have been established for many tertiary phosphine mercury(II) chloride complexes but insufficient iodide

or bromide complexes have been characterised to allow comparisons in these groups. For R_3PHgCl_2 complexes it would appear that 'small' strong σ-donating ligands give rise to extended polymer structures e.g. Me_3P, Et_3P, α-Bu_3P and $(NCCH_2CH_2)_3P$ have structures extended beyond the dimer stage whereas a weak donor such as Ph_3P results in a dimeric structure. The exceptions to this are $[Pr_3PHgCl_2]_2$ and $[Cy_3PHgCl_2]_2$ which have halogen-bridged dimeric structures despite the fact that both ligands have high pKa values (8.64 and 9.7 respectively). However, the large 'size' of the cyclohexyl groups probably inhibits the extension of its structure beyond the dimeric stage. Many R_3PHgX_2 complexes are found to have more than one form and it is possible the Pr_3PHgCl_2 is one of these and may therefore exist in an as yet unknown, more extended form.

The nature of the halogen atoms may play an important role in the extent of the association of $(R_3P)MX_2$ complexes. For example, the structural work on $(R_3P)CdX_2$ complexes[65] has shown that for a given phosphine, the more covalent Cd-I bonding gives rise to a less extended iodine-bridged dimer whilst the chloride gives rise to a more extended penta-coordinate arrangement. However, in the mercury series studied here (Table 4.3.15) for the limited number of structures for a particular phosphine, solved by full X-ray analysis, it appears that the halogen has little effect on the structure adopted. For both Pr_3P and Ph_3P mercury(II) halide complexes a dimeric arrangement is found except for one of the forms of Pr_3PHgI_2 which is polymeric.

In section 2.2 it was proposed that the extent of the interaction between the mercury and the donor ligand was dependent upon the electronic effect and the 'size' of the substituents attached to the donor atom. For the 2:1 series (section 4.2.3) stronger σ-donor ligands gave rise to short Hg-P bonds, long Hg-X bonds and large P-Hg-P bond angles. Parameters for

the structures of 1:1 complexes solved in this work and other analogous complexes solved by other workers are listed in table 4.3.16, along with pKa values for the phosphine ligands. Comparison of the Hg-X and Hg-P bond lengths does not show a marked distinction between phosphines of differing pKa values. However, the size of the P-Hg-$Cl_{terminal}$ angle does show marked variation for different strengths of the phosphine ligand. When R is Me, Et, Pr and Bu (pKa 8.65, 8.69, 8.64 and 8.43 respectively) the P - Hg-X angle is found to be large 162.1(1)°, 145.4(3)°, 148.7(2)° and 150.9(3)° respectively, compared to triphenylphosphine mercury(II) chloride (pKa Ph_3P 2.73) which has a much smaller P-Hg-$X_{terminal}$ angle of only 128.7(4)°. Tris(2-cyanoethyl)phosphine mercury(II) chloride has a similar P-Hg-$Cl_{terminal}$ angle (162.0(3)°) to trimethylphosphine mercury(II) chloride (pKa Me_3P is 8.65) which has a P-Hg-$Cl_{terminal}$ angle of 162.1(1)°, indicating $(NCCH_2CH_2)_3P$ is a strong σ-donor to mercury(II) halides although its pKa is only 1.36, as was also found for the 2:1 complex. This is further supported by the NMR data which shows the $(NCH_2CH_2)_3PHgCl_2$ has a similar chemical shift to Pr_3PHgCl_2 but smaller than for the weak donor complex with Ph_3P (table 4.3.17).

Only three mercury(II) iodide structures have been established, those of triphenyl phosphine and the α and β forms of tripropylphosphine. Although these three complexes have vastly differing structures there is little variation of bond angles and bond lengths despite the differing pKa of the phosphines (2.73 and 8.64 respectively). The average Hg-P bond lengths are 2.47 Å, 2.41 Å and 2.44 Å respectively and the P-Hg-$I_{terminal}$ bond angles are 128.4(2)° and for the α-Pr_3PHgI_2 124.8(6)°. This would indicate that for iodides of 1:1 complexes the differing donor strength of the ligands does not markedly affect the bond lengths and bond angles.

The effect of the anion on the geometry of 1:1 mercury(II) halide complexes can be seen from a comparison of the Hg-P and Hg-X_t bond lengths and size of the X_{br}-Hg-X_{br} and P-Hg-X_t angles. The only complete halide series is for tripropylphosphine, where the structures of chloride, bromide and iodide have been fully determined, but data is also available for the chloro and iodo mercury(II) halide complexes with triphenylphosphine. In both these cases the steric and electronic effects of the phosphine ligand may be ignored.

In the case of triphenylphosphine mercury(II) halides a comparison of the appropriate angles and lengths is straightforward, as both complexes being studied have a halogen-bridged dimeric structure, the chloride having a centrosymmetrical structure whilst the iodide has an asymmetric structure. Triphenylphosphine mercury(II) chloride has shorter Hg-P and Hg-X_t bond lengths 2.406(7) Å and 2.370(10) Å respectively and a smaller X_{br}-Hg-X_{br} angle 85.4(3)° than its iodide analogue which has corresponding bond lengths of 2.461(8) Å and 2.671(2) Å and an I-Hg-I angle of 94.8(1)°. The P-Hg-X_t angle in these cases are very similar 128.7(4)° for the chloride and 127.5(2)° for the iodide.

In the case of tripropylphosphine mercury(II) halides the iodides have vastly different structures from the chloride and bromide, both the latter being halogen-bridged dimers. Tripropylphosphine mercury(II) bromide is unusual in that the terminal Hg-Br bond length (2.507(2) Å) and the bridging Hg-Br bond length 2.667(2) Å are similar, whereas there is a marked difference for the chloride which has bond lengths of 2.348(5) Å and 2.638(4) Å respectively. The β-form of the iodide is a halogen-bridged dimer but is most unusual in having both phosphine groups bonded to the same mercury atom. In contrast the α-version of the iodide is a polymeric halogen-bridged structure. Despite the structural variations it is

possible to see an increase in the X_{br}-Hg-X_{br} angle from 96.5(2)° for the chloride, 102.5(1)° for the bromide to 112.5(2)° for the α-form of the iodide and 108.3(2)° for the β-form. The P-Hg-X_t angle however shows a decrease from chloride to iodide (148.7(2), 135.9(1) and 123.7(6)° av. respectively) and these variations are accompanied by an increase in the Hg-P (2.358(4), 2.408(4), 2.406(17) and 2.439(14) av. Å) and Hg-X_t (2.348(5), 2.507(2), 2.723(6) and 2.694(4) Å) bond lengths from X= Cl to I. The increase in Hg-P distance from chloride to iodide for both the Ph_3P and Pr_3P complexes may result from both the higher electronegativity of chlorine compared to iodide and also if the iodide is a stronger donor to mercury than chlorine as was discussed in section 4.2.3.

An increase in the Hg-X (X = Cl → Br → I) bond length would be expected due to the electronegativity and bulk of the halogen atoms. A comparison of this bond length (table A) for HgX_2 (I) and Pr_3PHgX_2 (II) shows that Hg-Cl is 2.52 Å in (I) and 2.348(5) Å in (II), Hg-Br for (I) 2.57 Å for (II) 2.507(2) Å and for Hg-I (I) 2.60 Å for (II) 2.69 Å av. The differences between I and II would indicate that in the 1:1 complexes the chlorine atom is acting as the stronger σ-donor. Similarly, a comparison shown below between the Hg-X distances in the complexes and the sum of the covalent radii leads to the same conclusions.

Table A Comparison of Hg-X covalent radii and Hg-X bond distances

sum covalent radii Hg-X (Å)		Hg-X_t bond distance (Å)		Difference (Å)	
		(Pr_3P) (I)	(Ph_3P) (II)	(I)	(II)
X = Cl	2.44	2.348	2.370	0.092	0.07
X = Br	2.58	2.507		0.073	
X = I	2.77	2.69	2.68	0.08	0.09

A similar comparison may be made between the Hg-P bond distances and the sum of the covalent radii for mercury and phosphorus (table B).

Table B Comparison of Hg-P covalent radii and Hg-P bond distances (Å)

sum covalent radii Hg-P (Å)		Hg-P distance (Å)		Difference (Å)	
		(Pr_3P) (I)	(Ph_3P) (II)	(I)	(II)
X = Cl	2.54	2.358	2.406	-.182	-.134
X = Br	2.54	2.408		-.132	
X = I	2.54	2.457	2.483	-.083	-.017

In all cases the Hg-P bond distance is smaller than the sum of the covalent radii indicating a strong mercury-ligand reaction.

Table 4.3.17 shows a decrease from the chloride to the iodide for both chemical shifts and coupling constants with a corresponding increase in the Hg-P bond lengths. The exception being the polymeric $[\alpha\text{-}Pr_3PHgI_2]_n$ which has a Hg-P bond length comparable to its bromo-analogue, but a similar chemical shift and coupling constant to $[\beta\text{-}Pr_3PHgI_2]_2$.

This trend of decreasing chemical shifts and coupling constants is also shown by the 2:1 complexes, but in the case of the 2:1 complexes the chemical shifts and coupling constants are lower.

Comparison of $\beta\text{-}(Pr_3P)_2Hg(\mu\text{-}I)_2HgI_2$ (I) and $(Pr_3P)_2Hg(\mu\text{-}I)_2CdI_2$ (II)

Fig. 4.3.8

A comparison of the bond lengths and bond angles for the complexes $[\beta\text{-}Pr_3PHgI_2]_2$ (I) and $(Pr_3P)_2Hg(\mu\text{-}I)_2CdI_2$ (II) shows them to be remarkably similar. Both have a halogen-bridged dimer structure with the two phosphine ligands coordinated to the same mercury atom and thus (I) is the only 1:1 mercury(II) halide tertiary phosphine complex known to be of this structure. The geometry about the Cd atom in (II) and the analogous Hg atom in (I), which is also bonded to two terminal iodine atoms, is only

slightly distorted from the tetrahedral, while the geometries about the other mercury atom, in each case, are highly distorted from tetrahedral and angles range from 89.5° to 149.1° in (I) and from 88.6° to 152.8° in (II). The similarity of the structures is not unexpected as $[\beta\text{-}Pr_3PHgI_2]_2$ can be prepared by the treatment of $(Pr_3P)HgI_2CdI_2$ with excess mercuric iodide.[24] The 1:2:1 triplet nature of the ^{199}Hg NMR spectrum for complex (II) indicates the bonding of two equivalent phosphine ligands to the mercury atom. ^{199}Hg NMR data are not available for $(\beta\text{-}Pr_3PHgI_2)_2$. The ^{31}P NMR data given in table 4.3.17 for both complexes surprisingly shows no similarity, the chemical shifts and coupling constants being markedly different.

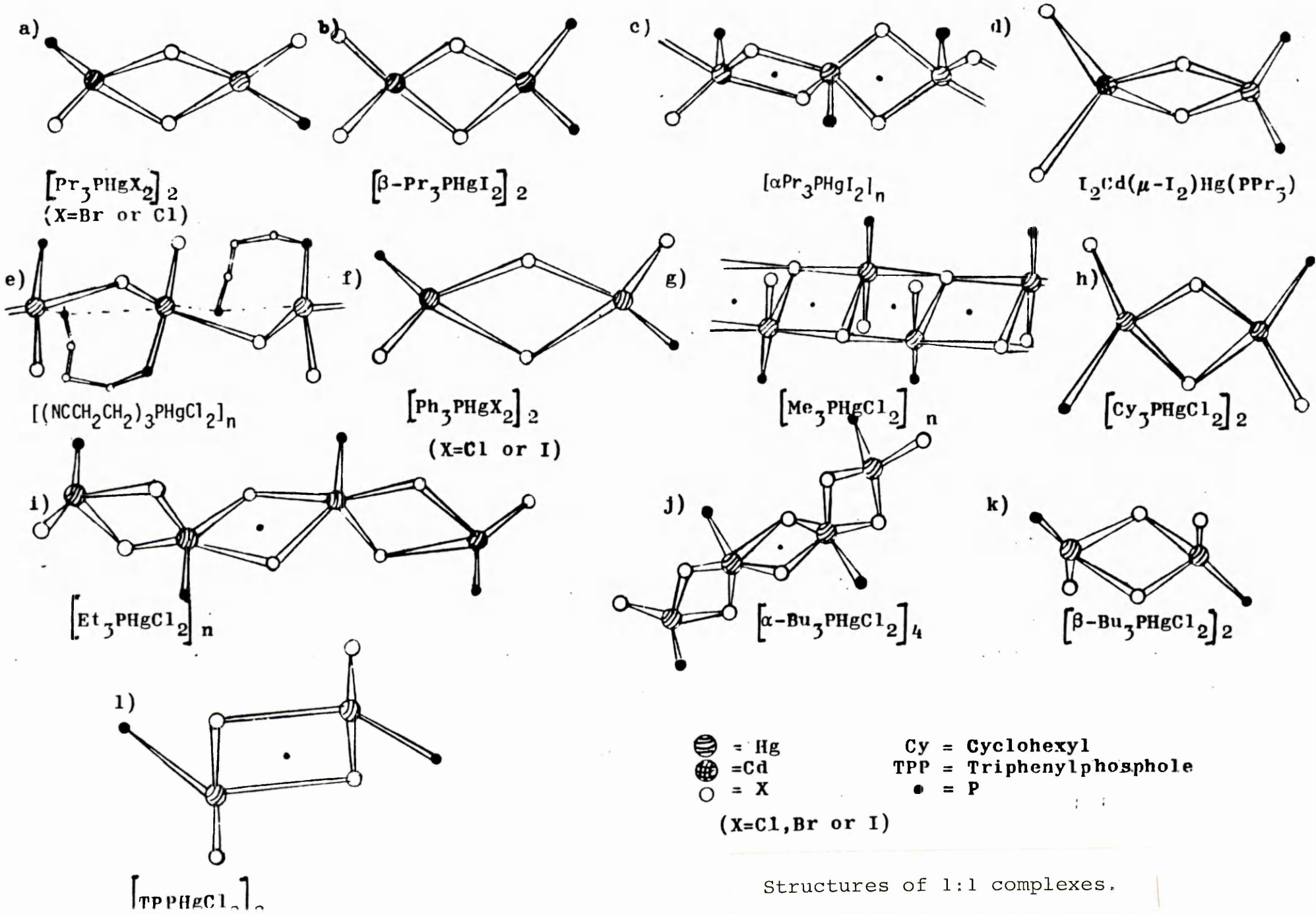

Fig 4.3.8

Structures of 1:1 complexes.

Table 4.3.15 Summary of Structures of $HgX_2(PR_3)$ Complexes Determined[a]

PR_3	Cl	Br	I
TPP[b]	Asymmetric dimer[d]	Assymetric dimer[d]	-
PPh_3	Symmetric dimer	Symmetric dimer	Asymmetric dimer
PPh_2Me	(α *Chain polymer* (β *Symmetric dimer*	*Ionic chain*	*Symmetric dimer*
$PPhMe_2$	*Ionic chain*	*Ionic chain*	*Symmetric dimer*
PMe_3	Ionic chain	Ionic chain	*New form*
PEt_3	Chain polymer	*Chain polymer*	*Symmetric dimer*
PPr_3	Asymmetric dimer[d]	Asymmetric dimer[d]	β: Unsymmetric dimer α: Weakly linked monomer units
PBu_3	(α Pseudo-tetramer (β Symmetric dimer	*Pseudo-tetramer*	*Pseudo-tetramer*
PCy_3[c]	Two independent dimers	*Symmetric dimer*	*Symmetric dimer*
$P(CH_2CH_2CN)_3$	Chain polymer		

(a) Structures underlined have been determined by full X-ray analysis: Structures in normal type have been deduced by comparison of preliminary single crystal X-ray data: Structures in *italics* are those proposed from comparative vibrational spectroscopy.

(b) TPP = 1,2,5-triphenylphosphole.

(c) Cy - cyclohexyl.

(d) In an asymmetric dimer the Hg-X bond lengths in the centrosymmetric HgX_2Hg unit are distinctly unequal.

Table 4.3.16 Comparison of Bond Lengths (Å) and Bond Angles (°) for Some $(R_3P)HgX_2$ Complexes

$(R_3P)HgX_2$	Hg-X_{br} (Å)	Hg-X_t (Å)	Hg-P (Å)	X_b-Hg-X_b (°)	P-Hg-X_t (°)	R_3P
$(Me_3P)HgCl_2$[a]	2.782(4) 2.941(4) 3.489(4)	2.355(4)	2.365(3)	98.2(1)	162.1(1)	8.65
$(Et_3P)HgCl_2$[a]	2.56(1) 3.04(1) 3.21(1)	2.42(1)	2.35(1)	98.7(3)	145.4(3)	8.69
$(Pr_3P)HgCl_2$[b]	2.638(4)	2.348(5)	2.358(4)	96.5(2)	148.7(2)	8.64
$(Pr_3P)HgBr_2$[b]	3.051 2.667(2)	2.507(2)	2.408(4)	102.5(1)	135.9(1)	8.64
$(\alpha\text{-}Pr_3P)HgI_2$[b]	3.566(6) 3.612(6)	2.723(6) 2.622(6)	2.406(17)	112.5(2)	122.6(6) 124.8(6)	8.64
$(\beta\text{-}Pr_3P)HgI_2$[b]	3.027(4) 3.050(5) 2.937(5) 2.921(4)	2.694(4) 2.685(2)	2.457(14) 2.421(15)	109.6(2) 109.8(2) 109.5(2) 106.3(2)	-	8.64
$(NCCH_2CH_2)_3PHgCl_2$[b]	2.780(7) 2.714(7)	2.331(7)	2.393(5)	98.8(3) 98.1(3) 99.0(3)	90.2(2) 95.8(2) 162.0(3)	1.36
$(\alpha\text{-}Bu_3P)HgCl_2$[c]	2.709(20) 2.895(21) 2.626(19) 2.304(21) 2.664(18) 3.375(25)	2.289(21)	2.363(21) 2.337(19)	92.6(6) 88.3(7) 87.8(6)	147.8(7)	8.43
$(\beta\text{-}Bu_3P)HgCl_2$[d]	2.720(6) 2.736(6)	2.348(8)	2.377(6)	89.0(3)	150.9(3)	8.43

Ph_3PHgCl_2[c]		2.658(8) 2.623(8)	2.370(10)	2.406(7)	85.4(3)	128.7(4)	2.73
Ph_3PHgI_2[b]		2.990(2) 2.860(2) 2.960(2) 2.846(2)	2.671(2) 2.684(2)	2.461(8) 2.438(8)	94.8(1) 95.8(1)	128.4(2) 126.6(2)	2.73
Cy_3PHgCl_2[e]	1	2.641(4) 2.665(4)	2.391(5)	2.416(3)	95.2(2)	139.6(2)	9.7
	2	2.602(4) 2.779(4)	2.413(3)	2.412(3)	101.5(2)	132.0(1)	
$TPPHgCl_2$[c]		2.542(13) 2.747(14)	2.404(11)	2.438(10)	86.5(4)	127.8(5)	-

a = ref. 36

b = this work

c = ref. 34

d = ref. 38

e = ref. 39

t = terminal

Table 4.3.17 NMR Parameters for $(R_3P)HgX_2$ Complexes (where X = Cl, Br or I and R = Pr, Ph and $(NCCH_2CH_2)$)

Complex	(^{31}P)/ppm (±1)	J(Hg-P) Hz (±5)	Hg-P (Å)
$(Pr_3P)HgCl_2$[a]	33.0	7389	2.358(4)
$(Pr_3P)HgBr_2$[a]	27.2	6611	2.407(4)
$CdHgI_4(PPr_3)_2$[c]	17.5	4340	2.436(24)
$\beta(Pr_3P)HgI_2$	6.2	5071	2.431(25)
$\alpha(Pr_3P)HgI_2$[a]	6.9	5053	2.406(17)
$(Ph_3P)HgCl_2$	38.8	7431	2.406(7)
$(Ph_3P)HgBr_2$[b]	36.1	6464	-
$(Ph_3P)HgI_2$[b]	12.2	4700	2.461(8) 2.483(8)
$(NCCH_2CH_2)_3PHgCl_2$[c]	33.39	-	2.393(5)
$(NCCH_2CH_2)_3PHgBr_2$[c]	29.25	-	-
$(NCCH_2CH_2)_3PHgI_2$[c]	-	-	-

All measurements relative to H_3PO_4

[a]ref. 61 solvent 20% CD_2Cl_2 in CH_2Cl_2 at 300 K

[b]ref. 63 solvent DMF at 243 K

[c]Personal communication B. Taylor (solvent acetone)

Summary

The nature of both the phosphine ligand and halogen atom play an important role in the structures adopted by $(R_3P)_nHgX_2$ complexes (where n = 1 or 2).

The 2:1 mercury(II) halide complexes all have distorted monomeric tetrahedral structures in which the σ-donor ability of the phosphine ligand plays a dominant role in the size of the P-Hg-P angles and the lengths of the Hg-P bonds (Table 4.2.7). The stronger σ-donor phosphine ligands give rise to larger P-Hg-P angles, smaller X-Hg-X angles and short Hg-P bond lengths. Insufficient data is available for any meaningful deductions concerning the effect of the halide atom as the full structures are only available for one series $(Ph_3P)_2HgX_2$ (where X = Cl, Br or I). From the limited information available the effects of the halide on the 2:1 structures appears to be a decrease in the size of the P-Hg-P angle where X varies from Cl to Br to I with a corresponding increase of the Hg-P bond lengths.

For the 1:1 mercury(II) halide complexes a variety of the gross structural types has been found, and these are summarised in Table 4.3.15. Complexes which contain strong σ-donor phosphine ligands tend to give a large number of different structures. These vary from symmetrical halogen-bridged dimers (e.g. $(Pr_3PHgCl_2)_2$) to chain polymers (e.g. $(Et_3PHgCl_2)_n$). The only weak σ-donor phosphine studied is triphenylphosphine which results in halogen-bridged dimer structures for both the iodide and chloride complexes. The only complete halide series studied is for tripropylphosphine where the structures vary from a symmetrical halogen-bridged dimer where X = Cl and Br, to an extended pentaco-ordinate iodine-bridged structure or an unusual halogen-bridged dimer, having both phosphine

ligands co-ordinated to the same mercury atom in the two forms of Pr_3PHgI_2. A complete study of the iodine analogues where R = Et, Me and ($NCCH_2CH_2$) would be necessary to provide a meaningful comparison of the effect of the halogen atom on the structures of the 1:1 mercury(II) halide tertiary phosphine complexes.

REFERENCES

1. R.W.G. Wyckoff, Crystal Structures, Vol. I, 2nd edition, Wiley (1965).
2. M. Atoji, J.E. Schirber and C.A. Swenson, J. Chem. Phys., 31, 1628 (1959).
3. B. Kamenar and A. Nagl, Acta Cryst., B32, 1414 (1976).
4. G. Bandoli, D.A. Clement, L. Sindellari and E. Tondello, J. Chem. Soc., Dalton Trans., 449 (1975).
5. A. Forbes Cameron and K.P. Forrest, J. Chem. Soc. A, 1286 (1971).
6. N.A. Bell, M. Goldstein, T. Jones and I.W. Nowell, Acta Cryst., B36, 710 (1980).
7. S. Kulpe, Z. Anorg. Chem., 349, 314 (1967).
8. A. Mitschler, J. Fischer and R. Weiss, Acta Cryst., 22, 236 (1967).
9. M. Frey, Compt. Rend., 270, 1265 (1970).
10. D. Grdenic and C. Djordjevic, J. Chem. Soc., 1316 (1956).
11. W.H. Bauer, Acta Cryst. II, 488 (1958).
12. F. Ebert and H. Woitniek, Z. Anorg. Chem., 210, 269 (1933).
13. T. Donoghue and R.S. Drago, Inorg. Chem., 1, 866 (1962).
14. D.P. Graddon, K.B. Heng and E.C. Watton, Aust. J. Chem., 19, 1801 (1966).
15. C.W. Frank and L.B. Rogers, Inorg. Chem., 5, 615 (1966).
16. N.R. Kunchur and M.R. Truter, J. Chem. Soc., 3478 (1958).
17. M. Nardelli, L. Coghi and G. Mazzoni, Gazz. Chim. Ital., 88, 235 (1958).
18. L.R. Nassimbeni and A.L. Rogers, Acta Cryst., B32, 257 (1976).
19. M.M. Rolies and C.J. DeRanter, Acta Cryst., B34, 3216 (1978).
20. C.H. MacGillavry and J.M. Bijvoet, Z. Krist., 94, 231 (1936).
21. R. Zannetti, Gazz. Chim. Ital., 90, 1428 (1960).

22. M. Nardelli, L. Cavalca and A. Braibanti, Gazz. Chim. Ital., 87, 137 (1957).

23. C.I. Branden, Arkiv. Chem., 22, 83 (1964).

24. R.C. Evans, F.G. Mann, H.S. Peiser and D. Purdie, J. Chem. Soc., 1209 (1940).

25. C.I. Branden, Arkiv. Chem., 22, 485 (1964).

26. P.D. Brotherton, P.C. Healy, C.L. Raston and A.H. White, J. Chem. Soc. Dalton, 334 (1973).

27. A.J. Canty, C.L. Raston, B.W. Skelton and A.H. White, J. Chem. Soc. Dalton, 15 (1982).

28. H. Brusset and F. Madaule-Aubry, Bull. Soc. Chim. France, 10, 3122 (1966).

29. D. Grdenic and I. Kristanovic, Arkiv. Chem., 27, 143 (1955).

30. R.G. Goel and W.O. Ogini, Inorg. Chem., 16, 8 (1977).

31. R.G. Goel, W.P. Henry and N.K. Tha, Inorg. Chem., 21, 2551 (1982).

32. F.G. Moers and J.P. Langhout, Rec. Trav. Chim. Pays Bas, 92, 996 (1973).

33. N.A. Bell, T.D. Dee, M. Goldstein and I.W. Nowell, Inorg. Chim. Acta, 38, 191 (1980).

34. N.A. Bell, M. Goldstein, T. Jones and I.W. Nowell, Inorg. Chim. Acta, 43, 81 (1980).

35. N.A. Bell, M. Goldstein, T. Jones and I.W. Nowell, Inorg. Chim. Acta, 28, L169 (1978).

36. N.A. Bell, M. Goldstein, T. Jones and I.W. Nowell, Inorg. Chim. Acta, 48 185 (1981).

37. N.A. Bell, M. Goldstein, T. Jones and I.W. Nowell, Inorg. Chim. Acta, 69, 155 (1983).

38. N.A. Bell, M. Goldstein, T. Jones, L.A. March and I.W. Nowell, Inorg. Chim. Acta, 61, 83 (1982).

39. N.A. Bell, T.D. Dee, M. Goldstein and I.W. Nowell, Inorg. Chim. Acta, 70, 215 (1983).

40. L. Fälth, Chem. Scripta., 9, 71 (1976).

41. T. Jones, Sheffield City Polytechnic, PhD Thesis (1979).

42. N.A. Bell, T.D. Dee, P.L. Goggin, M. Goldstein, R.J. Goodfellow, T. Jones, K. Kessler, D.M. McEwan and I.W. Nowell, J. Chem. Research, 2, 0201 (1981).

43. N.A. Bell, T.D. Dee, M. Goldstein, P.J. McKenna and I.W. Nowell, Inorg. Chim. Acta, 71, 135 (1983).

44. R.W. Goel, W.P. Henry and R.C. Srivastava, Inorg. Chem., 20, 1727 (1981).

45. S. Grim, D. Shah, C. Hass, J. Ressner and P. Smith, Inorg. Chim. Acta, 36, 139 (1979).

46. R. Colton and D. Dakternieks, Aust. J. Chem., 33, 1677 (1980).

47. C.A. Tolman, J. Am. Chem. Soc., 92, 2953 (1970).

48. C.A. Streuli, Anal. Chem., 32, 985 (1960).

49. S. Grim, P. Lui and R. Keiter, Inorg. Chem., 13, 342 (1974).

50. E.C. Alyea, S.A. Dias, R.G. Goel, W.O. Ogini, P. Pilon and D.W. Meek, Inorg. Chem., 17, 1697 (1978).

51. R.G. Pearson, J. Chem. Ed., 45, 581 (1968).

52. W.A. Henderson and C.A. Streuli, J. Am. Chem. Soc., 82, 5791 (1960).

53. G. Ferguson, P.J. Roberts, E.C. Alyea and M. Khan, Inorg. Chem., 17, 2965 (1978).

54. M.F.C. Ladd and R.A. Palmer, 'Structure Determination by X-ray Crystallography', Plenum Press, New York (1977).

55. W.L. Bragg, Proc. Cambridge Philos. Soc., 17, 43 (1913).

56. A.J.C. Wilson, Nature, 150, 152 (1942).

57. D. Sayre, Acta Cryst., 15, 60 (1952).

58. G.M. Sheldrick, 'Shelx 76, Program for Crystal Structure Determination', University of Cambridge (1976).

59. E.S. Raper, Personal Communication.

60. L.G. Sillen, 'Stability Constants of Metal-Ion Complexes', Chemical Society Special Publication, 17 (1964).

61. N.A. Bell, M. Goldstein, T. Jones and I.W. Nowell, Inorg. Chim. Acta, 75, 21 (1983).

62. N.A. Bell, M. Goldstein, L.A. March and I.W. Nowell, Inorg. Chim. Acta, 83, 75 (1984).

63. E.C. Alyea, S.A. Dias, R.G. Goel, W.O. Ogini, P. Pilon and D.W. Meek, Inorg. Chem., 17, 1697 (1978).

64. J. Karle and H. Hauptmann, Acta Cryst., 9, 635 (1958).

65. T.D. Dee, Sheffield City Polytechnic, PhD Thesis (1981).

66. N.W. Alcock, "The Analytical Method for Absorption Correction in Crystallographic Computing", edited by F.R. Ahmed, Munksgaard, Copenhagen (1970).

Details of Programme of Study

(a) Completed a computing course in Basic at the Polytechnic.

(b) Completed a computing course in the use of IBM 4341 computer at the Polytechnic.

(c) Attended a final year degree course of lectures on X-ray Crystallography, given by the Director of Studies.

(d) Completed the following reading study programme.

(i) Crystal Structure Analysis. J.P. Glusker and K.N. Trueblood, Oxford University Press, (1972).

(ii) X-ray Structure Determination, a Practical Guide. G.H. Stout and L.H. Jensen, Macmillan, New York, (1968).

(iii) Direct Methods in Crystallography. M.M. Woolfson, Oxford Clarendon Press, (1961).

(iv) Structure Determination by X-ray Crystallography. M.F.C. Ladd and R.A. Palmer, Plenum Press, (1977).

(v) Inorganic Chemistry, Principles of Structure and Reactivity, J.E. Huheey, Harper and Row, (1978).

(vi) The Chemistry of Zinc, Cadmium and Mercury. B.J. Aylett, Pergamon. Texts in Inorganic Chemistry Vol. 18, Pergamon Press.

Appendices

A1. Final Positional Parameters and Thermal Parameters

Anisotropic temperature factors are of the form:-

$$\exp[-2\pi^2(U_{11}h^2a^{*2} + U_{22}k^2b^{*2} + U_{33}l^2c^{*2} + 2U_{12}hka^*b^* + 2U_{13}hla^*c^* + 2U_{23}klb^*c^*] \quad 1$$

Isotropic temperature factors are of the form:

$$\exp -8\pi^2U(\sin^2\theta/\lambda^2) \quad 2$$

Table 1 Final Fractional Coordinates (Hg x 10^5; other atoms x 10^4) with Estimated Standard Deviations in Parentheses[a] for $[(2\text{-thienyl})_3P]_2HgCl_2$

	x	y	z
Hg	44386(3)	15488(2)	25479(2)
Cl(1)	2726(3)	498(1)	2070(2)
Cl(2)	3613(3)	2619(1)	1614(2)
P(1)	4303(2)	1891(1)	3969(1)
P(2)	6592(2)	1169(1)	2004(1)
C(11)	5500(9)	1340(5)	4713(6)
S(12)	5150(4)	1115(2)	5635(2)
C(13)	6690(12)	596(6)	5880(8)
C(14)	7429(13)	609(7)	5317(8)
C(15)	6783(10)	1024(7)	4635(8)
C(21)	4783(9)	2821(5)	4209(6)
S(22)	3989(4)	3524(1)	3592(2)
C(23)	4924(13)	4153(6)	4218(8)
C(24)	5875(11)	3868(6)	4890(8)
C(25)	5810(9)	3072(5)	4920(7)
C(31)	2587(8)	1791(4)	4225(5)
S(32)	2027(3)	2290(2)	4948(2)
C(33)	507(12)	1780(7)	4872(7)
C(34)	425(11)	1247(5)	4301(7)
C(35)	1597(10)	1217(5)	3913(7)
C(41)	7385	328	2451
S(42A)	6473	-299	2789
S(42B)	9009	46	2462
C(43A)	7916	-865	3019
C(43B)	8741	-751	2934
C(44A)	9125	-564	2925
C(44B)	7465	-868	3062
C(45A)	8780	80	2453
C(45B)	6576	-230	2717
C(51)	6112(9)	1016(5)	923(5)
S(52)	7229(3)	654(1)	337(2)
C(53)	5943(11)	679(5)	-535(6)
C(54)	4707(12)	970(5)	-418(6)
C(55)	4828(10)	1175(5)	431(6)
C(61)	8001	1836	2212

	x	y	z
S(62A)	9401	1822	1763
S(62B)	8056	2439	2936
C(63A)	10153	2562	2308
C(63B)	9690	2748	2835
C(64A)	9333	2794	2804
C(64B)	10294	2327	2345
C(65A)	8004	2411	2783
C(65B)	9112	1868	1779

Final Positional Parameters (x 10^4) for Hydrogen atoms

H(13)	6988	289	6446
H(14)	8445	334	5378
H(15)	7230	1086	4094
H(23)	4820	4733	4095
H(24)	6573	4194	5348
H(25)	6419	2726	5394
H(33)	-289	1871	5236
H(34)	-463	871	4154
H(35)	1728	825	3448
H(53)	6100	489	-1125
H(54)	3754	1038	-893
H(55)	3967	1430	658

Table 2 Final Thermal Parameters for Non-Hydrogen Atoms with Estimated Standard Deviations in Parentheses for $[(2\text{-thienyl})_3P]_2HgCl_2$

(a) Anisotropic temperature factors ($\times 10^4$)

	U_{11}	U_{22}	U_{33}	U_{23}	U_{13}	U_{12}
Hg	334(2)	318(2)	289(2)	-11(1)	96(2)	9(1)
Cl(1)	502(13)	412(13)	412(13)	-119(10)	120(11)	-134(10)
Cl(2)	550(13)	331(11)	398(13)	67(10)	67(11)	54(10)
P(1)	274(10)	242(10)	246(10)	-5(9)	66(8)	-6(8)
P(2)	257(10)	250(10)	305(11)	-18(9)	84(9)	-1(8)
C(11)	309(42)	326(46)	314(50)	-3(42)	94(37)	-27(37)
S(12)	763(20)	804(23)	463(17)	285(16)	253(15)	303(17)
C(13)	646(69)	539(65)	605(73)	287(57)	113(58)	139(53)
C(14)	546(65)	713(78)	602(84)	252(67)	82(60)	93(58)
C(15)	309(47)	658(76)	696(85)	371(67)	96(50)	323(50)
C(21)	334(44)	292(46)	361(50)	-60(41)	101(38)	-31(37)
S(22)	717(19)	342(13)	454(16)	21(11)	12(14)	-7(12)
C(23)	712(76)	289(55)	638(80)	99(56)	115(64)	-96(53)
C(24)	464(52)	431(56)	647(77)	-167(53)	136(53)	-134(44)
C(25)	290(40)	230(45)	643(63)	-108(44)	107(42)	-32(34)
C(31)	322(39)	209(37)	318(47)	-65(35)	28(35)	40(32)
S(32)	457(13)	461(13)	487(15)	-161(12)	189(12)	9(11)
C(33)	524(60)	707(75)	463(62)	70(59)	279(51)	163(58)
C(34)	465(56)	329(49)	652(70)	83(48)	199(51)	-85(42)
C(35)	347(46)	348(49)	569(64)	-116(46)	170(44)	21(38)
C(51)	365(43)	292(42)	268(44)	-64(36)	174(36)	-43(35)
S(52)	488(13)	451(13)	428(14)	-76(11)	207(11)	76(11)
C(53)	691(62)	333(47)	330(50)	-156(42)	174(45)	-152(46)
C(54)	575(62)	428(52)	333(51)	56(44)	76(46)	-42(47)
C(55)	472(53)	403(51)	345(52)	13(43)	153(43)	-16(42)

(b) Isotropic temperature factors ($\times 10^3$)

	U		U
C(41)	38(2)	C(61)	37(2)
S(42A), S(42B)	52(1)	S(62A), S(62B)	47(1)
C(43A), C(43B)	63(4)	C(63A), C(63B)	35(2)
C(44A), C(44B)	64(4)	C(64A), C(64B)	77(5)
C(45A), C(45B)	156(14)	C(65A), C(65B)	167(15)

Table 3 Final Fractional Coordinates for $[(NCCH_2CH_2)_3P]_2HgBr_2.OC(CH_3)_2$ (Hg x 10^5, other atoms x 10^4) with Estimated Standard Deviations in Parentheses

Atom	x	y	z
Hg	26835(7)	12825(4)	26700(2)
Br(1)	5682(2)	1215(1)	2708(1)
Br(2)	1913(4)	2934(1)	2618(1)
P(1)	2393(4)	1019(2)	3816(1)
P(2)	2351(4)	870(2)	1538(1)
C(11)	2793(18)	1971(8)	4291(6)
C(12)	4291(23)	2310(10)	4166(8)
C(13)	4628(21)	3107(9)	4503(7)
N(13)	4822(19)	3735(10)	4745(7)
C(21)	3661(19)	245(9)	4141(6)
C(22)	3604(24)	-585(9)	3747(9)
C(23)	4521(21)	-1255(10)	4034(7)
N(23)	5222(22)	-1738(9)	4254(7)
C(31)	623(18)	685(10)	4069(7)
C(32)	-647(19)	1270(14)	3853(8)
C(33)	-1919(23)	968(15)	4167(8)
N(33)	-2885(25)	764(19)	4460(10)
C(41)	3574(18)	7(8)	1381(6)
C(42)	3589(23)	-275(12)	665(7)
C(43)	4545(27)	-998(11)	582(8)
N(43)	5286(27)	-1571(12)	514(9)
C(51)	551(17)	519(9)	1258(6)
C(52)	-622(18)	1148(10)	1426(7)
C(53)	-2048(22)	869(12)	1132(8)
N(53)	-3108(19)	645(12)	891(8)
C(61)	2789(17)	1742(8)	1002(6)
C(62)	4282(21)	2120(11)	1171(9)
C(63)	4561(24)	2874(10)	790(9)
N(63)	4820(27)	3471(11)	514(9)
O	-556(28)	-332(15)	2626(9)
C(1)	-1536(39)	-882(17)	2559(13)
C(2)	-1880(45)	-1310(20)	1923(13)
C(3)	-2469(38)	-1141(26)	3087(14)

Final Positional Parameters (x 10^4) for Hydrogen atoms

	x	y	z
H(111)	2749	1820	4798
H(112)	1987	2448	4163
H(121)	4351	2415	3653
H(122)	5094	1844	4323
H(211)	3401	105	4631
H(212)	4751	503	4137
H(221)	3953	-455	3267
H(222)	2493	-814	3715
H(311)	673	655	4590
H(312)	399	62	3873
H(321)	-834	1241	3335
H(322)	-405	1914	3996
H(411)	3258	-531	1663
H(412)	4667	200	1535
H(421)	3964	247	380
H(422)	2493	-445	498
H(511)	327	-81	1481
H(512)	528	443	740
H(521)	-356	1766	1241
H(522)	-683	1182	1944
H(611)	1974	2231	1038
H(612)	2770	1508	512
H(621)	5105	1652	1082
H(622)	4344	2289	1676

Table 4 Final Anisotropic Thermal Parameters for Non-Hydrogen Atoms with Estimated Standard Deviations in Parentheses for $[(NCCH_2CH_2)_3P]_2HgBr_2.OC(CH_3)_2$

	U_{11}	U_{22}	U_{33}	U_{23}	U_{13}	U_{12}
Hg	501(4)	405(3)	210(2)	-11(3)	35(2)	12(4)
Br(1)	43(11)	978(13)	385(7)	-18(9)	15(6)	3(11)
Br(2)	1643(27)	410(9)	519(10)	11(8)	36(12)	303(12)
P(1)	410(25)	315(17)	212(14)	1(11)	59(13)	14(14)
P(2)	422(26)	318(16)	221(14)	-14(12)	40(13)	-22(15)
C(11)	481(110)	303(70)	402(69)	-31(54)	100(59)	-42(65)
C(12)	638(150)	436(90)	517(86)	-83(66)	118(78)	-123(85)
C(13)	700(131)	336(74)	397(71)	-86(59)	-94(67)	-143(73)
N(13)	960(132)	485(78)	598(76)	-117(77)	54(71)	-171(97)
C(21)	531(119)	361(73)	293(63)	83(55)	5(58)	19(69)
C(22)	774(160)	252(67)	747(106)	-64(70)	-52(91)	107(78)
C(23)	825(134)	301(74)	513(80)	30(71)	90(75)	207(92)
N(23)	1056(161)	454(83)	554(84)	19(68)	-1(83)	94(91)
C(31)	366(107)	406(76)	526(82)	118(63)	110(64)	39(65)
C(32)	440(116)	691(102)	641(94)	12(96)	180(74)	96(110)
C(33)	297(130)	1283(179)	502(94)	265(99)	4(75)	-24(105)
N(33)	585(165)	1942(251)	824(133)	437(148)	15(104)	-140(150)
C(41)	557(116)	317(64)	294(81)	43(49)	71(78)	50(65)
C(42)	714(149)	606(104)	356(82)	-237(75)	161(77)	32(94)
C(43)	922(192)	449(91)	528(92)	-170(71)	237(93)	-146(103)
N(43)	1324(220)	574(98)	869(132)	-130(87)	438(123)	155(115)
C(51)	353(102)	516(86)	382(66)	-37(57)	40(55)	76(68)
C(52)	473(106)	450(94)	471(71)	-110(67)	-19(59)	-108(76)
C(53)	554(139)	755(108)	470(84)	-150(76)	60(76)	30(91)
N(53)	413(114)	1167(131)	656(93)	-289(91)	-11(73)	89(91)
C(61)	577(109)	281(64)	323(64)	80(51)	20(57)	40(61)
C(62)	465(130)	490(94)	659(106)	243(81)	39(80)	-33(80)
C(63)	657(155)	444(87)	634(117)	150(83)	97(93)	-54(83)
N(63)	1311(209)	578(106)	846(124)	211(87)	30(114)	-329(103)
O	1601(226)	1333(169)	933(124)	42(115)	483(125)	-61(149)
C(1)	1174(263)	860(160)	960(174)	275(133)	197(155)	268(165)
C(2)	2733(419)	1046(191)	924(166)	-241(167)	576(193)	-191(259)
C(3)	1246(280)	2334(379)	1107(195)	253(213)	426(176)	-261(245)

Table 5 Final Fractional Coordinates ($\times 10^4$) with Estimated Standard Deviations in Parentheses for $[(NCCH_2CH_2)_3P]_2HgCl_2$

	Molecule 1			Molecule 2		
	x	y	z	x	y	z
Hg	1638(1)	1948(2)	4198(1)	6578(0)	2437(2)	2564(1)
Cl(1)	1606(5)	-721(11)	4683(4)	7244(4)	1005(11)	2132(4)
Cl(2)	2215(4)	3363(14)	5228(4)	6806(4)	5281(11)	2385(5)
P(1)	2256(4)	1341(12)	3692(4)	7179(3)	1856(10)	3608(3)
P(2)	724(4)	3050(14)	4100(4)	5706(3)	2188(11)	1622(3)
C(11)	2526	-683	3827	7482	-116	3717
C(12)	2030	-1759	3526	7068	-1378	3361
C(13)	2308	-2934	3851	6712	8508	3556
N(13)	2454	-4258	4183	6372	7864	3828
C(21)	1906	1497	2849	7858	2999	3934
C(22)	1741	3003	2582	8131	3036	3517
C(23)	1445	3828	2812	8630	3979	3758
N(23)	1163	4674	3022	9131	4322	4125
C(31)	2886	2434	3896	6890	-8001	4160
C(32)	3223	2437	4631	6768	-6546	4263
C(33)	3711	3585	4795	6329	-5792	3897
N(33)	4117	4336	5017	5869	-5518	3414
C(41)	118	3060	3377	5427	265	1383
C(42)	-201	1525	3072	5881	-929	1514
C(43)	160	877	3126	5697	-2320	1148
N(43)	606	4	2942	5556	-3392	903

Cont.

	x	y	z	x	y	z
C(51)	852	5327	4155	5052	3109	1611
C(52)	627	5593	4510	5164	4579	1841
C(53)	307	6464	4035	4769	5510	1942
N(53)	-203	6997	3204	4340	5382	2089
C(61)	447	2158	4577	5941	2989	1063
C(62)	908	2500	5166	5449	3004	406
C(63)	819	1509.	5353	5740	3652	39
N(63)	638	700	5844	5916	4264	-277

Table 6 Final Thermal Parameters for Non-Hydrogen Atoms with Estimated Standard Deviations in Parentheses for $[(NCCH_2CH_2)_3P]_2HgCl_2$

Anisotropic Thermal Parameters ($x10^4$)

	Molecule 1						Molecule 2					
	U_{11}	U_{22}	U_{33}	U_{23}	U_{13}	U_{12}	U_{11}	U_{22}	U_{33}	U_{23}	U_{13}	U_{12}
Hg	605(8)	812(10)	577(8)	16(8)	273(7)	51(8)	524(7)	723(8)	432(6)	7(7)	197(5)	22(7)
Cl(1)	1289(88)	809(70)	577(58)	104(53)	409(59)	69(64)	682(59)	967(70)	871(61)	-50(54)	461(52)	98(53)
Cl(2)	891(74)	1334(101)	855(69)	-391(70)	249(58)	-417(73)	939(68)	661(64)	1115(76)	-22(56)	472(61)	-134(54)
P(1)	623(58)	819(72)	568(59)	57(53)	234(48)	-14(53)	554(50)	690(59)	370(43)	53(45)	149(39)	14(49)
P(2)	559(60)	1156(92)	663(57)	-1(61)	207(49)	184(62)	579(52)	678(64)	454(43)	-6(47)	220(41)	70(49)

Isotropic Thermal Parameters (x 10^4)

	Molecule 1	Molecule 2		Molecule 1	Molecule 2
C(11)	988(138)	1384(175)	C(41)	1212(134)	630(85)
C(12)	1122(132)	1110(140)	C(42)	2554(357)	1168(162)
C(13)	2179(305)	2671(347)	C(43)	2145(316)	1051(126)
N(13)	2198(293)	3335(350)	N(43)	2224(209)	1096(90)
C(21)	1252(151)	1418(141)	C(51)	1505(170)	760(90)
C(22)	1001(137)	1288(134)	C(52)	4628(1317)	1343(153)
C(23)	1618(265)	1660(140)	C(53)	2425(265)	1993(309)
N(23)	1751(170)	2765(139)	N(53)	3571(322)	2586(422)
C(31)	1003(113)	1442(180)	C(61)	1814(170)	640(88)
C(32)	973(115)	1526(270)	C(62)	1862(234)	837(105)
C(33)	1235(172)	1907(333)	C(63)	2231(547)	943(112)
N(33)	1905(167)	2967(319)	N(63)	2528(287)	1403(134)

Table 7 Final Fractional Coordinates for $[(NCCH_2CH_2)_3PHgCl_2]_n$ (Hg x 10^5; other atoms x 10^4) with Estimated Standard Deviations in Parentheses

Atom	x	y	z
Hg	-520(4)	14470(14)	4988(18)
Cl(1)	197(4)	4615(10)	1767(15)
Cl(2)	-1139(3)	1754(17)	-84(15)
P	1072(3)	960(8)	250(12)
C(11)	1469(12)	414(25)	1932(31)
C(12)	1326(9)	1692(28)	3403(31)
C(13)	1746(14)	1306(31)	4749(31)
N(13)	2074(13)	1038(29)	5689(33)
C(21)	1293(11)	-819(26)	-1191(28)
C(22)	933(14)	-2443(31)	-801(33)
C(23)	283(15)	-2267(36)	-1467(39)
N(23)	-235(14)	-2333(33)	-1654(32)
C(31)	1436(10)	2910(27)	-555(33)
C(32)	2173(10)	2809(27)	-796(29)
C(33)	2389(12)	4279(34)	-1558(36)
N(33)	2516(20)	5568(32)	-2147(36)

Final hydrogen positions (x10^4)

	x	y	z
H(111)	1977	428	1695
H(112)	1324	-856	2264
H(121)	833	1549	3761
H(122)	1409	2989	3033
H(211)	1801	-1059	-1122
H(212)	1170	-424	-2367
H(221)	906	-2607	456
H(222)	1173	-3525	-1316
H(311)	1336	3945	244
H(312)	1216	3171	-1677
H(321)	2287	1708	-1502
H(322)	2406	2701	331

Table 8 Final Thermal Parameters for $[(NCCH_2CH_2)_3PHgCl_2]_n$ with Estimated Standard Deviations in Parentheses

Anisotropic Thermal Parameters

	U_{11}	U_{22}	U_{33}	U_{23}	U_{13}	U_{12}
Hg	261(4)	433(5)	441(6)	11(7)	15(5)	25(4)
Cl(1)	540(38)	431(38)	768(81)	-62(48)	10(44)	100(32)
Cl(2)	319(30)	1133(95)	785(102)	34(71)	-7(34)	11(42)
P	278(25)	302(31)	442(61)	42(33)	-19(30)	-48(21)
C(11)	465(127)	134(101)	488(242)	-43(127)	-136(134)	73(90)
C(12)	195(85)	452(185)	490(209)	11(158)	127(109)	27(97)
C(13)	572(147)	559(193)	359(238)	-31(199)	-254(155)	-63(153)
C(21)	371(110)	236(105)	202(158)	-47(11)	73(107)	18(91)
C(23)	353(159)	1170(465)	2202(930)	-840(560)	60(300)	-305(225)
N(23)	648(171)	1171(307)	636(317)	-696(257)	-119(173)	-264(189)
C(33)	269(123)	899(338)	844(394)	145(294)	-110(161)	-128(152)
N(33)	1398(384)	796(265)	1072(511)	841(347)	-451(340)	-646(278)

Isotropic Thermal Parameters

	U		U
C(22)	498(79)	C(31)	347(52)
C(32)	320(55)	N(13)	590(80)

Table 9 Final Fractional Coordinates for $[Ph_3PHgI_2]_2$ ($\times 10^4$) with Estimated Standard Deviations in Parentheses

	x	y	z
Hg1	6775(1)	1399(1)	8340(1)
Hg2	8118(1)	923(1)	6831(1)
I1	6949(1)	36(2)	9479(1)
I2	6766(1)	-187(2)	7162(1)
I3	8141(1)	2511(2)	7999(1)
I4	7928(1)	2166(2)	5641(1)
P1	6002(3)	3138(8)	8177(3)
C11	5204(13)	2975(36)	8698(13)
C12	4907(16)	2050(42)	8774(18)
C13	4307(16)	1887(51)	9184(20)
C14	4029(12)	2803(45)	9463(16)
C15	4347(16)	3951(41)	9400(15)
C16	4943(13)	4029(38)	9070(14)
C21	6466(13)	4491(35)	8392(15)
C22	6836(17)	4474(36)	9013(17)
C23	7145(22)	5395(64)	9264(26)
C24	7151(27)	6484(57)	8828(27)
C25	6741(27)	6493(62)	8106(29)
C26	6405(19)	5316(41)	8010(20)
C31	5712(11)	3213(30)	7302(12)
C32	5022(12)	3384(35)	7114(15)
C33	4825(17)	3439(31)	6414(17)
C34	5308(17)	3250(30)	5878(14)
C35	6033(15)	3227(28)	6043(14)
C36	6208(12)	3200(29)	6776(14)
P2	8949(3)	-749(8)	7026(4)
C41	9278(12)	-812(31)	7938(13)
C42	8826(16)	-672(36)	8416(16)
C43	9020(21)	-863(33)	9183(15)
C44	9738(24)	-1033(51)	9279(18)

C45	10196(21)	-1197(34)	8773(21)
C46	9968(13)	1016(35)	8028(17)
C51	9673(12)	-559(30)	6445(11)
C52	9974(16)	530(47)	6339(18)
C53	10505(19)	675(38)	5874(21)
C54	10821(18)	-317(43)	5588(17)
C55	10563(14)	-1457(45)	5668(14)
C56	9930(15)	-1573(43)	6058(19)
C61	8553(14)	-2130(30)	6834(13)
C62	8595(18)	-3050(40)	7240(18)
C63	8261(26)	-4251(55)	7115(29)
C64	7978(29)	-4247(63)	6475(28)
C65	7881(21)	-3545(78)	6038(26)
C66	8154(26)	-2254(38)	6196(18)

Final Hydrogen Positions (x 10^4)

	x	y	z
H12	5116	1286	8498
H13	4104	998	9279
H14	3539	2727	9728
H15	4112	4740	9627
H16	5227	4865	9075
H22	6814	3678	9335
H23	7436	5326	9748
H24	7440	7243	9027
H25	6679	7240	7750
H26	6073	5179	7559
H32	4636	3474	7517
H33	4288	3601	6281
H34	5130	3127	5346
H35	6421	3270	5640
H36	6747	3108	6925
H42	8306	-402	8275
H43	8647	-899	9604
H44	9938	-1022	9809
H45	10724	-1442	8896
H46	10325	-1061	7597
H52	9804	1289	6645
H53	10667	1563	5716
H54	11287	-205	5284
H55	10833	-2233	5469
H56	9643	-2406	6037
H62	8935	-2973	7690
H63	8241	-4921	7523
H64	7824	-5136	6308
H65	7590	-3691	5560
H66	8070	-1515	5839

Table 10 Final Thermal Parameters for $[Ph_3PHgI_2]_2$ with Estimated Standard Deviations in Parentheses

Anisotropic Thermal Parameters

	U_{11}	U_{22}	U_{33}	U_{12}	U_{13}	U_{23}
Hg1	457(6)	536(14)	652(6)	99(6)	17(5)	97(6)
Hg2	425(6)	604(15)	720(7)	47(6)	22(5)	102(6)
I1	764(13)	740(22)	543(9)	101(10)	3(9)	-16(13)
I2	478(9)	643(22)	672(10)	-116(10)	74(8)	-222(10)
I3	430(9)	542(22)	805(12)	-117(11)	59(8)	-122(10)
I4	549(11)	781(23)	685(11)	136(11)	108(8)	106(12)
P1	365(32)	422(75)	652(38)	41(38)	66(28)	70(35)
C11	324(138)	634(362)	610(149)	50(175)	-99(115)	92(171)
C12	485(176)	901(439)	1055(241)	-116(240)	170(164)	-211(218)
C13	456(174)	1872(550)	1447(327)	-719(343)	498(207)	-512(258)
C14	185(128)	1546(478)	819(195)	-43(241)	143(127)	-88(203)
C15	528(181)	1053(408)	782(188)	-316(210)	89(146)	000(221)
C16	304(128)	1069(385)	800(190)	7(205)	98(126)	63(172)
C21	334(130)	1083(358)	802(180)	553(206)	197(125)	134(169)
C22	863(229)	216(326)	950(227)	-342(195)	-213(177)	-108(207)
C23	797(276)	2611(796)	1162(357)	-111(456)	226(256)	808(382)
C31	333(117)	750(274)	528(132)	43(145)	-68(100)	-2(139)
C32	237(118)	1325(385)	856(188)	-44(206)	44(122)	164(172)
C33	766(207)	568(316)	947(214)	277(196)	-408(182)	0(199)
C34	971(229)	642(306)	507(141)	83(151)	-208(149)	380(210)
C35	731(185)	251(277)	721(169)	170(150)	-115(144)	-138(170)
C36	334(126)	792(309)	911(196)	356(188)	160(128)	346(156)
P2	306(30)	498(76)	639(37)	-80(39)	-2(27)	2(35)
C41	336(124)	707(299)	612(150)	50(160)	-7(110)	25(146)
C42	634(187)	1038(396)	866(206)	-464(215)	-6(163)	218(206)
C43	1267(316)	600(340)	593(171)	-244(177)	-160(185)	363(259)
C44	1277(373)	2129(619)	567(198)	-589(282)	-83(231)	-356(400)
C45	1050(278)	384(359)	1272(296)	123(243)	-739(249)	-140(236)
C46	298(127)	952(362)	1088(239)	246(222)	-26(144)	55(170)

	U_{11}	U_{22}	U_{33}	U_{12}	U_{13}	U_{23}
C51	371 (128)	351 (303)	488 (126)	-137 (140)	27 (101)	299 (155)
C52	516 (186)	1548 (500)	930 (232)	-200 (265)	54 (163)	-444 (260)
C53	1039 (297)	236 (336)	1696 (350)	-266 (260)	833 (265)	-26 (222)
C54	708 (219)	1051 (471)	805 (210)	-41 (231)	261 (172)	-234 (259)
C55	338 (143)	1394 (476)	610 (162)	-44 (210)	-71 (121)	39 (211)
C56	381 (152)	1337 (459)	1251 (279)	243 (288)	6 (174)	96 (217)
C65	729 (258)	3381 (979)	1300 (370)	-91 (528)	-479 (254)	364 (421)
C66	2171 (487)	326 (344)	917 (250)	-216 (217)	-480 (275)	-87 (324)

Isotropic Thermal Parameters

	U
C24	1504 (202)
C25	1564 (209)
C26	892 (105)
C61	584 (71)
C62	937 (110)
C63	1488 (191)
C64	1501 (205)

Table 11 Final Fractional and Thermal Parameters for $[\beta Pr_3PHgI_2]_2$ ($\times 10^4$) with Estimated Standard Deviations in Parentheses

	x	y	z
Hg1	6109(2)	1511(2)	6051(1)
Hg2	2373(2)	2357(2)	5958(1)
I1	4608(4)	2804(3)	6798(2)
I2	3685(4)	946(3)	5281(2)
I3	764(4)	1423(3)	6601(2)
I4	1739(5)	3917(3)	5270(3)
P1	6478(15)	99(11)	6719(7)
P2	6946(15)	2768(11)	5454(7)
C11	7831(55)	-643(44)	6468(25)
C12	8187(76)	-1455(57)	6989(34)
C13	8949(108)	-2100(85)	6746(48)
C21	5102(50)	-709(37)	6617(23)
C22	4008(59)	-250(46)	6902(25)
C23	2949(75)	-1009(57)	6827(34)
C31	6630(56)	453(44)	7500(24)
C32	7979(49)	1024(39)	7633(24)
C33	8064(65)	1277(47)	8325(30)
C41	7320(77)	3895(62)	5881(35)
C42	8265(60)	3736(48)	6418(28)
C43	8680(111)	4712(92)	6665(47)
C51	8188(56)	2555(45)	5102(25)
C52	8327(53)	1539(41)	4958(25)
C53	9363(89)	1446(63)	4674(38)
C61	5464(83)	3108(72)	4799(39)
C62	5796(77)	3922(63)	4422(36)
C63	4677(85)	3885(65)	3853(40)

Anisotropic Thermal Parameters

	U_{11}	U_{22}	U_{33}	U_{23}	U_{13}	U_{12}
Hg1	84(2)	55(2)	85(2)	11(1)	17(1)	-1(1)
Hg2	81(2)	72(2)	97(2)	6(1)	14(2)	-5(1)
I1	80(3)	91(3)	100(3)	-6(2)	10(2)	-10(2)
I2	80(3)	74(2)	67(2)	-17(2)	6(2)	-7(2)
I3	94(3)	103(3)	112(4)	17(3)	38(3)	-4(3)
I4	140(4)	82(3)	171(5)	54(3)	26(4)	5(3)
P1	80(11)	67(10)	85(10)	18(8)	13(9)	-4(8)
P2	67(10)	72(11)	91(11)	18(9)	-1(9)	-1(8)

Isotropic Thermal Parameters

	U		U		U
C11	9(2)	C21	8(2)	C31	9(2)
C12	13(3)	C22	10(2)	C32	8(2)
C13	20(4)	C23	13(3)	C33	11(2)
C41	14(3)	C51	9(2)	C61	16(3)
C42	10(2)	C52	8(2)	C62	14(3)
C43	21(5)	C53	15(3)	C63	16(3)

Table 12 Final Fractional and Thermal Parameters for $[Pr_3PHgCl_2]_2$ with Estimated Standard Deviations in Parentheses

Final Positional Parameters (Hg x 10^5, other atoms x 10^4)

$[Pr_3PHgCl_2]_2$ with Estimated Standard Deviations in Parentheses

(i) Non-hydrogen atoms

	x	y	z
Hg	-7296(0)	37958(1)	-3011(0)
C11	-1593(3)	4242(5)	683(3)
C12	456(2)	4031(4)	1089(4)
P	-451(2)	2811(4)	-1680(3)
C11	508(8)	2987(16)	-1782(14)
C12	1055(10)	2399(22)	-1056(18)
C13	1810(10)	2499(31)	-1303(28)
C21	-992(9)	3408(17)	-2786(12)
C22	-1772(11)	3525(20)	-2786(17)
C23	-2223(20)	4065(27)	-3772(25)
C31	-642(13)	1228(14)	-1694(18)
C32	-1274(17)	882(22)	-1270(26)
C33	-1386(16)	-394(22)	-1209(23)

(ii) Hydrogen atoms

	x	y	z
H111	631	3919	-1739
H112	564	2656	-2493
H121	1063	2800	-348
H122	911	1478	-1027
H131	2207	2053	-749
H132	1959	3419	-1330
H133	1807	2096	-2009
H211	-933	2828	-3383
H212	-779	4273	-2903
H221	-1993	2661	-2681

	x	y	z
H222	-1846	4093	-2185
H231	-2798	4129	-3726
H232	-2165	3501	-4380
H233	-2012	4933	-3884
H311	-160	789	-1289
H312	-742	935	-2448
H321	-1197	1240	-537
H322	-1764	1258	-1714
H331	-1863	-562	-888
H332	-905	-789	-759
H333	-1472	-771	-1937

Anisotropic Thermal Parameters ($\AA^2 \times 10^4$ for Hg, Cl, P, $\times 10^3$ for carbon atoms)

	U_{11}	U_{22}	U_{33}	U_{23}	U_{13}	U_{12}
Hg	648(6)	524(5)	503(6)	-40(3)	163(4)	36(3)
Cl1	610(27)	730(29)	652(28)	38(24)	240(23)	71(22)
Cl2	580(25)	550(24)	640(27)	86(21)	31(21)	24(19)
P	488(23)	472(23)	529(25)	-80(20)	150(20)	13(19)
C11	37(8)	56(10)	78(12)	-6(9)	4(9)	3(8)
C12	58(12)	94(16)	104(17)	1(13)	22(12)	11(11)
C13	27(9)	144(25)	216(34)	-19(24)	20(14)	10(12)
C21	47(9)	86(12)	33(8)	-2(9)	5(7)	-15(9)
C22	56(11)	100(17)	79(14)	18(13)	6(10)	16(11)
C23	127(25)	119(24)	125(26)	33(20)	-1(20)	7(18)
C31	77(13)	47(10)	88(14)	-7(9)	31(11)	-7(9)
C32	120(22)	84(16)	172(30)	-19(18)	85(22)	-32(15)
C33	140(23)	66(14)	189(31)	-29(17)	101(23)	-16(15)

Table 13 Final Fractional and Thermal Parameters for $[Pr_3PHgBr_2]_2$

Final Fractional Coordinates (Hg x 10^5; other atoms x 10^4) for $[Pr_3PHgBr_2]_2$ with Estimated Standard Deviations in Parentheses

(i) Non-hydrogen atoms

	x	y	z
Hg	-16426(1)	52282(1)	38966(0)
Br1	-3155(2)	3161(2)	3827(2)
Br2	443(2)	3661(2)	4180(1)
P	-1812(4)	7871(4)	3463(3)
C11	-2632(15)	8877(16)	3984(10)
C12	-3943(17)	8287(22)	3752(13)
C13	-4623(19)	9126(25)	4191(16)
C21	-290(13)	8774(15)	3802(9)
C22	462(15)	8110(19)	3349(10)
C23	1661(16)	9002(23)	3580(12)
C31	-2684(14)	8132(16)	2283(9)
C32	-2838(17)	9830(19)	1987(11)
C33	-3613(15)	9966(20)	985(11)

(ii) Hydrogen Atoms

	x	y	z
H111	-2709	10060	3786
H112	-2079	8792	4696
H121	-3867	7102	3947
H122	-4498	8376	3040
H131	-5549	8631	3989
H132	-4720	10313	3998
H133	-4090	9039	4905
H211	250	8636	4511
H212	-439	9975	3643
H221	-109	8142	2638

	x	y	z
H222	703	6941	3561
H231	2176	8503	3248
H232	2239	8970	4290
H233	1427	10172	3367
H311	-3615	7644	2072
H312	-2195	7537	1962
H321	-1914	10322	2176
H322	-3312	10442	2313
H331	-3707	9966	985
H332	-4540	9480	793
H333	-3142	9359	656

Anisotropic Thermal Parameters ($\AA^2 \times 10^4$ for Hg, Br, P; $\times 10^3$ for all carbon atoms) with Estimated Standard Deviations in Parentheses

	U_{11}	U_{22}	U_{33}	U_{23}	U_{13}	U_{12}
Hg	828(5)	549(3)	603(4)	13(4)	284(4)	22(5)
Br1	1065(18)	720(11)	1537(21)	-71(13)	575(16)	-189(12)
Br2	850(14)	993(12)	501(11)	52(10)	311(10)	288(12)
P	546(29)	524(21)	574(27)	35(21)	231(24)	51(22)
C11	75(13)	62(9)	71(12)	18(9)	41(11)	8(10)
C12	79(15)	123(16)	149(19)	-11(14)	80(15)	13(14)
C13	123(18)	169(21)	240(28)	-26(20)	130(20)	-14(18)
C21	67(12)	60(9)	45(10)	23(8)	10(9)	14(9)
C22	66(13)	101(12)	78(13)	-5(10)	51(11)	-12(11)
C23	78(15)	140(18)	125(18)	-14(15)	52(14)	-15(14)
C31	64(12)	81(11)	61(11)	5(9)	24(10)	7(10)
C32	115(15)	96(13)	64(12)	29(11)	33(11)	31(13)
C33	92(15)	130(16)	90(16)	43(13)	23(12)	6(14)

Table 14 Final Fractional Parameters of $(Pr_3P)_2Hg(\mu\text{-}I)_2CdI_2$ (Hg, Cd, I x 10^5; other atoms x 10^4) with Estimated Standard Deviations in Parentheses

Atom	x	y	z
Hg	38275(5)	15282(4)	89433(2)
Cd	75301(10)	23481(8)	90295(5)
I(1)	62807(9)	9624(7)	97105(4)
I(2)	53776(10)	28099(9)	81895(5)
I(3)	92599(11)	14569(9)	84250(5)
I(4)	82386(14)	39229(10)	97022(7)
P(1)	3529(4)	127(3)	8290(2)
P(2)	3068(4)	2818(3)	9533(2)
C(11)	2200(15)	-611(10)	8471(6)
C(12)	1882(19)	-1464(14)	8056(9)
C(13)	984(28)	-2118(19)	8222(11)
C(21)	3231(13)	474(11)	7518(6)
C(22)	2062(16)	1038(12)	7378(7)
C(23)	1756(19)	1291(14)	6693(8)
C(31)	4947(16)	-649(11)	8348(7)
C(32)	6017(15)	-271(12)	8069(7)
C(33)	7112(17)	-966(14)	8137(8)
C(41)	1672(15)	2490(14)	9884(8)
C(42)	1614(19)	1505(15)	10081(9)
C(43)	452(18)	1268(15)	10381(8)
C(51)	2699(24)	3916(14)	9113(9)
C(52)	1812(21)	3847(17)	8597(10)
C(53)	1048(26)	4787(18)	8272(11)
C(61)	4305(23)	3128(20)	10130(11)
C(62)	4196(29)	3820(23)	10513(14)
C(63)	5330(24)	3774(19)	11094(11)

Atom	x	y	z
H(111)	1381	-150	8454
H(112)	2417	-888	8921
H(121)	2741	-1864	8024
H(122)	1540	-1178	7620
H(131)	845	-2687	7891
H(132)	106	-1742	8250
H(133)	1306	-2428	8654
H(211)	3165	-175	7248
H(212)	4011	909	7405
H(221)	1289	621	7516
H(222)	2152	1708	7628
H(231)	893	1702	6627
H(232)	1652	630	6435
H(233)	2515	1716	6547
H(311)	4685	-1336	8139
H(312)	5248	-761	8819
H(321)	5735	-155	7597
H(322)	6308	409	8278
H(331)	7884	-664	7926
H(332)	6831	-1647	7926
H(333)	7403	-1083	8608
H(411)	861	2621	9563
H(412)	1629	2953	10270
H(421)	1632	1038	9696
H(422)	2430	1364	10397
H(431)	480	516	10516
H(432)	-376	1396	10070
H(433)	422	1723	10771
H(511)	3565	4188	8970
H(512)	2337	4433	9413

H(521)	2214	3384	8279
H(522)	976	3511	8733
H(531)	735	4626	7890
H(532)	2221	5137	8121
H(533)	983	5263	8574
H(611)	5124	3303	9908
H(612)	4484	2476	10392
H(621)	4256	4508	10287
H(622)	3292	3759	10681
H(631)	5202	4361	11400
H(632)	6239	3839	10931
H(633)	5275	3091	11325

Table 15 Final Thermal Parameters for $(Pr_3P)_2Hg(\mu\text{-}I)_2CdI_2$ with Standard Deviations in Parentheses

Anisotropic Thermal Parameters (C x 10^3, other atoms x 10^4)

Atom	U_{11}	U_{22}	U_{33}	U_{23}	U_{13}	U_{12}
Hg	752(4)	601(4)	703(4)	-84(3)	256(3)	4(3)
Cd	643(6)	656(7)	770(7)	-15(6)	260(6)	41(5)
I(1)	712(6)	791(7)	636(6)	167(5)	156(5)	42(5)
I(2)	748(7)	989(8)	922(7)	438(6)	216(6)	18(6)
I(3)	851(7)	1048(9)	995(8)	-172(7)	426(6)	50(7)
I(4)	1308(12)	887(9)	1738(14)	-498(9)	410(10)	-19(8)
P(1)	744(26)	677(24)	624(23)	-109(20)	185(20)	21(21)
P(2)	764(26)	736(27)	858(28)	-181(23)	238(23)	45(23)
C(11)	101(12)	71(10)	77(10)	-18(8)	27(9)	-25(9)
C(12)	115(15)	113(15)	119(15)	-39(13)	34(13)	-38(13)
C(13)	318(36)	169(25)	178(24)	-77(20)	164(25)	-128(27)
C(21)	60(91)	93(11)	67(9)	-7(8)	17(7)	16(9)
C(22)	100(13)	77(11)	111(13)	20(10)	36(11)	5(10)
C(23)	129(16)	121(16)	102(14)	13(12)	22(12)	-5(13)
C(31)	110(13)	67(10)	73(10)	-21(8)	10(9)	19(10)
C(32)	86(11)	85(12)	82(11)	-13(9)	27(9)	9(10)
C(33)	103(14)	125(16)	124(15)	-17(13)	15(12)	26(14)
C(41)	75(11)	106(14)	134(15)	-12(13)	44(11)	15(10)
C(42)	119(16)	126(17)	109(14)	21(13)	61(12)	16(14)
C(43)	115(15)	159(20)	106(14)	49(14)	30(12)	3(14)
C(51)	181(23)	95(15)	122(17)	-13(13)	35(17)	48(16)
C(52)	132(19)	126(19)	147(21)	14(16)	12(16)	-7(16)
C(53)	227(31)	112(19)	220(28)	5(19)	-56(23)	72(20)
C(61)	98(15)	206(25)	196(22)	-114(20)	34(15)	-11(16)
C(62)	212(24)	210(25)	183(24)	-28(21)	46(19)	-31(20)
C(63)	165(23)	168(23)	174(21)	-23(17)	-9(18)	-78(20)

Table 16 Final Fractional and Thermal Parameters ($\times 10^4$) for $[\alpha Pr_3PHgI_2]_n$ with Estimated Standard Deviations in Parentheses

Final Fractional Coordinates (Hg $\times 10^5$, other atoms $\times 10^4$)

	x	y	z
Hg	27729(4)	47693(2)	4650(2)
I1	4289(7)	6567(3)	392(3)
I2	573(6)	4308(4)	-1184(3)
P	3500(24)	3720(15)	1844(11)

Anisotropic Thermal Parameters ($\AA^2 \times 10^4$ for Hg, I; $\times 10^3$ for P)

	U_{11}	U_{22}	U_{33}	U_{23}	U_{13}	U_{12}
Hg	1384(28)	1092(22)	941(19)	248(16)	37(17)	-308(20)
I1	1504(42)	963(30)	1077(31)	-156(23)	671(30)	-353(29)
I2	1061(34)	1267(38)	956(28)	-126(25)	92(24)	-147(29)
P	113(15)	122(15)	88(10)	7(10)	11(10)	27(12)

Table 17 Torsion Angles for the 2:1 Complex $[(NCCH_2CH_2)_3P]_2HgCl_2$

	Angle (°) with E.S.D's in Parenthesis	
	Dimer I	Dimer II
P1-C11-C12-C13	160.8(4.8)	178.4(1.3)
P1-C21-C22-C23	48.9(6.2)	176.9(3.2)
P1-C31-C32-C33	171.3(3.1)	85.7(10.9)
P2-C41-C42-C43	56.5(7.8)	158.3(3.3)
P2-C51-C52-C53	120.9(7.6)	173.9(5.1)
P2-C61-C62-C63	151.3(8.0)	178.7(2.4)

Table 18 Torsion angles for 1:1 $(R_3P)HgX_2$ complexes

(a) Pr_3PHgCl_2

	Angle (°) with E.S.D's in Parenthesis
Cl2-Hg1-P1-C11	25.8(0.7)
Cl2-Hg1-P1-C21	144.2(0.6)
Cl2-Hg1-P1-C31	96.3(0.8)
Cl2*-Hg1-P1-C11	65.2(0.6)
Cl2*-Hg1-P1-C21	53.3(0.6)
Cl2*-Hg1-P1-C31	172.8(0.8)
Cl1-Hg1-P1-C11	176.5(0.7)
Cl1-Hg1-P1-C21	65.1(0.7)
Cl1-Hg1-P1-C31	54.4(0.9)
Hg1-P1-C31-C32	0.7(24.1)
Hg1-P1-C21-C22	48.5(22.0)
Hg1-P1-C11-C12	69.4(1.6)
P1-C31-C32-C33	151.6(22.0)
P1-C21-C22-C23	179.5(1.7)
P1-C11-C12-C13	173.1(1.7)
C11-P1-C21-C22	170.6(1.4)
C11-P1-C31-C32	124.2(24.0)
C21-P1-C31-C32	122.2(24.0)

(b) Pr_3PHgBr_2

Br2-Hg1-P1-C11	143.4(0.6)
Br2-Hg1-P1-C21	24.2(0.6)
Br2-Hg1-P1-C31	97.5(0.6)
Br2*-Hg1-P1-C11	53.9(0.6)

	Angle (°) with E.S.D's in Parenthesis
Br2*-Hg1-P1-C21	65.3(0.5)
Br2*-Hg1-P1-C31	173.1(0.6)
Br1-Hg1-P1-C11	55.6(0.6)
Br1-Hg1-P1-C21	174.8(0.5)
Br1-Hg1-P1-C31	63.5(0.6)
Hg1-P1-C11-C12	59.0(1.3)
Hg1-P1-C -C22	65.0(1.2)
Hg1-P1-C31-C32	178.5(1.0)
P1-C11-C12-C13	179.8(1.4)
P1-C21-C22-C23	174.2(1.1)
P1-C31-C32-C33	178.5(1.2)
C11-P1-C21-C22	175.4(1.1)
C11-P1-C31-C32	58.9(1.3)
C21-P1-C31-C32	56.8(1.3)

(c) Pr_3PHgI_2

I1-Hg1-P1-C11	167.1(1.5)
I1-Hg1-P1-C21	54.7(1.7)
I1-Hg1-P1-C31	36.8(2.6)
I2-Hg1-P1-C11	130.7(1.5)
I2-Hg1-P1-C21	7.5(1.7)
I2-Hg1-P1-C31	98.9(2.6)
P1-C11-C12-C13	170.8(5.6)
P1-C21-C22-C23	146.8(6.3)
P1-C31-C32-C33	178.3(4.4)
C11-P1-C21-C22	57.7(7.5)
C11-P1-C31-C32	35.1(3.9)

	Angle (°) with E.S.D's in Parenthesis
C21-P1-C31-C32	173.6(2.9)
Hg1-P1-C11-C12	170.4(4.6)
Hg1-P1-C21-C22	173.5(5.8)
Hg1-P1-C31-C32	79.9(2.7)
Hg1-P2-C41-C42	87.4(6.3)
Hg1-P2-C51-C52	27.7(6.7)
Hg1-P2-C61-C62	176.3(5.6)
P2-C41-C42-C43	163.5(8.1)
P2-C51-C52-C53	179.9(4.2)
P2-C61-C62-C63	167.1(5.6)

(d) $(NCCH_2CH_2)_3PHgCl_2$

P-C11-C12-C13	170.3(1.9)
P-C21-C22-C33	74.5(2.7)
P-C31-C32-C33	171.3(1.9)

A2. The Absorption Correction

Absorption corrections have been made for $[\beta\text{-}Pr_3PHgI_2]_2$ and $[(NCCH_2CH_2)_3PHgCl_2]_n$ using ABSCOR.[66] An outline of this method follows.

The intensity of the emergent X-ray beam may be reduced by the absorption of the X-rays by the crystal. The extent of the absorption is given by:

$$I = I_0 \exp(-\mu X) \qquad 3$$

Where I = measured intensity of emergent beam

I_0 = intensity of emergent beam at zero absorption

X = total path length of the X-ray through the crystal in cm

μ = linear absorption coefficient (cm^{-1}) and is given by

$$\mu = \frac{N}{V_c} \Sigma_{aj} (\mu_{aj}) \qquad 4$$

N = number of molecules per unit cell

V_c = volume of unit cell

μ_a = atomic absorption coefficient

j = the j^{th} atom

The transmission factor T is equal to I/I_0 and is obtained by integration over the volume of the crystal.

$$T = I/I_0 = \frac{1}{V} \int_V \exp[-\mu(X_1 + X_2)].dV \qquad 5$$

where X_1 = length of incident beam from point of entry to the element of volume dV.

X_2 = length of diffracted beam from the point of emergence from element dV, to the point of emergence from the crystal.

The crystal is considered as a convex polyhedron, for which every reflection may be divided into a number of tetrahedra. The absorption correction for one tetrahedron is calculated and the summation of the

corrections for all tetrahedra gives the total absorption correction required by a particular reflection.

To enable an absorption correction to be made the crystal shape must be defined. The faces of the crystal are defined in terms of their Miller indices. A point of origin within the crystal is chosen and the perpendicular distances from all the faces to this origin are measured. Having defined the crystal shape the value of T in equation 5 may be calculated using the Abscor computer program which will also give corrected intensities for each reflection. For example, this is illustrated below in Fig. A1 for $[(NCCH_2CH_2P)_3HgCl_2]_n$.

Fig. A1 Schematic Diagram of the $[(NCCH_2CH_2P)_3HgCl_2]_n$ crystal

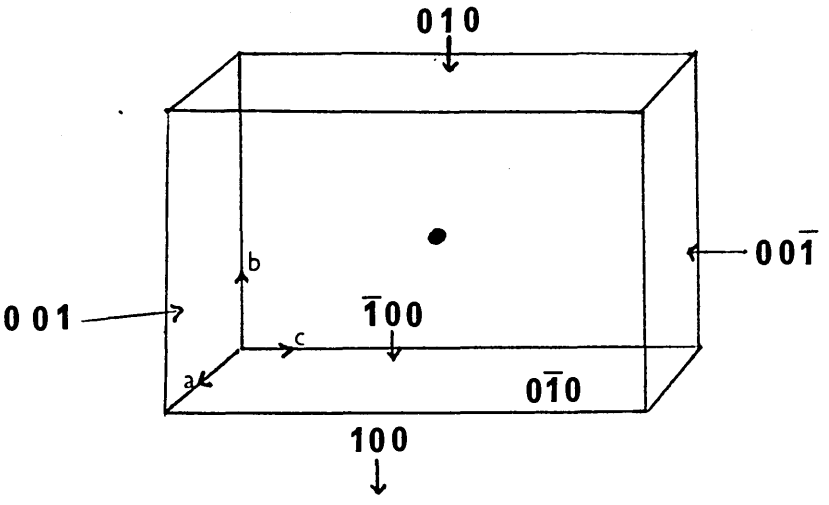

A3. Preparative Methods

(a) Preparation of Ph_3PHgI_2

Equimolar portions of ligand and mercury(II) halide were dissolved separately in minimal quantities of warm ethanol. The solution of ligand was added dropwise to the mercury(II) halide solution, the resulting precipitate being filtered off and recrystallised from DMF/H_2O mixture as white crystals and dried *in vacuo*.

(b) Preparation of Pr_3PHgX_2 (where X =Cl or Br)

These were similarly prepared by the action of an alcoholic solution of the ligand (1 mole) on the alcoholic mercury(II) halide solution.[24] The product was recrystallised from ethanol as white needle shaped crystals.

(c) Preparation of Pr_3PHgI_2 (α- and β-forms)

The reaction of alcoholic solutions of the ligand and mercury(II) iodide gave a pale yellow mass. Recrystallisation of the product from alcohol/acetone (4:1 by vol.) gave white needle shaped crystals of the α-form of the product. The β-form is deposited from the mother-liquor as yellow crystals. The α-form of the iodide may also be formed by the rapid recrystallisation of the β-form.

(d) Preparation of $[(NCCH_2CH_2)_3P]_nHgX_2$ (when X = Cl n = 1 and 2 when X =Br n = 2)

These complexes were prepared by mixing alcoholic solutions of the ligand and the appropriate mercury(II) halide in the required mole ratio. The resultant precipitate were recrystallised from acetone as white crystals and dried *in vacuo*.

(e) Preparation of $[(2\text{-thienyl})_3P]_2HgCl_2$

A hot solution of the phosphine ligand in ethanol (2.5 mol) was added to a hot solution of the mercury(II) chloride. The solution was allowed to

cool and the resulting precipitate was filtered off, washed with ethanol and dried. The product was recrystallised from hot ethanol as colourless needles.

(f) Preparation of $(Pr_3P)_2Hg(\mu\text{-}I)_2CdI_2$

This complex was prepared by the treatment of hot ethanolic $(Pr_3P)_2CdI_2$ solution with 1 mole solution of hot mercury(II) iodide. On standing a white crystalline product was formed,[41] which was recrystallised from ethanol as fine colourless needles.

A4. Analytical Data

Compound	% C		% H	
	Calculated	Found	Calculated	Found
‡Ph_3PHgI_2	30.16	30.25	2.10	2.02
*Pr_3PHgCl_2	25.04	25.07	4.90	4.92
*Pr_3PHgBr_2	20.76	20.97	4.07	4.04
‡Pr_3PHgI_2 (α-form)	17.58	17.77	3.44	3.38
‡Pr_3PHgI_2 (β-form)	17.58	17.77	3.44	3.34
*$(NCCH_2CH_2)_3PHgCl_2$	23.40	23.30	2.60	2.55
*$[(NCCH_2CH_2)_3P]_2HgCl_2$	32.85	32.95	3.65	3.60
*$[(NCCH_2CH_2)_3P]_2HgBr_2Me_2CO$	31.33	31.36	3.76	3.73
*$[(2\text{-thienyl})_3P]_2HgCl_2$	34.65	34.65	2.15	2.10
‡$(Pr_3P)_2HgI_2CdI_2$	18.94	18.89	3.70	3.61

*Analysis carried out by Elemental Micro-Analysis Ltd., Devon.

‡Analysis carried out by The City University Chemistry Department, London.

Structure Factors for $[(2\text{-thienyl})_3P]_2HgCl_2$

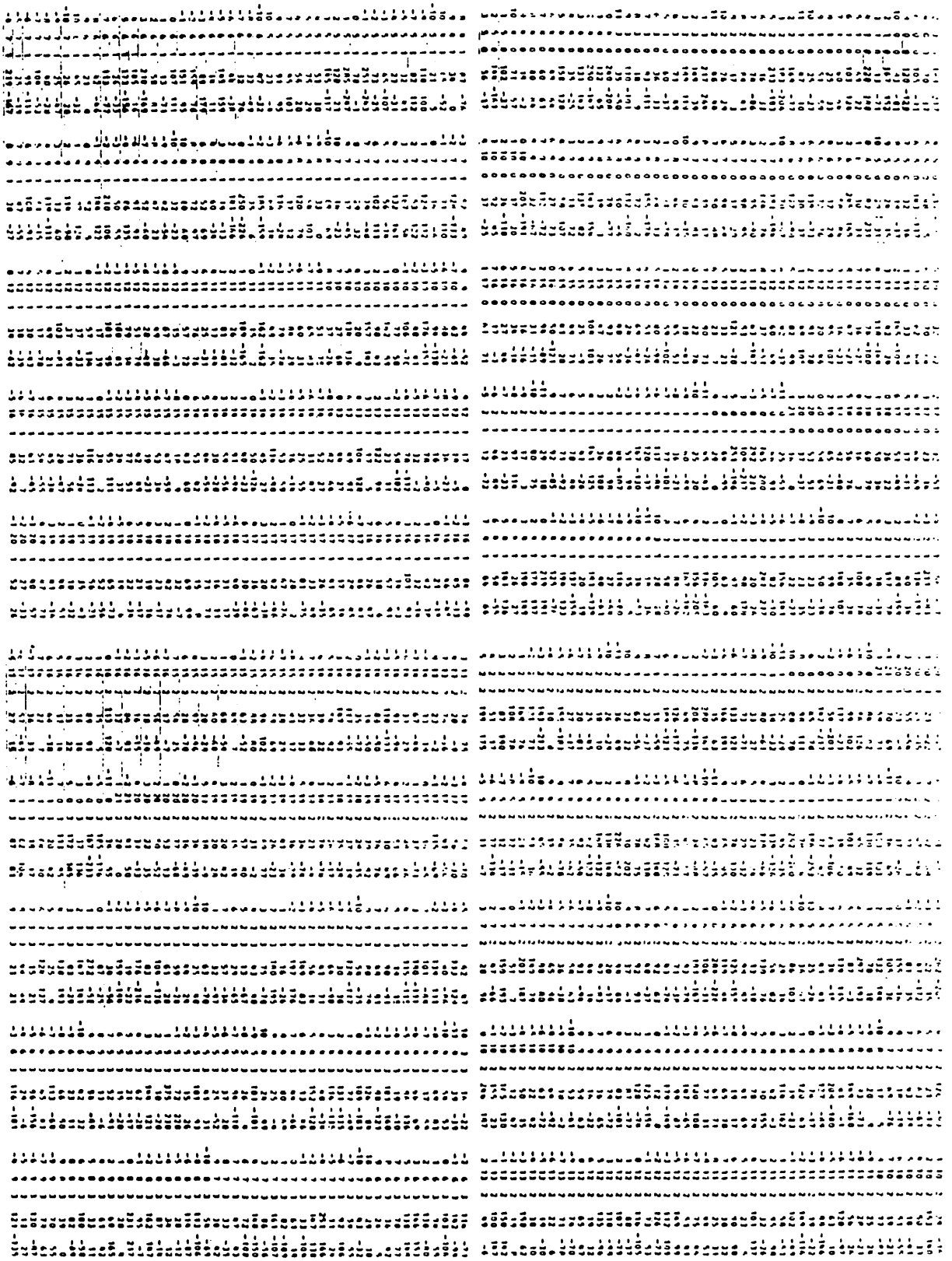

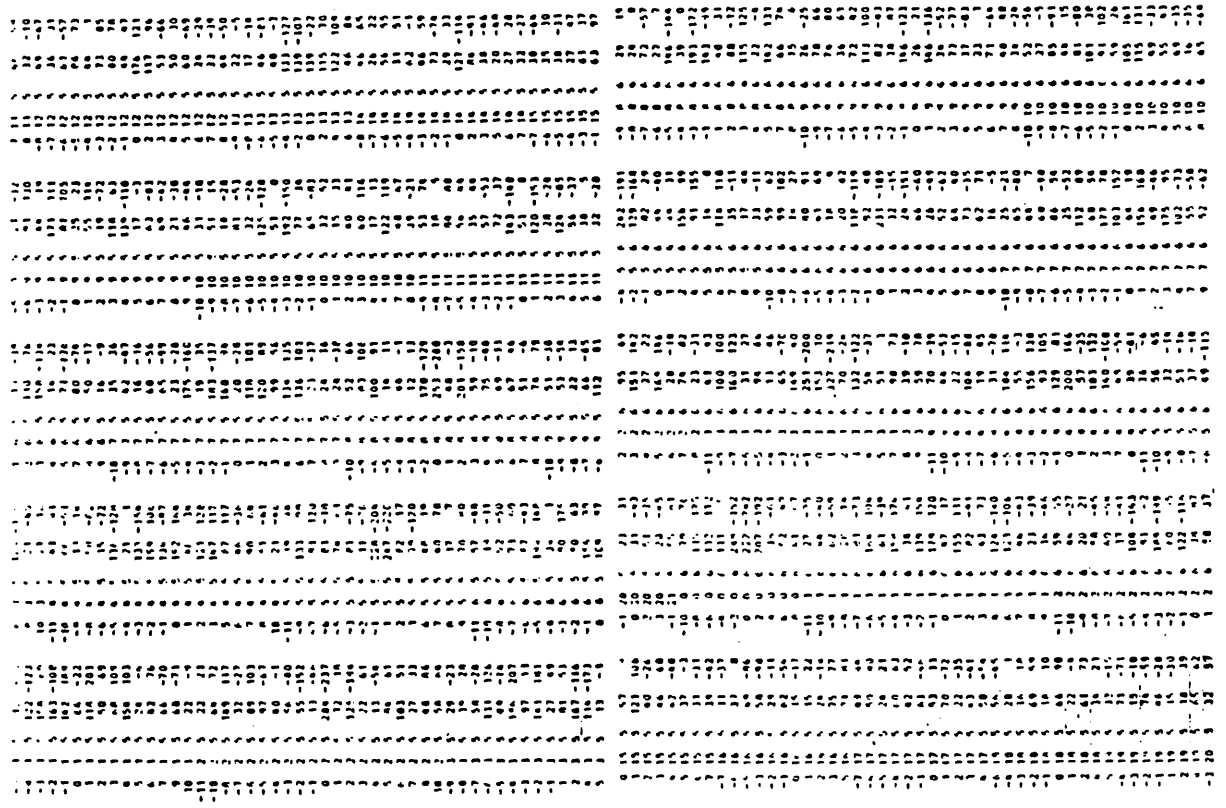

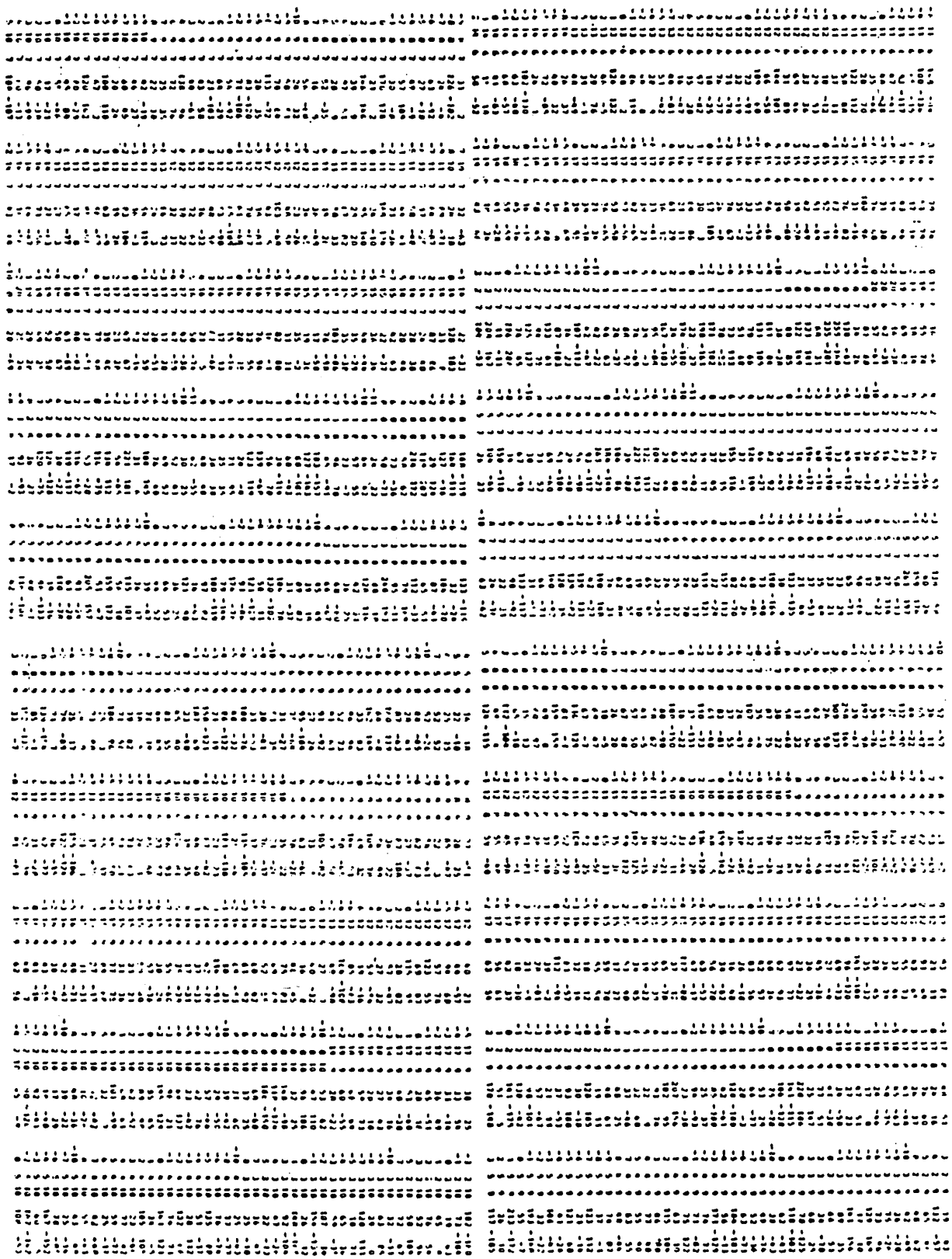

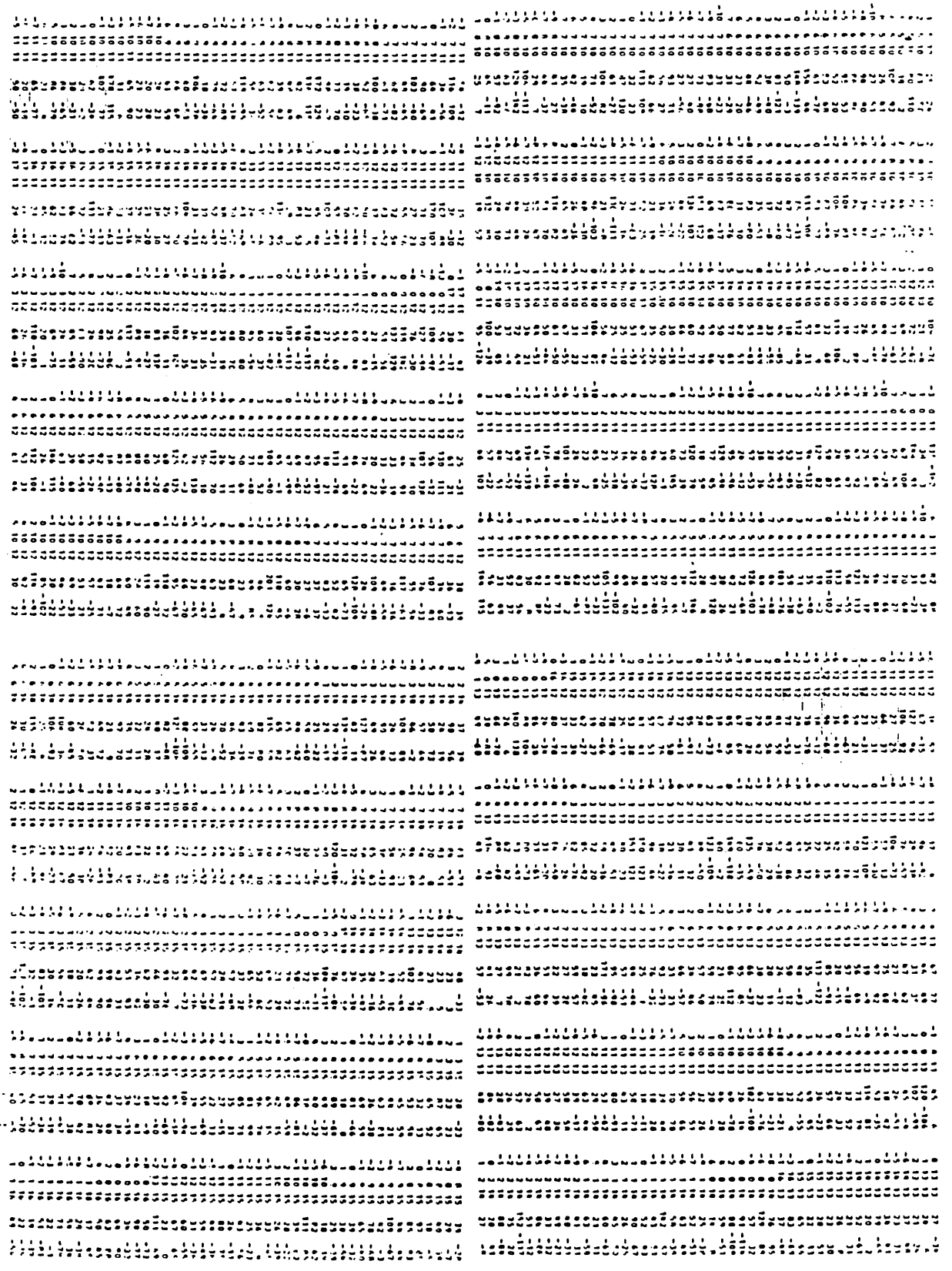

Structure Factors for $[(NCCH_2CH_2)_3P]_2HgCl_2$

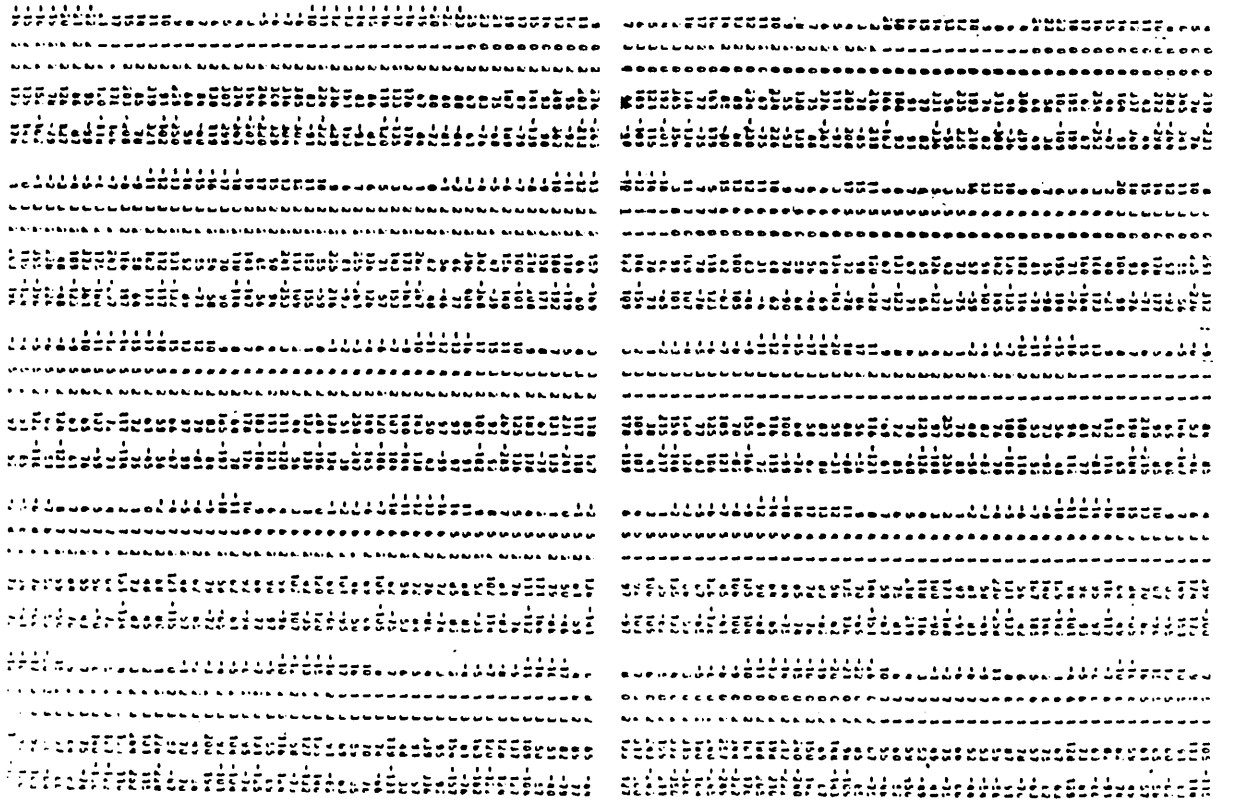

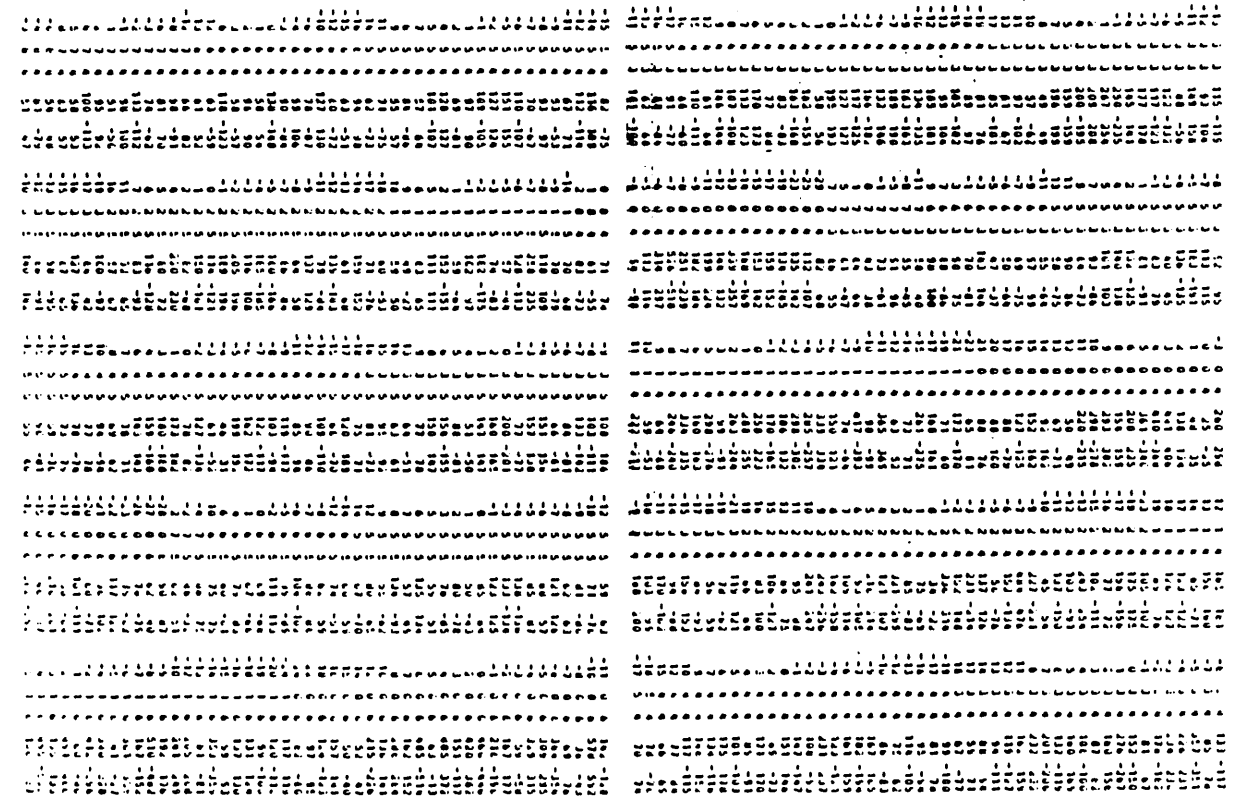

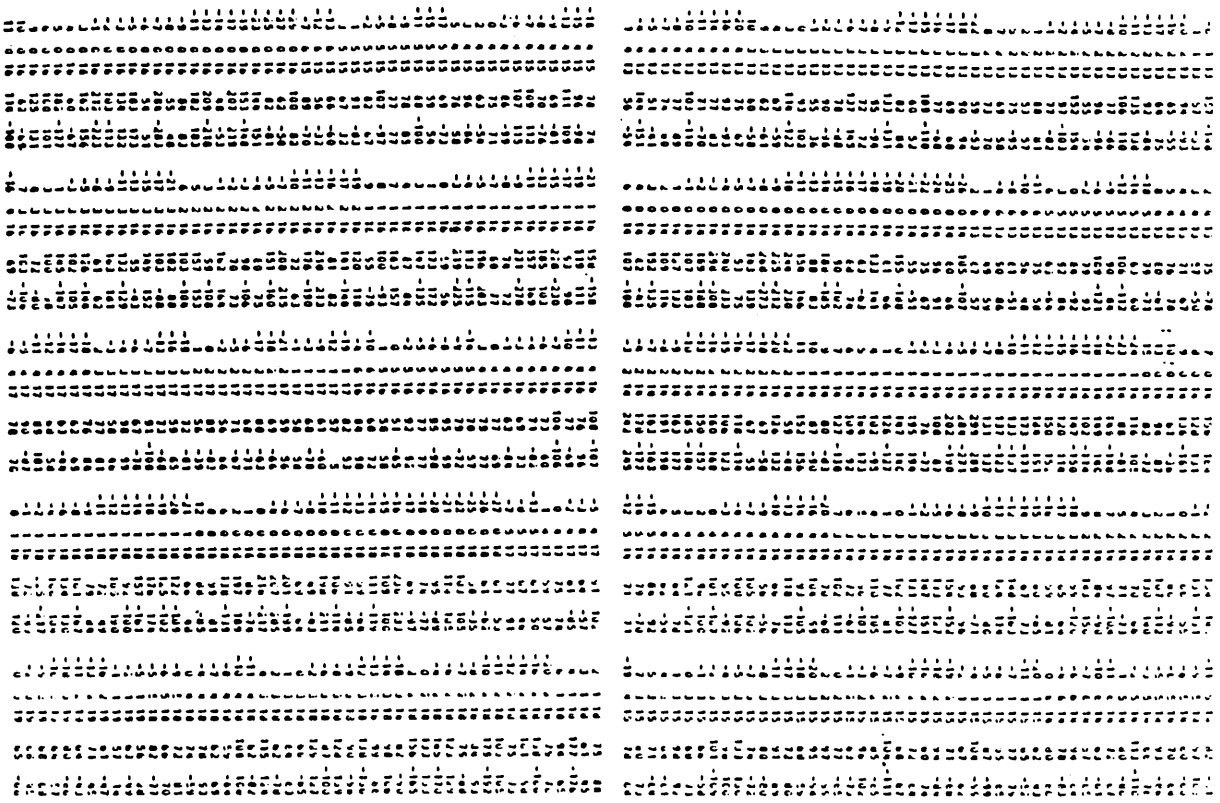

Structure Factors for $[(NCCH_2CH_2)_3P]_2HgBr_2.OC(CH_3)_2$

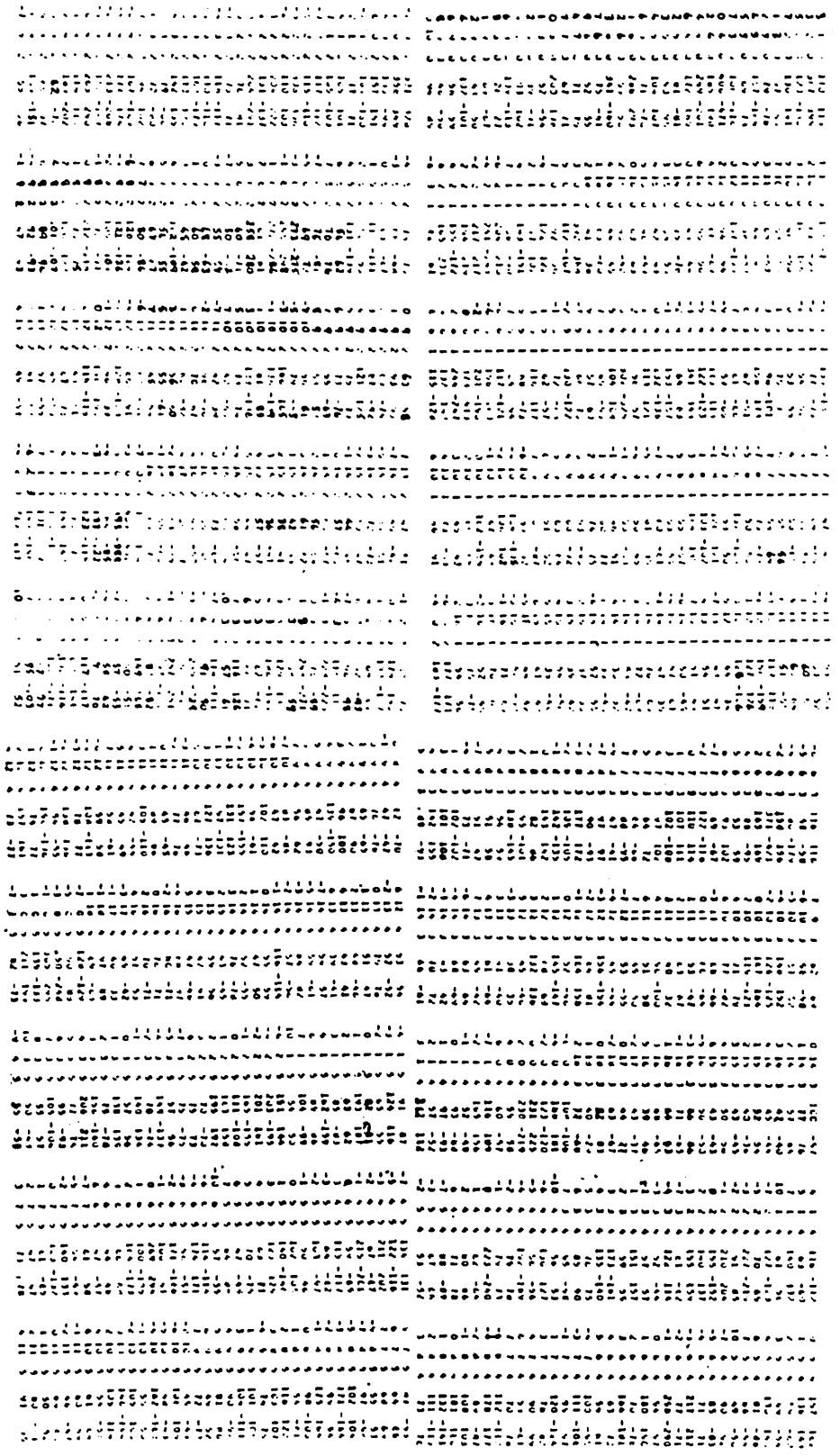

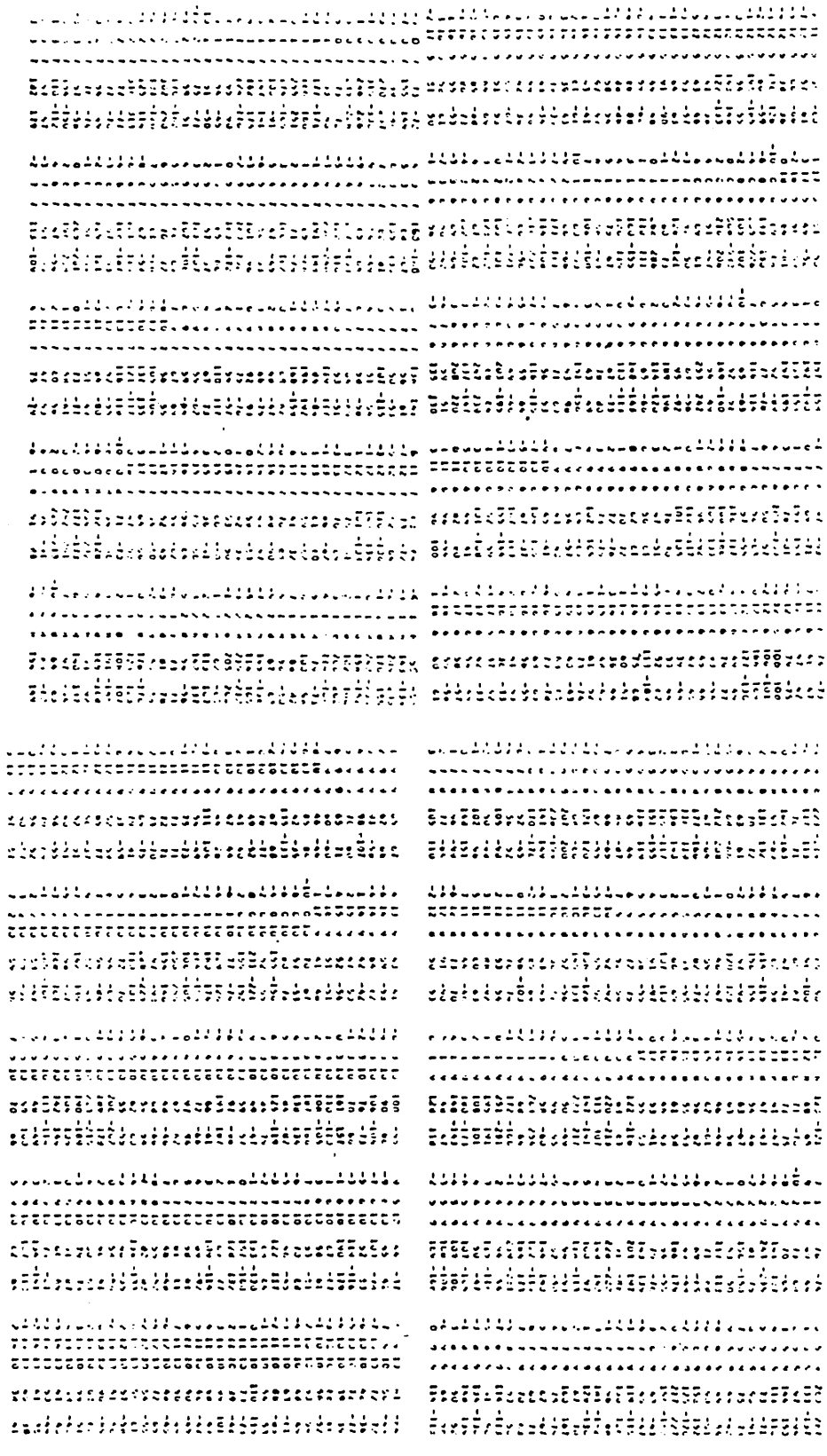

Structure Factors for $[(NCCH_2CH_2)_3PHgCl_2]_n$

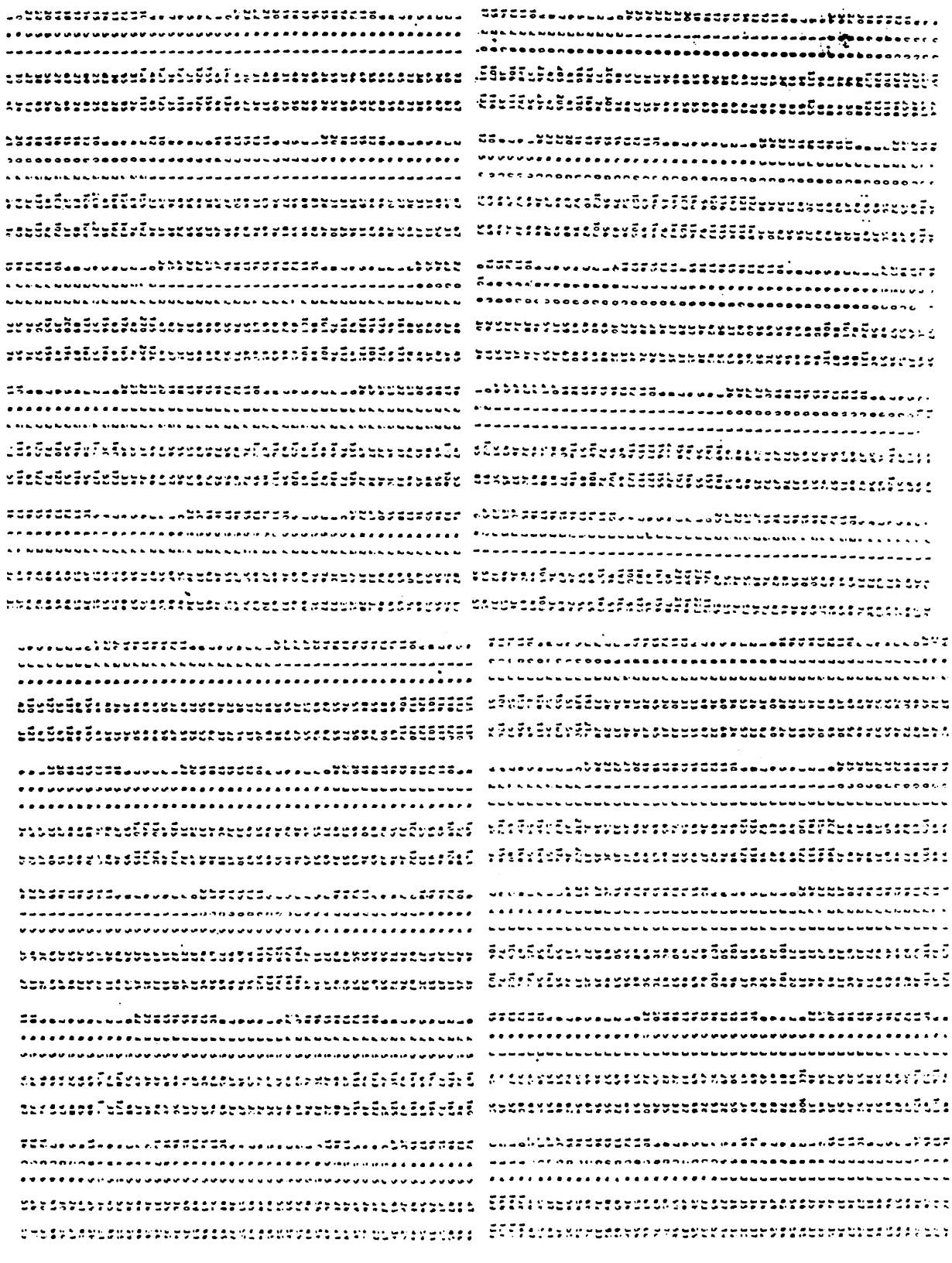

Structure Factors for $[Ph_3PHgI_2]_2$

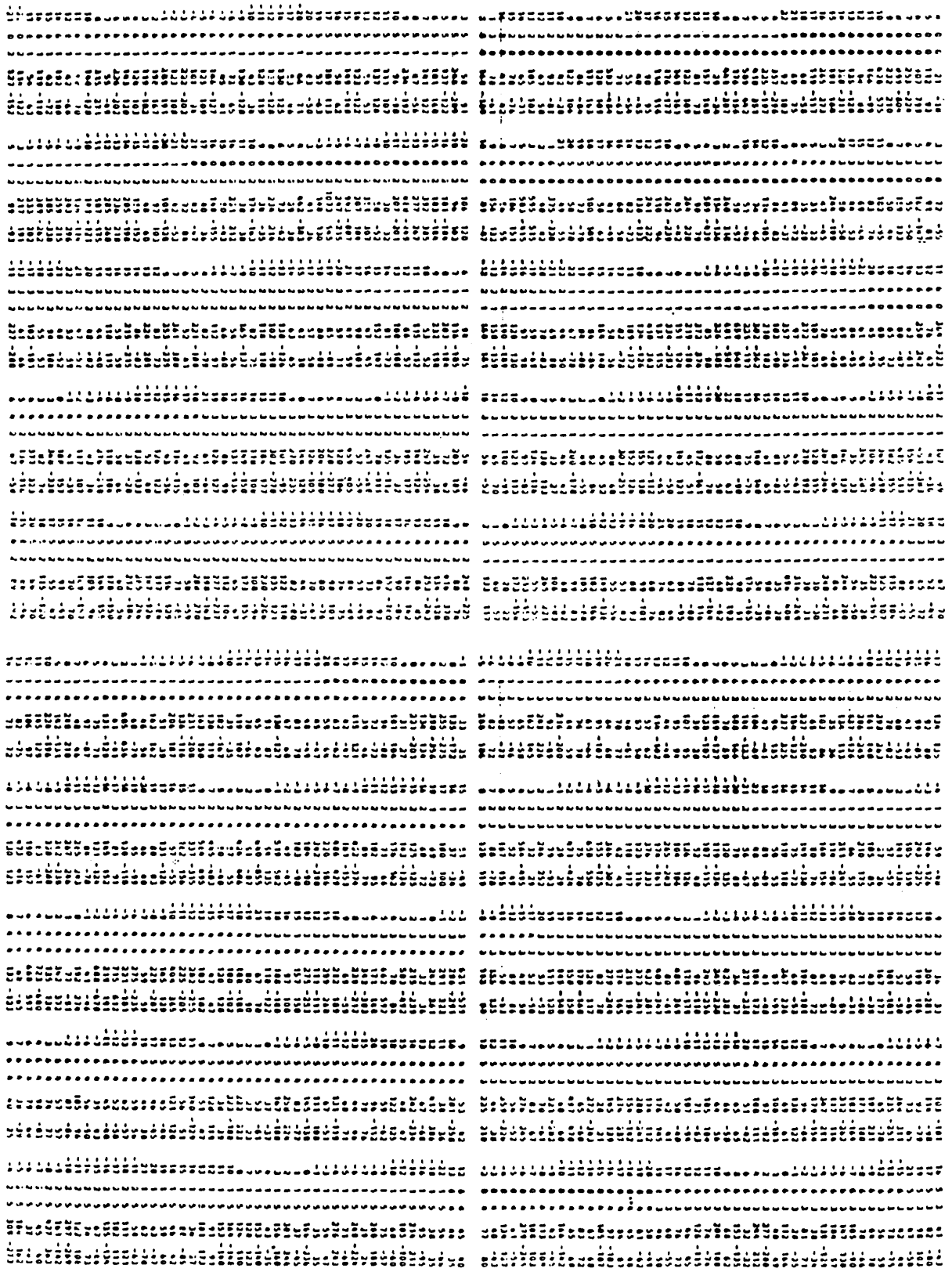

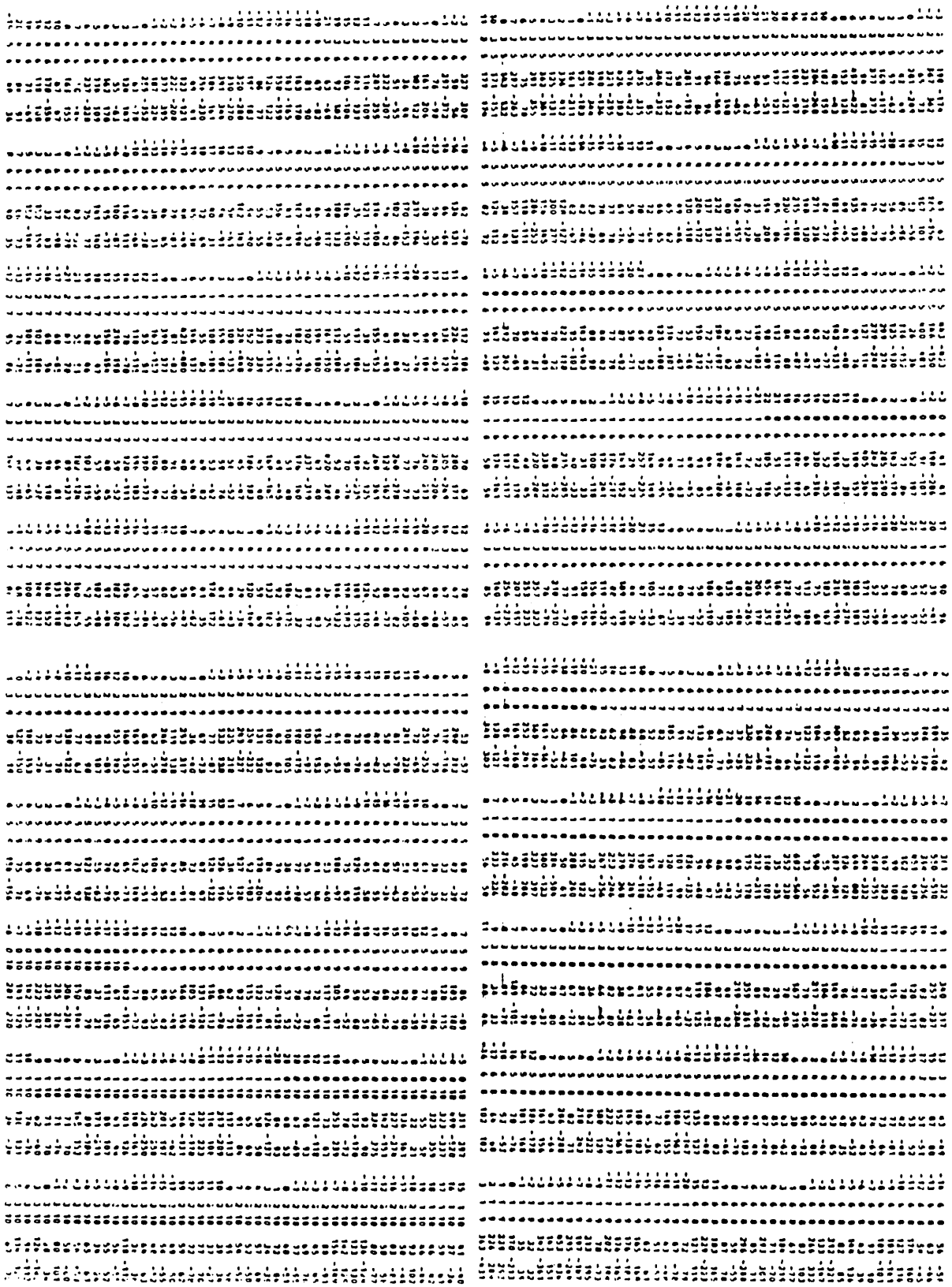

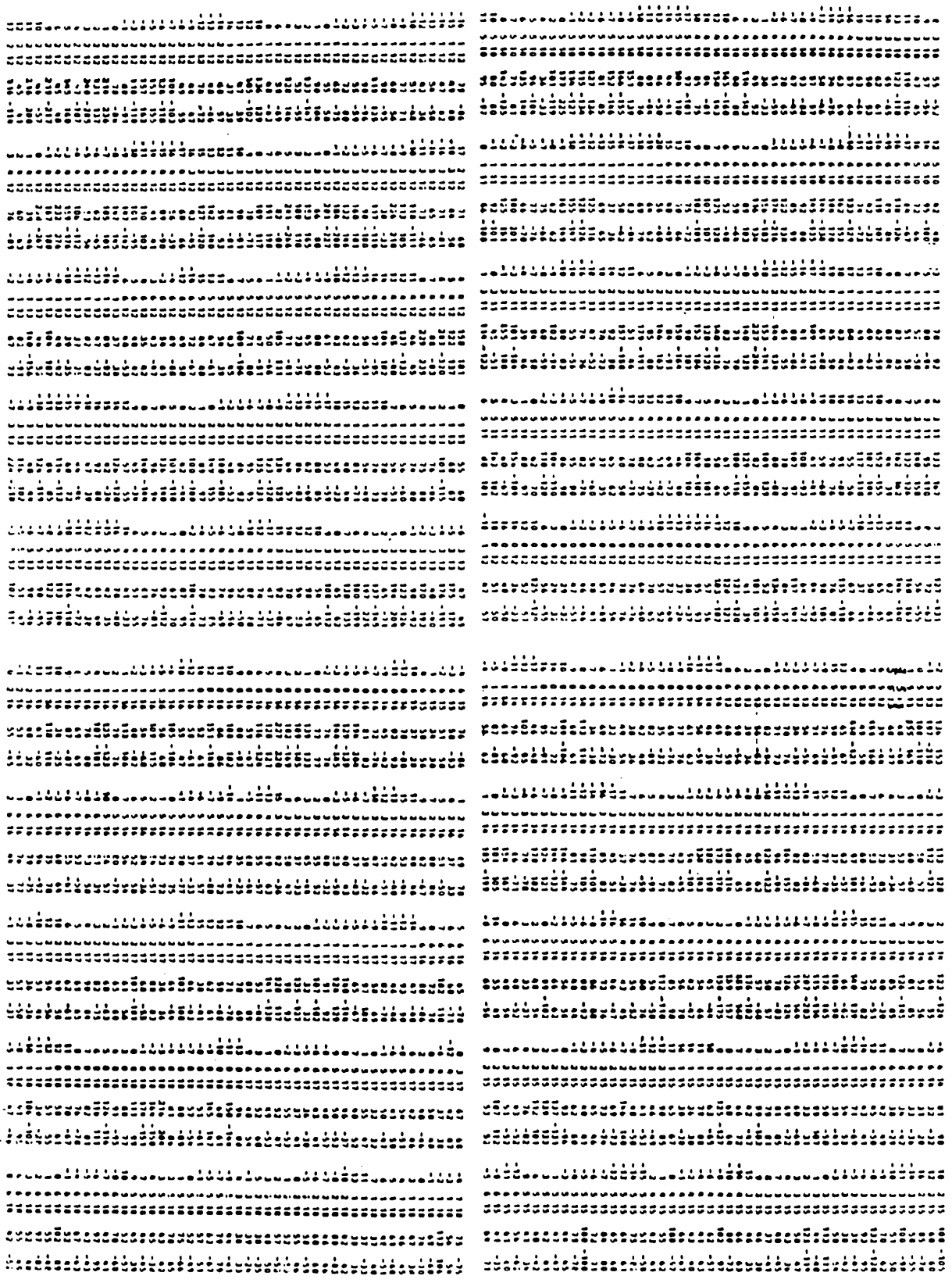

-10	1	19	73	78	1	3	19	51	40	-3	1	20	36	36	1	4	20	56	58	-3	3	21	69	56
-9	1	19	56	-51	3	3	19	42	-31	0	1	20	31	25	2	4	20	54	-52	-2	3	21	51	-39
-8	1	19	67	-73	4	3	19	41	37	5	1	20	43	-32	5	4	20	49	-40	0	3	21	78	64
-7	1	19	56	62	7	3	19	39	39	6	1	20	45	38	6	4	20	48	47	2	3	21	51	-45
-6	1	19	43	35	2	4	19	77	67	-4	2	20	51	-44	7	4	20	69	65	3	3	21	84	68
-2	1	19	96	-87	4	4	19	44	-44	-2	2	20	48	33	8	4	20	72	-70	5	3	21	55	-45
-1	1	19	39	43	-7	5	19	41	35	2	2	20	43	-31	-5	5	20	43	35	6	3	21	71	59
0	1	19	73	-62	3	5	19	56	48	3	2	20	63	47	0	5	20	40	-28	-2	4	21	54	34
1	1	19	54	-44	5	5	19	63	-53	4	2	20	58	48	1	5	20	40	35	0	4	21	50	-41
-8	1	19	38	24	7	5	19	43	42	5	2	20	-63	-57	-2	6	20	47	-33	-2	5	21	57	-39
6	1	19	47	38	8	5	19	39	43	6	2	20	50	-43	-3	1	21	37	32	-1	5	21	43	33
7	1	19	38	-36	-3	6	19	72	-60	-8	3	20	43	-51	-2	1	21	35	-29	0	5	21	73	59
-9	2	19	76	77	-1	6	19	60	49	0	3	20	82	69	4	1	21	37	-22	1	5	21	50	-46
-7	2	19	44	-46	3	6	19	57	-39	2	3	20	82	-70	5	1	21	44	-38	2	5	21	52	-40
-1	2	19	71	-68	5	6	19	62	54	5	3	20	57	43	7	1	21	42	28	-2	2	22	96	-72
0	2	19	61	50	-7	0	20	69	66	7	3	20	49	-47	-7	2	21	45	41	-1	2	22	51	41
1	2	19	60	54	-5	0	20	58	-45	8	3	20	50	-35	-5	2	21	45	-41	0	2	22	54	41
2	2	19	37	-31	-1	0	20	37	37	-7	4	20	50	-50	1	2	21	73	-60	1	2	22	50	-26
5	2	19	49	-52	-8	1	20	39	-40	-5	4	20	47	24	7	2	21	44	-35	1	3	22	59	47
6	2	19	42	39	-6	1	20	46	36	-1	4	20	79	-67	-6	3	21	42	32	2	3	22	65	55
8	2	19	38	-30	-5	1	20	37	-31	0	4	20	70	54	-5	3	21	51	-55					

Structure Factors for $[\beta\text{-}Pr_3PHgI_2]_2$

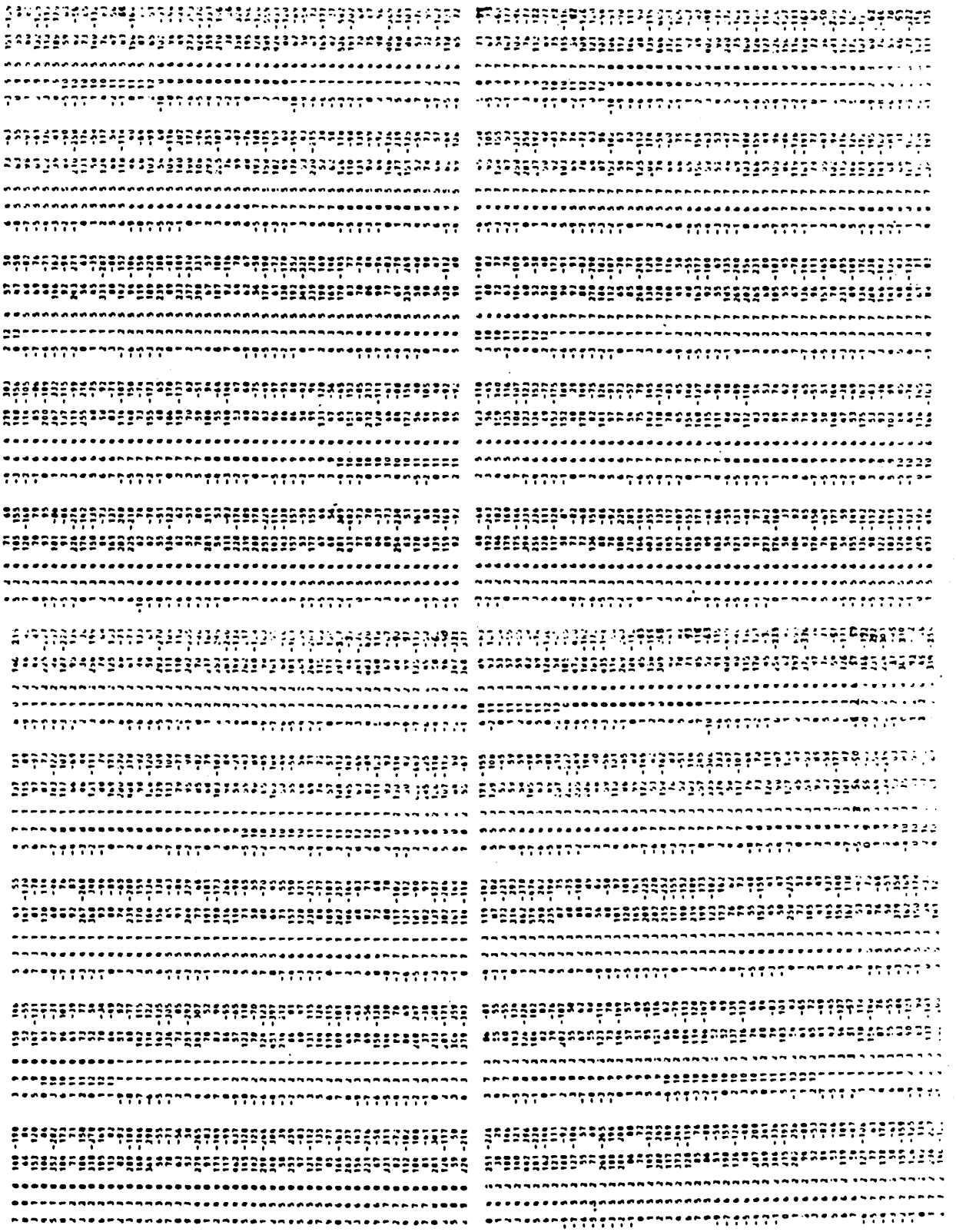

Structure Factors for $[Pr_3PHgBr_2]_2$

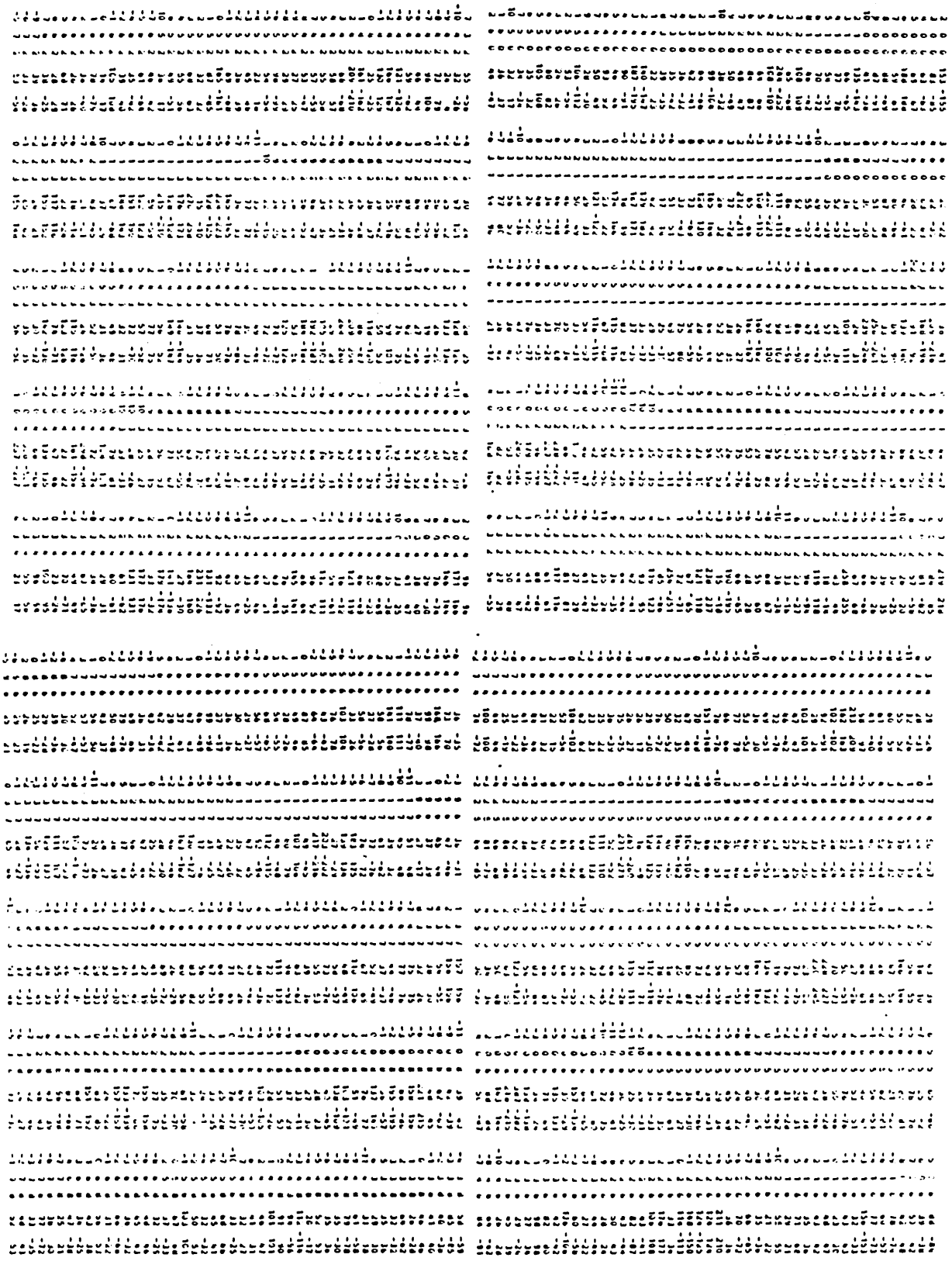

Structure Factors for $[Pr_3PHgBr_2]_2$

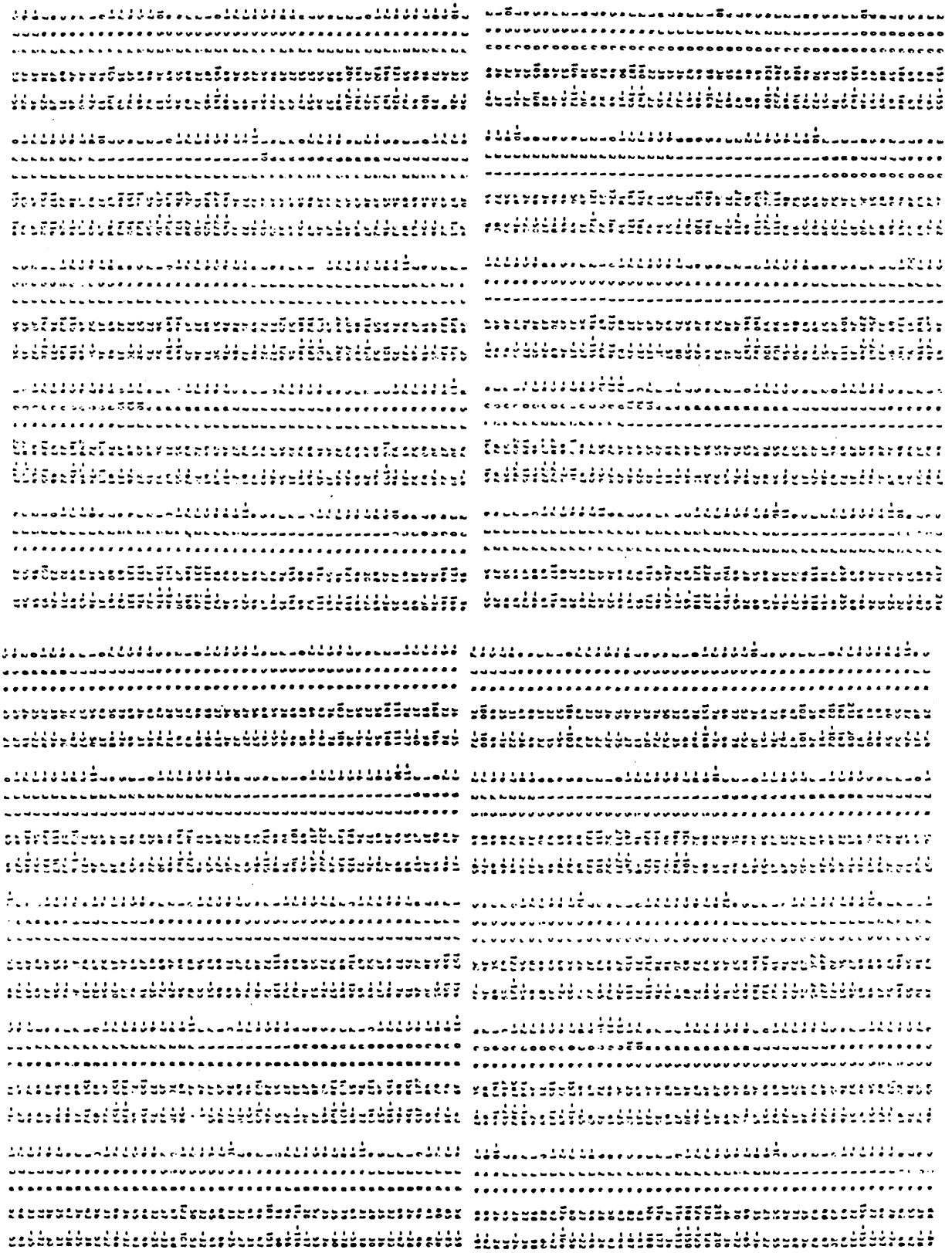

Structure Factors for $[Pr_3PHgCl_2]_2$

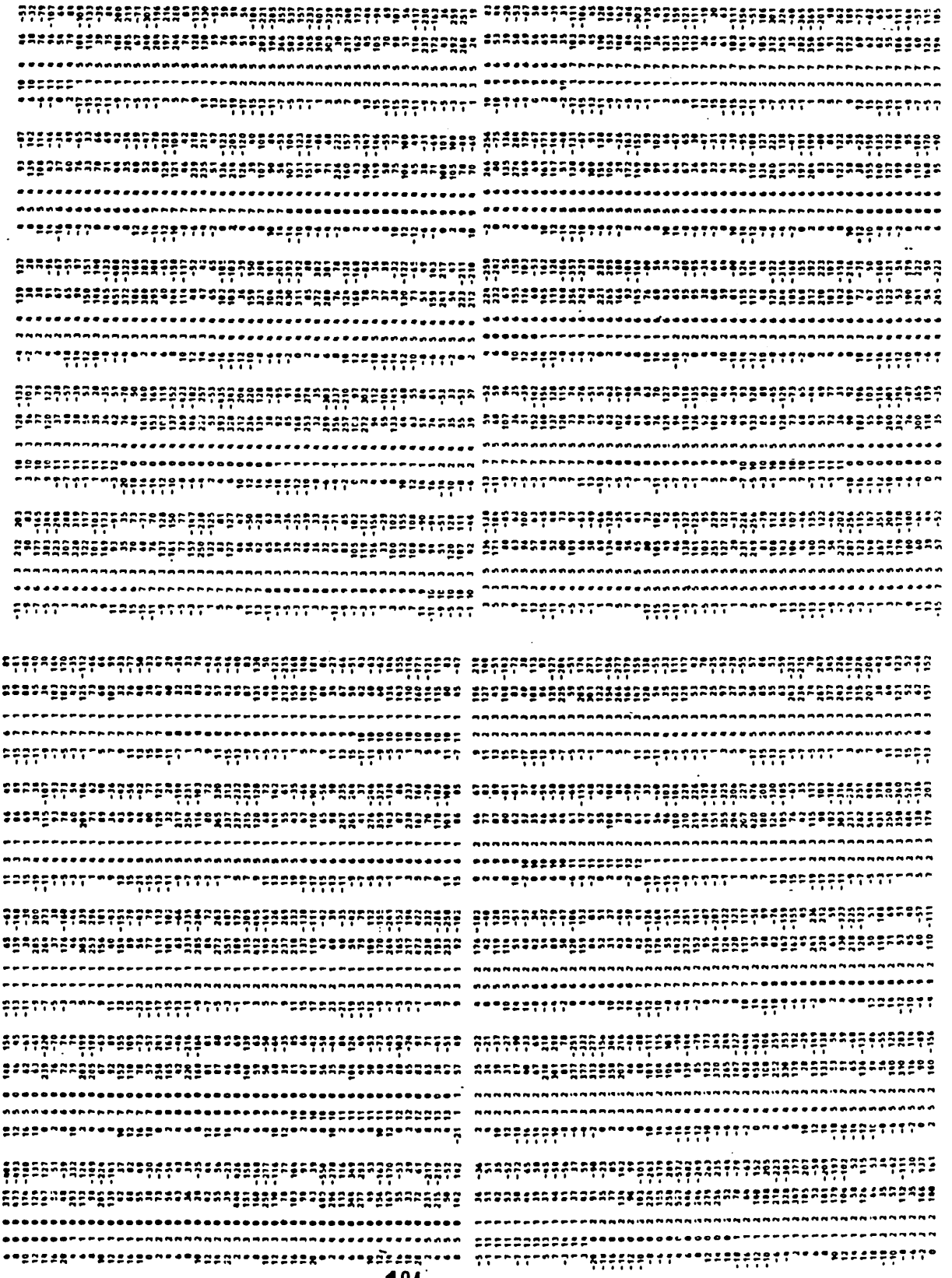

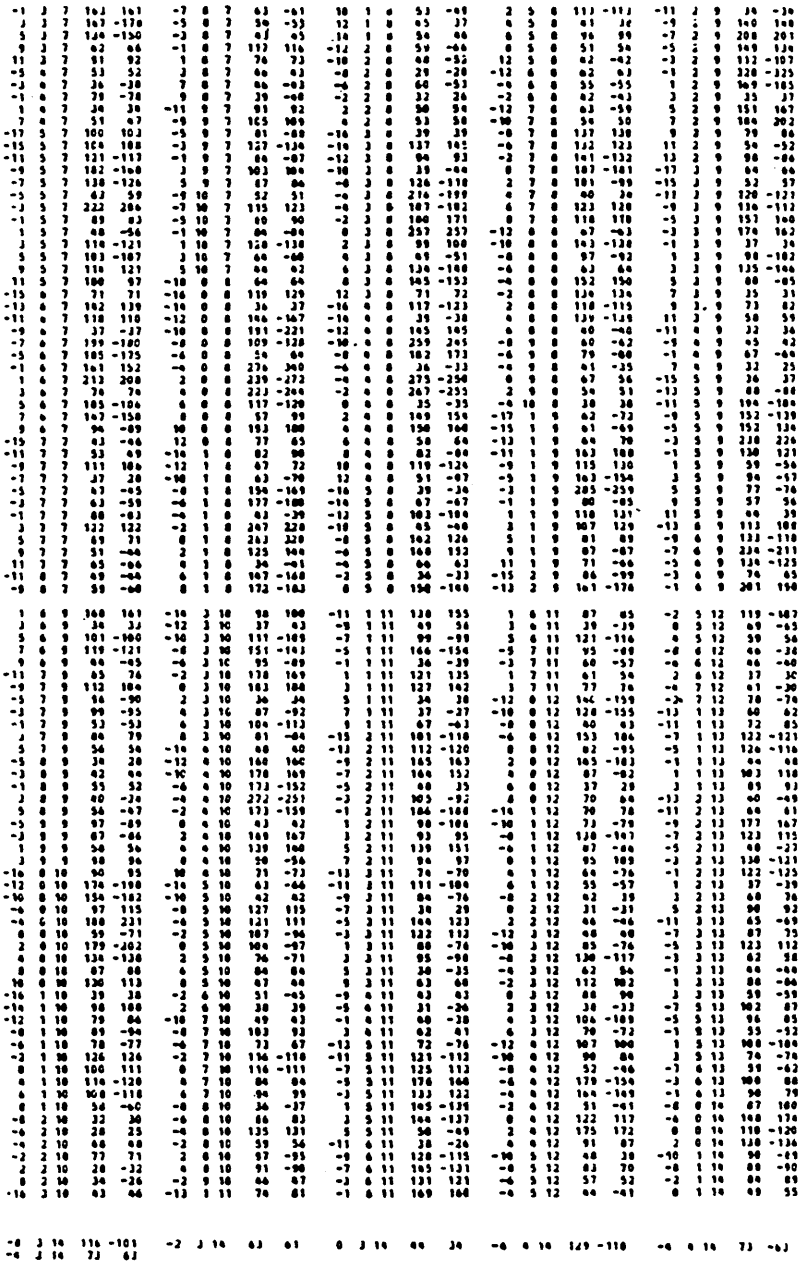

Structure Factors for $(Pr_3P)_2Hg(\mu\text{-}I)_2CdI_2$

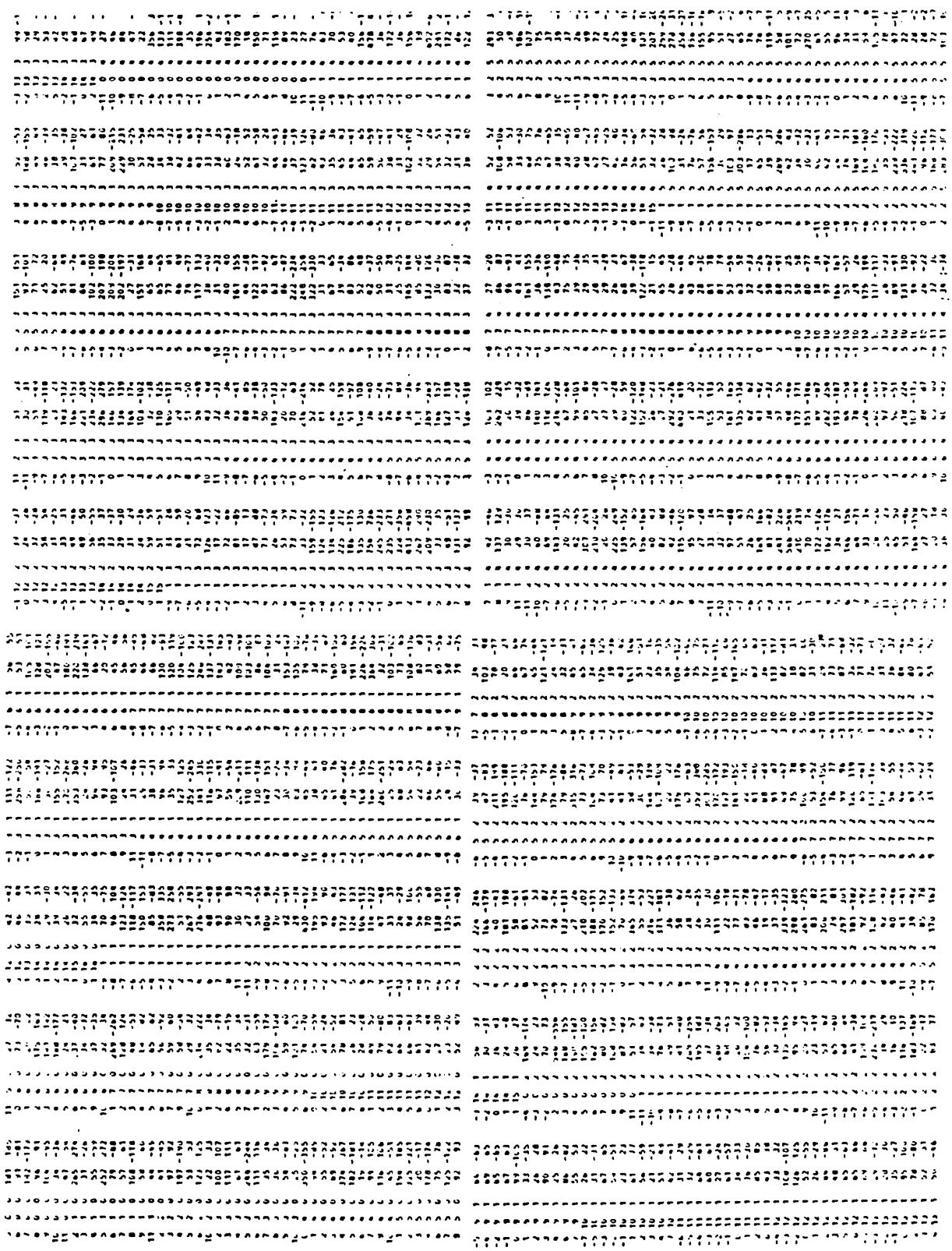

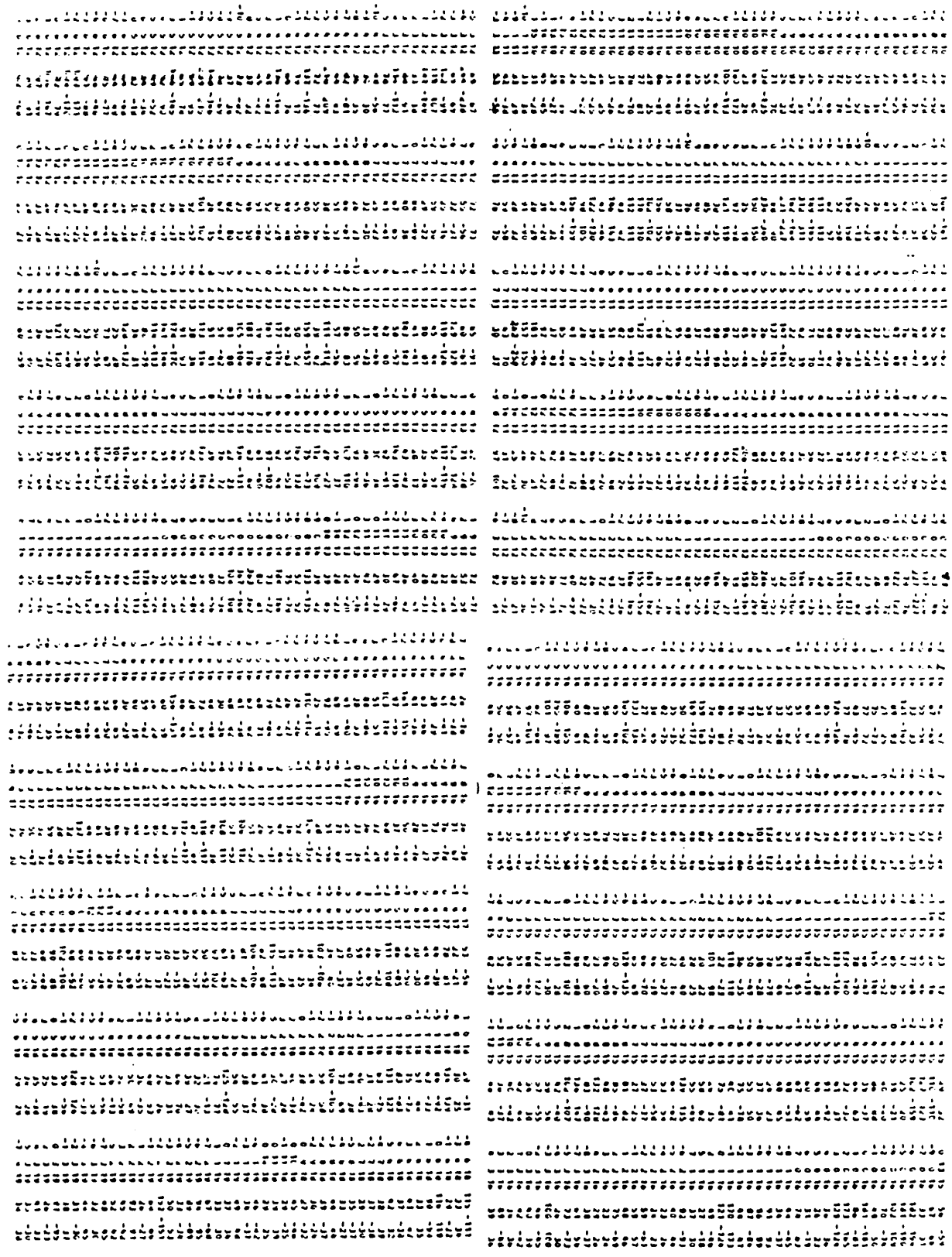

Structure Factors for $[\alpha\text{-}Pr_3PHgI_2]_n$